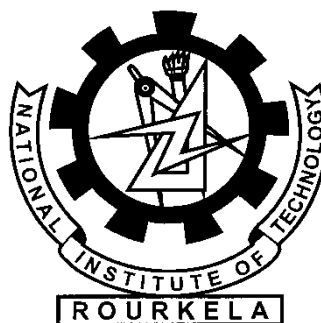# On The Dynamic Stability of Functionally Graded Material Plates Under Parametric Excitation

A THESIS SUBMITTED IN PARTIAL FULFILMENT OF

THE REQUIREMENT FOR THE DEGREE

OF

DOCTOR OF PHILOSOPHY

IN

MECHANICAL ENGINEERING

BY

RAMU INALA

(ROLL NO. 511ME109)

Department of Mechanical Engineering

National Institute of Technology

Rourkela -769008 Odisha (India)

June-2015

On The Dynamic Stability of Functionally Graded Material Plates Under Parametric Excitation

A THESIS SUBMITTED IN PARTIAL FULFILMENT OF

THE REQUIREMENT FOR THE DEGREE

OF

DOCTOR OF PHILOSOPHY

IN

MECHANICAL ENGINEERING

BY

RAMU INALA

(ROLL NO. 511ME109)

UNDER THE SUPERVISION OF

Prof. S. C. Mohanty

Department of Mechanical Engineering

National Institute of Technology

Rourkela -769008 Odisha (India)

June-2015

CERTIFICATE

This is to certify that the thesis entitled "On the Dynamic Stability of Functionally Graded Material Plates Under Parametric Excitation" submitted by Mr. Ramu Inala for the award of the degree of Doctor of Philosophy (Mechanical Engineering) of NIT Rourkela, Odisha, India, is a record of bonafide research work carried out by him under my supervision and guidance. Mr. Ramu Inala has worked for more than three and half years on the above problem and this has reached the standard, fulfilling the requirements and the regulation relating to the degree. The contents of this thesis, in full or part, have not been submitted to any other university or institution for the award of any degree or diploma.

Place: Rourkela
Date:

(Dr. Sukesh Chandra Mohanty)
Associate Professor
Department of Mechanical Engineering
National Institute of Technology
Rourkela-769008
Orissa, India.

Acknowledgement

I avail this unique opportunity to express my gratitude and heartfelt reverence to my thesis supervisor, **Dr. S.C. Mohanty**, Associate Professor, Department of Mechanical Engineering, National Institute of Technology, Rourkela. He introduced me to the field of structural vibration, educated me with the methods and principles of research and guided me patiently throughout this thesis work. I am highly indebted and express my deep sense of gratitude to him for his supervision, valuable suggestions, constructive criticism and motivation with enormous moral support during my difficult phase to complete this work.

I express my sincere thanks to **Prof. S.K. Sarangi**, Director, **Prof. S.S. Mohapatra**, Head of Mechanical Engineering Department, and **Prof. K.P. Maity**, Ex-Head of Mechanical Engineering Department, National Institute of Technology, Rourkela, for their kind support and concern regarding my academic requirements.

I am grateful to my Doctoral Scrutiny committee Members, **Prof. S.K. Sahoo, Prof. H. Ray, Prof. R.K. Behara**, Department of Mechanical Engineering and **Prof. P. Sarkar**, Department of Civil Engineering, for their valuable suggestions and comments during this research work.

I owe my largest debt to my family. I would like to express my gratitude towards my family members: I. Venkateswararao, I. Naga kumari, G. Sudha, G. Raju, K. Shanta kumari, K. Praveen, Hasini and Joel for their love, affection and encouragement which help me in completion of this work. I also want to express my sincere thanks to my spouse Indhu for her sacrifice, endless inspiration and active cooperation throughout the course of my doctoral dissertation.

I would also thank my friend Mr. G. Raghavendra for his valuable thoughts in my research and personal career.

It is a great pleasure for me to acknowledge and express my appreciation to all my well-wishers for their understanding, relentless supports, and encouragement during my research work. I wish to express my sincere thanks to all those who helped me directly or indirectly at various stages of this work.

Last, but not the least, I am grateful to **The Almighty God** for bestowing upon me the courage to face the complexities of life and giving me the strength during the course of this research work.

RAMU INALA

i

ABSTRACT

The objective of this thesis is to study the dynamic stability of functionally graded material (FGM) plates under parametric excitation. Third order shear deformation theory is used for the analysis of the plates. The equations of motion have been derived using finite element method in conjunction with Hamilton's principle. The boundaries of stable and unstable regions in the parameter space are determined by using Floquet's theory. FGMs are microscopically inhomogeneous spatial combination of materials, usually made up of ceramic and metal constituents. A steel-alumina FGM plate with steel-rich bottom and alumina reach top is considered for the analysis. The properties of the functionally graded material plates are assumed to vary along the thickness direction, according to a power law distribution in terms of the volume fractions of the constituents.

The effect of power law index on the critical buckling load, natural frequencies and dynamic stability of plates is determined. In case of FGM plate, an increase of power law index value decreases the natural frequencies. If aspect ratio is increased, the critical buckling load decreases for both uniaxial and biaxial loading cases and it is also observed that increase of power law index value decreases critical buckling load. With increase of the power index there is deteriorating effect on the dynamic stability of the FGM plate.

The influence of temperature rise on the dynamic stability of the FGM plate in thermal environment is investigated. The natural frequencies and dynamic stability behaviour are found to be highly sensitive to the temperature change between the bottom and top surfaces. In high temperature environment the dynamic stability of the plate deteriorates.

The effect of foundation stiffness coefficients on the dynamic stability of FGM plates are examined in detail through parametric studies. The frequencies of FGM plate resting on Pasternak foundation increase with the increase of Winkler foundation constant and shear layer constant. The Winkler and shear foundation constants have significant effect on the critical buckling load of FGM plates resting on Pasternak foundation. An increase of these constants increases the critical buckling load of the plate. Increase of Winker foundation constant and shear layer constant improves the dynamic stability of FGM plate. Shear layer constant has got more prominent effect compared to the Winkler foundation constant, on the dynamic stability of FGM plate resting on Pasternak foundation.

Parametric investigation is carried out to study thoroughly the effect of the temperature rise, hub radius and rotational speed on the vibration and dynamic stability of rotating plate in

thermal environment. It is observed that the natural frequencies reduce with an increase in temperature rise. The increase in rotational speed and hub radius results in increase of natural frequencies. The increase in temperature leads to reduction in the dynamic stability of plate. Increase in hub radius and rotational speed improves the stability of the rotating plate.

The effects of moisture concentration, temperature rise and power law index on the dynamic stability of FGM plates in hygrothermal environment are investigated. The observations made from the dynamic stability diagrams are: with increase in moisture concentration and temperature the instability of the plate is more probable, the combined effect of moisture and temperature on the dynamic instability of FGM plates is more severe than the effect of individual parameter.

The effect of skew angle on dynamic stability of FGM plate in thermal environment is discussed. The natural frequencies increase with an increase of skew angle. Increase in aspect ratio of FGM skew plate increases its instability. The increase in the value of power law index is found to have enhancing effect on the parametric instability of the skew FGM plate. The increase in skew angle of the plate reduces the chance of dynamic instability of the plate.

Keywords: FGM plates; Third order shear deformation theory; Power law; Dynamic stability; Dynamic load factor; Thermal environment; Foundation constant; Hygrothermal environment; Rotating plate; Skew angle.

CONTENTS

LIST OF TABLES

LIST OF FIGURES

NOMENCLATURE

Although all the principal symbols used in this thesis are defined in the text as they occur, a list of them is presented below for easy reference.

a, b	Length and width of the element
C_m, C_c	Moisture concentration at metal and ceramic side
c_k, d_k	Coefficients of polynomial
d	Distance between the central plane to neutral plane
$E(z)$	Effective Young's modulus
E_c	Young's modulus of ceramic
E_m	Young's modulus of metal
(e)	Element
$F_c^{(e)}$	Centrifugal force
h	Plate thickness
l	Moment of inertia of cross-section
k	Power law index
k_s	Shear foundation constant
k_w	Winkler's foundation constant
L	Length of the plate
M_x, M_y	Bending moments about Y and X axis
$\bar{N}$	Critical buckling load parameter
N_i	Shape functions for ith node
P(t)	Dynamic axial load
P^{cr}	Critical buckling load
P_s	Static load component
P_t	Time dependent dynamic load component
$P_0, P_{-1}, P_1, P_2, P_3$	Coefficients of temperature dependent material constants
Q_x, Q_y	Shear forces
Q_{11}, Q_{22}, Q_{21}, Q_{44}	Stiffness coefficients
R	Hub radius
$R(z)$	Effective material property
R_c	Material property at ceramic side layer
R_m	Material property at the metallic side layer
T_c, T_m	Temperature at ceramic surface and metal surface
V_c	Ceramic volume fraction
V_m	Metal volume fraction

u, v	Axial displacements of reference plane
W	Plate width
w	Transverse displacement in z-direction

Matrices

$\left[K^{(e)} \right]$	Element stiffness matrix
$\left[K_c^{(e)} \right]$	Element centrifugal matrix
$\left[K_{ef} \right]$	Global effective stiffness matrix
$\left[K_{ef}^{(e)} \right]$	Element effective stiffness matrix
$\left[K_g \right]$	Global geometric stiffness matrix
$\left[K_g^{(e)} \right]$	Element geometric stiffness matrix
$\left[K_H^{(e)} \right]$	Element moisture matrix
$\left[K_T^{(e)} \right]$	Element thermal stiffness matrix
$\left[K_{sl}^{(e)} \right]$	Shear layer element matrix
$\left[K_{wk}^{(e)} \right]$	Winkler's foundation element matrix
$\left[M \right]$	Global mass matrix
$\left[M^{(e)} \right]$	Element mass matrix
$\left\{ q \right\}$	Global displacement vector
$\left\{ q^{(e)} \right\}$	Element displacement vector
$\left[T_r \right]$	Transformation matrix

Greek symbols

α, β	Static and dynamic load factors
$\hat{\beta}$	Natural frequency parameter
$\varepsilon_{xx}, \varepsilon_{yy}$	Normal strain
$\gamma_{xz}, \gamma_{yz}, \gamma_{xy}$	Shear strain
ω	Natural frequency
ϕ	Skew angle of the plate
ψ	Coefficient of linear expansion
$\rho(z)$	Effective mass density

ρ_c	Mass density of ceramic
ρ_m	Mass density of metal
σ_{xx}, σ_{yy}	Normal stress
σ_{xx}^H, σ_{yy}^H	Moisture stress
σ_{xx}^T, σ_{yy}^T	Thermal stress
τ_{xy}, τ_{yz}, τ_{xz}	Shear stress
θ_x, θ_y	Transverse normal rotation about the y and x axis respectively.
$\upsilon(z)$	Poisson's ratio
υ_c	Poisons ratio of ceramic
υ_m	Poisson's ratio of metal
ς	Thermal conductivity
ΔC	Moisture difference
ΔT	Temperature change
Γ	Moisture expansion coefficient
Ω	Excitation frequency
ϖ	Non-dimensional frequency parameter
ϖ_r	Angular velocity of plate

Chapter 1

BACKGROUND AND MOTIVATION

1.1 Introduction

Structural systems by virtue of their interaction with environmental forces may undergo dynamic or parametric instability. In recent years, parametric instability of structural systems has gained importance. Parametric resonance can cause a number of catastrophic incidents. The environmental interaction with the deformable continuum is complex in nature and is usually represented by means of static and dynamic loads. The static loads are dead loads acting on the deformable bodies and they don't change their magnitude as well as their initial directions. The forces acting on the body may not always be static loads. In many realistic situations, the dynamic loads are time dependent and may change their direction. Also, the dynamic loading may go through two forms such as periodic and non-deterministic. Harmonic or superposition of several harmonic functions is used in representing periodic loading. Propeller force on a ship, unbalanced masses of rotating machinery, wind loading induced by vortex shedding on tall slender structures, helicopter blades in forward flight in a free-stream that varies periodically and spinning satellites in elliptic orbits passing through a periodically varying gravitational field are the examples of periodic forces. Non-periodic loads cannot be defined explicitly as functions of time and statistical parameters best describe them. Examples are earthquake, wind and ocean waves acting on on-shore and off-shore structures and aircraft structures subjected to turbulent flow. The uncoupled flapping motion of rotor blades in forward flight under the effect of atmospheric turbulence is an example of system subjected to both periodic components and non-deterministic fluctuations.

A second order non-homogenous equation generally describes a resonant system. When the elastic system under goes normal resonance or forced resonance, the external excitation frequency is equal to natural frequency of the system. Normal resonance correspond to the oscillatory response of the system in the direction of external excitation and is as shown in figure 1.1(a). In normal resonance, systems response amplitude increases linearly with time and can be reduced by providing damping. Figures 1.1 (b) and (c) show the normal resonant system and its response curve with time.
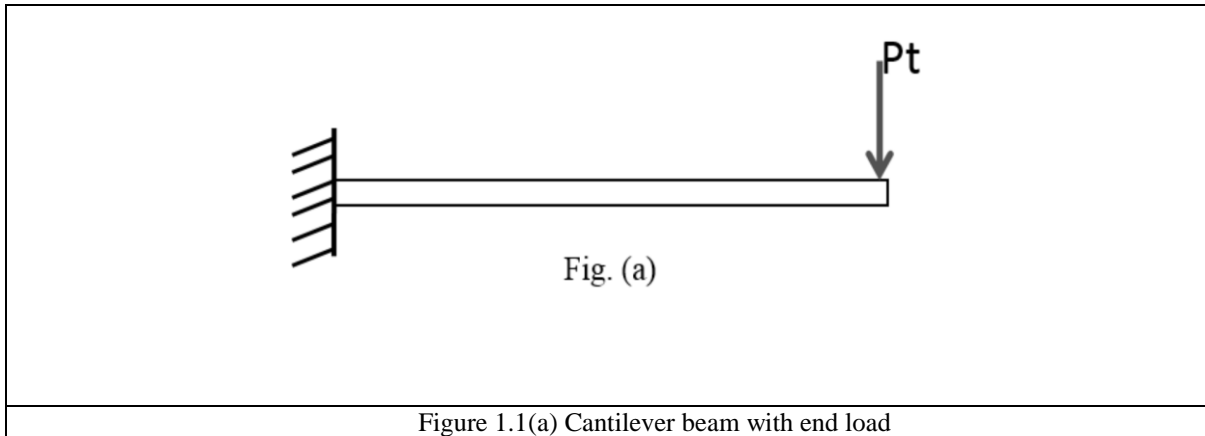
Figure 1.1(a) Cantilever beam with end load

Figure 1.1(b) Frequency verses amplitude diagram of a normal excited system.	Figure 1.1(c) Response variation with time of a normal system.
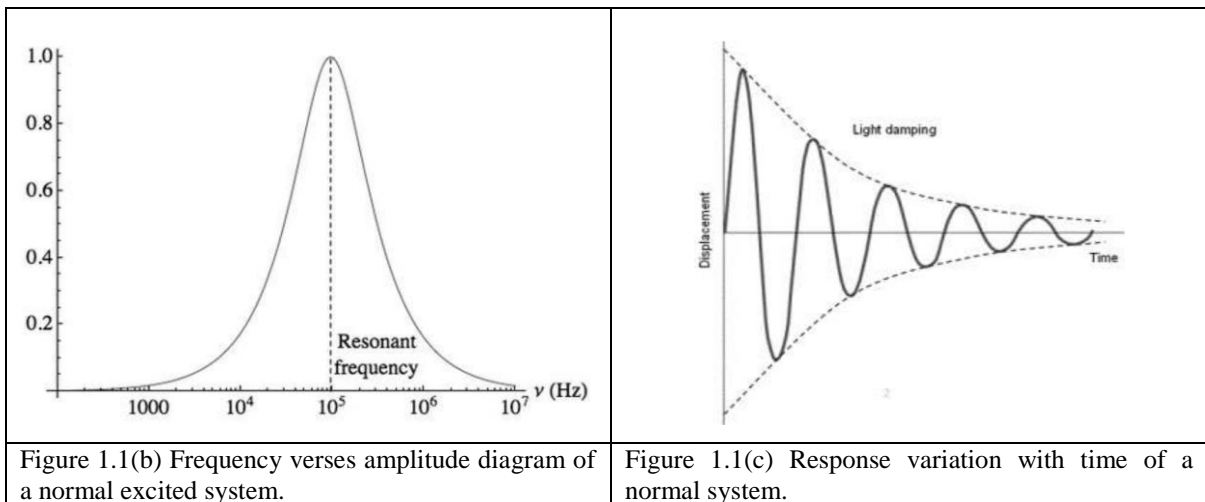
The phenomenon of dynamic stability is analyzed by second order homogenous equations. Parametric resonance refer to an oscillatory motion in a mechanical system due to time varying external excitation. The external applied loading terms appear as parameters or coefficients in the equation of motion of an elastic system. System undergoes parametric resonance when the external excitation is equal to an integral multiple of natural frequency of the system. The response of the system is orthogonal to the direction of external excitation, as shown in figure 1.2(a). In parametric resonance, systems amplitude increases exponentially and may grow without limit. This exponential unlimited increase of amplitude is potentially

dangerous to the system. Parametric resonance is also known as parametric instability or dynamic instability. Damping has little effect on the severity of parametric resonance but may only decrease the rate of increase of response.

Figure 1.2 (a) Cantilever beam subjected to axial load

| Figure 1.2(b) Stability diagram of a parametrically excited system. | Figure 1.2(c) Response variation with time of a parametrically excited unstable system. |
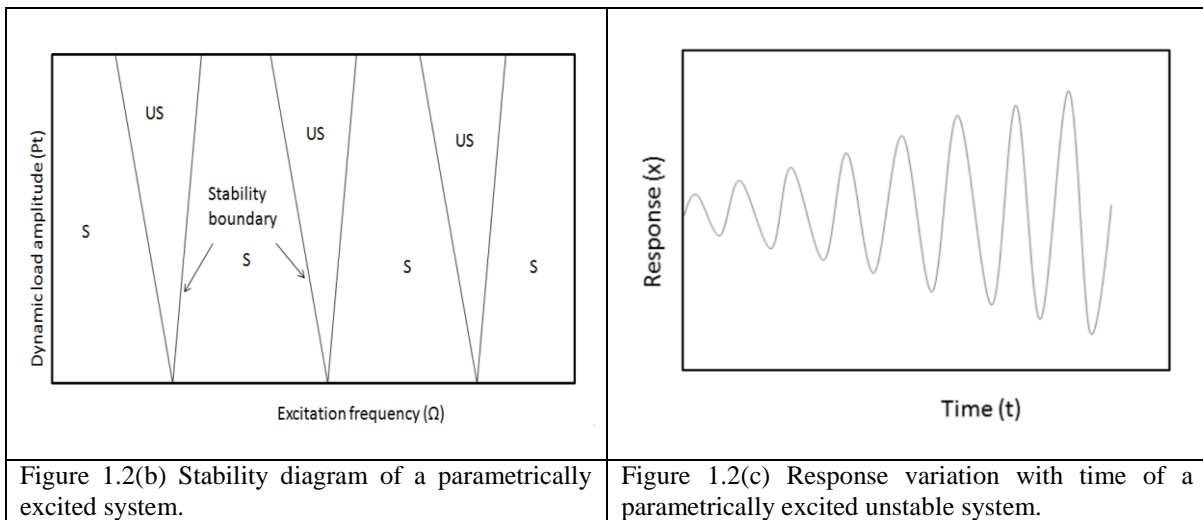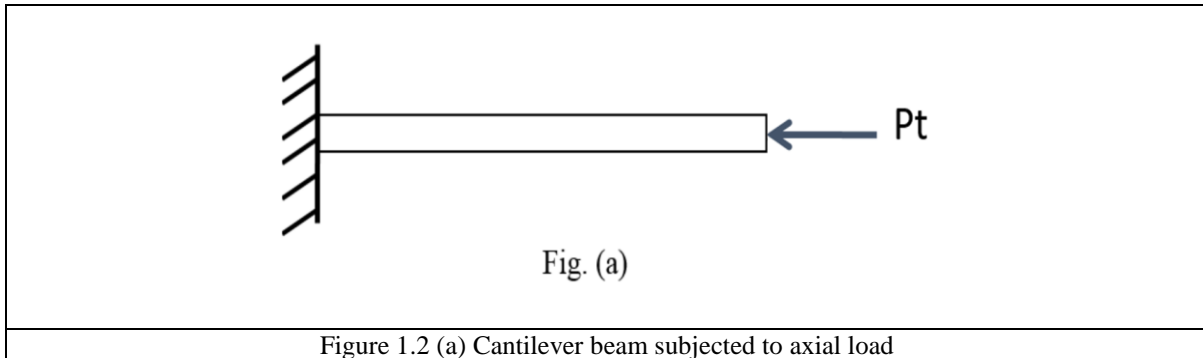
The system can experience parametric instability (resonance), when the excitation frequency or any integer multiple of it, is twice the natural frequency, that is to say

$$m\Omega = 2\omega_n$$

where m=1, 2, 3 … n. and ω_n natural frequency of the system.

The case $\Omega = 2\omega_n$ is known as to be the most significant in application and is called main parametric resonance.

Main objective of analysis of parametrically excited system is to establish the regions in the parameter space in which the system becomes unstable. These areas are known as regions of dynamic instability. The boundary separating a stable region from an unstable one is called a stability boundary. These boundaries drawn in the parameter space i.e. dynamic load amplitude, excitation frequency and static load component is called a stability diagram. Figure 1.2(b) shows a typical dynamic stability diagram. Parametrically excited unstable system's

response variation with time is as shown in figure 1. 2(c). The dynamic load component is the time dependent component of the axial force. It can be seen from the figure 1.2 (b) that the instability of the system doesn't occur at a single excitation frequency rather occurs over a range of frequency which makes the parametrically excited systems more dangerous than ordinary resonant systems. In addition, as the amplitude of the time dependent component of the axial force increases, the range of frequency over which the system becomes unstable increases. The location of the unstable region closer to the dynamic load axis indicates that the system is more liable to dynamic instability, as the instability occurs at lower excitation frequencies. In contrast, if the unstable region is located farther from the dynamic load axis, it indicates that the system is less prone to dynamic instability. If the area of the instability region is large, it indicates instability over a wider frequency range. If the instability region shifts towards the dynamic load axis or there is an increase in its area, the instability of the system is said to be enhanced and when contrary to it happens, the stability is said to be improved.

Structural components like plates are subjected to periodic loads under different environmental and operating conditions and this may lead to their parametric resonance. These members may have different boundary conditions depending upon their applications. The parametric resonance may cause the loss of functionality of plate structures. One of the controlling method of parametric resonance is by changing mass/stiffness. To reduce or prevent the structural vibration, the designer has to choose better materials with suitable mass/stiffness. Alloys and composite materials having high strength to weight ratio have been produced due to advancement in material science technology. Laminated composite materials have been successfully used in many engineering applications such as aircraft, marine and automotive industries. These are of lightweight and high strength. However, large inter-laminar stresses are developed due to the mismatch of two different materials properties across the interface. Particularly in high temperature environments, debonding and delamination problems occur in composite materials. In the materials, a group of metals have high strength and toughness, while the ceramics are good in thermal resistance. Hence, to improve the thermal resistance, ceramics can be used to mix with metals in order to combine their specific advantages.

Functionally Graded Materials (FGM) have successfully replaced the debonding and delamination problems of composite materials due to their gradual variation of properties. FGMs are microscopically heterogeneous advanced composites usually made from a mixture of metals and ceramics, mixture properties vary smoothly from one surface to the other. The gradual properties change is not observed in traditional composite materials. Our ability to

fabricate FGMs appears to be a modern engineering innovation, though FGM is not a new concept. These type of materials also occur in nature. Some examples for natural FGMs have been shown in figure 1.3. Bamboo and bones have functional grading. Even our skin is also graded to provide certain toughness, tactile and elastic qualities as a function of skin depth and location on the body.

The concept of FGM was first introduced in Japan in 1984 during a space plane project, where a combination of materials used would serve the purpose of a thermal barrier capable of withstanding a surface temperature of $2000K$ and a temperature gradient of $1000K$ across a 10 mm deep section. In recent years, its applications have been extended also to the structural components of solar energy generators, chemical plants, high efficiency combustion and heat exchangers. In the literature two types of gradation laws have been used for mathematical formulation of FGMs for structural analysis. One is exponential law, in which studies concentrate on fracture mechanics and another simple power law, it covers the stress analysis of FGM structural components.

Figure 1.3(a) Natural FGMs (a & b) bamboo tree (c) human bone
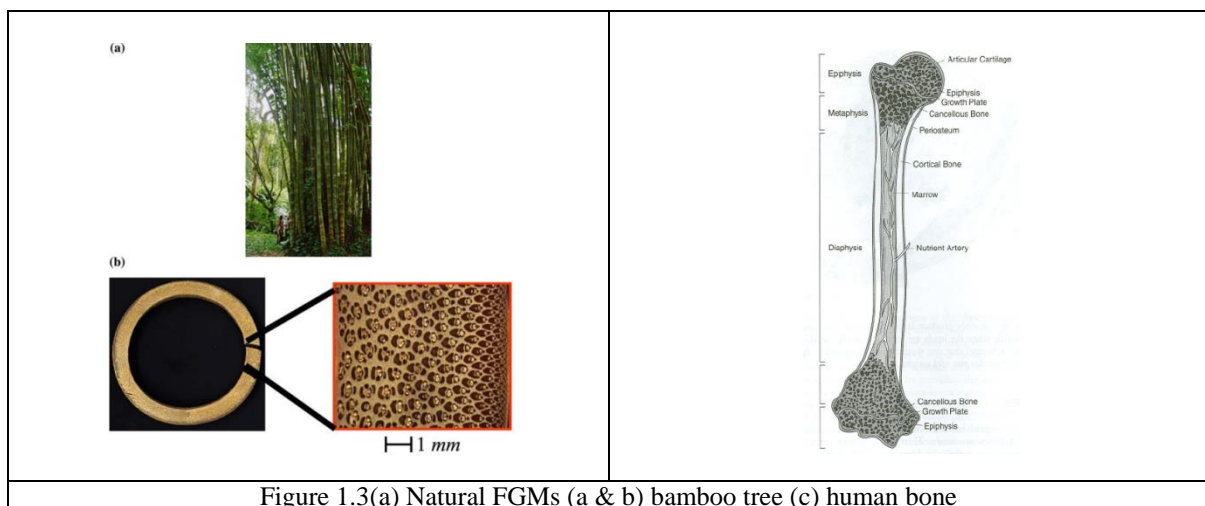
FGM structures are designed in such way as to overcome the demerits of ordinary materials. These materials have many advantages such as high resistance to temperature gradients, high wear resistance, reduction in residual and thermal stresses and an increase in strength to weight ratio. Because of these inherent properties, structure's stability also increases. An example of use of FGMs is re-entry vehicle in space. The FGMs can be used to produce the shuttle structures. When the space shuttle reenters in to atmosphere of the earth, heat source is generated by the air friction of high velocity movement. If the structures of the space shuttles are made from FGMs, the hot air flow is blocked by the outside surface of ceramic and transfers slightly into the lower surface. Consequently, the temperature at the lower surface is much reduced, which therefore avoids or reduces structural damage due to

thermal stresses and thermal shock. Due to the outstanding properties of FGMs they are used in many engineering applications such as aerospace, aircraft, defense, space shuttle, gas turbine blades, rocket engine parts, biomedical and electronic industries. In future the availability and production cost of FGMs may be cheap, so that they can be used in helicopter rotor blades, turbo machinery parts and automobile parts etc.

Importance of the present study

Many structural components can be modelled as plate like structures. These structures are often subjected to dynamic loads, among which the periodic in-plane force may cause dynamic instability, in which case there is an unbounded exponential built up of the response. It is of enormous practical importance to understand the dynamic stability of systems under periodic loads. Therefore, a broad understanding of the dynamic stability characteristics of structural materials in periodic loading environments is a matter of importance for the design against structural failure.

1.2 Research objective

The extensive use of FGM plates has generated considerable interests among many researchers working in the field of modelling, analysis and design. Accurate prediction of structural response characteristics is a demanding problem for the analysis of FGM, due to the anisotropic structural behavior and the presence of various types of complicated constituents. This is because the material composition of an FGM changes gradually, usually varying through the thickness. The present investigation mainly focuses on the study of vibration, buckling and dynamic stability of FGM plates under parametric excitation. A third order shear deformation theory based finite element model is formulated for studying the buckling, free vibration and dynamic instability characteristics of FGM plates in different environments and operating conditions. The effect of various environment and operating condition parameters such as index value, temperature rise, foundation stiffness, rotational speed, skew angle and dynamic load factor on vibration and dynamic stability behavior of FGM plates are examined numerically. Comprehensive literature survey uncovers that vibration and dynamic stability of FGM structures have been investigated to some extent. In this course, the present work on the investigation of dynamic stability of FGM plates is to contribute towards improved understanding of parametric resonance phenomenon. Moreover, for predictable applications of FGM structures, reliable analysis and results are required and hence in the present work an appropriate finite element based mathematical modelling of FGM plates has been attempted.

Depending on these guiding concepts, the objectives of present analyses are as follows:

- ✓ Study on the effect of power law property distribution on critical buckling load, natural frequencies and dynamic stability of FGM plates.
- ✓ Investigation in to the effect of power law property distribution and temperature rise on the buckling load, natural frequencies and dynamic instability of FGM plates in the thermal environment.
- ✓ Investigation in to the effect of power law property distribution, foundation properties and temperature environment on the critical buckling load, natural frequencies and dynamic instability of FGM plate supported on foundation.
- ✓ Study of the effect of power law property distribution, temperature rise and moisture concentration on the critical buckling load, natural frequencies and dynamic instability of FGM plates in hygrothermal environment.
- ✓ Investigation of the effect of power law property distribution, rotating speed, and hub radius on the natural frequencies, critical buckling load and parametric instability of rotating FGM plates in high temperature fields.
- ✓ Study on the effect of power law property distribution and skew angle on critical buckling load, natural frequencies and dynamic instability of skew FGM plates in high temperature thermal environment.

1.3 Outline of the present work

The present thesis is composed of eight main chapters including this section.

- ✓ Chapter 2: Literature review

  A detailed survey of the literature, pertinent to the previous works done in this field has been reported. A critical discussion of the earlier investigations is done.
- ✓ Chapter 3: Dynamic stability of functionally graded material plates under parametric excitation.

  Formulation of the problem based on the third order shear deformation theory is described in detail. The plate is modeled using a four node finite element. Effect of different system and forcing parameters on buckling load, free vibration and dynamic stability of the plate is studied.
- ✓ Chapter 4: Dynamic stability of functionally graded material plates in high temperature thermal environment under parametric excitation.

This section presents the effect of temperature rise on vibration and dynamic stability of functionally graded material plates in uniform, linear and nonlinear thermal environments.

✓ Chapter 5: Dynamic stability of functionally graded material plates on elastic foundations under parametric excitation.

The effect of Winkler and Pasternak foundation parameters on vibration and dynamic stability of functionally graded material plates supported on elastic foundation is investigated.

✓ Chapter 6: Dynamic stability of functionally graded material plates in hygrothermal environment under parametric excitation.

The influence of temperature and moisture concentration rise on vibration and dynamic stability of functionally graded material plates in hygrothermal environment is presented in detail.

✓ Chapter 7: Dynamic stability of rotating functionally graded material plate under parametric excitation.

The effect of the hub radius and rotational speed on vibration and dynamic stability of functionally graded material plates in high temperature environment is explained in detail.

✓ Chapter 8: Dynamic stability of skew functionally graded plates under parametric excitation.

The influence of skew angle on vibration and dynamic stability of functionally graded material plates in thermal environments is investigated.

✓ Chapter 9: Conclusion and scope for future work.

The conclusions drawn from the above studies are described. There is also a brief note on the scope for further investigation in this field.

1.4 Closure

Present section gives a sustenance to thought about functionally graded material suitable for various applications.

✓ A material advantageous over composite materials and having tailored properties.
✓ A material appropriate for application in extreme working circumstances.
✓ A material having enhanced residual stress distribution.
✓ A material, the characteristics of constituent phases of which can be completely used without any compromise.

The above features offer the scope for various prospective applications. To have a knowledge of the static and dynamic behavior of these FGM plates, research objectives are presented here. The next chapter presents an extensive literature review on the proposed field of research.

Chapter 2
REVIEW OF LITERATURE

2.1 Introduction

The phenomenon of parametric resonance was discovered way back in the year 1831. Faraday [39] was one of the first scientists to study the parametric resonance phenomenon when he observed that surface waves in a fluid-filled cylinder under vertical excitation showed half the frequency of the container. Melde [120] was the first to observe the phenomenon of parametric resonance in structural dynamics. He found that the string could oscillate latterly although the excitation force was longitudinal, at twice the natural frequency of the fork, under a number of critical conditions. Lord Rayleigh [192-194] provided a theoretical basis for understanding the parametric resonance of strings and conducted several experiments. Beliaev [11] studied the response of a straight elastic hinged-hinged column subjected to periodic axial load. Alexanderson [5] was the first to investigate the use of parametric amplifiers for radio telephony from Berlin to Vienna and Moscow.

A number of review articles on the parametric resonance have been reported. Evan – Iwanowski [37], Ibrahim and co-workers [67-73], Ariarathnam [7] and Simitses [185] presented a review of researches on vibration and stability of parametrically excited systems. Furthermore, books by Bolotin [14], Schmidt [173] and Nayfeh and Mook [131] deal comprehensively with the basic theory of dynamic stability of systems under parametric excitations. Thorough review work on FGM about its various aspects like stress, stability, manufacturing and design, applications, testing, and fracture has been presented by Victor and Larry and his co-workers[209]. A critical review on free, forced vibration analysis and

dynamic stability of ordinary and functionally grade material plates was reported by Ramu and Mohanty [153]. Review of the thermo-elastic and vibration analyses of functionally graded plates with an emphasis on the recent works published since 1998 were discussed by Jha et al. [78]. Their review carried out was concerned with deformation, stress, vibration and stability problems of FG plates.

2.2 Types of Parametric Resonance

Simple resonance, the resonance of sum type or resonance of difference type may be exhibited for a system with multi-degrees of freedom depending upon the type of loading, support conditions and system parameters.

Classification of different types of resonances exhibited by a linear periodic system was presented by Melde [120]. Iwatsubo et al. [75] and [76] investigated the stability of uniform columns with simply supported ends and concluded that combination type resonance would not occur for this system. Saito and Otomi [169] from their investigation on stability of viscoelastic beams with viscoelastic support showed that this system did not exhibit combination resonances of difference type for axial loading, but those did exhibit the above-mentioned resonance for tangential type of loading. Celep [22] on the basis of his investigation on stability of simply supported pre-twisted column found that combination resonances of the sum type may exist or disappear depending on the pre-twist angle and rigidity ratio of the cross-section. Elastic shaft with a disk can exhibit only difference type combination resonances was showed by Ishida et al. [74]. Chen and Ku [24] investigated the effect of the gyroscopic moment on the principal region of instability of a cantilever shaft disk system.

2.3 Methods of Stability Analysis of Parametrically Excited Systems

Parametrically excited system's governing equations are represented by second order differential equation with periodic coefficients. The exact solutions are not available for parametrically excited systems. The researchers for a long time have been involved to explore different solution methods for this kind of problem. The objectives of these kind of investigators are to establish the existence of periodic solutions and their stability. A number of methods have been applied for the solutions of the governing equations of parametrically excited systems. The most common among them are method proposed by Bolotin based on Floquet's theory, the Galerkin's method, perturbation and iteration techniques, the Lyapunov second method and the asymptotic technique by Krylov, Bogoliubov and Mitroploskii.

Satisfactory results can be obtained for simple resonance case using Bolotin [14] method based on Floquet's theory. Burney and Jaeger [20] have used this method to determine the region of the dynamic instability of a uniform column for different end conditions. They assumed the column to be consisting of different segments, each segment being considered as a massless spring with lumped masses. Piovan and Machado [147] used the method to determine the dynamic instability regions of a functionally graded thin-walled beam subjected to heat conduction. Machado et al. [107] have also used the Bolotin's method for studying the parametric instability of a thin-walled composite beam. This method has been modified by Stevens [190] for a system with complex differential equations of motion. Hsu [58] and [59] proposed an approximate method of stability analysis of systems having small parameter excitations. Hsu's method can be used to obtain instability zones of main, combination and difference types. Later Saito and Otomi [169] modified Hsu's method to suit systems with complex differential equations of motion. Takahashi [197] has proposed a method free from the limitations of small parameter assumption. This technique establishes both the simple and combination type instability zones. Lau et al. [96] proposed a variable parameter increment method, which is free from limitations of small excitation parameters. It has the advantage of treating non-linear systems.

Several investigators, to study the parametric instability of elastic systems have used finite element method (FEM). Brown et al. [18] investigated the dynamic stability of uniform bars by using this method. Abbas and Thomas [1] studied the dynamic stability of beams by using finite element method for different end conditions. Shastry and Rao [179] and [180] used finite element method to plot the stability boundaries of a cantilever column acted upon by an intermediate periodic load at different positions. The parametric instability behaviour of a non-prismatic bar with localized zone of damage and supported on an elastic foundation was studied by Dutta and Nagraj [34] using finite element analysis. Öztürk and Sabuncu [139] used finite element method to study the dynamic stability of beams on elastic supports. Mohanty [123] have used this method to study the effect of localised damage on the dynamic stability of beams. Mohanty et al. [124], [125] have investigated the static and dynamic behaviour of functionally graded Timoshenko beams using this method also. Ramu and Mohanty [154], [155] studied the buckling and free vibration analysis of functionally graded material thin plates using finite element method. Lucia and Paolo [94] developed finite element method for static analysis of functionally graded Reissner–Mindlin plate. Briseghella et al. [17] studied the dynamic stability of elastic structures like beams and frames using finite element method.

Kugler et al. [88] proposed an efficient low order shell finite element with six degrees of freedom per node. They established its effectiveness and accuracy through numerical calculations.

Patel et al. [143] employed the method of the finite element to study the influence of foundation parameters on the dynamic instability of layered anisotropic composite plates. Myung-Hyun and Sang-Youl [128] have used finite element method to study the dynamic stability of delaminated composite skew plates under combined static and dynamic loads based on higher-order shear deformation theory. Desai et al. [32] used a layer-wise mixed finite element model for the free vibration analysis of multi-layered thick composite plates. Young et al. [230] studied the dynamic stability of skew plates subjected to an aerodynamic force in the chordwise direction and a random in-plane force in the spanwise direction using finite element analysis.

2.4.1 Different shear deformation theories

FGMs are made of ceramic and metal in such a way that the ceramic can resist the thermal loading in the high-temperature environment. The material properties of FGMs vary continuously from one surface to the other surface and this results in eliminating surface problems of composite materials in achieving the smooth stress distribution. Theoretical modelling and analysis of FGM plates has become an important topic of discussion at the present stage. Static analysis of functionally graded plate using higher-order shear deformation theory was performed by Mantari et al. [114]. Gulshan Taj et al. [45] assumed transverse shear stresses variation as quadratic through thickness and therefore, no need of shear correction factor. Xiang and Kang [217] analyzed the static response of FG plates based on various higher order shear deformation theories. Beena and Parvathy [9] proposed spline finite strip method for static analysis of FG plates. The static response of functionally graded plates was presented by Belabed et al. [10] using an efficient and simple higher order shear and normal deformation theory. The concept of the neutral surface for the FGM plates was proposed by Da-Guang and You-He [30].

Free vibration analysis of FGM rectangular plates has been numerically performed by number of researchers. Theoretical formulation and finite element models for functionally graded plates based on the third-order shear deformation theory was presented by Reddy [163]. The finite element model accounts for the thermo-mechanical coupling and geometric non-linearity. Zhao et al. [236] have studied the free vibration of FGPs with arbitrary boundary

conditions using the element free kp-Ritz method. In their analysis, a mesh-free kernel particle functions were used to approximate the two-dimensional displacement fields. Refined two-dimensional shear deformation theory was investigated by Fares et al. [40] for orthotropic FG plates. For obtaining this theory, a modified version of the mixed variational principle of Reissner was used. This approach does not require any shear correction factor. An exact analytical solution was developed by Hasani and Saidi [50] for free vibration analysis of thin FG rectangular plates by using the classical plate theory. In their study the effects of inplane displacement on the vibration of FG rectangular plates were studied and also a closed-form solution for finding the natural frequencies of FG simply supported rectangular plates was presented. A 2-D higher order theory was developed by Matsunaga [117] for analyzing natural frequencies and buckling stresses of FG plates. They used Hamilton's principle for the dynamic analysis of a rectangular functionally graded plate with two-dimensional higher-order theory. A finite element method (FEM) of B-spline wavelet on the interval (BSWI) was used to solve the free vibration and buckling analysis of plates by Zhibo Yang et al. [237]. In their analysis BSWI functions were considered for structural analysis, the proposed method used to obtain a faster convergence and a satisfying numerical accuracy with seven degrees of freedom. Senthil and Batra [175] investigated an exact solution for the vibration of simply supported rectangular thick plate. They assumed that the plate was made of an isotropic material with material properties varying in the thickness direction only.

In the last few decades, researchers have been investigating the vibration of FGM plates. Nguyen et al. [134] modeled functionally graded material plates based on first-order shear deformation theory. Hosseini-Hashemi et al. [56] proposed a new exact closedform approach for free vibration analysis of thick rectangular FG plates based on the third-order shear deformation theory of Reddy [165]. In their study, Hamilton's principle was used to extract the equations of dynamic equilibrium and natural boundary conditions of the plate. Ferreira et al. [42] introduced a meshless method for free vibration analysis of functionally graded plates with multi-quadric radial basis functions to approximate the trial solution. Suresh Kumar et al. [195] presented the free vibration analysis of functionally graded material plates without enforcing zero transverse shear stress conditions on the top and bottom surfaces of the plate using higher-order displacement model. Hosseini et al. [57] investigated the free vibration analysis of functionally graded rectangular plates by considering the first-order shear deformation plate theory.

Khorramabadi et al. [84] have proposed an analytical approach for the free vibration behaviour analysis of simply supported functionally graded plates by using the first-order and third-order shear deformation theories. Rastgoftar et al. [159] have proposed a solution for the boundary stabilization of an FGM plate in free transverse vibration. Li and Zhang [100] have investigated the extended Melnikov method for the global dynamics of a simply supported functionally graded materials rectangular plate. In their analysis, the transvers and in-plane excitations are considered and the properties are assumed to be temperature-dependent. The Hamilton's principle and the Galerkin's method were used to derive the governing equation of motion of the FGM rectangular plate with two degrees of freedom. Zhu and Liew [240] have investigated a Kriging meshless method for free vibration analysis of metal and ceramic functionally graded plates. The Kriging technique developed to construct shape functions can be derived from Kronecker delta function property and thus make it easy to implement the essential boundary conditions. Jha et al. [80] studied the free vibration of FGM plates with higher order and normal shear deformation theories. Wu and Li [216] developed a finite prism method based on the Reissner's mixed variational theorem for the three-dimensional free vibrational analysis of functionally graded carbon nanotube-reinforced composite plates with different boundary conditions. Shariat et al. [177] derived the equilibrium, stability and compatibility equations of an imperfect functionally graded plates using classical plate theory. Bouazza et al. [16] approached analytically for stability analysis of thick functionally graded plates. They assumed first order shear deformation theory for deriving stability and equilibrium equations.

Hossein et al. [54] have developed a solution for large deflection free transverse vibration of FGM plates for boundary stabilization. Fourth order nonlinear partial differential equations are used for dynamic analysis of FGM plates. Singh and Kari [186] have carried out vibration analysis of the functionally graded material plates and shells using semiloof shell element with nonlinear formulation. Singha and Prakash [187] have outlined the nonlinear characteristics of functionally graded plates when subjected to transverse distributed load. In their analysis, they considered the material properties of the plate varying in the thickness direction according to a simple power-law distribution in terms of volume fractions of the constituents. Hashemi et al. [51] have developed a new analytical approximation method for free vibration analysis of moderately thick rectangular plates with two opposite edges simply supported by using Reissner–Mindlin plate theory.

Abrate [3] has calculated proportionality constant for the natural frequencies of functionally graded plates and compared with homogeneous isotropic plates. He also studied the free vibrations, buckling, and static deflection of functionally graded plates in which material properties vary along the thickness. Altay and Dokmeci [6] have developed a unified variational principle from a differential form, which is expressed in variational in the three-dimensional fundamental equations. Hashemi et al. [56] presented a new exact closedform solution for the vibration analysis of FG rectangular plates based on the Reddy's [165] third-order shear deformation plate theory. Neves et al. [132] have used an original hyperbolic sine shear deformation theory for the bending and free vibration analysis of functionally graded plates. Jha et al. [80] performed the free vibration analysis of functionally graded thick plates by using higher order shear/shear-normal deformation theories. Huu-Tai and Dong [66] presented the bending and free vibration analysis of FG plates by a simple first order shear deformation theory. Free vibration analysis of arbitrarily thick functionally graded rectangular plates with general boundary conditions was given by Guoyong et al. [47] by using three-dimensional elasticity theory. Efraim and Eisenberger [35] presented the free vibration analysis of annular FGM plates.

Bodaghi and Saidi [13] have studied a new analytical approach for buckling analysis of thick functionally graded rectangular plates. Higher-order shear deformation plate theory was adopted for equilibrium and stability equations derivation. Boundary layer functions of two uncoupled partial differential equations in terms of transverse displacement are derived from the coupled governing stability equations of the functionally graded plate. Mechanical and thermal buckling analysis of thick functionally graded plates with closed form solution was reported by Samsam and Eslami [170]. Latifi et al. [95] investigated the buckling of rectangular FG plates subjected to biaxial compression loadings with different boundary conditions using Fourier series expansion. Buckling behaviour of simply supported functionally graded material plates under constant and linearly varying periodic loads was investigated by Rohit and Maiti [164]. The effect of shear deformation was studied using higher order shear deformation theory and first order shear deformation theory for the case of uniform compression loading. They concluded that the influence of transverse shear on buckling loads was almost similar for all types of FGMs. Xinwei et al. [219] solved the critical buckling problem of thin rectangular plates with cosinedistributed load along the two opposite plate edges. This analysis requires first the plane elasticity problem to be solved to obtain the distribution of inplane stresses and then the buckling problem. Mokhtar et al. [126] investigated the buckling of rectangular thin

functionally graded plates under uniaxial and biaxial compression by using classical plate theory and Navier's solution. Buckling of functionally graded material plates was studied by Choi [27]; Sidda Reddy et al. [184]. To account for the transverse shear deformation effects, Thai et al. [206] employed a refined shear deformation theory for bending, buckling and vibration analysis of FG plates resting on elastic foundation.

2.4.2 Effect of thermal environment

Most of the researchers have dealt with free, forced vibration and buckling analysis of FGM plates with temperature-independent properties by using different theories. Due to the increased applicability of functionally graded materials in the diversified field, it is important to find out the vibration characteristics of functionally graded plates in thermal environments. Praveen and Reddy [148] found non-linear static and dynamic response of functionally graded ceramic- metal plates in a steady temperature environment and subjected to lateral dynamic loads by using finite element method. Reddy and Chin [163] have investigated a wide range of problems on FGM cylinders and plates including thermo-mechanical coupling effects, among which transient response of the plate due to heat flux was discussed. Yang and Shen [225] explained the vibration characteristics and transient response of FGM plates made of temperature dependent materials in thermal environments considering shear deformation. Huang and Shen [65] studied the nonlinear vibration and dynamic response of functionally graded material plates in thermal environments. For this analysis, the steady state heat conduction and temperature dependent material properties were assumed. Li et al. [99] have studied the free vibration analysis of functionally graded material rectangular plates in the thermal environment. The formulation was based on the three-dimensional linear theory of elasticity.

Talha and Singh [201] developed a higher-order shear deformation theory and it provides additional freedom to the displacements through the thickness and thus eliminates the over prediction. Bouazza et al. [15] have studied buckling of FGM plate under thermal loads. Two types of thermal loads namely; uniform temperature rise and linear temperature rise through the thickness were assumed in this analysis. Talha and Singh [199] presented the thermo-mechanical buckling behaviour of FGM plate using higher order shear deformation theory. The proposed structural kinematics assumed cubically varying in-plane displacement and quadratically varying transverse displacement through the thickness. Maziar and Amian [119] studied the free vibration of functionally graded non uniform straight-sided plates with circular and non-circular cut outs. Moreover, thermal effects on free vibration and the effects

of various parameters on natural frequencies of these plates were evaluated. Matsunaga [117] studied the thermal buckling of FG plates with 2D higher-order shear deformation theory. Nuttawit et al. [137] applied an improved third-order shear deformation theory for free and forced vibration response study of functionally graded plates. For this analysis, both temperature independent and dependent materials were considered. Leetsch at al. [98] studied the 3D thermo-mechanical behavior of functionally graded plates subjected to transverse thermal loads by a series of 2D finite plate elements. Shahrjerdi et al. [176] demonstrated the analytical solution for the free vibration characteristics of solar functionally graded plates under temperature field, using second order shear deformation theory. Yang-Wann [232] found the analytical solution for the vibration characteristics of FGM plates under temperature field. The frequency equation was obtained using the Rayleigh–Ritz method based on the third-order shear deformation plate theory. Malekzadeh et al. [112] have investigated the free vibration of functionally graded (FG) thick annular plates subjected to the thermal environment using 3D elasticity theory.

2.4.3 Effect of foundation

Extensive studies about plates on elastic foundation can be found in the literature. These studies were carried out by means of both numerical and analytical approaches. Many of these studies were based on classical plate theory namely by Chucheepsakul and Chinnaboon [28], Civalek [29], first-order shear deformation theory by Qin [149], Eratll and Akiiz [38], Liew et al. [101], Han and Liew [48], Shen et al. [182], Xiang [218], Abdalla and Ibrahim [2], Buczkowski and Torbacki [19], Ozgan and Daloglu [138], Ferreira et al. [43], Liu [106], and higher-order shear deformation theory by Thai and Choi [203], [204], Zenkour [235].

Different methods used for free vibration analysis of rectangular plates resting on elastic foundation are available in the literature. Huang and Thambiratnam [63] proposed the finite strip method for static, free vibration and critical buckling analysis of plate resting on elastic foundation. They simulated the spring system as elastic support with different boundary conditions. Thai and Kim [205] investigated a simple refined theory for bending, buckling and vibration study of thick plate resting on elastic foundation. This theory is based on the assumption that in-plane and transverse displacements consist of bending and shear components in which the bending components do not contribute towards shear forces and similarly, the shear components do not contribute toward bending moments. The most interesting feature of simple refined theory is that it contains two unknowns as against three in the case of other shear deformation theories. Hasani et al. [49] developed an analytical method

for free vibration analysis of FG plate resting on two parameter elastic foundation. They used boundary layer function for decoupling the governing equations and solved for the levy type boundary conditions. Dehghan and Baradaran [33] proposed a coupled FE-DQ method for 3-D analysis of thick rectangular plates resting on elastic foundations with various boundary conditions. This method benefits the ability of FEM in modeling of complicated geometry and at the same time gains the simplicity and accuracy of DQM.

An outstanding work on the free vibration analysis of Mindlin plate resting on Pasternak elastic foundation with different boundary conditions was carried out by Akhavan et al. [4]. Exact solutions have been obtained for all possible combinations of boundary conditions along the edges in the presence of in-plane loading. Yas and Aragh [227] used the differential quadrature method to study the free vibration of continuous grading fiber reinforced plates rested on elastic foundations. Jahromi et al. [77] studied the free vibration of Mindlin plates partially resting on elastic foundation by generalized differential quadrature method. Sharma et al. [178] presented the free vibration analysis of moderately thick antisymmetric cross-ply laminated rectangular plates with elastic edge constraints using differential quadrature Method. Yaghoobi and Fereidoon [221] analyzed both the mechanical and thermal buckling of FGM plates resting on elastic foundation with simply supported boundary conditions by an assessment of a simple refined n^{th}-order shear deformation theory. Yang et al. [226] investigated the reciprocal theorem method for the theoretical solutions of rectangular plates supported on the elastic foundation with free edges.

Hosseini et al. [56] have carried out analytical solutions for free vibration analysis of moderately thick rectangular plates, which were collection of functionally graded materials and supported by either Pasternak or Winkler elastic foundations. These rectangular plates had two opposite edges simply supported, whereas all possible combinations of free, simply supported and clamped boundary conditions were applied to the other two edges. Rashed et al. [157] presented the boundary element method for a Reissner plate on a Pasternak foundation. Chinnaboon et al. [26] developed a BEM-based meshless method for the analysis of plates on a biparametric elastic foundation, in addition to the boundary supports. Zenkour et al. [234] investigated the bending response of an orthotropic rectangular plate resting on two-parameter elastic foundation. Nobakhti and Aghdam [135] studied the bending of a moderately thick plate resting on the elastic foundation by using generalized differential quadrature (GDQ) method. They assumed that the plate was resting on two-parameter elastic (Pasternak) foundation or strips with a finite width. Malekzadeh [111] used three-dimensional elasticity theory to study

the free vibration analysis of FG plates resting on two parameter elastic foundation with different boundary conditions. Sheikholeslami and Saidi [181] analyzed the free vibration of FG plates resting on the elastic foundation using higher-order shear and normal deformable plate theory. Bahmyari and Khedmati [8] proposed a shear deformable plate theory in combination with Element-Free Galerkin Method (EFGM) for vibration analysis of nonhomogeneous moderately thick plates with point supports, resting on Pasternak elastic foundation. Hsu [60] developed a new version of differential quadrature method for free vibration analysis of rectangular plates resting on elastic foundations and carrying any number of spring masses. Mantari et al. [116] studied the free vibration of functionally graded plates resting on elastic foundation.

Geoige and Voyiadjis [46] investigated the refined theory for bending of moderately thick plates on elastic foundations. This method included the transverse normal strain effect in addition to the transverse shear and normal stress effects. The bending problem of rectangular plates with free edges on elastic foundations using Galerkin's variational method was presented by Cheng Xiang-sheng [25]. Ramesh and Sekhar [158] studied the behavior of flexible rectangular plates resting on tensionless elastic foundations by finite-element method (FEM). Conical exact solutions using Green's functions approach was presented by Lam et al. [93] to study the bending, buckling and vibration analysis of Levy-plates on two-parameter elastic foundations.

Shen et al. [182] have presented free and forced vibration analysis of Reissner-Mindlin plates with four free edges resting on a Pasternak-type elastic foundation. Their approach was based on the Reissner-Mindlin first order shear deformation theory. Özdemir [139] developed a new fourth order finite element for thick plates resting on a Winkler foundation and the element was free from shear locking problem. This new fourth order finite element gave excellent results for static and dynamic analyses. Kumar [90] studied a differential transform method (DTM) for the free transverse vibration of isotropic rectangular plates resting on a Winkler foundation. An exact solution for free vibration analysis of simply supported rectangular plates on the elastic foundation has been presented by Dehghany and Farajpour [33] employing the three-dimensional elasticity theory. Seyedemad et al. [172] adopted a novel mathematical approach for study of free vibration of thin rectangular plates on Winkler and Pasternak elastic foundation. The closed form solutions were developed for solving the governing differential equations of plates.

2.4.4 Effect of hygrothermal environment

Parhi et al. [144] studied the effect of hygrothermal environment on free vibration and transient response of multiple delaminated composite plates and shells. They used finite element method based on the first order shear deformation theory for calculating the fundamental frequency of composite plates under temperature and moisture effect. Mahato and Maiti [109] have studied the capabilities of active fiber composite to control the undesirable response due to hygrothermal effect. The effect of delamination on the natural frequencies of delaminated woven fiber composite plates in the hygrothermal environment was studied by Panda et al. [141] numerically as well as experimentally. Nayak et al. [130] studied the influence of environment on the free vibration of laminated composite plates with experimental investigation, using frequency response function spectrum and coherences techniques. Rajesh and patil [151] have analyzed the hygrothermally induced free vibration of laminated composite plates with random material properties using higher-order shear deformation theory. Mahapatra et al. [108] presented vibration characteristics of laminated flat panel subjected to hygrothermal environment based on higher order shear deformation theory. Lee and Kim [97] investigated the effect of hygrothermal environment on post-buckling behavior of FGM plates based on first order shear deformation theory and Von Karman strain displacement relations.

A few works in literature are available on free vibration, critical buckling and static instability of composite plates in temperature and moisture environment. Direct and straightforward method was used by Benkhedda et al. [12] to determine hygrothermal stresses produced in the polymer matrix composite plates with the variation of temperature and moisture. Patel et al. [146] proposed a higher-order theory to study the effect of moisture concentration and temperature distribution on deflection, buckling and natural frequency of composite laminates. The vibration characteristics of laminated composite plates under varying temperature and moisture was presented by Rath and Sahu [161]. Sai Ram and Sinha [168] studied the moisture and temperature effects on the static instability of laminated composite plates. Lal et al. [92] investigated the post buckling response of functionally graded materials plate based on higher order shear deformation theory using von-Karman nonlinear strain kinematics and nonlinear finite element method.

2.4.5 Effect of rotation

Some of the researcher's works on vibration analysis of rotating cantilever isotropic and composite plates are reflected here. Free vibration analysis of rotating composite pretwisted

cantilever plate was presented by Karmakar and Singh [81]. They developed a nine node three dimensional degenerated composite shell element for modal analysis of composite plate using finite element method. Yoo and Kim [229] derived the linear equation of motion for the flapwise bending vibration analysis of rotating plates. Vibration analysis of rotating composite plates was presented by Kim [85]. He considered the in-plane and bending motion coupling effects for deriving the explicit mass and stiffness matrices. The effect of geometric non linearity on free vibration analysis of thin isotropic plates was studied by Saha [166] using numerical methodology.

Sreenivasamurthy and Ramamurti [188] investigated the Coriolis effect on first bending and torsional frequencies of flat rotating low aspect ratio cantilever plates using finite element method. Wang et al. [210] studied on the effects of hub size, rotating speed and setting angle free vibration of rotating cantilever rectangular plates. Shiaut et al. [183] investigated the vibration and optimum design of a rotating laminated blade. They used optimality criterion method for optimum design of rotating laminate blade with multiple frequencies. The vibration analysis of rotating annular plates has been studied by Liu et al. [105] using finite element method. Karmakar and Sinha [82] investigated the failure of pretwisted rotating plates subjected to centre point transverse load using finite element method. Hu et al. [62] applied the principle of virtual work and the Rayleigh–Ritz method for the vibration analysis of rotating cantilever plate with pre-twist. Hashemi et al. [53] used finite element method to determine the natural frequencies of a rotating thick plate. Sun et al. [194] investigated the vibration behavior of a rotating blade with an arbitrary stagger angle and rotation speed. They derived the equations of motion using the Hamilton's principle, which are discretised by a novel application of the fast and efficient collocation method for rotating structures. Farhadi and Hosseini [41] studied the aeroelastic behavior of a supersonic rotating rectangular plate in the air medium. For modal analysis of the plate, the Mindlin first-order shear deformation plate theory along with Von Karman nonlinear terms were used. Kee and Kim [83] investigated the vibration of a rotating composite blade. Their analysis included the effect of centrifugal force and Coriolis acceleration for an initially twisted rotating shell structure. Carrera et al. [21] presented the free-vibrational analysis of rotating beam using Carrera Unified Formulation. CUF is a hierarchical formulation which offers a procedure to obtain refined structural theories that account for variable kinematic description.

The exact solution for vibration and buckling of non-uniform plates subjected to in-plane loads with time-dependent boundary condition was studied by Saeidifar and Ohadi [165].

The nonlinear flutter and thermal buckling behavior of a ceramic-metal functionally graded plate subjected to combined thermal and aerodynamic loads were studied by Tawfik [202] using nonlinear finite element method based on von Karman strain displacement relations. Hosseini et al. [56] proposed an exact closed form solution for free vibration analysis of moderately thick FG plates based on first order shear deformation theory. For extracting dynamic equilibrium equation, Hamiltonian principle was used. Zarrinzadeh et al. [233] studied the free vibration of rotating axially functionally graded tapered beam with different boundary conditions using finite element method. A two-node beam element was used in terms of basic displacement functions for this analysis.

2.4.6 Effect of skew angle

Existing literature show that a lot of studies have been carried out on the free vibration of isotropic skew plates. Liew and Han [102] presented the bending analysis of a simply supported, thick skew plate based on the first-order shear deformation Reissner/Mindlin plate theory. Nair and Durvasula [129] used variational Ritz method for solution of the free vibration problems of skew plates with different boundary conditions. This study was approached by using the variational method of Ritz, a double series of beam characteristic functions being used in an appropriate combination of different boundary conditions. Sathyamoorthy [171] using Hamilton's principle, developed the governing dynamic equations for skew plates and also presented numerical results. Mizusawa and Kajita [121] applied the spline finite method to analyze the vibration of skew plates with point supports. Rajamohan and Ramachandran [150] presented a new fundamental solution in oblique coordinates for the analysis of isotropic skew plates subjected to transverse loading. Wang [211] studied the buckling of skew fibre-reinforced composite laminates using B-spline Rayleigh-Ritz method based on first order shear deformation theory. Wang et al. [213] used a new version differential quadrature method for buckling of thin anisotropic rectangular and isotropic skew plates. Hu and Tzeng [61] studied the buckling of skew composite laminated plates subjected to uniaxial in-plane compressive forces. Differential quadrature large amplitude free vibration analysis of laminated skew plates was investigated by Malekzadeh [110]. Dey and Singha [145] considered composite skew plates to investigate the instability regions subjected to periodic inplane loads. Elastic buckling behavior of uniaxially loaded skew plates with openings was presented by Tahmasebi and Shanmugam [196]. Krishna and Palaninathan [87] employed a general high precision triangular plate bending finite element to study the free vibration of skew laminates. The frequencies were calculated for different skew angles of simply supported and clamped conditions.

Upadhyay and Shukla [208] presented the large deformation flexural response of composite laminated skew plates subjected to uniform transverse pressure. Muhammad and Singh [127] proposed an energy method using polynomial for the linear static analysis of skew plates with simply supported and clamped boundaries. They assumed first order shear deformation theory for analysis of skew plate. Ganapathi and Prakash [44] have analyzed the thermal buckling of simply supported functionally graded skew plates using first-order shear deformation theory in conjunction with the finite element approach. Zhou et al. [238] derived the three-dimensional elasticity solution for vibration analysis of cantilevered skew plates. Zhou and Zheng [239] employed the moving least square Ritz (MLS-Ritz) method to study the free vibration of skew plates. Skew plates with various combinations of edge support conditions were considered and good convergence and accuracy were demonstrated in their study. Liew et al. [102], [103] studied the vibration and buckling of thick skew plate using Mindlin shear deformation plate theory. Sengupta [174] studied the skew rhombic plates in transverse bending using a simple finite element method. Woo et al. [215] used integrals of Legendre polynomials on p-version finite element method to obtain the natural frequencies and mode shapes of skew plates with and without cut-outs. Eftekhari and Jafari [36] investigated the free vibration of rectangular and skew Mindlin plates with different boundary conditions by mixed finite element-differential quadrature method. Combination of these two methods are simpler than the case where either the FEM or DQM is individually applied to the problem. Xinwei et al. [220] applied the differential quadrature method (DQM) for an accurate free vibration analysis of skew plates. Pang-jo and Yun [142] developed the analytical solutions for skewed thick plates on elastic foundation. The free vibration of isotropic and laminated composite skew plates was studied by Srinivasa et al. [189] with the help of experimental and finite element methods. Lai et al. [91] have developed new discrete singular convolution-element method for free vibration analysis of skew plates using the first-order shear deformable plate theory. Recently, accurate vibration analysis of skew plates was done by using the new version of the differential quadrature method by Wang et al. [213].

2.5 Closure

This chapter delivers the understanding into various past developments in the area of structural dynamics, particularly of plates. For the sake of simplicity, it is divided into five main sections. In section 2.1, introduction and a review of the literature on parametric resonance are presented. Section 2.2 describes a brief classification of parametric resonance. Various methods used by several researchers for the analysis of dynamic stability are described in section 2.3. The section

2.4 is devoted to the findings regarding the effect of various system parameters on the vibration and stability of plates. The effect of spatial variation of properties on the static, free vibration, forced vibration and buckling behavior of FGM plates is discussed in section 2.4.1. The vibration and buckling of FGM plates in high thermal environments are presented in section 2.4.2. The section 2.4.3 presents an exhaustive review of the literature on vibration of isotropic and FGM plates on elastic foundation. The section 2.4.4 presents the literature review on the vibration and stability of composite plates in the hygrothermal environment. Vibration of rotating isotropic and composite plates are discussed in section 2.4.5. Section 2.4.6 describes the different aspects of dynamics of skew plates.

It is observed from the reported literature that a worthy of work have been done on the dynamic stability of structural components made of metals, alloys and composites. A review of the literature shows that a lot of work have been done on the free, forced vibration and buckling of FGM plates. Some works has been done on the dynamic stability of isotropic and composite plates. Very little work has been done on the dynamic stability of FGM plates. Therefore, it may be concluded in this section that dynamic stability study of FGM plates remains an open problem to be taken up.

Based on the review of the literature, the different problems identified for the present investigation are presented as follows.

- ✓ Vibration, buckling and parametric resonance characteristics of FGM plates.
- ✓ Vibration and parametric resonance characteristics of FGM plates in high thermal environments.
- ✓ Vibration, buckling and parametric resonance characteristics of FGM plates resting on elastic foundation.
- ✓ Vibration, buckling and parametric resonance characteristics of FGM plates in hygrothermal environments.
- ✓ Vibration, buckling and parametric resonance characteristics of rotating FGM plates in high temperature thermal environments.
- ✓ Vibration, buckling and parametric resonance characteristics of skew FGM plates in high temperature thermal environments.

The influence of various parameter such as index value, boundary conditions, aspect ratio, temperature rise, moisture concentration, foundation stiffness, rotational speed and skew angle on the parametric instability characteristics of FGM plates are studied numerically.

Chapter 3

DYNAMIC STABILITY OF FUNCTIONALLY GRADED MATERIAL PLATES UNDER PARAMETRIC EXCITATION

3.1 Introduction

In the past the stability analysis of functionally graded material plates have been dealt by some of the researchers. Kima and Kim [86] presented the dynamic stability analysis of a plate under a follower force by using the finite element method based on the Kirchhoff-Love plate theory and Mindlin plate theory. Tylikowski [207] studied the stability of functionally graded rectangular plate described by geometrically nonlinear partial differential equations using the direct Liapunov method. In their analysis an oscillating temperature caused generation of inplane time-dependent forces destabilizing plane state of the plate equilibrium. Ng et al. [133] investigated the parametric resonance or dynamic stability of functionally graded cylindrical shells under periodic axial loading, using Bolotin's first approximation. Chattopadhyay and Radu [23] investigated the dynamic instability of laminated composite plates subjected to dynamic loads using finite element method. Sahu and Datta [167] investigated the dynamic instability of isotropic, cross-ply and angle-ply laminated composite plates subjected to uniaxial harmonically varying in plane point or patch loads. Mohanty et al. [122] studied the parametric instability of delaminated composite plates under in-plane periodic loads. They assumed a first order shear deformation theory.

Structural components like plates made of FGMs are suitable to apply for aerospace structure applications, nuclear plants and semiconductor technology. The present work conducts the parametric instability study of functionally graded material plates under uniaxial and biaxial in plane time-varying pulsating force. Four node rectangular elements are used for

modelling the FGM plate using finite element method. Hamilton's principle is employed to establish the governing equation, which is a linear system of Mathieu–Hill type equation in matrix form, from which the boundaries of stable and unstable regions are determined by using Floquet's theory. Free vibration and static stability analyses are also discussed as parting problems. Numerical analysis are presented in both dimensionless parameters and graphical forms. The influences of various parameters on parametric instability of FGM plate are studied in detail.

3.2 Methodology

3.2.1 Formulation of the problem

The plate is of uniform rectangular cross-section having a length L, width W and thickness h. The plate is subjected to a pulsating in plane axial force $P(t)$ represented as

$$P(t) = P_s + P_t \cos\Omega t \tag{3.1}$$

where Ω is the excitation frequency of the dynamic load component, P_s is the static and P_t is the amplitude of the time dependent component of the load, respectively. A typical FGM plate subjected to uniaxial and biaxial in-plane dynamic loads is shown in figures. 3.1and 3.2 respectively.

| Figure 3.1 Plate under in-plane uniaxial periodic loads | Figure 3.2 Plate under in-plane biaxial periodic loads |
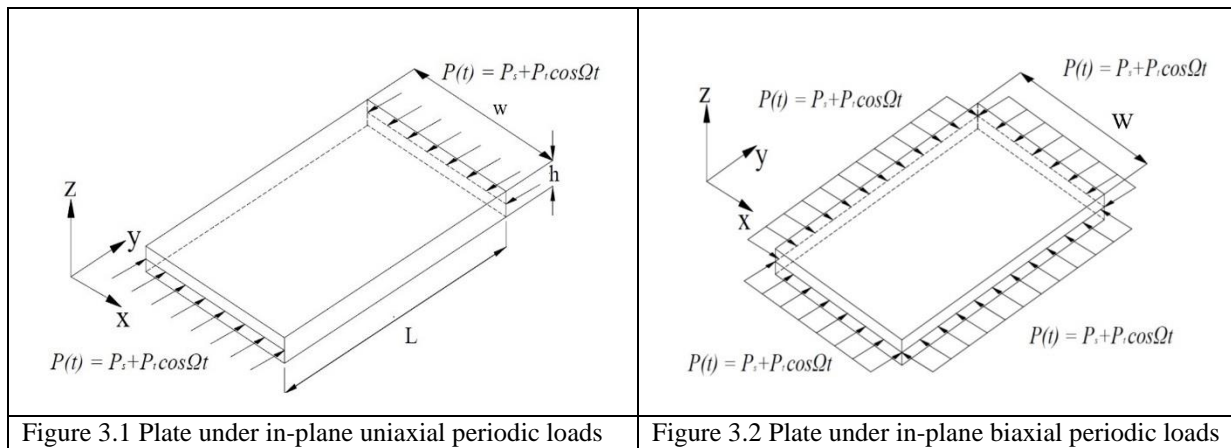
3.2.2The simple power law

The properties of functionally graded material plate is assumed to vary along the thickness. The properties $R\,(z)$ along the thickness of the functionally graded materials in terms of two constituent materials properties can be expressed as

$$R(z) = R_c(z)V_c(z) + R_m(z)V_m(z) \tag{3.2}$$

where $R(z)$ represents the effective material properties with two constituents. R_c and R_m are ceramic and metal properties, V_c and V_m are volume fraction of ceramic and metal constituents respectively.

The constituent volume fraction of ceramic V_c (z) and metal V_m (z) at any location z from mid-plane axis using rule of mixture is represented as

$$V_c(z) + V_m(z) = 1 \tag{3.3}$$

$V_c(z)$ is the volume fraction variation of the ceramic material and it is assumed to follow a simple power-law distribution as

$$V_c = \left(\frac{1}{2} + \frac{z}{h}\right)^k, 0 \leq k \leq \infty \tag{3.4}$$

where $-h/2 \leq z \leq h/2$ is the coordinate through the thickness from the middle surface to ceramic and metal sides and k is a gradient index. Figure 3.3 shows the working range variation of material properties (Young's modulus) along the thickness, based on a grading index.

Based on the volume fraction of the constituent materials, the effective material properties such as Young's modulus $E(z)$, Poison's ratio $\upsilon(z)$ and mass density $\rho(z)$ of FGM plate material properties are obtained using the following expression.

$$
\begin{aligned}
E(z) &= E_m + (E_c - E_m)\left(\frac{1}{2} + \frac{z}{h}\right)^k \\
\rho(z) &= \rho_m + (\rho_c - \rho_m)\left(\frac{1}{2} + \frac{z}{h}\right)^k \\
\upsilon(z) &= \upsilon_m + (\upsilon_c - \upsilon_m)\left(\frac{1}{2} + \frac{z}{h}\right)^k
\end{aligned}
\tag{3.5}
$$

where the subscripts m and c represent the metallic and ceramic constitutes, k is the power law index.
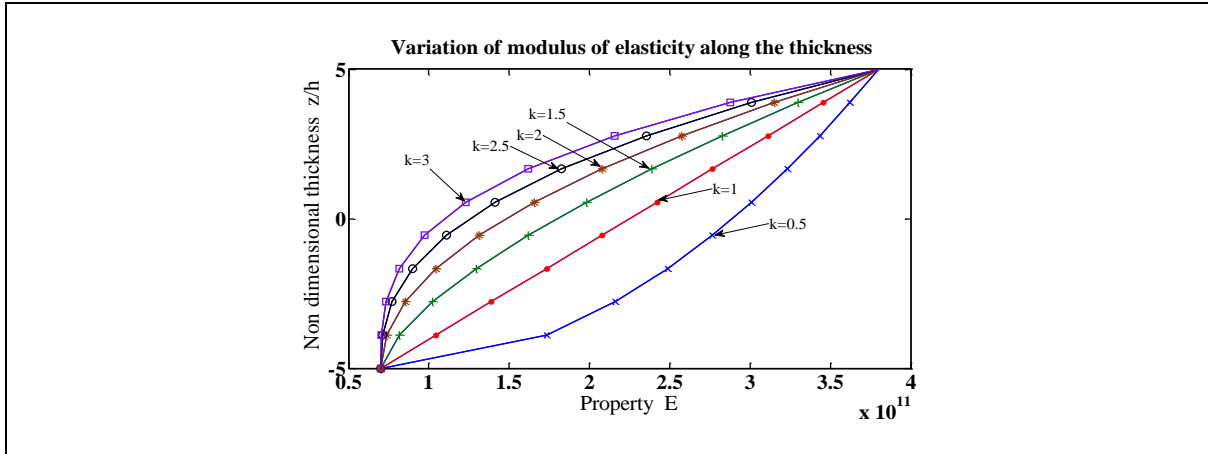
Figure 3.3 Variation of Young's modulus along the thickness of the FGM plate
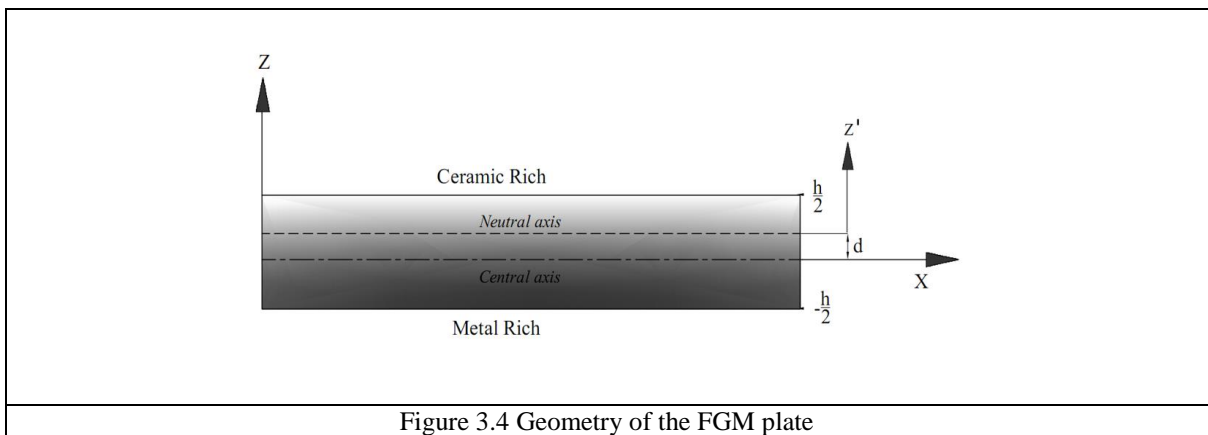
Figure 3.4 Geometry of the FGM plate

3.2.3 Physical neutral surface of the FGM plate

In the present work neutral plane concept has been employed in the analysis. For a FGM plate due to the variation of the material properties along the thickness, the neutral plane does not coincide with the geometrical mid-plane of the plane as shown in figure 3.4. The distance (d) of the neutral surface from the geometric mid-surface may be expressed as

$$d = \frac{\int\limits_{-h/2}^{h/2} zE(z)dz}{\int\limits_{-h/2}^{h/2} E(z)dz} \tag{3.6}$$

For homogeneous isotropic or symmetrical composite plates the neutral and geometric middle surfaces are same.

3.2.4 Kinematics

In the present work, the mechanics of deformation of the plate structure made up of functionally graded material is characterized by third order shear deformation theory using Reddy's equations. Figure 3.5 shows the plate cross-section before and after deformation about the

neutral axis. In-plane displacements *u, v* and the normal displacement *w* are expressed with respect to neutral plane and are expressed as

$$u = u_n + z'\theta_x - c_1 z'^3 \left(\theta_x + w_{n,x}\right),$$
$$v = v_n + z'\theta_y - c_1 z'^3 \left(\theta_y + w_{n,y}\right)$$
$$w = w_n$$

(3.7)

where u_n, v_n, w_n, θ_x and θ_y are functions of x, y, and t (time). u_n, v_n and w_n denote the displacements of a point on the neutral surface of the plate. Here θ_x and θ_y are the rotations of transverse normal about the y and x axes, respectively.
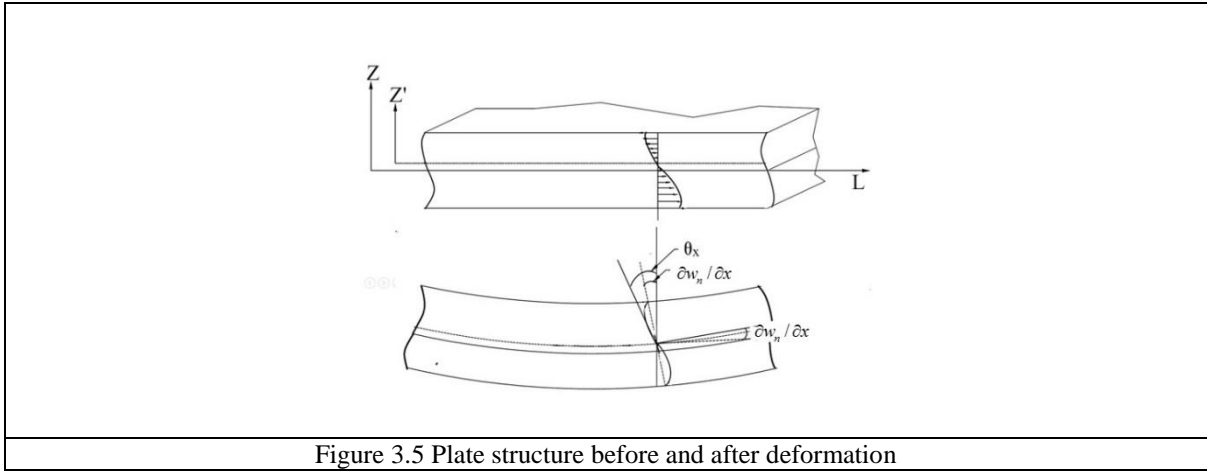
Figure 3.5 Plate structure before and after deformation

Inplane and transverse plane strain-displacement constitutive relations with respect to neutral plane can written as

$$\{\varepsilon^b\} = \begin{Bmatrix} \varepsilon_{xx} \\ \varepsilon_{yy} \\ \gamma_{xy} \end{Bmatrix} = \begin{Bmatrix} \varepsilon_{xx}^{(n)} \\ \varepsilon_{yy}^{(n)} \\ \gamma_{xy}^{(n)} \end{Bmatrix} + z' \begin{Bmatrix} \varepsilon_{xx}^{(1)} \\ \varepsilon_{yy}^{(1)} \\ \gamma_{xy}^{(1)} \end{Bmatrix} - z'^3 \begin{Bmatrix} \varepsilon_{xx}^{(3)} \\ \varepsilon_{yy}^{(3)} \\ \gamma_{xy}^{(3)} \end{Bmatrix}$$

(3.8)

$$\{\gamma^s\} = \begin{Bmatrix} \gamma_{yz} \\ \gamma_{xz} \end{Bmatrix} = \begin{Bmatrix} \gamma_{yz}^{(n)} \\ \gamma_{xz}^{(n)} \end{Bmatrix} + z'^2 \begin{Bmatrix} \gamma_{yz}^{(2)} \\ \gamma_{xz}^{(2)} \end{Bmatrix}$$

(3.9)

where

$$\varepsilon^{(n)} = \begin{Bmatrix} \varepsilon_{xx}^{(n)} \\ \varepsilon_{yy}^{(n)} \\ \gamma_{xy}^{(n)} \end{Bmatrix} = \begin{Bmatrix} u_{n,x} \\ v_{n,y} \\ u_{n,y} + v_{n,x} \end{Bmatrix},$$

$$\varepsilon^{(1)} = \begin{Bmatrix} \varepsilon_{xx}^{(1)} \\ \varepsilon_{yy}^{(1)} \\ \gamma_{xy}^{(1)} \end{Bmatrix} = \begin{Bmatrix} \theta_{x,x} \\ \theta_{y,y} \\ \theta_{x,y} + \theta_{y,x} \end{Bmatrix}, \qquad (3.10)$$

$$\varepsilon^{(3)} = \begin{Bmatrix} \varepsilon_{xx}^{(3)} \\ \varepsilon_{yy}^{(3)} \\ \gamma_{xy}^{(3)} \end{Bmatrix} = -c_1 \begin{Bmatrix} \theta_{x,x} + w_{n,xx} \\ \theta_{y,y} + w_{n,yy} \\ \theta_{x,y} + \theta_{y,x} + 2w_{n,xy} \end{Bmatrix}$$

$$\gamma^{(n)} = \begin{Bmatrix} \gamma_{yz}^{(n)} \\ \gamma_{xz}^{(n)} \end{Bmatrix} = \begin{Bmatrix} w_{n,x} + \theta_x \\ w_{n,y} + \theta_y \end{Bmatrix},$$

$$\gamma^{(2)} = \begin{Bmatrix} \gamma_{yz}^{(2)} \\ \gamma_{xz}^{(2)} \end{Bmatrix} = -c_2 \begin{Bmatrix} w_{n,x} + \theta_x \\ w_{n,y} + \theta_y \end{Bmatrix} \qquad (3.11)$$

where $c_1 = \dfrac{4}{3h^2}$ and $c_2 = 3c_1$.

The stress-strain relationships of the functionally graded material plate in the global x, y and z coordinate system can be written as

$$\begin{Bmatrix} \sigma_{xx} \\ \sigma_{yy} \\ \tau_{yz} \\ \tau_{xz} \\ \tau_{xy} \end{Bmatrix} = \begin{bmatrix} Q_{11} & Q_{12} & 0 & 0 & 0 \\ Q_{21} & Q_{22} & 0 & 0 & 0 \\ 0 & 0 & Q_{44} & 0 & 0 \\ 0 & 0 & 0 & Q_{55} & 0 \\ 0 & 0 & 0 & 0 & Q_{66} \end{bmatrix} \begin{Bmatrix} \varepsilon_{xx} \\ \varepsilon_{yy} \\ \gamma_{yz} \\ \gamma_{xz} \\ \gamma_{xy} \end{Bmatrix} \qquad (3.12)$$

where $Q_{11} = Q_{22} = \dfrac{E(z')}{\left(1 - v^2(z')\right)}, Q_{12} = Q_{21} = \dfrac{E(z')v(z')}{\left(1 - v^2(z')\right)}$ \qquad (3.13)

$$Q_{44} = Q_{55} = Q_{66} = \dfrac{E(z')}{2\left(1 + v(z')\right)} \qquad (3.14)$$

The stress resultants are expressed as follows

$$
\begin{bmatrix} N_{xx} \\ N_{yy} \\ N_{xy} \end{bmatrix} = \int\limits_{-h/2-d}^{h/2-d} \begin{bmatrix} \sigma_{xx} \\ \sigma_{yy} \\ \tau_{xy} \end{bmatrix} dz'
$$

$$
\left.
\begin{aligned}
\begin{bmatrix} M_{xx} \\ M_{yy} \\ M_{xy} \end{bmatrix} &= \int\limits_{-h/2-d}^{h/2-d} \begin{bmatrix} \sigma_{xx} \\ \sigma_{yy} \\ \tau_{xy} \end{bmatrix} z' dz' \\[4pt]
\begin{bmatrix} P_{xx} \\ P_{yy} \\ P_{xy} \end{bmatrix} &= \int\limits_{-h/2-d}^{h/2-d} \begin{bmatrix} \sigma_{xx} \\ \sigma_{yy} \\ \tau_{xy} \end{bmatrix} z'^3 dz'
\end{aligned}
\right\}
\tag{3.15}
$$

$$
\left.
\begin{aligned}
\begin{bmatrix} Q_{xz} \\ Q_{yz} \end{bmatrix} &= \int\limits_{-h/2-d}^{h/2-d} \begin{bmatrix} \tau_{xz} \\ \tau_{yz} \end{bmatrix} dz' \\[4pt]
\begin{bmatrix} R_{xz} \\ R_{yz} \end{bmatrix} &= \int\limits_{-h/2-d}^{h/2-d} \begin{bmatrix} \tau_{xz} \\ \tau_{yz} \end{bmatrix} z'^2 dz'
\end{aligned}
\right\}
\tag{3.16}
$$

Substitution of equation (3.12) in equations (3.15) and (3.16) yields the following relations

$$
\left.
\begin{aligned}
\begin{bmatrix} N \\ M \\ P \end{bmatrix} &= \begin{bmatrix} [A] & [B] & [E] \\ [B] & [D] & [F] \\ [E] & [F] & [H] \end{bmatrix} \begin{Bmatrix} \varepsilon^{(n)} \\ \varepsilon^{(1)} \\ \varepsilon^{(3)} \end{Bmatrix} \\[6pt]
\begin{bmatrix} Q^s \\ R^s \end{bmatrix} &= \begin{bmatrix} [A^s] & [D^s] \\ [D^s] & [F^s] \end{bmatrix} \begin{Bmatrix} \gamma^{(n)} \\ \gamma^{(2)} \end{Bmatrix}
\end{aligned}
\right\}
\tag{3.17}
$$

For all of the stiffness components are expressed as:

$$
\left(A_{ij} \quad B_{ij} \quad D_{ij} \quad E_{ij} \quad F_{ij} \quad H_{ij} \right) = \int\limits_{-h/2-d}^{h/2-d} Q_{ij} \left(1, z', z'^2, z'^3, z'^4, z'^6 \right) dz'
\tag{3.18}
$$

$$
\left(i, j = 1, 2, 6 \right)
$$

$$
\left(A_{ij}^s \quad D_{ij}^s \quad F_{ij}^s \right) = \int\limits_{-h/2-d}^{h/2-d} Q_{ij} \left(1, z'^2, z'^4 \right) dz' \qquad \left(i, j = 4, 5 \right)
\tag{3.19}
$$

3.2.5 Energy equations

The total strain energy $\left(U_P^{(e)} \right)$ of the plate element due to vibratory stresses according to the third order shear deformation theory can expressed as,

$$U_P^{(e)} = \frac{1}{2} \int_0^b \int_0^a \left[[N]^T \{\varepsilon^{(n)}\} + [M]^T \{\varepsilon^{(1)}\} + [P]^T \{\varepsilon^{(3)}\} + [Q^s]^T \{\gamma^{(n)}\} + [R^s]^T \{\gamma^{(2)}\} \right] dxdy \quad (3.20)$$

The kinetic energy of the plate element is given by

$$T^{(e)} = \frac{1}{2} \rho \int_A \left(\dot{u}^2 + \dot{v}^2 + \dot{w}^2 \right) dA \qquad (3.21)$$

where $\rho = \int_{-h/2-d}^{h/2-d} \rho(z')dz'$.

The work done by the plate element due to in-plane loads is:

$$W^{(e)} = \frac{1}{2} \int_A \left[P(t) \left(\frac{\partial w}{\partial x} \right)^2 + P(t) \left(\frac{\partial w}{\partial y} \right)^2 \right] dA \qquad (3.22)$$

where $P(t)$ represents the applied in-plane load along the x and y axes respectively.

3.2.6 FE formulation of a 4-noded rectangular element

A rectangular four node element having one node at each corner as shown in figure 3.6 is considered. There are seven degrees of freedom at each node, two in plane displacements u and v along x and y axes, one transverse displacement w along the thickness direction, two rotations and two slopes about x and y directions in terms of the (x, y) coordinates.

The element displacement vector $\{q^{(n)}\}$ is written as

$$\{q^{(n)}\} = \sum_{i=1}^k N_i q_i, \qquad (3.23)$$

where $\{q^{(n)}\} = \left\{ u, v, w, \theta_x, \theta_y, \frac{\partial w}{\partial x}, \frac{\partial w}{\partial y} \right\}$, q_i is the displacement vector corresponding to node i,

N_i is the shape function associated with node i and k is the number of nodes per element, which is four in the present analysis.
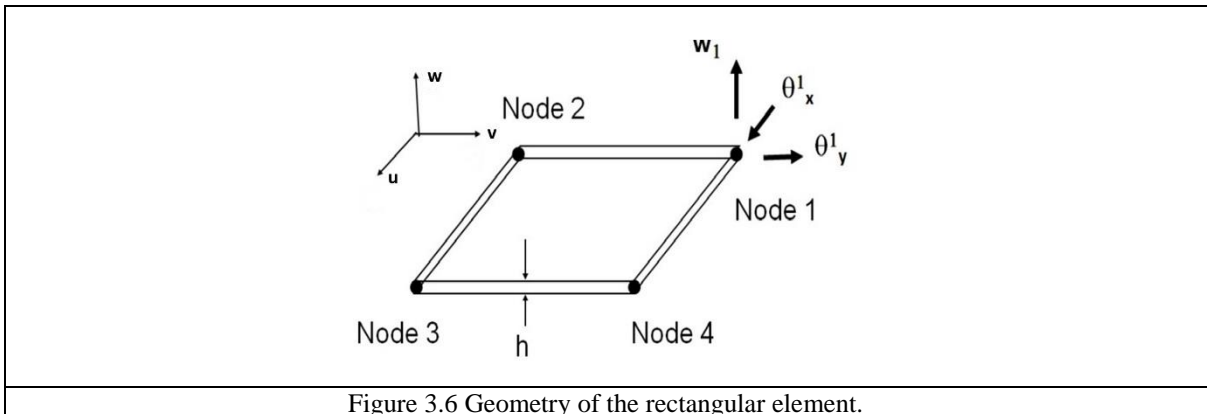
Figure 3.6 Geometry of the rectangular element.

The element nodal displacement vector

$$\left\{q^{(e)}\right\} = \left\{u_i, v_i, w_i, \theta_{xi}, \theta_{yi}, \left(\frac{\partial w}{\partial x}\right)_i, \left(\frac{\partial w}{\partial y}\right)_i\right\}_{i=1,2,3,4}$$ (3.24)

$$u = \sum_{i=1}^{4} N_i u_i, v = \sum_{i=1}^{4} N_i v_i, w = \sum_{i=1}^{4} N_i w_i, \theta_x = \sum_{i=1}^{4} N_i \theta_x^i, \theta_y = \sum_{i=1}^{4} N_i \theta_y^i,$$

$$\frac{\partial w}{\partial x} = \sum_{i=1}^{4} N_i \frac{\partial w_i}{\partial x}, \frac{\partial w}{\partial y} = \sum_{i=1}^{4} N_i \frac{\partial w_i}{\partial y}$$ (3.25)

N is the shape functions matrix

$$[N] = \left\{\left[N_{u_n}\right]\left[N_{v_n}\right]\left[N_{w_n}\right]\left[N_{\theta_x}\right]\left[N_{\theta_y}\right]\left[N_{\partial w/\partial x}\right]\left[N_{\partial w/\partial y}\right]\right\}^T$$

$$[N] = \sum_{i=1}^{4} \begin{bmatrix} N_i & 0 & 0 & 0 & 0 & 0 & 0--- \\ 0 & N_i & 0 & 0 & 0 & 0 & 0--- \\ 0 & 0 & N_i & 0 & 0 & 0 & 0--- \\ 0 & 0 & 0 & N_i & 0 & 0 & 0--- \\ 0 & 0 & 0 & 0 & N_i & 0 & 0--- \\ 0 & 0 & 0 & 0 & 0 & N_i & 0--- \\ 0 & 0 & 0 & 0 & 0 & 0 & N_i --- \end{bmatrix}$$ (3.26)

$$N_1 = \frac{(1-\xi)(1-\eta)}{4}, N_2 = \frac{(1+\xi)(1-\eta)}{4}$$

$$N_3 = \frac{(1+\xi)(1+\eta)}{4}, N_4 = \frac{(1-\xi)(1+\eta)}{4}$$ (3.27)

where $\xi = x/a, \eta = y/b$, a and b are the element length and width.

The strain vector can be expressed in terms of nodal displacement vector   as

$$\left\{\varepsilon^b\right\} = [B_b]\left\{q^{(e)}\right\}$$ (3.28)

$$\left\{\gamma^s\right\} = [B_s]\left\{q^{(e)}\right\}$$ (3.29)

where, $[B_b] = [B_0] + z'[B_1] + z'^3[B_2]$ and

$$[B_s] = [B_3] + z'^2[B_4]$$

where, $[B_0], [B_1], [B_2], [B_3] \, and \, [B_4]$ are defined as follows

$$[B_0] = \begin{bmatrix} \dfrac{\partial}{\partial x} & 0 & 0 & 0 & 0 & 0 & 0 \\[2mm] 0 & \dfrac{\partial}{\partial y} & 0 & 0 & 0 & 0 & 0 \\[2mm] \dfrac{\partial}{\partial y} & \dfrac{\partial}{\partial x} & 0 & 0 & 0 & 0 & 0 \end{bmatrix} [N],$$

$$[B_1] = \begin{bmatrix} 0 & 0 & 0 & \dfrac{\partial}{\partial x} & 0 & 0 & 0 \\[2mm] 0 & 0 & 0 & 0 & \dfrac{\partial}{\partial y} & 0 & 0 \\[2mm] 0 & 0 & 0 & \dfrac{\partial}{\partial y} & \dfrac{\partial}{\partial x} & 0 & 0 \end{bmatrix} [N] \ ,$$

$$[B_2] = c_1 \begin{bmatrix} 0 & 0 & 0 & \dfrac{\partial}{\partial x} & 0 & \dfrac{\partial}{\partial x} & 0 \\[2mm] 0 & 0 & 0 & 0 & \dfrac{\partial}{\partial y} & 0 & \dfrac{\partial}{\partial y} \\[2mm] 0 & 0 & 0 & \dfrac{\partial}{\partial y} & \dfrac{\partial}{\partial x} & \dfrac{\partial}{\partial y} & \dfrac{\partial}{\partial x} \end{bmatrix} [N],$$

$$[B_3] = \begin{bmatrix} 0 & 0 & \dfrac{\partial}{\partial x} & 0 & 1 & 0 & 0 \\[2mm] 0 & 0 & \dfrac{\partial}{\partial x} & 1 & 0 & 0 & 0 \end{bmatrix} [N], \quad [B_4] = c_2 \begin{bmatrix} 0 & 0 & 0 & 1 & 0 & 1 & 0 \\ 0 & 0 & 0 & 0 & 1 & 0 & 1 \end{bmatrix} [N]$$

Substituting equation (3.28) and equation (3.29) in equation (3.20), the element strain energy can be expressed as

$$U_p^{(e)} = \frac{1}{2}\left[\{q^{(e)}\}^T \left(\left[K_b^{(e)} \right] + \left[K_s^{(e)} \right] \right) \{q^{(e)}\} \right] \tag{3.30}$$

The element stiffness matrix is expressed as

$$\left[K^{(e)} \right] = \left[K_b^{(e)} \right] + \left[K_s^{(e)} \right] \tag{3.31}$$

where, $\left[K_b^{(e)} \right] = \left[K_{00}^{(e)} \right] + \left[K_{01}^{(e)} \right] + \left[K_{11}^{(e)} \right] + \left[K_{02}^{(e)} \right] + \left[K_{12}^{(e)} \right] + \left[K_{22}^{(e)} \right]$ (3.32)

$$\left[K_{00}^{(e)}\right] = \int\limits_0^a \int\limits_0^b [B_0]^T [A][B_0] dxdy$$

$$\left[K_{01}^{(e)}\right] = \int\limits_0^a \int\limits_0^b \left([B_0]^T [B][B_1] + [B_1]^T [B][B_0]\right) dxdy$$

$$\left[K_{11}^{(e)}\right] = \int\limits_0^a \int\limits_0^b [B_1]^T [D][B_1] dxdy$$

$$\left[K_{02}^{(e)}\right] = \int\limits_0^a \int\limits_0^b \left([B_0]^T [E][B_2] + [B_2]^T [E][B_0]\right) dxdy \tag{3.33}$$

$$\left[K_{12}^{(e)}\right] = \int\limits_0^a \int\limits_0^b \left([B_1]^T [F][B_2] + [B_1]^T [F][B_2]\right) dxdy$$

$$\left[K_{22}^{(e)}\right] = \int\limits_0^a \int\limits_0^b [B_2]^T [H][B_2] dxdy$$

$$\left[K_s^{(e)}\right] = \left[K_{33}^{(e)}\right] + \left[K_{34}^{(e)}\right] + \left[K_{44}^{(e)}\right] \tag{3.34}$$

$$\left[K_{33}^{(e)}\right] = \int\limits_0^a \int\limits_0^b [B_3]^T \left[A^s\right][B_3] dxdy$$

$$\left[K_{34}^{(e)}\right] = \int\limits_0^a \int\limits_0^b \left([B_3]^T \left[D^s\right][B_4] + [B_4]^T \left[D^s\right][B_3]\right) dxdy \tag{3.35}$$

$$\left[K_{44}^{(e)}\right] = \int\limits_0^a \int\limits_0^b [B_4]^T \left[F^s\right][B_4] dxdy$$

Reproducing equation (3.21), the kinetic energy of the plate element is expressed as

$$T^{(e)} = \frac{1}{2}\rho \int\limits_A \left(\dot{u}^2 + \dot{v}^2 + \dot{w}^2\right) dA \tag{3.36}$$

The velocities $\dot{u}, \dot{v}$ and $\dot{w}$ can be written in terms of shape functions and nodal velocity vector as

$$\dot{u} = \left[\left[N_{u_n}\right] + z'\left[N_{\theta_x}\right] - c_1 z'^3 \left(\left[N_{\theta_x}\right] + \left[N_{\partial w/\partial x}\right]\right)\right]\left\{\dot{q}^{(e)}\right\}^T$$

$$\dot{v} = \left[\left[N_{v_n}\right] + z'\left[N_{\theta_y}\right] - c_1 z'^3 \left(\left[N_{\theta_y}\right] + \left[N_{\partial w/\partial y}\right]\right)\right]\left\{\dot{q}^{(e)}\right\}^T \tag{3.37}$$

$$\dot{w} = \left[N_{w_n}\right]\left\{\dot{q}^{(e)}\right\}^T$$

Substituting equation (3.37) in equation (3.36) the element kinetic energy, $T^{(e)}$ can be expressed as

$$
\begin{aligned}
T^{(e)} = \frac{1}{2}\int_0^a\int_0^b \{q^{(e)}\}^T \Big[& I_0\Big([N_{u_n}]^T[N_{u_n}]+[N_{v_n}]^T[N_{v_n}]+[N_{w_n}]^T[N_{w_n}]\Big)+ \\
& I_1\Big([N_{u_n}]^T[N_{\theta_x}]+[N_{\theta_x}]^T[N_{u_n}]+[N_{v_n}]^T[N_{\theta_y}]+[N_{\theta_y}]^T[N_{v_n}]\Big)+ \\
& I_2\Big([N_{\theta_x}]^T[N_{\theta_x}]+[N_{\theta_y}]^T[N_{\theta_y}]\Big)+ \\
& I_3\Big([N_{u_n}]^T\big[[N_{\theta_x}]+[N_{\partial w/\partial x}]\big]+\big[[N_{\theta_x}]+[N_{\partial w/\partial x}]\big]^T[N_{u_n}]+ \\
& \quad [N_{v_n}]^T\big[[N_{\theta_y}]+[N_{\partial w/\partial y}]\big]+\big[[N_{\theta_y}]+[N_{\partial w/\partial y}]\big]^T[N_{v_n}]\Big)+ \\
& I_4\Big([N_{\theta_x}]^T\big[[N_{\theta_x}]+[N_{\partial w/\partial x}]\big]+\big[[N_{\theta_x}]+[N_{\partial w/\partial x}]\big]^T[N_{\theta_x}]+ \\
& \quad [N_{\theta_y}]^T\big[[N_{\theta_y}]+[N_{\partial w/\partial y}]\big]+\big[[N_{\theta_y}]+[N_{\partial w/\partial y}]\big]^T[N_{\theta_y}]\Big)+ \\
& I_6\Big(\big[[N_{\theta_x}]+[N_{\partial w/\partial x}]\big]^T\big[[N_{\theta_x}]+[N_{\partial w/\partial x}]\big]+\big[[N_{\theta_y}]+[N_{\partial w/\partial y}]\big]^T\big[[N_{\theta_y}]+[N_{\partial w/\partial y}]\big]\Big)\Big]\{q^{(e)}\}\,dx\,dy
\end{aligned}
$$
(3.38)

$$
T^{(e)} = \frac{1}{2}\Big[\{\dot{q}^{(e)}\}^T\big[M^{(e)}\big]\{\dot{q}^{(e)}\}\Big]
$$
(3.39)

where $\big[M^{(e)}\big]$ is the element mass matrix

$$
\begin{aligned}
\big[M^{(e)}\big] = \int_0^a\int_0^b \Big[& I_0\Big([N_{u_n}]^T[N_{u_n}]+[N_{v_n}]^T[N_{v_n}]+[N_{w_n}]^T[N_{w_n}]\Big)+ \\
& I_1\Big([N_{u_n}]^T[N_{\theta_x}]+[N_{\theta_x}]^T[N_{u_n}]+[N_{v_n}]^T[N_{\theta_y}]+[N_{\theta_y}]^T[N_{v_n}]\Big)+ \\
& I_2\Big([N_{\theta_x}]^T[N_{\theta_x}]+[N_{\theta_y}]^T[N_{\theta_y}]\Big)+ I_3\Big([N_{u_n}]^T\big[[N_{\theta_x}]+[N_{\partial w/\partial x}]\big]+\big[[N_{\theta_x}]+[N_{\partial w/\partial x}]\big]^T[N_{u_n}]+ \\
& \quad [N_{v_n}]^T\big[[N_{\theta_y}]+[N_{\partial w/\partial y}]\big]+\big[[N_{\theta_y}]+[N_{\partial w/\partial y}]\big]^T[N_{v_n}]\Big)+ \\
& I_4\Big([N_{\theta_x}]^T\big[[N_{\theta_x}]+[N_{\partial w/\partial x}]\big]+\big[[N_{\theta_x}]+[N_{\partial w/\partial x}]\big]^T[N_{\theta_x}]+ \\
& \quad [N_{\theta_y}]^T\big[[N_{\theta_y}]+[N_{\partial w/\partial y}]\big]+\big[[N_{\theta_y}]+[N_{\partial w/\partial y}]\big]^T[N_{\theta_y}]\Big)+ \\
& I_6\Big(\big[[N_{\theta_x}]+[N_{\partial w/\partial x}]\big]^T\big[[N_{\theta_x}]+[N_{\partial w/\partial x}]\big]+\big[[N_{\theta_y}]+[N_{\partial w/\partial y}]\big]^T\big[[N_{\theta_y}]+[N_{\partial w/\partial y}]\big]\Big)\Big]\,dx\,dy
\end{aligned}
$$
(3.40)

where $I_i = \displaystyle\int_{-h/2-d}^{h/2-d} \rho(z')\big(1, z', z'^2, c_1 z'^3, c_1 z'^4, c_1^2 z'^6\big)\,dz'$, $\qquad (i = 0,1,2,3,4,6)$

Using expressions for $\dfrac{\partial w}{\partial x}$ and $\dfrac{\partial w}{\partial y}$ from equation (3.25) in equation (3.22) the elemental

work done can be written in terms of nodal displacement vector as

$$W^{(e)} = \frac{1}{2} \int_A \left\{ q^{(e)} \right\}^T \left[P(t) \left[N_{\partial w / \partial x} \right]^T \left[N_{\partial w / \partial x} \right] + P(t) \left[N_{\partial w / \partial y} \right]^T \left[N_{\partial w / \partial y} \right] \right] \left\{ q^{(e)} \right\} dx \, dy$$

$$= \frac{1}{2} \left\{ q^{(e)} \right\}^T \left(P(t) \right) \left[K_g \right] \left\{ q^{(e)} \right\} \tag{3.41}$$

$$\left[K_g^{(e)} \right] = \int_0^a \int_0^b \left[\left[N_{\partial w / \partial x} \right]^T \left[N_{\partial w / \partial x} \right] + \left[N_{\partial w / \partial y} \right]^T \left[N_{\partial w / \partial y} \right] \right] dx \, dy \tag{3.42}$$

where $\left[K_g^{(e)} \right]$ is the element geometric stiffness matrix and it contains the terms with axial forces only.

3.3 Governing Equations of Motion

The element equation of motion subjected to axial force is obtained by using Hamilton's principle.

$$\delta \int_{t_1}^{t_2} \left(U_p^{(e)} - T^{(e)} + W^{(e)} \right) dt = 0 \tag{3.43}$$

where $U_p^{(e)}$ is the element strain energy, $T^{(e)}$ is kinetic energy of element and $W^{(e)}$ is work done by the plate element.

By dividing the plate in to a number of elements and using equations (3.30), (3.39) and (3.41) in equation (3.43), the equation of motion of plate element in matrix form for the axially loaded discretized system is obtained as follows

$$\left[M^{(e)} \right] \left\{ \ddot{q}^{(e)} \right\} + \left[K^{(e)} \right] \left\{ q^{(e)} \right\} - P(t) \left[K_g^{(e)} \right] \left\{ q^{(e)} \right\} = 0 \tag{3.44}$$

The governing equation of motion of plate in terms of global displacement matrix obtained as follows.

$$[M] \{ \ddot{q} \} + [K] \{ q \} - P(t) \left[K_g \right] \{ q \} = 0 \tag{3.45}$$

where $[K]$, $[M]$ and $\left[K_g \right]$ are global stiffness, global mass and global geometric stiffness matrices respectively.

$$[M] \{ \ddot{q} \} + [K] \{ q \} - \left(P_s + P_t \cos \Omega t \right) \left[K_g \right] \{ q \} = 0 \tag{3.46}$$

where P_s is the static and P_t is the amplitude of time dependent component of the load, can be represented as a function of the fundamental static buckling load P^{cr} of a reference plate,

having required boundary conditions. Hence substituting, $P(t) = \alpha P^{cr} + \beta P^{cr} \cos \Omega t$ with α and β, called static and dynamic load factors respectively, equation (3.46) can be written as

$$[M]\{\ddot{q}\} + \left([K] - \alpha P^{cr} \left[K_g \right]_s \right) \{q\} - \beta P^{cr} \cos \Omega t \left[K_g \right]_t \{q\} = 0 \qquad (3.47)$$

where $\left[K_g \right]_s$ and $\left[K_g \right]_t$ reflect the influence of P_s and P_t respectively. If the static and time dependent components of the load are applied in the same manner then.

$$\left[K_g \right]_t = \left[K_g \right]_s = \left[K_g \right]$$

3.3.1 Parametric instability regions

The above equation (3.47) represents a system of second order differential equations with periodic coefficients of Mathieu-Hill type. From the theory of Mathieu function it is evident that the nature of solution is dependent on the choice of load frequency and load amplitude. The frequency amplitude domain is divided in two regions, which give raise to stable solutions and to regions, which cause unstable solutions. According to the Floquet's theory the periodic solutions characterize the boundary conditions between the dynamic stability and instability zones.

The equation does not change its form on addition of the period $T = \dfrac{2\pi}{\Omega}$ to t.

This follows from the fact that $\cos \Omega (t + T) = \cos \Omega t$ therefore if $q(t)$ is a solution of the equation (3.47), and then $q(t+T)$ is also its solution.

According to the Floquet's solutions the mth solution of equation (3.47) can be written as,

$$q_m (t+T) = \lambda_m q_m (t) \qquad (3.48)$$

where λ_m is the characteristic constant

These solutions which acquire a constant multiplier by the addition of the period T to t can be represented in the form

$$q_m (t) = \gamma_m (t) e^{\left(1/T \right) In \lambda_m} \qquad (3.49)$$

where $\gamma_m (t)$ is a periodic function of period T.

It follows from the equation (3.49) that the behaviour of the solutions as $t \to \infty$ depends on the value of the characteristic roots, more precisely, on the value of its moduli.

Taking in to account that $In \lambda_m = In |\lambda_m| + i \arg \lambda_m$

$$q_m(t) = \varphi_m(t) e^{\left(\frac{1}{T}\right) \ln|\lambda_m|} \tag{3.50}$$

where $\varphi_m = \gamma_m(t) e^{\left(\frac{it}{T}\right) \arg \lambda_m}$

If the characteristic number λ_m is greater than unity, then the corresponding solution, equation will have an unbounded exponential multiplier, hence the solution is unlimited. If the same characteristic number is less than unity, then the corresponding solution is damped as t increases. Finally, if the characteristic number is equal to unity then the solution is periodic, i.e. it will be bounded in time. These are the conclusions of the Floquet's theory.

So the periodic solution can be expressed as Fourier series.

The boundaries of the principal instability regions with period 2T are of practical importance. A solution with period 2T is represented by:

$$q(t) = \sum_{n=1,3,\ldots}^{\infty} \left[\{c_n\} \sin \frac{n\Omega t}{2} + \{d_n\} \cos \frac{n\Omega t}{2} \right] \tag{3.51}$$

A solution with period T is represented by:

$$q(t) = \{c_0\} + \sum_{n=2,4,\ldots}^{\infty} \left[\{c_n\} \sin \frac{n\Omega t}{2} + \{d_n\} \cos \frac{n\Omega t}{2} \right] \tag{3.52}$$

If the series expansions of eq. (3.51), term wise comparisons of the sine and cosine coefficients will give infinite system of homogeneous algebraic equations for the vectors $\{c_n\}$ and $\{d_n\}$ for the solutions on the stability borders. Non-trivial solutions exist if the determinant of the coefficient matrices of these equation systems of infinite order vanishes. When looking for numerical solutions, systems of finite order are required and as it is revealed in reference Bolotin [17], a sufficiently close approximation of the infinite Eigen value problem is obtained by taking $n=1$ in the expansion in equation (3.51) and putting the determinant of the coefficient matrices of the first order equal to zero. The first order expansion of equation (3.51) gives

$$q(t) = \{c_1\} \sin \frac{\Omega t}{2} + \{d_1\} \cos \frac{\Omega t}{2} \tag{3.53}$$

Substituting the first order (*n=1*) Fourier series expansion of equation (3.53) in equation (3.47) and comparing the coefficients of $\cos \frac{\Omega t}{2}$ and $\sin \frac{\Omega t}{2}$ terms, the condition for existence of these boundary solutions with period 2T is given by

$$\left([K] - \left(\alpha \pm \frac{\beta}{2} \right) P^{cr} \times [K_g] - \frac{\Omega^2}{4} [M] \right) \{q\} = 0 \tag{3.54}$$

The above equation represents an eigenvalue problem for known values of α, β and P^{cr}. This equation gives two sets of eigenvalues of Ω bounding the regions of instability due to the presence of plus and minus sign. The instability boundaries can be determined from the solution of the equation.

$$\left| [K] - \left(\alpha \pm \frac{\beta}{2} \right) P^{cr} \times [K_g] - \frac{\Omega^2}{4} [M] \right| = 0 \tag{3.55}$$

Also the equation (3.55) represents the solution to a number of related problems

(1) For natural frequencies:

$\alpha = 0$, $\beta = 0$ and $\omega = \frac{\Omega}{2}$, ω represents the natural frequencies of the plate.

The equation becomes

$$\left| [K] - \omega^2 [M] \right| = 0 \tag{3.56}$$

(2) For static stability or buckling analysis:

$\alpha = 1$, $\beta = 0$ and $\omega = 0$

The equation becomes

$$\left| [K] - P^{cr} \times [K_g] \right| = 0 \tag{3.57}$$

(3) For dynamic instability, when all terms are present

$$\left| [K] - \left(\alpha \pm \frac{\beta}{2} \right) P^{cr} \times [K_g] - \iota \frac{\omega^2_1}{4} [M] \right| = 0 \tag{3.58}$$

where $\iota = \left(\frac{\Omega}{\omega_1} \right)^2$

The solution of equation (3.58) gives two sets of values of $\left(\frac{\Omega}{\omega_1} \right)$ forgiven values of α, β, P^{cr}, and ϖ_1. The plot between β and $\left(\frac{\Omega}{\omega_1} \right)$ gives the regions of dynamic instability.

3.4 Results and Discussion

To study the vibration and dynamic instability of the FGM plates the numerical results are computed using the proposed numerical model. A computer code has been developed in MATLAB environment. The element stiffness, geometric stiffness and mass matrices are derived using the standard procedure. Numerical integration technique, Gaussian quadrature is

used for the element matrices calculation. The global matrices $[K]$, $[K_g]$ and $[M]$ are obtained by assembling the corresponding element matrices. The boundary conditions are applied by restraining the generalized displacements in different nodes of the discretized structure. The validation of the proposed program is observed by comparing the results with those available in published literature.

3.4.1 Validation of results

The results for FGM plate free vibration and buckling analysis obtained by applying third order shear deformation theory in this study are compared with the available literature results of Hosseini et al. [56] (Exact closedform procedure); Hosseini et al. [57] (Analytical approach); Zhao et al. [236] (Element-free kp-Ritz method). The natural frequencies are obtained by considering a combination of Al/Al$_2$O$_3$ FGM, where the top surface is ceramic rich and the bottom surface is metal rich.

The dimensionless frequency parameter $\hat{\beta}$ considered as defined by Hosseini et al [56]:

$\hat{\beta} = \omega h \sqrt{\rho_c / E_c}$, where E_c and ρ_c are Young's modulus and mass density of ceramic material. The plate is discretized in to 10X10 elements. Validation has been done by considering the values of length L=1 m, width W=1m, and thickness h=0.05 m, respectively. Poisson's ratio, mass density and Young's modulus of the ceramic and metal Zhao et al. [236]:

Al, $\rho = 2702 kg/m^3$, $E = 70 \text{X} 10^9 Pa$, $\nu = 0.3$, SUS304, $\rho = 8166 kg/m^3$, $E = 207.78 \text{X} 10^9 Pa$, $\nu = 0.3177$, Al$_2$O$_3$, $\rho = 2707 kg/m^3$, $E = 380 \text{X} 10^9 Pa$, $\nu = 0.3$

Table 3.1 Comparison of the natural frequency parameter for simply supported FGM (Al/Al$_2$O$_3$) square plates.

h/a	Mode Number	Method	Power law index (k)				
			0	0.5	1	4	10
0.05	(1,1)	Present	0.0146	0.0127	0.0118	0.0102	0.0091
		Hosseini [57]	0.0148	0.0128	0.0115	0.0098	0.0094
		Hosseini [56]	0.0148	0.0125	0.0113	0.0101	0.0096
0.1	(1,1)	Present	0.0566	0.0491	0.0453	0.0392	0.0350
		Hosseini [57]	0.0577	0.0492	0.0445	0.0383	0.0363
		Hosseini [56]	0.0577	0.0490	0.0442	0.0382	0.0366
	(1,2), (2,1)	Present	0.1365	0.1172	0.1074	0.0928	0.0835
		Zhao [236]	0.1354	0.1154	0.1042	-	0.0850
		Hosseini [56]	0.1376	0.1173	0.1059	0.0911	0.0867
	(2,2)	Present	0.2095	0.1784	0.1624	0.1453	0.1271
		Zhao [236]	0.2063	0.1764	0.1594	0.1397	0.1324
		Hosseini [56]	0.2112	0.1805	0.1631	-	0.1289
0.2	(1,1)	Present	0.2072	0.1766	0.1608	0.1390	0.1258
		Zhao [236]	0.2055	0.1757	0.1587	0.1356	0.1284
		Hosseini [56]	0.2112	0.1805	0.1631	0.1397	0.1324

Table 3.1 shows the natural frequency parameter obtained from the present study using third order shear deformation theory and reference results. There is a good agreement between the presented results and those from Hosseini et al. [56]; Hosseini et al. [57]; Zhao et al. [236].

Buckling analysis has been performed for FGM rectangular plates with different values of power law index. To validate the present calculation method, comparison of critical buckling loads for simply supported FGM plates is shown in table 3.2 (a-b). There is good agreement between the present and results of Choi [27]; Sidda Reddy et al. [184] for uniaxial and biaxial loading cases with different power law index.

Non-dimensional critical buckling load parameter by Choi [27] is: $(\bar{N} = N_{cr}\left(L^2 / E_m h^3\right))$

Table 3.2(a) Comparison of non-dimensional critical buckling load of simply supported FGM (Al/Al$_2$O$_3$) plate subjected to uniaxial loading.

Loading	L/h		Power law index (k)				
			0	0.5	1	5	10
Uniaxial	10	Present	18.49	11.99	9.58	6.43	5.22
		Choi [27]	18.57	12.12	9.33	6.03	5.45
		Sidda Reddy [184]	18.54	12.08	9.299	5.99	5.42
	20	Present	19.52	12.72	10.35	7.29	5.59
		Choi [27]	19.57	12.56	9.66	6.34	5.76
		Sidda Reddy [184]	19.35	12.53	9.649	6.32	5.75
	50	Present	19.83	12.97	10.35	7.47	5.70
		Choi [27]	19.58	12.69	9.763	6.42	5.84
		Sidda Reddy [184]	19.54	12.67	9.743	6.45	5.87
	100	Present	19.88	12.79	10.45	7.49	5.72
		Choi [27]	19.61	12.71	9.77	6.45	5.87
		Sidda Reddy [184]	19.57	12.69	9.75	6.43	5.86

Table 3.3(b) Comparison of non-dimensional critical buckling load of simply supported FGM (Al/Al$_2$O$_3$) plate subjected biaxial loading

Loading	L/h		Power law index (k)				
			0	0.5	1	5	10
Biaxial	10	Present	9.102	6.009	4.717	3.322	2.572
		Choi [27]	9.289	6.062	4.670	3.018	2.726
		Sidda Reddy [184]	9.273	6.045	4.650	2.998	2.715
	20	Present	9.610	6.257	5.091	3.589	2.753
		Choi [27]	9.676	6.283	4.834	3.172	2.883
		Sidda Reddy [184]	9.658	6.270	4.821	3.162	2.876
	50	Present	9.762	6.380	5.208	3.589	2.753
		Choi [27]	9.791	6.349	4.882	3.219	2.931
		Sidda Reddy [184]	9.772	6.336	4.872	3.212	2.825
	100	Present	9.787	6.398	5.223	3.685	2.805
		Choi [27]	9.807	6.358	4.889	3.225	2.938
		Sidda Reddy [184]	9.788	6.345	4.879	3.219	2.932

3.4.2 Natural frequency and buckling analysis

The following numerical results are obtained by considering the steel (SUS304) as the bottom surface and alumina (Al$_2$O$_3$) as the top surface in the FGM plate. The geometry of the plate is as follows: length L=1 m, width W=1 m, thickness h=0.1 m.

The frequency parameter (ϖ) as defined by Talha and Singh [199] has been adopted for this numerical analysis and is expressed as

$$\varpi = \omega\sqrt{12\left(1-v^2\right)\rho_c L^2 W^2 / \pi^4 E_c h^2}$$

The variation of natural frequency parameter in FGM (SUS304/Al$_2$O$_3$) plate with different boundary conditions are shown in figures 3.7-3.10. The effect of power law index k on the frequencies can be seen for different boundary conditions. Increasing index value leads to reduce the natural frequencies. These plots, 3.7-3.10 reveal that the effect of power law index value from k=0 to 3 is more prominent than the higher values of k. The increase in power law index reduces the ceramic content and increases the metal content, hence there is a reduction in effective Young's modulus, so the frequencies decrease.
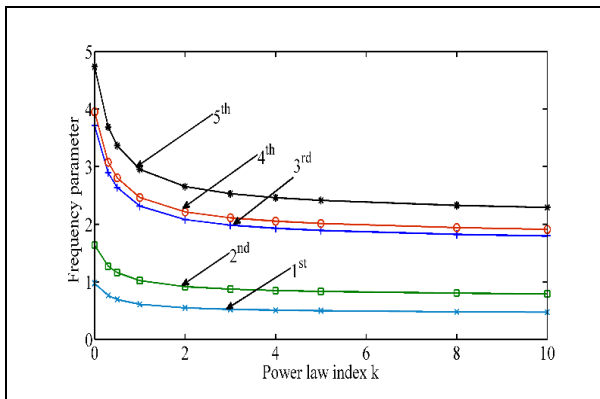
Figure 3.7 First five frequency parameters verses index value with SFSF boundary conditions.	Figure 3.8 First five frequency parameters verses index value with SSSS boundary conditions.
Figure 3.9 First five frequency parameters verses index value with SCSC boundary conditions.	Figure 3.10 First five frequency parameters verses index value with CCCC boundary conditions.
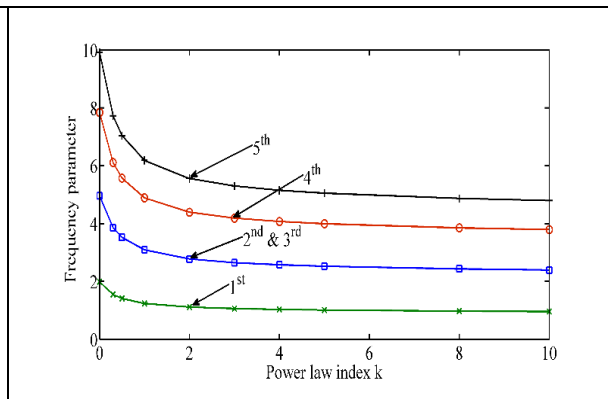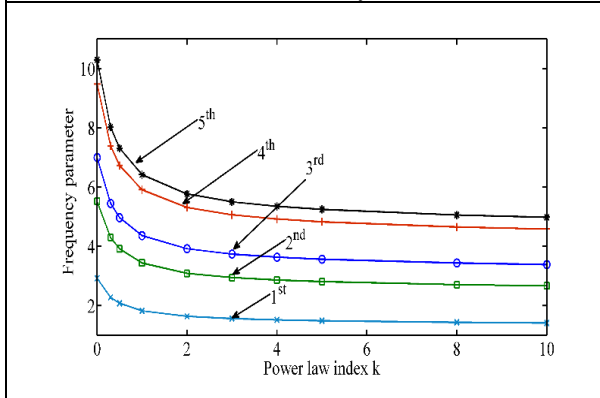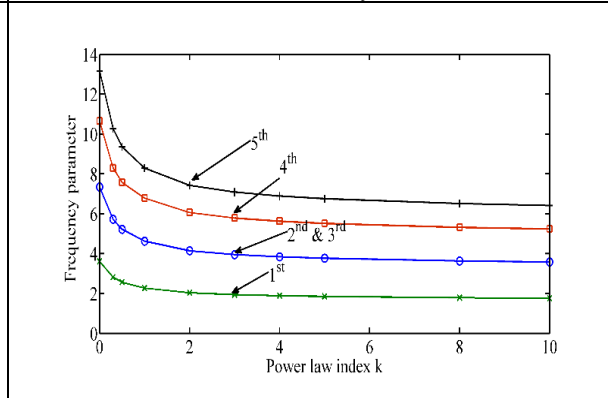
The effect of aspect ratio on the first five natural frequencies of FGM (k=1) plate is investigated and is presented in figure 3.11 and 3.12 for SSSS and CCCC boundary conditions

respectively. It is observed from the figures that the increase in aspect ratio decreases the first five natural frequencies.

| Figure 3.11 Variation of first five frequency parameters verses aspect ratio with SSSS boundary condition. | Figure 3.12 Variation of first five frequency parameters verses index value with CCCC boundary condition. |
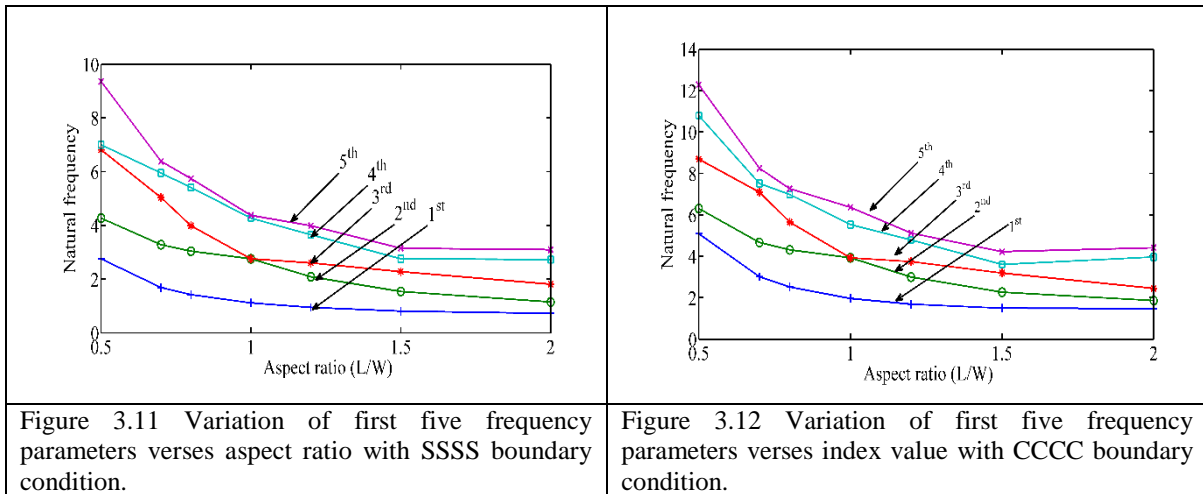
Figures 3.13 and 3.14 show the results of critical buckling load of simply supported FGM rectangular plate. The critical buckling load decreases when the power law index value increases, both in uniaxial and biaxial compression cases. This happens due to the reduction in effective Young's modulus of the FGM with increasing power law index value.

| Figure 3.13 Variation of critical buckling load verses index value under uniaxial compression. | Figure 3.14 Variation of critical buckling load verses index value under biaxial compression. |
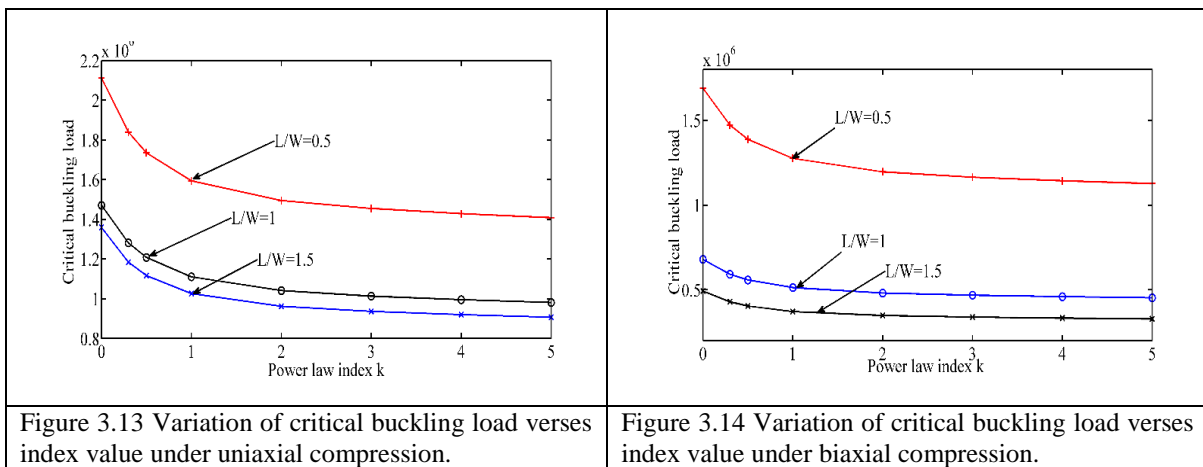
3.4.3 Dynamic stability analysis

The dynamic stability of FGM plates under parametric excitation has been investigated. The power law index value, the length, the width and the thickness of the FGM plates are varied to assess their effects on the parametric instability behaviour. For dynamic stability study the first, second and third mode instability regions are represented through key as '——' $2\omega_1$, '- - -' $2\omega_2$, '·········' $2\omega_3$.
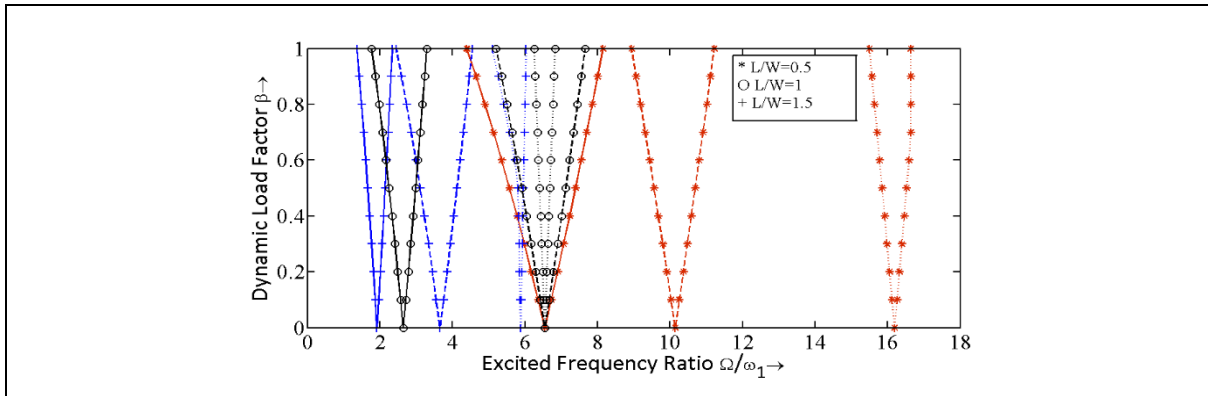
Figure 3.15 Dynamic stability of simply supported FGM plate under uniaxial loading with different aspect ratios, k=1, '——' $2\omega_1$, '－－－' $2\omega_2$, '·········' $2\omega_3$.

Figures 3.15-3.17 show the dynamic stability regions of simply supported FGM plate with aspect ratio L/W=0.5, 1, 1.5 and plate thickness h=0.1m. Figures 3.15-3.17 reveal that for plate under uniaxial loading with increasing aspect ratio, the instability regions shift to lower frequencies of excitation. Structural plates are usually subjected to low frequency vibration. So when the instability regions shift to lower frequencies of excitation, the chance of occurrence of instability is more. Hence with increase in aspect ratio of the FGM plate the instability is enhanced.
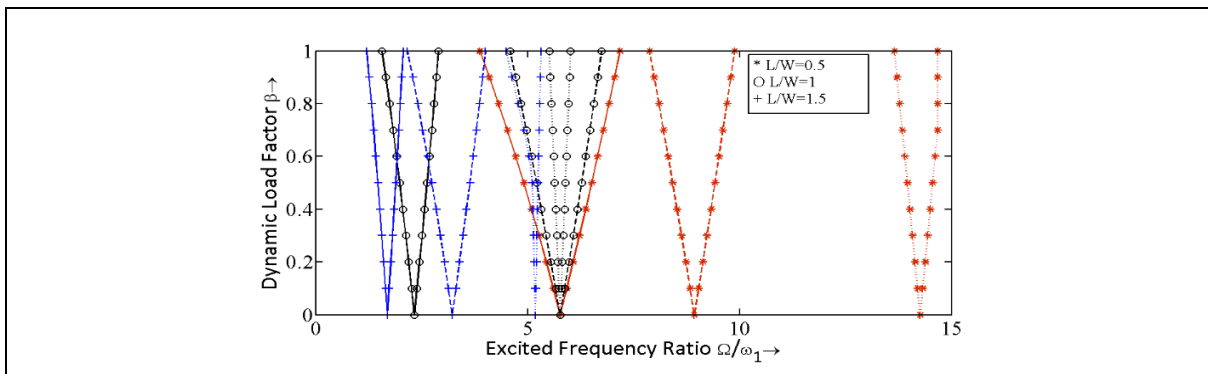
Figure 3.16 Dynamic stability of simply supported FGM plate under uniaxial loading with different aspect ratios, k=2, key as in fig. 3.15.
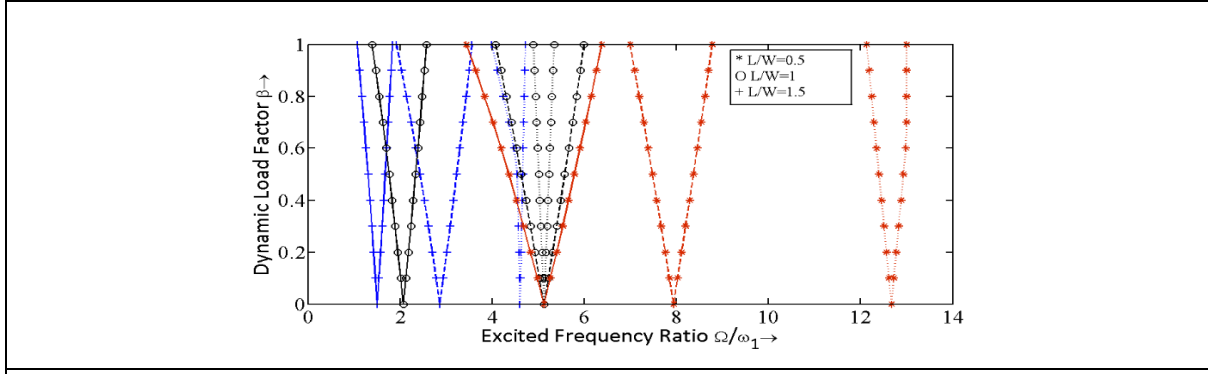
Figure 3.17 Dynamic stability of simply supported FGM plate under uniaxial loading with different aspect ratios, k=5, key as in fig. 3.15.

Figure 3.18-3.20 show that increase in power law index value (k=1, 2 and 5) reduces stability of FGM plate under uniaxial periodic loads. It can be seen that the instability regions are shifted towards the dynamic load axis with increase in power law index value, thus occurring at lower excitation frequencies. The effect is more significant on higher mode instability regions than on the first mode region. Hence, increase in power law index increases the dynamic instability of the FGM plate.
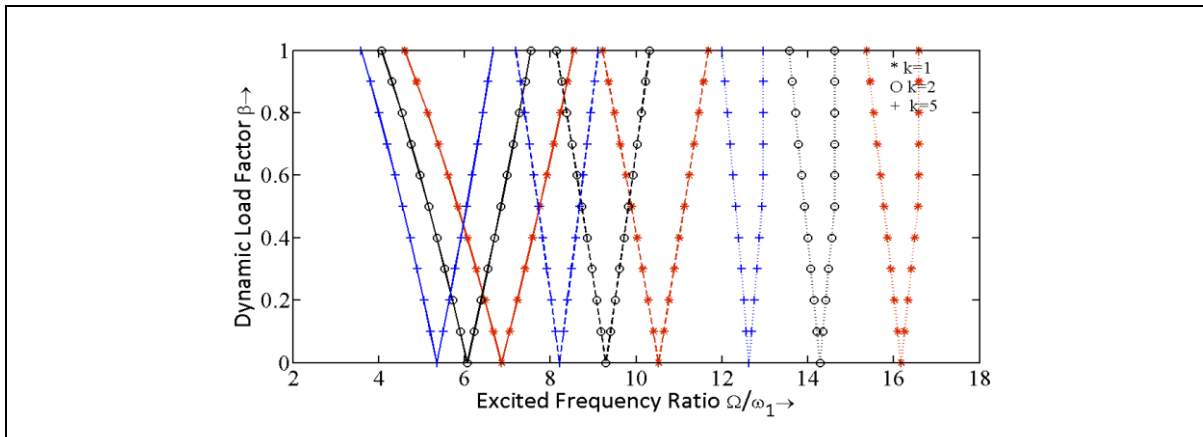
Figure 3.18 Stability regions for simply supported FGM plate under uniaxial loading with different index values, L/W=0.5, key as in fig. 3.15.
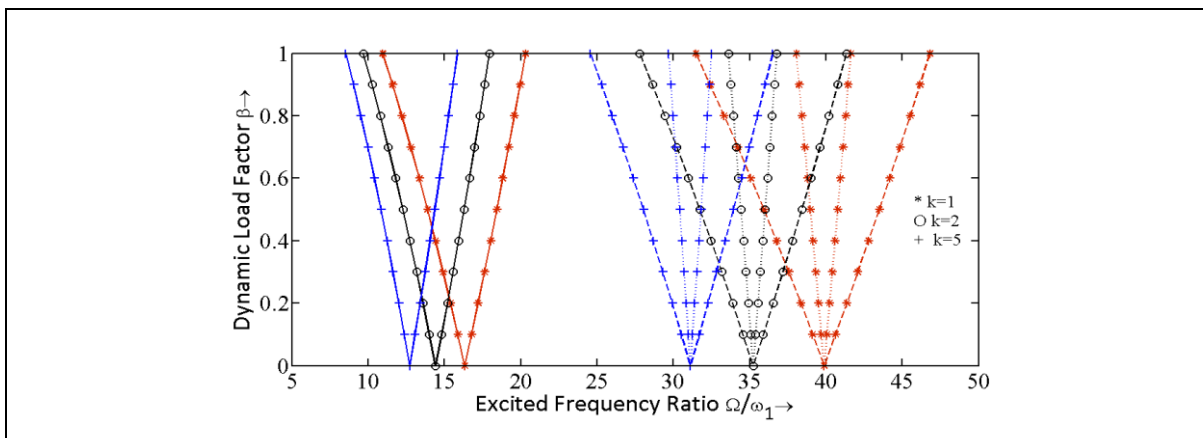
Figure 3.19 Stability regions for simply supported FGM plate under uniaxial loading with different index values, L/W=1, key as in fig. 3.15.
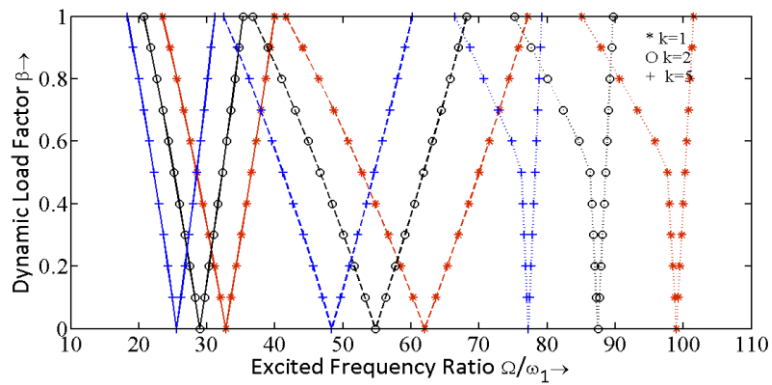
Figure 3.20 Stability regions for simply supported FGM plate under uniaxial loading with different index values, L/W=1.5, key as in fig. 3.15.

The effect of aspect ratio on the first three instability regions of simply supported plate subjected to biaxial loading are presented in figures 3.21-3.23. The unstable regions are relocated nearer to the dynamic load axis with increase of aspect ratio L/W. So increase of aspect ratio increases the probability of dynamic instability of FGM plate under biaxial periodic loads.
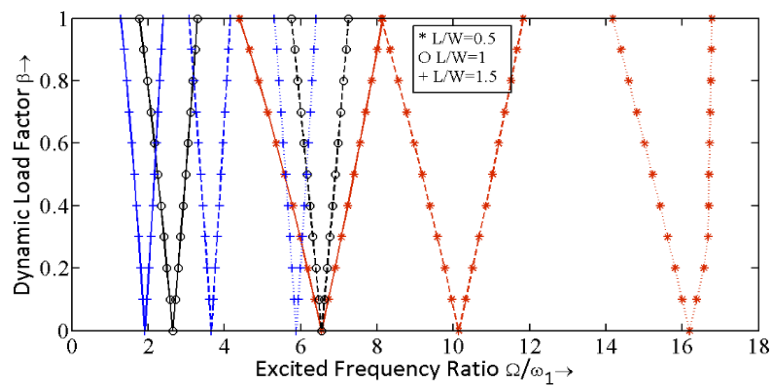
Figure 3.21 Stability regions for simply supported FGM plate under biaxial loading, k=1, key as in fig. 3.15.
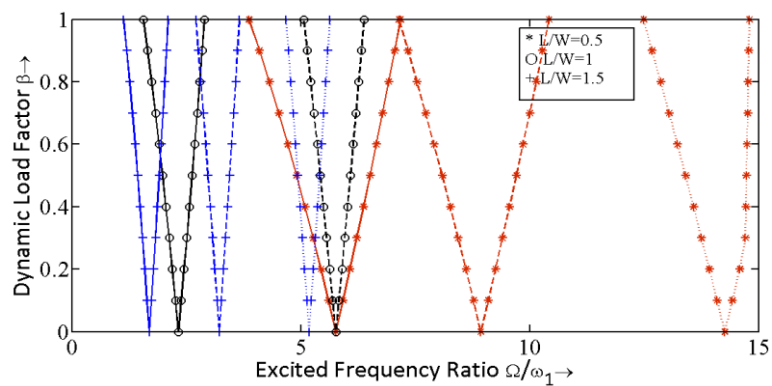
Figure 3.22 Dynamic stability regions for simply supported FGM plate under biaxial loading, k=2, key as in fig. 3.15.
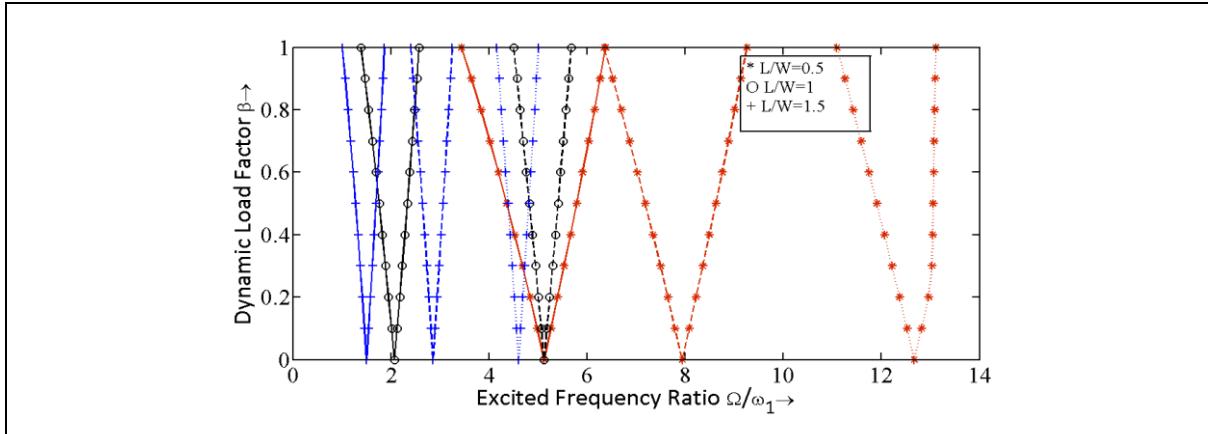
Figure 3.23 Dynamic stability regions for simply supported FGM plate under biaxial loading, k=5, key as in fig. 3.15.

The first three principal parametric instability regions of FGM plate of rectangular cross-section with various index values and aspect ratio under biaxial dynamic loading is examined through figures 3.24-3.26. The first three principal instability regions are shifted towards the dynamic load factor axis as the power law index increases from 1, 2 to 5, thereby enhancing the chance of parametric instability. As the value of power law index increases, the stiffness of the plate reduces and hence the excitation frequency to cause instability decreases, making the plate more prone to instability.
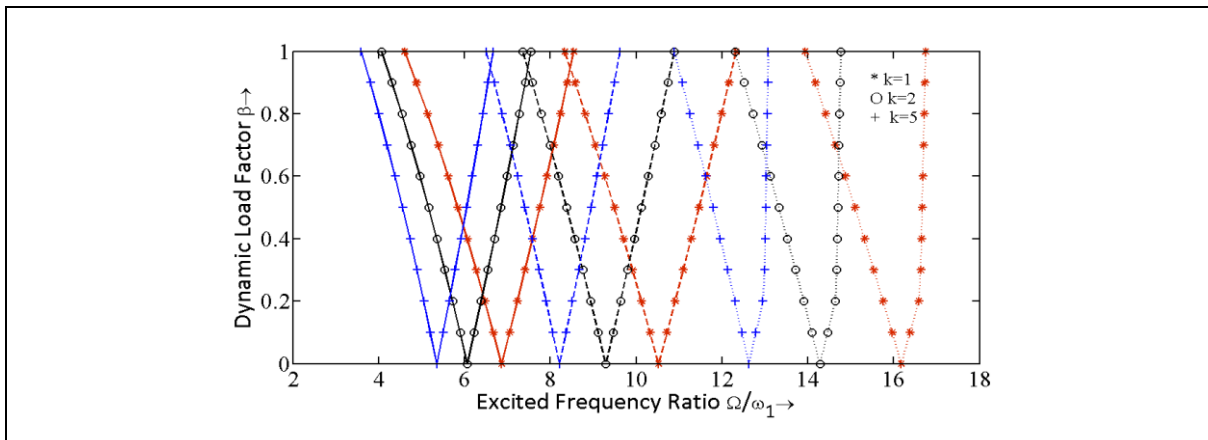
Figure 3.24 Dynamic stability of simply supported FGM plate under biaxial loading, L/W=0.5, key as in fig. 3.15.
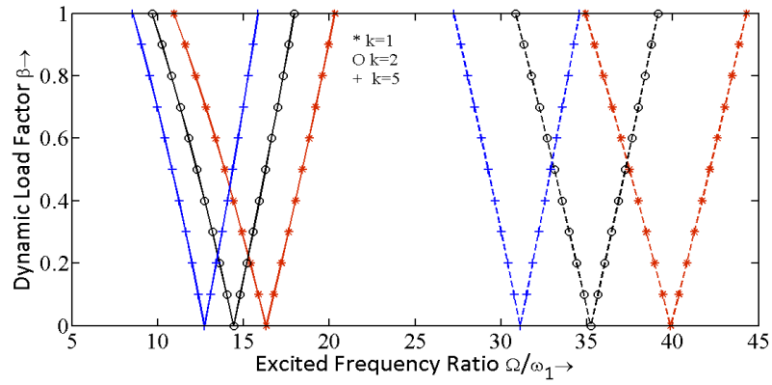
Figure 3.25 Dynamic stability of simply supported FGM plate under biaxial loading, L/W=1, '——' $2\omega_1$, '----' $2\omega_2$.
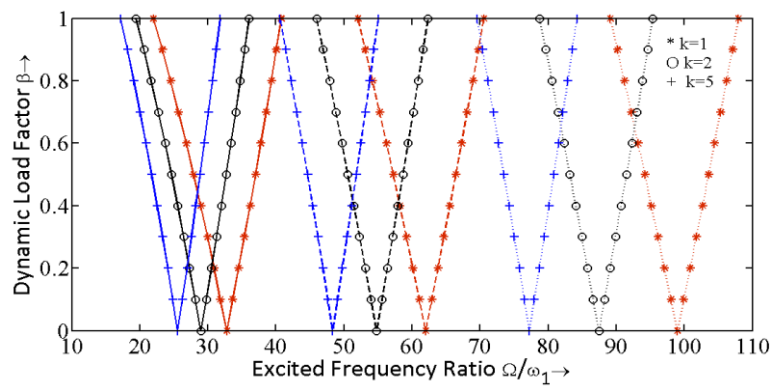
Figure 3.26 Dynamic stability of simply supported FGM plate under biaxial loading, L/W=1.5, key as in fig. 3.15.
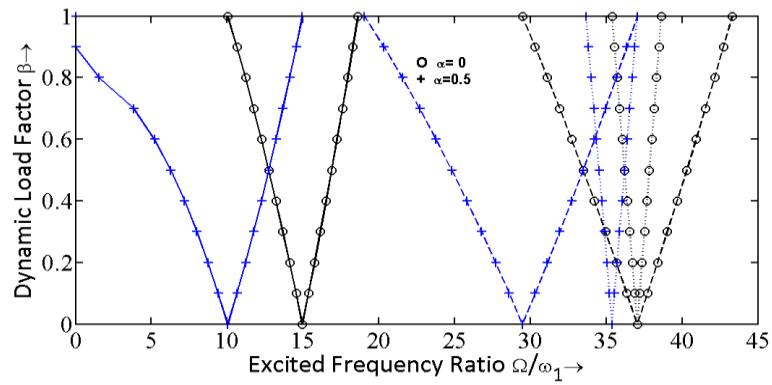
Figure 3.27 Dynamic stability diagram of simply supported FGM plate subjected to uniaxial loading for α=0 and 0.5, key as in fig. 3.15.

Figures 3.27 and 3.28 show the dynamic stability diagrams of simply supported FGM plate subjected to uniaxial and biaxial loading case respectively. Here the first two principal instability regions shift towards the dynamic load axis with an increase of static load factor α. The increasing static load factor reduces the stability of the FGM plate subjected to both uniaxial and biaxial loading case.

Figure 3.28 Dynamic stability diagram of simply supported FGM plate subjected to biaxial loading for α=0 and 0.5, key as in fig. 3.25.
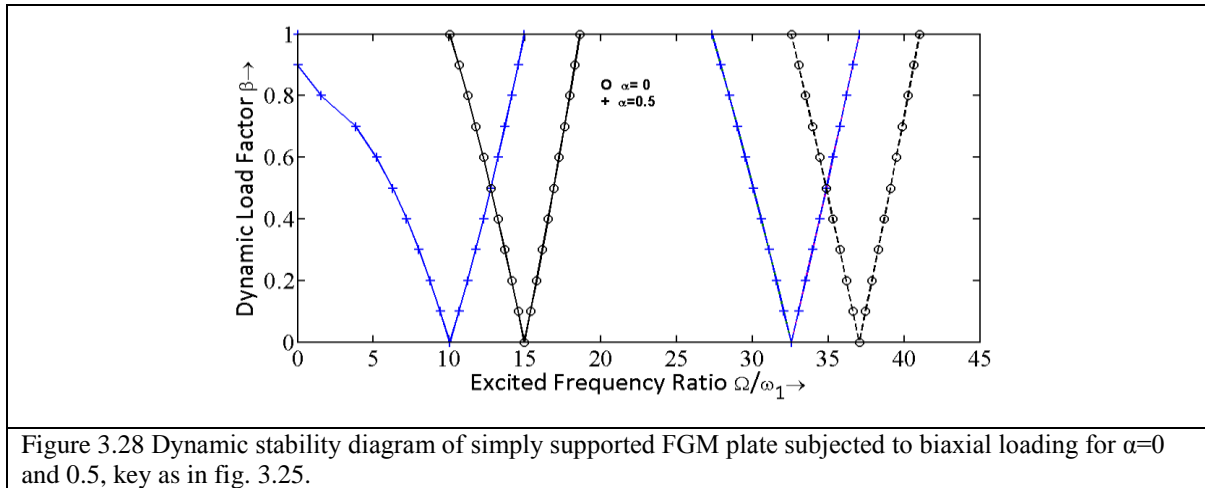
3.5 Conclusion

Finite element modelling of rectangular FGM plate has been developed using third order shear deformation theory. Based on the above formulation various types of analyses i.e. free vibration, buckling and dynamic stability have been carried out.

In case of FGM plate with increase of power law index value, the first five natural frequencies decrease. If aspect ratio is increased the critical buckling load decreases for uniaxial and biaxial loading and it is also observed that as the power law index value increases critical buckling load decreases.

Increase in aspect ratio of rectangular plate results in decrease of the stability of FGM plate for both uniaxial and biaxial loading cases. With increase of the power index value, instability regions moves closer to dynamic load axis with the different aspect ratios, it shows that there is deterioration of the dynamic stability. This happen both for uniaxial and biaxial dynamic loading. Increasing static load factor reduces the stability of simply supported FGM plate for both uniaxial and biaxial loading case.

Chapter 4

DYNAMIC STABILITY OF FUNCTIONALLY GRADED MATERIAL PLATES IN HIGH THERMAL ENVIRONMENT UNDER PARAMETRIC EXCITATION

4.1 Introduction

Functionally graded materials are advanced composite microscopically heterogeneous materials in which the mechanical properties vary smoothly and continuously along certain direction. This is achieved by gradually changing the volume fraction of the constituent materials. The main advantages of FGMs are diminished cracks and removal of the large inter laminar stresses at intersections between interfaces. The material properties of the FGM can be tailored to attain the specific requirements in different engineering applications in order to get the advantages of the properties of individual material. This is possible because the material composition of the FGM changes continuously in a preferred direction. In recent years, functionally graded material has become increasingly important especially in high temperature applications such as aerospace, nuclear reactors and power generation industries. FGM plate like structures may be subjected to periodically time-varying in-plane force, it may cause parametric resonance. Therefore understanding of the dynamic stability characteristics of FGM plates in thermal environments is important for the design of the structures.

Bouazza et al. [15] have studied buckling of FGM plate under thermal loads. Two types of thermal loads were assumed in this analysis namely; uniform temperature rise and linear temperature rise through the thickness. Talha and Singh [201] presented the thermo-mechanical buckling behaviour of FGM plate using higher order shear deformation theory. The proposed

structural kinematics assumed cubically varying in-plane displacement and quadratically varying transverse displacement through the thickness. Matsunaga [117] has presented the thermal buckling of temperature independent FG plates using a 2D higher-order shear deformation theory. Nuttawit et al. [137] investigated an improved third-order shear deformation theory for free and forced vibration response analysis of functionally graded plates. For this analysis, both temperature independent and dependent materials were considered. Leetsch et al. [98] studied the 3D thermo-mechanical behavior of functionally graded plates subjected to transverse thermal loads by a series of 2D finite plate elements. Young-Wann [232] found the analytical solution for the vibration characteristics of FGM plates under temperature field. The frequency equation was obtained using the Rayleigh–Ritz method based on the third-order shear deformation plate theory. Malekzadeh et al. [113] have investigated the free vibration of functionally graded thick annular plates subjected to thermal environment using the 3D elasticity theory.

As the importance of thermal resistance and strength in high temperature environment grows, the study on vibration and dynamic stability of FGM structures have actively progressed recently. Yang et al. [223] studied the dynamic stability of symmetrically laminated FGM rectangular plates with general out-of-plane supporting conditions subjected to a uniaxial periodic in-plane load and undergoing uniform temperature change. Previous studies on the dynamic stability of functionally graded material plates subjected to time-dependent compressive axial loads were mainly based on temperature independent material. It is evident from the available literature that the dynamic stability of temperature dependent FGM plate has not been thoroughly studied. In the present study, the dynamic stability behaviour of all side clamped and simply supported FGM plate in high temperature environment subjected to harmonically time-dependent in-plane force has been presented. Finite element method using four node rectangular elements has been used to model the FGM plate. Based on Bolotin's method the boundary frequencies of instability regions were determined. Also the free vibration and the buckling of the FGM plate were investigated as related problems.

4.2 Mathematical Modelling

4.2.1 Formulation of the Problem

Figure 4.1 shows the FGM plate subjected to thermal loading. The temperature of the plate varies along the thickness direction only as per certain rules, namely uniform, linear and non-linear temperature rise.
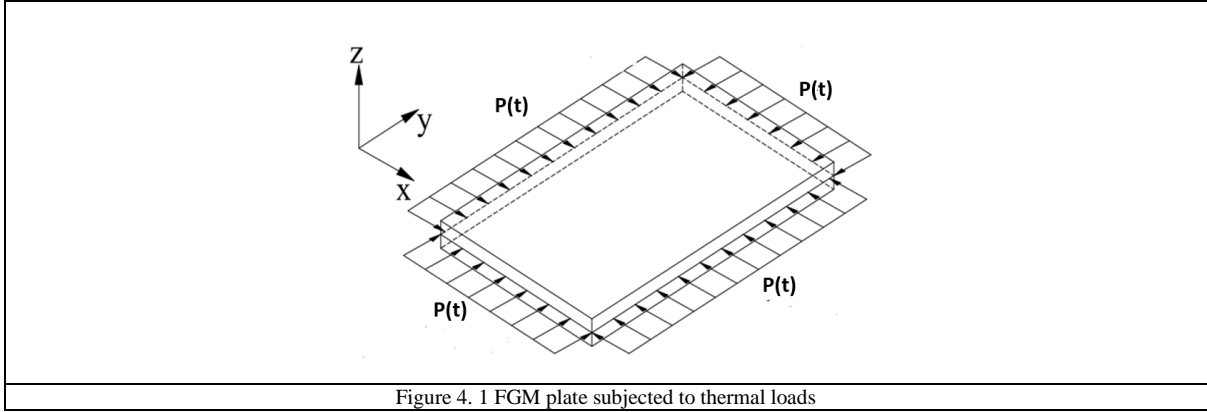
Figure 4. 1 FGM plate subjected to thermal loads

4.2.2 Functionally graded material plate constitutive law

A functionally graded material plate is made of metal and ceramic mixtures. The material composition is varied from the bottom surface to the top surface along thickness direction. The bottom surface ($z = -h/2$) of the plate is metal, whereas the top surface ($z = h/2$) is ceramic. The effective material property of FGM plate is needed for thermo-mechanical analysis. The effective material properties are calculated using a simple power law.

The effective material properties assumed to vary along the thickness direction of the plate can be expressed as

$$R(z) = R_c(z)V_c(z) + R_m(z)V_m(z) \tag{4.1}$$

where $R(z)$ represents the Young's modulus E, mass density ρ, Poisons ratio v, coefficient of thermal expansion ψ, moisture expansion coefficient Γ and thermal conductivity ζ of the temperature dependent FGM plate.

The volume fractions of the constituent materials, ceramic $V_c\ (z)$ and metal $V_m\ (z)$ at any location z from mid- plane are related as follows:

$$V_c(z) + V_m(z) = 1 \tag{4.2}$$

The volume fraction of the ceramic constituent material as per power law distribution can be written as

$$V_c = \left(\frac{1}{2} + \frac{z}{h}\right)^k, 0 \le k \le \infty \tag{4.3}$$

where k is the power law index, which prescribes the ceramic constituent material variation along the thickness direction of the plate.

The temperature dependent material properties are obtained using the following expression.

$$R(T) = P_0\left(P_{-1}T^{-1} + 1 + P_1T + P_2T^2 + P_3T^3\right) \tag{4.4}$$

where P_0, P_{-1}, P_2, and P_3 are the coefficients of temperature T in Kelvin and are unique to each constituent.

$T = T_0 + T(z)$, where $T(z)$ is temperature rise through the thickness direction and T_0 is room temperature.

From the above equations the effective material properties with two constituents for functionally graded material plates can be expressed as fallows

$$E(z,T) = E_m(T) + [E_c(T) - E_m(T)]\left(\frac{2z+h}{2h}\right)^k$$

$$\nu(z,T) = \nu_m(T) + [\nu_c(T) - \nu_m(T)]\left(\frac{2z+h}{2h}\right)^k$$

$$\psi(z,T) = \psi_m(T) + [\psi_c(T) - \psi_m(T)]\left(\frac{2z+h}{2h}\right)^k$$

$$\Gamma(z,T) = \Gamma_m(T) + [\Gamma_c(T) - \Gamma_m(T)]\left(\frac{2z+h}{2h}\right)^k \tag{4.5}$$

$$\rho(z) = \rho_m + [\rho_c - \rho_m]\left(\frac{2z+h}{2h}\right)^k$$

$$\zeta(z) = \zeta_m + [\zeta_c - \zeta_m]\left(\frac{2z+h}{2h}\right)^k$$

where the subscripts c and m represent ceramic and metal properties respectively. For the analysis, the temperature field is applied in the thickness direction only and the temperature field is assumed to be constant in the X Y plane of the plate.

4.2.3 Physical neutral surface of the FGM plate

In the present work neutral plane concept has been employed for the analysis. The distance (d) between the neutral plane to geometric mid-surface can be expressed by equation (3.6).

4.2.4 Thermal analysis

The behavior of FGM plate in thermal environments is considered for this study. The one dimensional temperature distribution through the thickness direction is assumed. In this case three thermal environments are considered: uniform, linear and nonlinear temperature distribution.

4.2.4.1 Uniform temperature distribution

In uniform temperature field, the temperature rise through the thickness is given as

$$T(z') = T_0 + \Delta T(z')$$ (4.6)

where $\Delta T(z') = T_c - T_m$ denotes the temperature gradient and $T_0 = 300K$ is room temperature.

T_c and T_m are temperature at ceramic surface and at metal surface respectively.

4.2.4.2 Linear temperature distribution

The variation of temperature distribution under linear rise through the thickness can be expressed as

$$T(z') = T_m + \Delta T(z')\left(\frac{z'}{h} + \frac{1}{2}\right)$$ (4.7)

4.2.4.3 Nonlinear temperature distribution

The one dimensional temperature distribution through the thickness direction is considered with $T = T(z')$. In order to obtain the temperature distribution along the thickness a steady-state heat transfer equation can be represented as

$$-\frac{d}{dz'}\left[\zeta(z')\frac{dT}{dz'}\right] = 0$$ (4.8)

where $\zeta(z')$ is the effective thermal conductive of the FGM.

This equation is solved by prescribing temperature at top and bottom surfaces such as

$T = T_c$ at $z' = h/2 - d$ and $T = T_m$ at $z' = -h/2 - d$.

The temperature rise through the thickness direction can be expressed as

$$T(z') = T_m + (T_c - T_m)\frac{\displaystyle\int_{-h/2-d}^{z'}\frac{1}{\zeta(z')}dz'}{\displaystyle\int_{-h/2-d}^{h/2-d}\frac{1}{\zeta(z')}dz'}$$ (4.9)

4.2.5 Constitutive relations

The stress-strain relationships of the FGM plate in the global x, y and z coordinate system, when there is a temperature change by ΔT can be written as

$$\begin{Bmatrix}\sigma_{xx}^T \\ \sigma_{yy}^T \\ \tau_{xy}^T\end{Bmatrix} = \begin{bmatrix}Q_{11} & Q_{12} & 0 \\ Q_{21} & Q_{22} & 0 \\ 0 & 0 & Q_{66}\end{bmatrix}\begin{Bmatrix}1 \\ 1 \\ 0\end{Bmatrix}\left(\psi(z',T)\Delta T(z')\right)$$ (4.10)

where $Q_{11} = Q_{22} = \dfrac{E(z',T)}{(1-\nu^2(z',T))}, Q_{12} = Q_{21} = \dfrac{\nu(z',T)E(z',T)}{(1-\nu^2(z',T))}, Q_{66} = \dfrac{E(z',T)}{2(1+\nu(z',T))}$

$\Delta T = T_c - T_m$, here T_m and T_c are reference temperature at metal surface and ceramic surface respectively. Also, ψ is the thermal expansion coefficient.

The in-plane force resultants, moments and higher order moments due to temperature rise are defined as

$$\left.\begin{aligned}
\begin{bmatrix} N_{xx}^T \\ N_{yy}^T \end{bmatrix} &= \int_{-h/2-d}^{h/2-d} \begin{bmatrix} \sigma_{xx}^T \\ \sigma_{yy}^T \end{bmatrix} dz' \\[6pt]
\begin{bmatrix} M_{xx}^T \\ M_{yy}^T \end{bmatrix} &= \int_{-h/2-d}^{h/2-d} \begin{bmatrix} \sigma_{xx}^T \\ \sigma_{yy}^T \end{bmatrix} z' dz' \\[6pt]
\begin{bmatrix} P_{xx}^T \\ P_{yy}^T \end{bmatrix} &= \int_{-h/2-d}^{h/2-d} \begin{bmatrix} \sigma_{xx}^T \\ \sigma_{yy}^T \end{bmatrix} z'^3 dz'
\end{aligned}\right\} \tag{4.11}$$

Substituting equation (4.10) in equation (4.11) yields the following relations

$$\begin{bmatrix} N^T \\ M^T \\ P^T \end{bmatrix} = \begin{bmatrix} [A^T] & [B^T] & [E^T] \\ [B^T] & [D^T] & [F^T] \\ [E^T] & [F^T] & [H^T] \end{bmatrix} \begin{Bmatrix} \varepsilon^{(n)T} \\ \varepsilon^{(1)T} \\ \varepsilon^{(3)T} \end{Bmatrix}, \tag{4.12}$$

The stiffness components are expressed as:

$$\begin{aligned}
& \left(A_{ij}^{\,T} \quad B_{ij}^{\,T} \quad D_{ij}^{\,T} \quad E_{ij}^{\,T} \quad F_{ij}^{\,T} \quad H_{ij}^{\,T} \right) \\
& = \int_{-h/2-d}^{h/2-d} Q_{ij} \left(\psi(z',T)\Delta T(z') \right) \left(1, z', z'^2, z'^3, z'^4, z'^6 \right) dz' \\
& (i, j = 1, 2)
\end{aligned} \tag{4.13}$$

The inplane strain-displacement relationship due to temperature change about neutral axis can written as

$$\{\varepsilon^{bT}\} = \begin{Bmatrix} \varepsilon_x^T \\ \varepsilon_y^T \end{Bmatrix} = \begin{Bmatrix} \varepsilon_x^{(n)T} \\ \varepsilon_y^{(n)T} \end{Bmatrix} + z' \begin{Bmatrix} \varepsilon_x^{(1)T} \\ \varepsilon_y^{(1)T} \end{Bmatrix} - z'^3 \begin{Bmatrix} \varepsilon_x^{(3)T} \\ \varepsilon_y^{(3)T} \end{Bmatrix} \tag{4.14}$$

$$\varepsilon^{(n)T} = \begin{Bmatrix} \varepsilon_x^{(n)T} \\ \varepsilon_y^{(n)T} \end{Bmatrix} = \begin{Bmatrix} u_{n,x} + w_{n,x} \\ v_{n,y} + w_{n,y} \end{Bmatrix},$$

$$\varepsilon^{(1)T} = \begin{Bmatrix} \varepsilon_x^{(1)T} \\ \varepsilon_y^{(1)T} \end{Bmatrix} = \begin{Bmatrix} \theta_{x,x} \\ \theta_{y,y} \end{Bmatrix},$$

$$\varepsilon^{(3)T} = \begin{Bmatrix} \varepsilon_x^{(3)T} \\ \varepsilon_y^{(3)T} \end{Bmatrix} = \begin{Bmatrix} \theta_{x,x} + w_{n,x} \\ \theta_{y,y} + w_{n,y} \end{Bmatrix}$$

The strain vector can be expressed in terms of nodal displacement vector $\{q^{(e)}\}$ as

$$\{\varepsilon^{bT}\} = [B_b^T]\{q^{(e)}\} \tag{4.15}$$

where $[B_b^T] = [B_0^T] + z'[B_1^T] + z'^3[B_2^T]$

$[B_0^T]$, $[B_1^T]$ and $[B_2^T]$ are defined as follows

$$[B_0^T] = \begin{bmatrix} \dfrac{\partial}{\partial x} & 0 & \dfrac{\partial}{\partial x} & 0 & 0 & 0 & 0 \\ 0 & \dfrac{\partial}{\partial y} & \dfrac{\partial}{\partial y} & 0 & 0 & 0 & 0 \end{bmatrix}[N], [B_1^T] = \begin{bmatrix} 0 & 0 & 0 & \dfrac{\partial}{\partial x} & 0 & 0 & 0 \\ 0 & 0 & 0 & 0 & \dfrac{\partial}{\partial y} & 0 & 0 \end{bmatrix}[N]$$

$$[B_2^T] = \begin{bmatrix} 0 & 0 & 0 & \dfrac{\partial}{\partial x} & 0 & \dfrac{\partial}{\partial x} & 0 \\ 0 & 0 & 0 & 0 & \dfrac{\partial}{\partial y} & 0 & \dfrac{\partial}{\partial y} \end{bmatrix}[N]$$

4.2.6. Finite Element Analysis

The element strain energy $\left(U_T^{(e)}\right)$ of the plate duo to thermal stresses is expressed as

$$U_T^{(e)} = \frac{1}{2}\int_0^b\int_0^a\left[[N^T]^T\{\varepsilon^{(n)T}\} + [M^T]^T\{\varepsilon^{(1)T}\} + [P^T]^T\{\varepsilon^{(3)T}\} \right]dxdy \tag{4.16}$$

Substituting equation (4.11) and (4.14) in equation (4.16), the element strain energy due to thermal stresses can be expressed as

$$U_T^{(e)} = \frac{1}{2}\left[\{q^{(e)}\}^T[K_T^{(e)}]\{q^{(e)}\} \right] \tag{4.17}$$

The element thermal stiffness matrix is expressed as

$$[K_T^{(e)}] = [K_{00}^{(e)T}] + [K_{11}^{(e)T}] + [K_{22}^{(e)T}] \tag{4.18}$$

$$\left.\begin{array}{l}\left[K_{00}^{(e)T}\right]=\int\limits_{0}^{a}\int\limits_{0}^{b}\left[B_{0}^{T}\right]^{T}\left[A^{T}\right]\left[B_{0}^{T}\right]dxdy \\[3mm] \left[K_{11}^{(e)T}\right]=\int\limits_{0}^{a}\int\limits_{0}^{b}\left[B_{1}^{T}\right]^{T}\left[D^{T}\right]\left[B_{1}^{T}\right]dxdy \\[3mm] \left[K_{22}^{(e)T}\right]=\int\limits_{0}^{a}\int\limits_{0}^{b}\left[B_{2}^{T}\right]^{T}\left[H^{T}\right]\left[B_{2}^{T}\right]dxdy\end{array}\right\}$$

Work done by the plate element due to external load is discussed in section 3.2. The geometric stiffness matrix $\left[K_{g}^{(e)}\right]$ considered for this analysis is given by equation (3.42).

$$\left[K_{g}^{(e)}\right]=\int\limits_{0}^{a}\int\limits_{0}^{b}\left[\left[N_{\partial w/\partial x}\right]^{T}\left[N_{\partial w/\partial x}\right]+\left[N_{\partial w/\partial y}\right]^{T}\left[N_{\partial w/\partial y}\right]\right]dx\,dy \tag{3.42}$$

4.3 Governing Equations of Motion

The equations of motion for a FGM plate element in thermo-mechanical environment is established by applying Hamilton's principle.

$$\delta\int\limits_{t_{1}}^{t_{2}}\left(U^{(e)}-T^{(e)}+W^{(e)}\right)dt=0 \tag{4.19}$$

The potential energy and the kinetic energy for plate element can be written in terms of displacement vector as

$$U^{(e)}=\frac{1}{2}\left\{q^{(e)}\right\}^{T}\left[K_{ef}^{(e)}\right]\left\{q^{(e)}\right\}-\frac{1}{2}\left\{q^{(e)}\right\}^{T}P(t)\left[K_{g}^{(e)}\right]\left\{q^{(e)}\right\} \tag{4.20}$$

$$T^{(e)}=\frac{1}{2}\left\{\dot{q}^{(e)}\right\}^{T}\left[M^{(e)}\right]\left\{\dot{q}^{(e)}\right\} \tag{4.21}$$

where $\left[K_{ef}^{(e)}\right]=\left[K^{(e)}\right]-\left[K_{T}^{(e)}\right]$

$\left[K_{ef}^{(e)}\right]$ is effective stiffness matrix and $\left[K^{(e)}\right]$, $\left[K_{T}^{(e)}\right]$, $\left[M^{(e)}\right]$ and $\left[K_{g}^{(e)}\right]$ are element stiffness matrix, thermal matrix $\left[K_{T}^{(e)}\right]$, mass matrix $\left[M^{(e)}\right]$ and $\left[K_{g}^{(e)}\right]$ geometric stiffness matrices respectively. The expressions for $\left[K^{(e)}\right]$, $\left[M^{(e)}\right]$ and $\left[K_{g}^{(e)}\right]$ are given by equations (3.31), (3.40) and (3.42) respectively in chapter 3.

The governing equation of motion of the axially loaded FGM plate element in matrix form can written as

$$\left[M^{(e)}\right]\left\{\ddot{q}^{(e)}\right\}+\left[K_{ef}^{(e)}\right]\left\{q^{(e)}\right\}-P(t)\left[K_{g}^{(e)}\right]\left\{q^{(e)}\right\}=0 \tag{4.22}$$

The governing equation of motion of the plate in terms of global displacement matrix can be obtained as follows

$$[M]\{\ddot{q}\} + [K_{ef}]\{q\} - P(t)[K_g]\{q\} = 0 \qquad (4.23)$$

where $P(t)$ is the time dependent dynamic load, can be represented in terms of static critical buckling load P^{cr} of metallic plate having similar applied boundary conditions. Hence substituting, $P(t) = P^{cr}(\alpha + \beta \cos \Omega t)$ with α and β as static and dynamic load factors respectively in equation (4.23). Equation (4.23) becomes

$$[M]\{\ddot{q}\} + [[K_{ef}] - P^{cr}(\alpha + \beta \cos \Omega t)[K_g]]\{q\} = 0 \qquad (4.24)$$

where $[K_{ef}] = [K] - [K_T]$

$[K_{ef}]$ is the global effective stiffness matrix and $[K], [K_T], [M]$ and $[K_g]$ are global elastic stiffness matrix, thermal matrix, mass matrix and geometric stiffness matrix respectively and $\{q\}$ is global displacement vector.

Referring to equation (3.54) of chapter 3, the condition for existence of the boundary solutions with period 2T is given by

$$\left([K_{ef}] - \left(\alpha \pm \frac{\beta}{2}\right)P^{cr} \times [K_g] - \frac{\Omega^2}{4}[M]\right)\{q\} = 0 \qquad (4.25)$$

The instability boundaries can be determined from the solution of the equation

$$\left| [K_{ef}] - \left(\alpha \pm \frac{\beta}{2}\right)P^{cr} \times [K_g] - \frac{\Omega^2}{4}[M] \right| = 0 \qquad (4.26)$$

Following the procedure described in section 3.3.1, the natural frequencies, critical buckling load and instability regions of FGM plate in high temperature thermal environment are determined.

4.4 Results and Discussion

4.4.1 Comparison study

To verify the present calculation method, the numerical results of clamped FGM (Si$_3$N$_4$/SUS304) square plates are compared with the available results in the literature.

Table 4.1 shows the temperature dependent material properties for this analysis. The plate has been discretized by 10X10 elements.

Table 4.1 Temperature dependent material properties [Reddy and Chin, [163]]

Materials		P_{-1}	P_0	P_1	P_2	P_3
Al_2O_3	E (Pa)	0	349.55×10^9	-3.853×10^{-4}	4.027×10^{-7}	-1.673×10^{-11}
	ψ (/K)	0	6.8269×10^{-6}	1.838×10^{-4}	0	0
	v	0	0.26	0	0	0
	ρ(kg/m³)	0	2700	0	0	0
Si_3N_4	E (Pa)	0	348.43×10^9	-3.070×10^{-4}	2.160×10^{-7}	-8.946×10^{-11}
	ψ (/K)	0	5.872×10^{-6}	9.065×10^{-4}	0	0
	v	0	0.24	0	0	0
	ρ(kg/m³)	0	2370	0	0	0
SUS304	E (Pa)	0	201.04×10^9	3.079×10^{-4}	-6.534×10^{-7}	0
	ψ (/K)	0	2.33×10^{-6}	8.086×10^{-4}	0	0
	v	0	0.3262	-2.002×10^{-4}	3.797×10^{-7}	0
	ρ(kg/m³)	0	8166	0	0	0

The dimensionless natural frequency parameter is defined as: $\varpi = \dfrac{\omega L^2}{\pi^2} \sqrt{\dfrac{I_0}{D_o}}$

where $I_0 = \rho h, D_0 = Eh^3/12(1-v^2)$. The material properties, ρ, E, and v are chosen to be the values of stainless steel (SUS304) at the reference temperature $T_0 = 300K$.

Table 4.2 shows the first five natural frequency parameters of clamped FGM (Si_3N_4/SUS304) plate. Present numerical experiment results are compared with the results of reference researchers Yang [222], Young [232] and Li et al. [99]. For this analysis the square plate with thickness to side ratio h/W=0.1 and power law index value k=2 is subjected to different uniform temperature distribution ($\Delta T = 0$, 300, $500 K$). Table 4.2 shows that present method results agree well with those of Yang [222], Young [232] and Li et al. [99].

Table 4. 2 Comparisons of first five natural frequency parameters for CCCC (Si_3N_4/SUS304) FGM plates under uniform temperature distribution (L=0.2 m, h/W=0.1, k=2, T_0=300⁰ K).

ΔT (K)	Source	ϖ_1	ϖ_2	ϖ_3	ϖ_4	ϖ_5
0	Yang [222]	4.1062	7.8902	7.8902	11.1834	12.5881
	Young[232]	4.1165	7.9696	7.9696	11.2198	13.1060
	Li et al.[99]	4.1658	7.9389	7.9389	11.1212	13.0973
	Present	4.0792	8.0195	8.0195	11.1770	13.8933
300	Yang [222]	3.6636	7.2544	7.2544	10.3924	11.7054
	Young [232]	3.6593	7.3098	7.3098	10.4021	12.1982
	Li et al.[99]	3.7202	7.3010	7.3010	10.3348	12.2256
	Present	3.6196	7.3580	7.3580	10.3559	12.9624
500	Yang [222]	3.2335	6.6281	6.6281	9.5900	10.8285
	Young [232]	3.2147	6.6561	6.6561	9.5761	11.2708
	Li et al.[99]	3.2741	6.6509	6.6509	9.5192	11.3126
	Present	3.1825	6.7173	6.7173	9.5450	11.5914
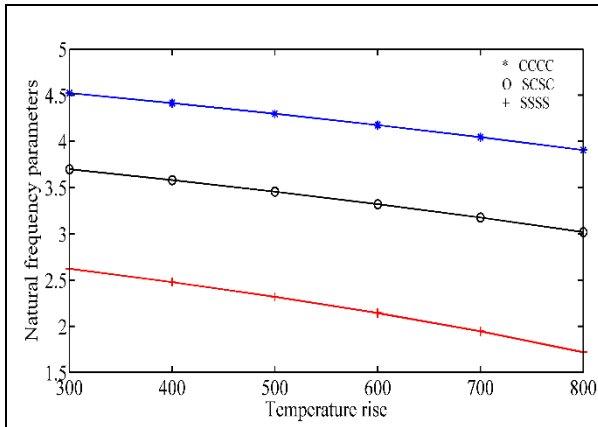
| Figure 4.2(a) Variation of first mode dimensionless frequency parameter of FGM plate in uniform temperature field for different boundary conditions, k=1. | Figure 4.2(b) Variation of second mode dimensionless frequency parameters of FGM plate in uniform temperature field for different boundary conditions, k=1. |

| Figure 4.3(a) Variation of first mode dimensionless frequency parameter of FGM plate in linear temperature field for different boundary conditions, k=1. | Figure 4.3(b) Variation of second mode dimensionless frequency parameter of FGM plate in linear temperature field for different boundary conditions, k=1. |
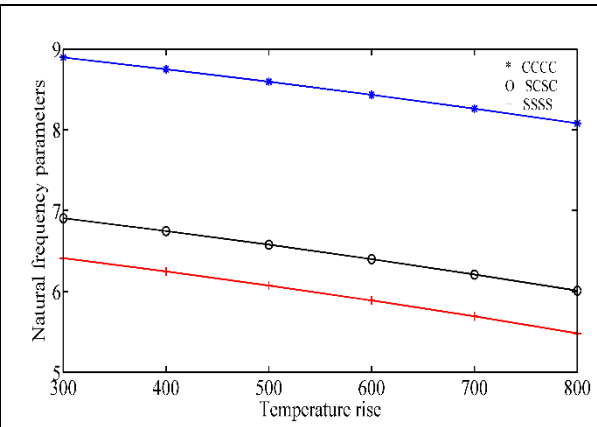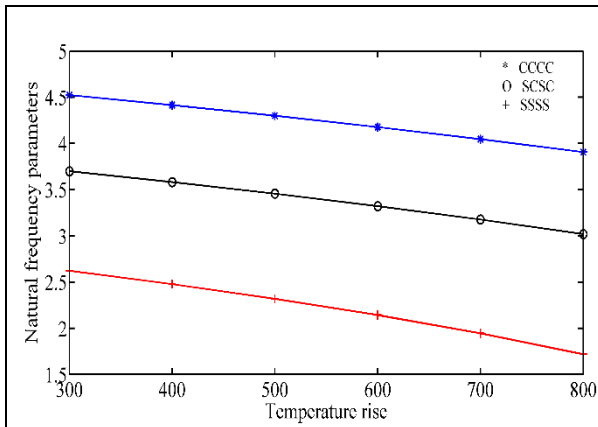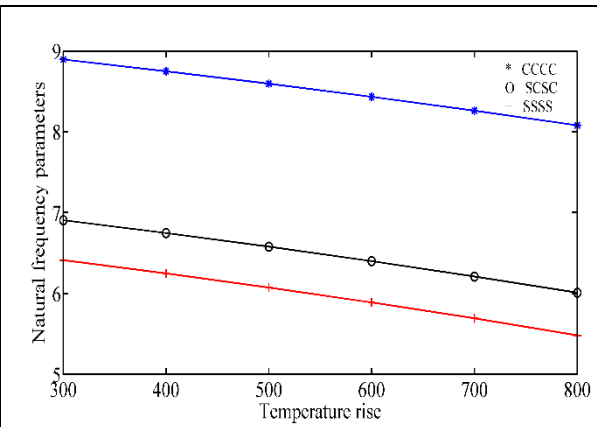
4.4.2 Natural frequency Analysis

For vibration and dynamic stability study a functionally graded material plate of (Al_2O_3/SUS304) of length 0.2 m, width 0.2 m and thickness ratio 0.025 m has been considered.

Figures 4.2 (a) and (b) depict the variation of dimensionless natural frequency parameters of FGM plate under uniform temperature environment for first and second mode respectively, with different boundary condition as mentioned in the figures. The effect of temperature rise on first and second mode dimensionless frequencies of FGM plates in linear temperature field are shown in figures 4.3 (a) and (b), respectively. Figure 4.4 (a) and (b) illustrate the effect of nonlinear temperature field on first and second mode dimensionless frequency parameters, respectively. It can be observed from these plots that increase in temperature decreases the first two mode frequencies in uniform, linear and nonlinear

temperature environments. It is also observed that the first two mode dimensionless frequencies of fully clamped FGM plate is the highest and that of SSSS plate is the lowest, in between is the SCSC corresponding to any thermal environment.

Figure 4.4(a) Variation of first dimensionless frequency parameters of FGM plate in nonlinear temperature field for different boundary conditions, k=1.	Figure4.4(b) Variation of second dimensionless frequency parameters of FGM plate in nonlinear temperature field for different boundary conditions, k=1.
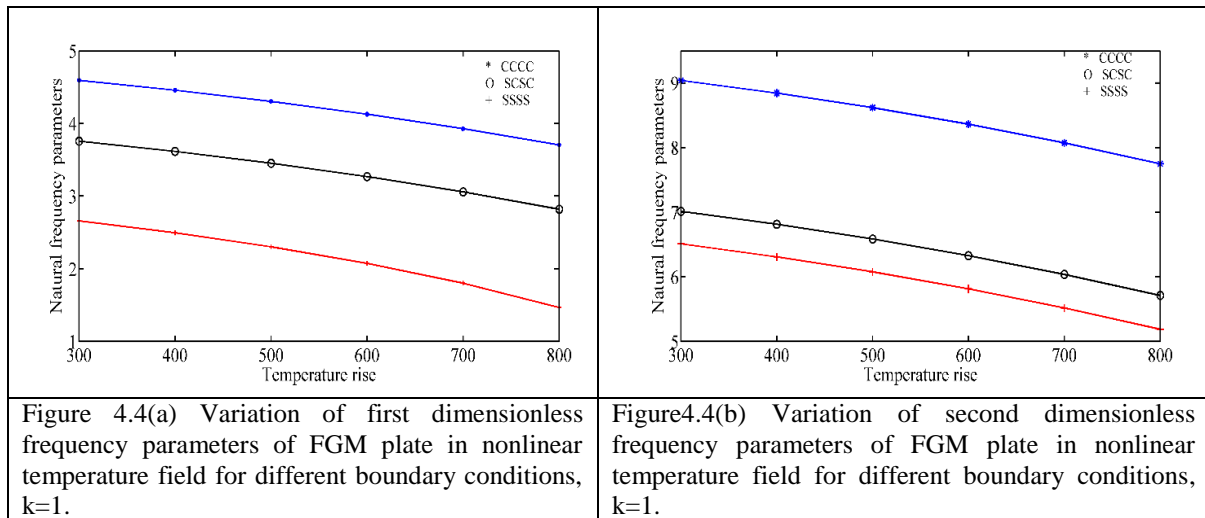
Figures 4.5 (a) and (b) display the first and second mode dimensionless frequency parameters versus temperature rise for SSSS (Al_2O_3/SUS304) FGM plates in different thermal environments respectively. The power law index is taken to be k=1, FGM plate subjected to uniform, linear, and nonlinear temperature distribution environments is considered. The uniform temperature change affects the natural frequencies considerably more than the linear and nonlinear temperature changes.

Figure 4.5(a) Variation of first mode frequency parameter of simply supported FGM plate with different temperature fields, k=1.	Figure 4.5(b) Variation of second mode frequency parameters of simply supported FGM plate with different temperature fields, k=1.
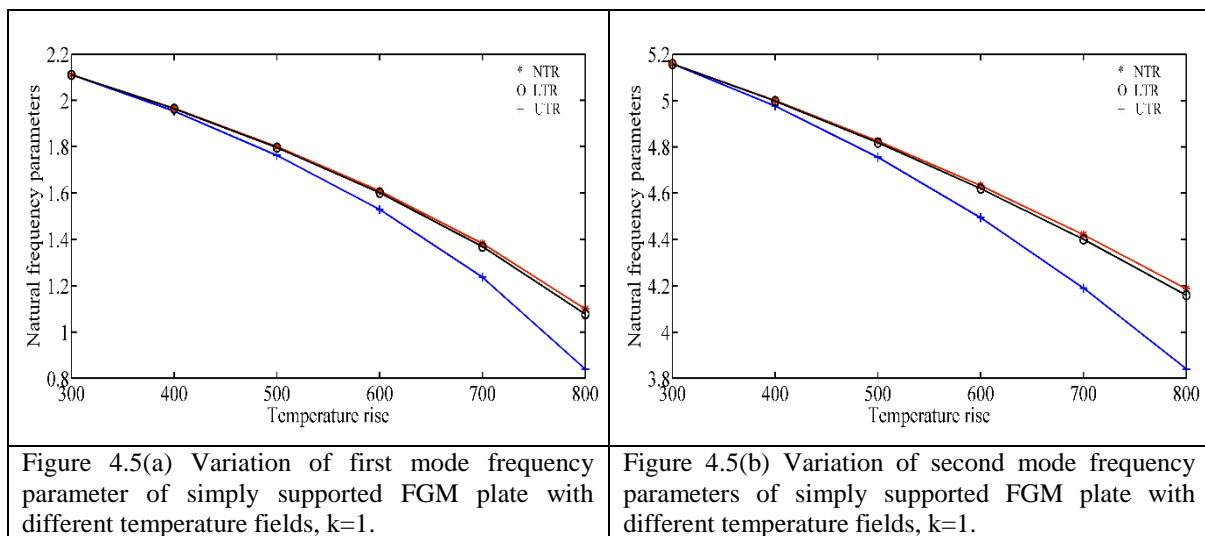
The variation of first and second mode dimensionless frequency parameters with temperature rise for a simply supported (SSSS) FGM plate in nonlinear thermal field for k=1 and 5 are plotted in figures 4.6 (a) and (b) respectively. It can be observed that the frequency for first two modes decrease with increase of index value and temperature also.

| Figure 4.6(a) Variation of first frequency parameter of simply supported FGM plate for index values k=1 and k=5. | Figure 4.6(b) Variation of second frequency parameter of simply supported FGM plate for index values k=1 and k=5. |
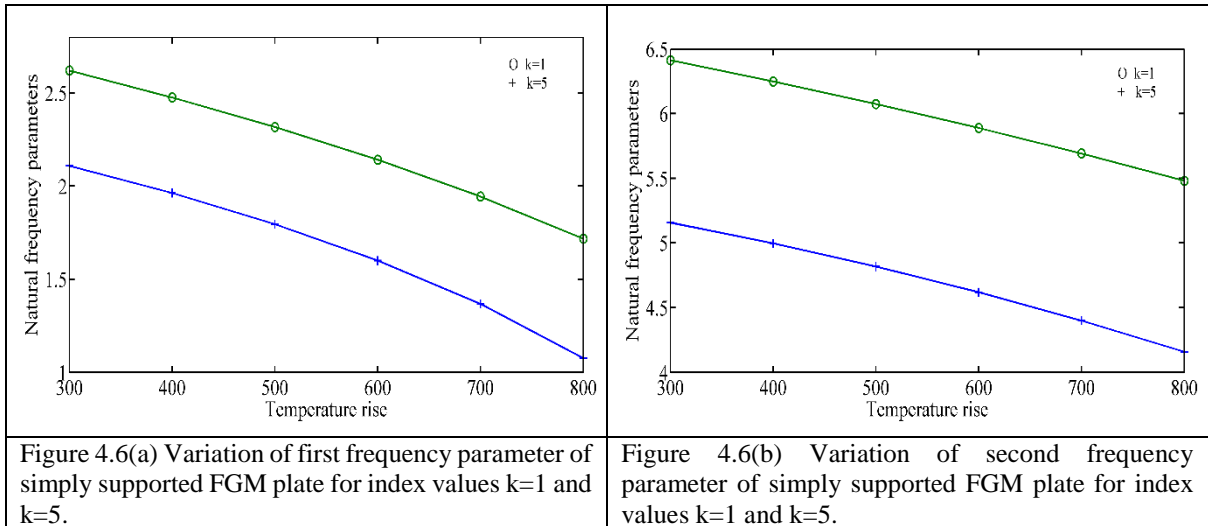
4.4.3 Dynamic stability analysis

Figures 4.7-4.9 display the dynamic stability behaviour of simply supported FGM plate under uniform temperature, linear temperature and nonlinear temperature distribution. The temperature rise causes the shitting of the stability regions towards the dynamic load factor axis, this indicates that the chances of system instability at lower excitation frequency is more and hence the dynamic stability is said to be deteriorated.

Figure 4.7 Dynamic stability diagram of simply supported FGM plate in uniform temperature field, k=5, '——' $2\omega_1$, '- - -' $2\omega_2$
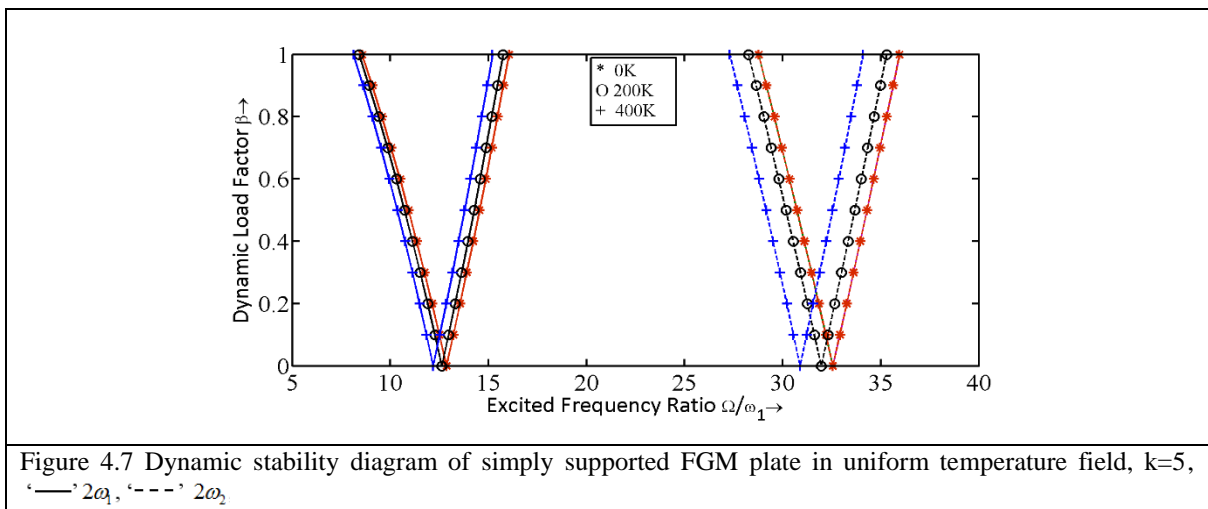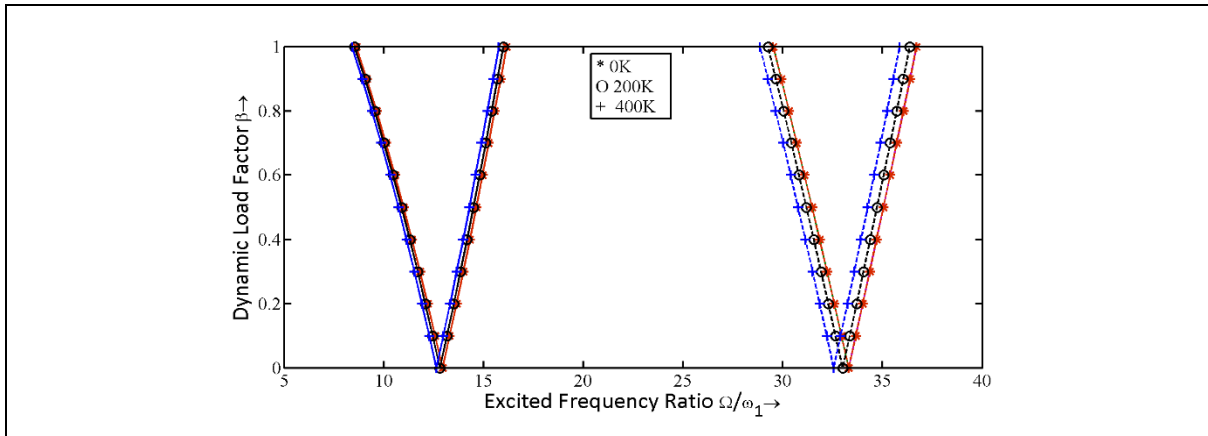
Figure 4.8 Dynamic stability diagram of simply supported FGM plate in linear temperature field, k=5, key as in fig. 4.7.
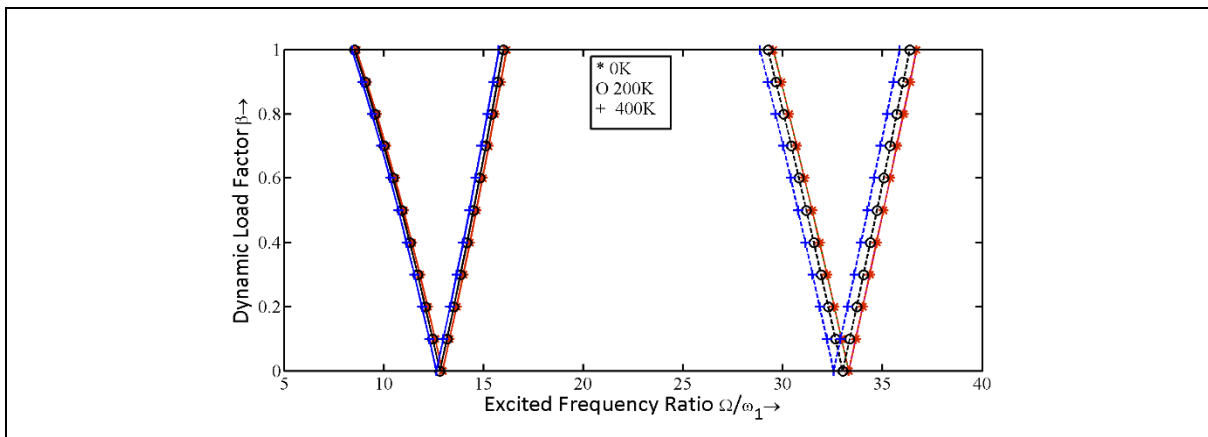
Figure 4.9 Dynamic stability diagram of simply supported FGM plate in nonlinear temperature field, k=5, key as in fig. 4.7.

Figures 4.10-4.12 illustrate the first two mode instability regions of all sides clamped FGM plate (k=5) for different temperature changes 0, 200 and 400 *K*. It is observed that in the presence of high temperature fields and increase in temperature, instability regions shift to lower excitation frequencies. When instability occurs at lower excitation frequency, the chance of occurrence of instability is more, hence with increase in environment temperature the instability of the plate increases. The increasing temperature degrades the structural strength of FGM plates, hence natural frequencies decrease. The reduced frequencies cause the shift of inability regions towards the lower excitation frequencies.
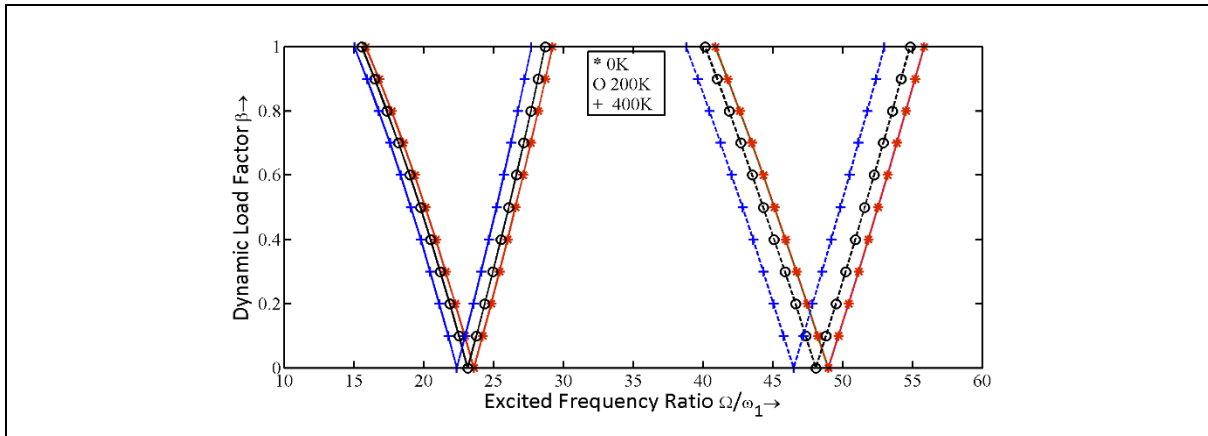
Figure 4.10 Dynamic stability diagram of fully clamped FGM plate in uniform temperature field, k=5, key as in fig. 4.7.
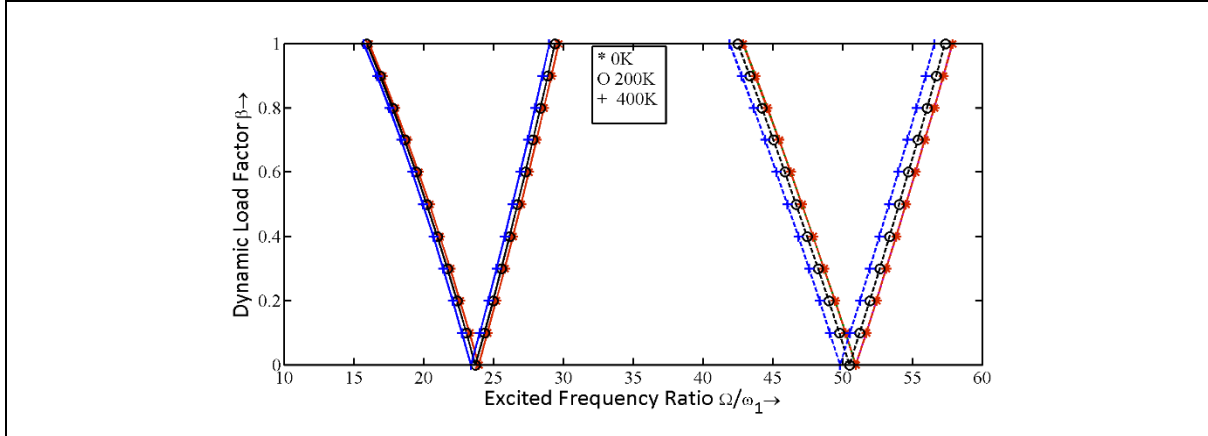
Figure 4.11 Dynamic stability diagram of fully clamped FGM plate in linear temperature field, k=5, key as in fig. 4.7.
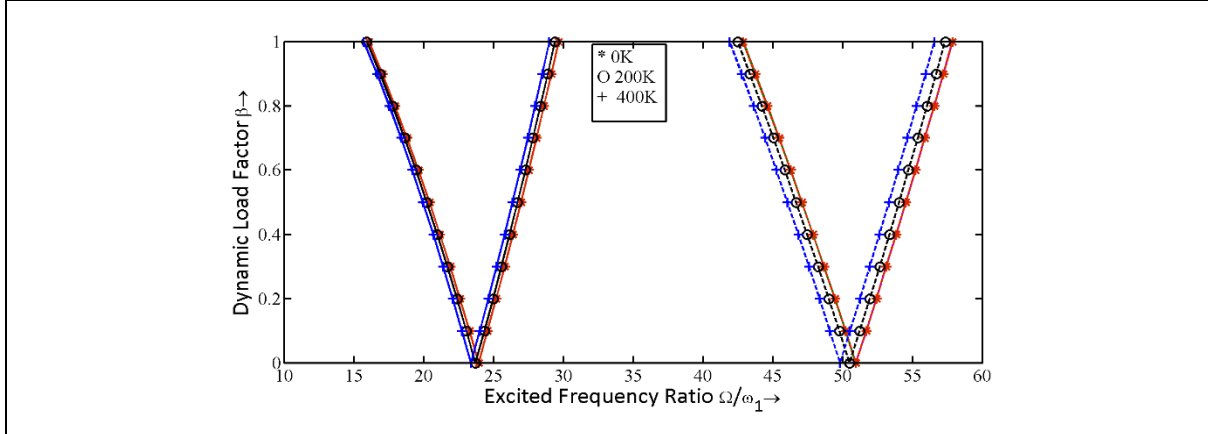
Figure 4.12 Dynamic stability diagram of fully clamped FGM plate in nonlinear temperature field, k=5, key as in fig. 4.7.

Figures 4.13 and 4.14 show the principal dynamic instability regions of simply supported and clamped FGM plates in thermal environments with uniform, linear and nonlinear temperature distribution respectively. The FGM plate with power law index k=5 and temperature change $200K$ is considered. The dynamic stability regions of FGM plate from Figures 4.13 and 4.14 illustrate that the temperature variation of uniform temperature type is more dominant than those of linear and nonlinear temperature distribution environments. It can

be observed that the effect of temperature rise on first principal instability region is less compared with the second principal instability region.
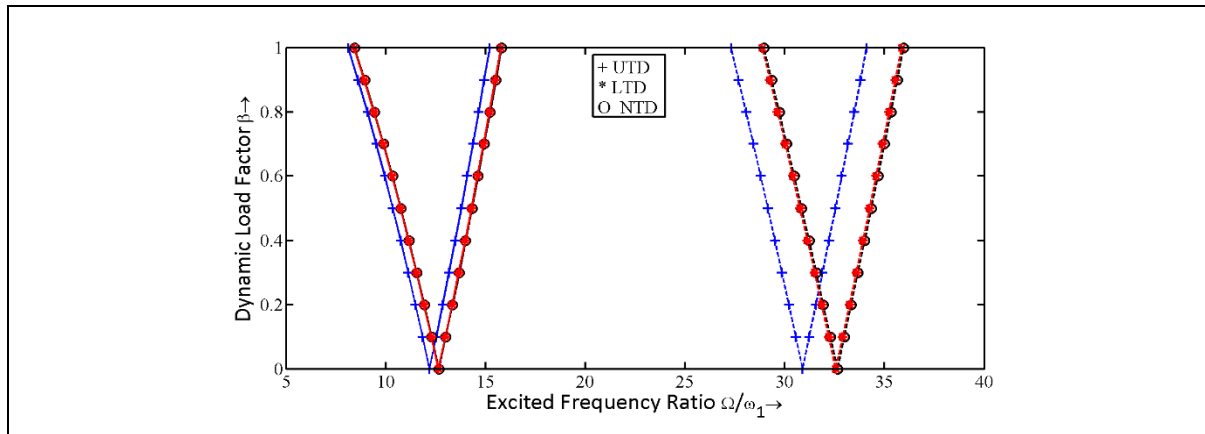
Figure 4.13 Dynamic stability diagram FGM plate with simply supported boundary conditions, k=5. $\Delta T = 200K$, key as in fig. 4.7
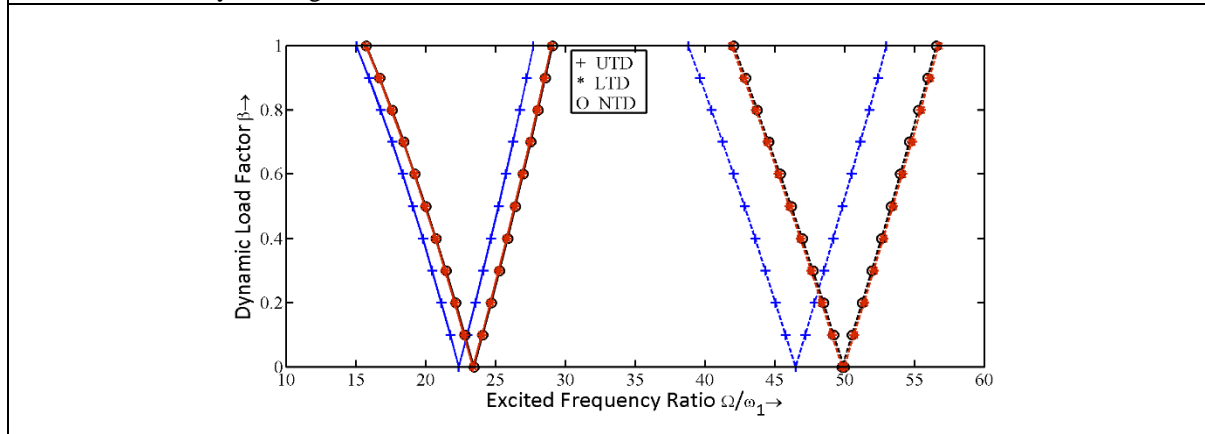
Figure 4.14 Dynamic stability diagram of FGM plate with fully clamped boundary conditions, k=5. $\Delta T = 200K$, key as in fig. 4.7.

Figure 4.15 shows the first two principal instability regions of simply supported FGM plate (k=1) and temperature rise 200*K*. It is observed that increase in thickness ratio (h/W) from 0.05 to 0.1 increases the stability of FGM plate in thermal environment. The first two instability regions shift away from the dynamic load axis when the thickness ratio increases. When instability regions shift to higher excitation frequencies, the dynamic stability is said to be enhanced, so increase of thickness of the plate enhances its dynamic stability.
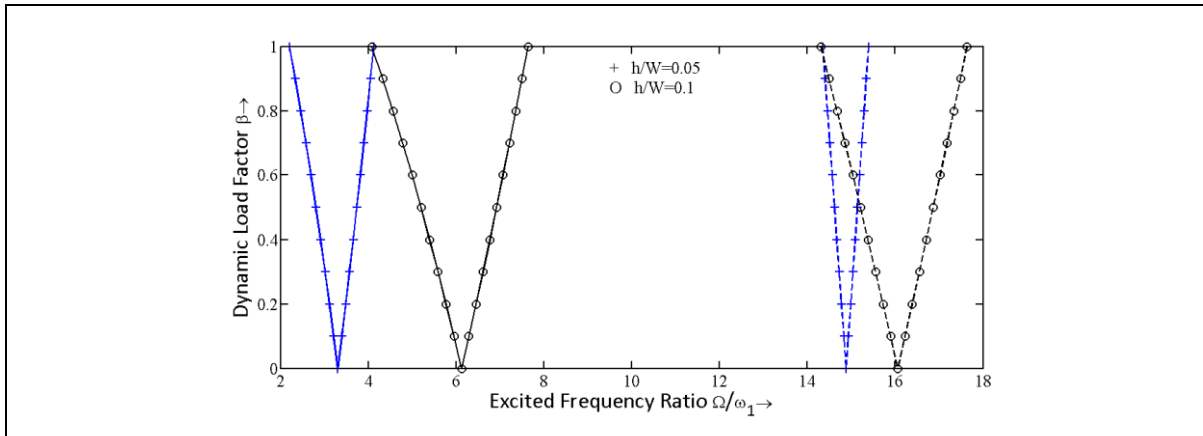
Figure 4.15 Dynamic stability diagram of simply supported FGM plate with thickness ratio h/W=0.05, 0.1, key as in fig. 4.7.
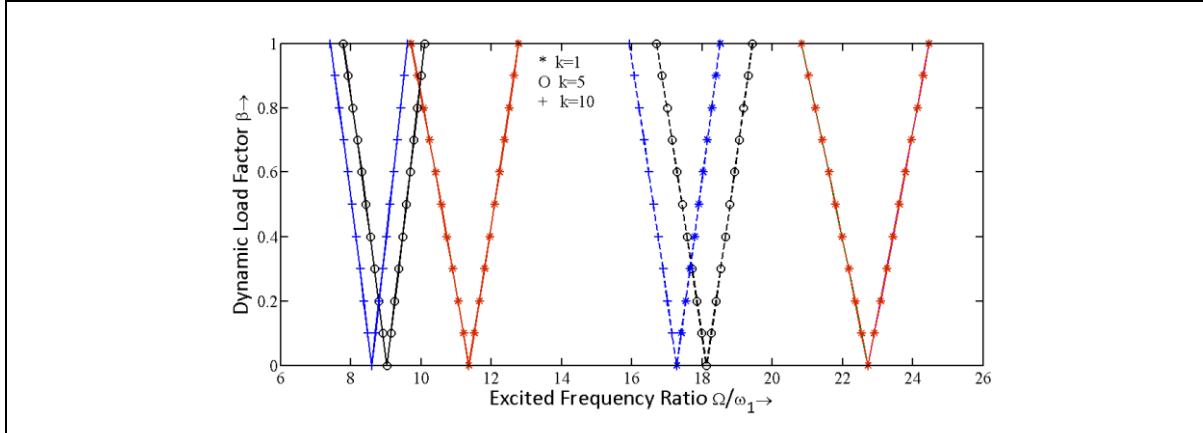
Figure 4.16 Dynamic stability diagram of simply supported FGM plate for different index values k=1, 5 and 10, key as in fig. 4.7.

The first two instability regions for temperature change $200K$ of a simply supported FGM plate with different index values k=1, 5 and 10 are shown in figure 4.16. The instability regions of FGM plate k=1 occur at higher excitation frequency. With increase of index value k=5 and 10, the instability regions move closer to the dynamic load factor axis. So with increase of index value the instability of the plate occurs at lower excitation frequencies and hence the stability of the FGM plate deteriorates with increase of power law index. With increase of power law index the natural frequencies of the plate reduce, this leads to the occurrence of instability at lower frequencies.

Figure 4.17 represents the first two mode instability regions of clamped FGM plate in thermal environment for different power law index values k=1, 5 and 10. The plate is exposed to an environment temperature change of $200K$. It is seen that the increase in power law index value reduces the stability of the FGM plate. The instability regions of FGM plate k=1 are located farthest from the dynamic load factor axis. Hence, it is most stable among the three cases. Similarly, the FGM plate k=5 and k=10 are respectively the intermediate and least stable plates.
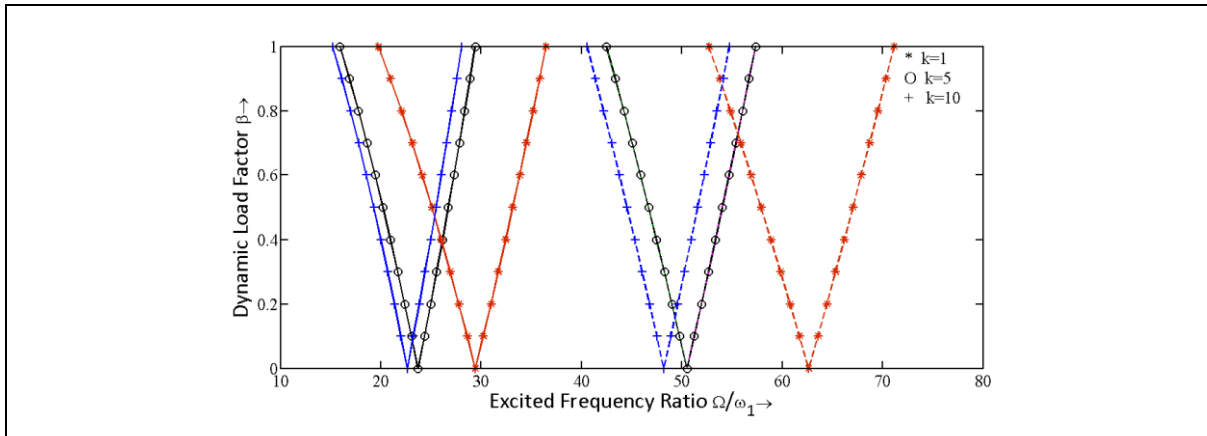
Figure 4.17 Dynamic stability diagram of clamped FGM plate for different index values k=1, 5 and 10, key as in fig. 4.7.

Figure 4.18 displays the first and second mode instability regions of FGM plate with simply supported and all sides clamped boundary conditions, k=1 and temperature change is 200 *K*. Plate with all sides clamped is more stable than simply supported condition. This is due to the fact that clamped end condition increases the rigidity of the plate compared to simply supported condition.
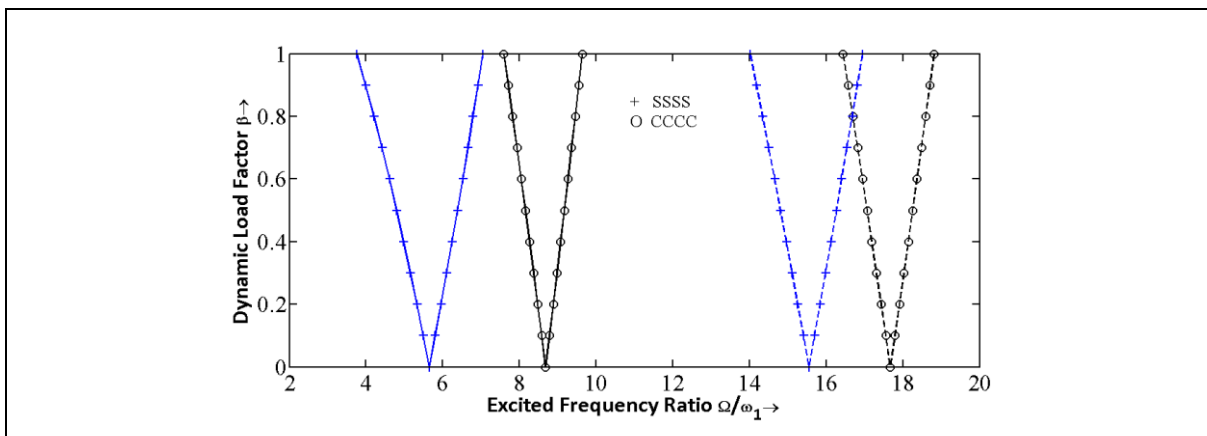
Figure 4.18 Dynamic stability FGM plate with simply supported and fully clamped boundary conditions. k=1, key as in fig. 4.7.

4.5 Conclusion

The free vibration and parametric instability characteristics of temperature dependent FGM plates in high temperature environment is investigated using finite element approach. Finite element model of a rectangular FGM plate has been developed using four node rectangular elements. The results are presented for FGM plates with different boundary conditions.

The FGM plate under uniform temperature, linear temperature and nonlinear temperature environment are considered. FGM plates in high temperature environment with the increase in temperature, the first two natural frequencies decrease. Increased temperature reduces the natural frequencies both for CCCC and SSSS plates. The natural frequencies are

found to be more sensitive to the uniform temperature change. The increase in index value reduces the natural frequencies of FGM plates in thermal environment.

Increase in environment temperature enhances the instability of simply supported and all sides clamped FGM plates. Lower values of power law index ensure better stability of FGM plates with simply supported and clamped boundary conditions compared to higher index values. The increase in index value reduces the stability of FGM plate for uniform, linear and nonlinear temperature distribution. The temperature rise reduces the stability of FGM plate in all the three thermal environments. All these factors contribute combinedly to the deterioration of dynamic stability of FGM plate under thermal environment.

Chapter 5

DYNAMIC STABILITY OF FUNCTIONALLY GRADED MATERIAL PLATES ON ELASTIC FOUNDATIONS UNDER PARAMETRIC EXCITATION

5.1 Introduction

Functionally graded material (FGM) plate structures resting on elastic foundation are extensively used in many engineering applications. Due to smooth distribution of material constituents, there is no abrupt change of stresses. These structural components like plates supported on an elastic foundation often find applications in the construction of nuclear, mechanical, aerospace, and civil engineering structures. These FGM plates can be subjected to external in plane periodic excitations, which may cause parametric resonance.

A few research papers have reported the dynamic stability of plates on elastic foundation. Hiroyuki [64] examined the two-dimensional higher-order theory for natural frequencies and buckling stresses of thick elastic plates resting on elastic foundations. Patel et al. [143] investigated the dynamic instability of laminated composite plates supported on elastic foundations, subjected to periodic inplane loads, using C^1 eight-noded shear-flexible plate element. Recent research works on vibration and buckling analysis, focus on the functionally graded material structures. Özdemir [140] developed a new fourth order finite element for thick plates resting on a Winkler foundation and the element was free from shear locking problem. A study of the literature reveals the existence of virtuous researches on buckling and free vibration analysis of FGM plates supported on elastic foundation.

From the literature review it seems that the dynamic stability of temperature dependent FGM plate supported on elastic foundation has not been studied. In the present work the dynamic stability of a FGM plate supported on Winkler and Pasternak foundations and subjected to uniform, linear and nonlinear thermal environment has been investigated. A four node finite element with seven degrees of freedom per node has been adopted to model the plate. Finite element method in conjunction with Hamilton's principle has been used to establish the governing equation. Third order shear deformation theory has been considered in the analysis. Floquet's theory has been used to establish the stability boundaries. Effects of different system parameters like foundation elastic constants, thickness ratio and power law index etc. on the dynamic stability behaviour of the FGM plate have been investigated.

5.2 Mathematical Formulation

The FGM plate of length L, width W, and thickness h, resting on elastic foundation and subjected to in-plane dynamic load is shown in figure 5.1. The plate is assumed to be subjected to biaxial in plane dynamic loading. The time varying load is $P(t) = P_s + P_t \cos \Omega t$. P_s is the static load component and P_t is the dynamic load component.

The plate with seven degrees of freedom assumed in this case is same as that shown in figure 3.4 and described in chapter 3. Neutral plane concept adopted and described in chapter 3 has also been adopted here. The element stiffness matrix, mass matrix and thermal stiffness matrix for FGM plate element derived in section 4.2 are also applicable in this case.

The effect of elastic foundation is introduced as elastic foundation stiffness matrix which is derived from the work done by the elastic foundation and is obtained as described below.
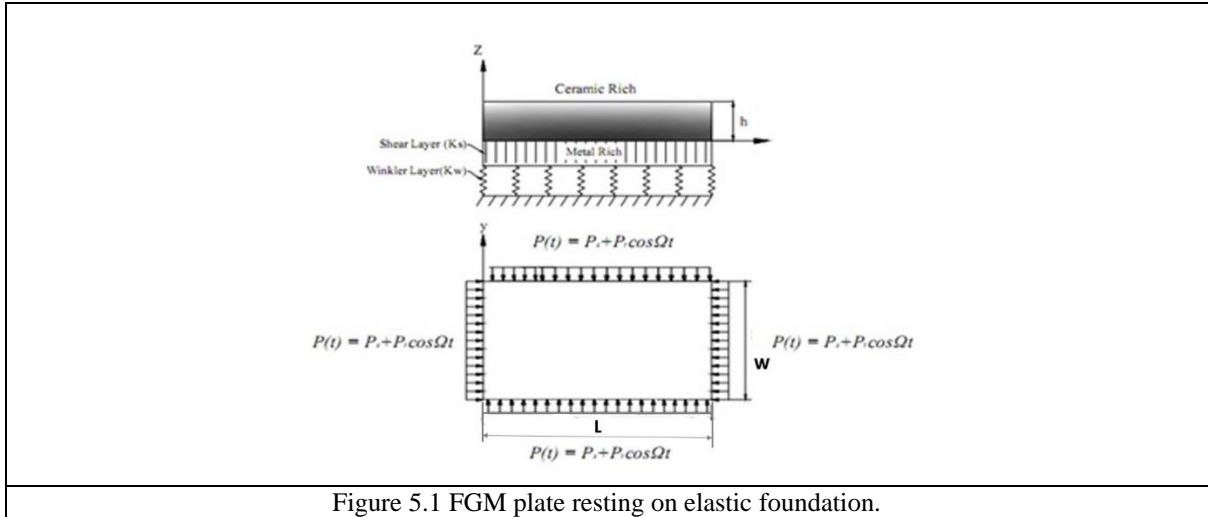
Figure 5.1 FGM plate resting on elastic foundation.

5.2.1 Energy equations

The strain energy of the foundation of plate element can be expressed as:

$$U_F^{(e)} = \frac{1}{2}\int_0^a\int_0^b\left[k_w w^2 + k_s\left(\left(\frac{\partial w}{\partial x}\right)^2 + \left(\frac{\partial w}{\partial y}\right)^2\right)\right]dxdy \tag{5.1}$$

where k_w is the Winkler foundation constant and k_s is the foundation shear layer constant.

5.2.2 Elastic foundation stiffness matrix

The Pasternak foundation element stiffness matrix $\left[K_F^e\right]$ is derived from the strain energy U_F^e of the foundation

$$U_F^{(e)} = \frac{1}{2}\int_0^a\int_0^b\left\{q^{(e)}\right\}^T\left[\left[k_w\left[N_w\right]^T\left[N_w\right]\right] + k_s\left[\left[N_{\partial w/\partial x}\right]^T\left[N_{\partial w/\partial x}\right] + \left[N_{\partial w/\partial y}\right]^T\left[N_{\partial w/\partial y}\right]\right]\right]\left\{q^{(e)}\right\}dx\,dy \tag{5.2}$$

$$= \frac{1}{2}\left[\left\{q^{(e)}\right\}^T\left[K_{wk}^{(e)}\right]\left\{q^{(e)}\right\}\right] + \frac{1}{2}\left[\left\{q^{(e)}\right\}^T\left[K_{sl}^{(e)}\right]\left\{q^{(e)}\right\}\right]$$

The element Winkler foundation stiffness $\left[K_{wk}^{(e)}\right]$ and shear foundation stiffness matrices $\left[K_{sl}^{(e)}\right]$ are expressed as

$$\left[K_{wk}^{(e)}\right] = k_w\int_0^a\int_0^b\left[N_w\right]^T\left[N_w\right]dx\,dy \tag{5.3}$$

$$\left[K_{sl}^{(e)}\right] = k_s\int_0^a\int_0^b\left[\left[N_{\partial w/\partial x}\right]^T\left[N_{\partial w/\partial x}\right] + \left[N_{\partial w/\partial y}\right]^T\left[N_{\partial w/\partial y}\right]\right]dx\,dy \tag{5.4}$$

The element foundation stiffness matrix is

$$\left[K_F^{(e)} \right] = \left[K_{wk}^{(e)} \right] + \left[K_{sl}^{(e)} \right] \tag{5.5}$$

5.3 Governing Equation of Motion

In order to derive the equations of motion of a plate element, section 3.3 can be suitably modified for the present case. Using equations (3.30), (3.39), (5.5) and (3.41) in equation (3.43) element equation of motion can be written as,

$$\left[M^{(e)} \right] \{ \ddot{q}^{(e)} \} + \left[K_{ef}^{(e)} \right] \{ q^{(e)} \} - P(t) \left[K_g^{(e)} \right] \{ q^{(e)} \} = 0 \tag{5.6}$$

where $\left[K_{ef}^{(e)} \right] = \left[K^{(e)} \right] + \left[K_F^{(e)} \right] - \left[K_T^{(e)} \right]$

$\left[K_{ef} \right]$ is effective stiffness matrix and $\left[K^{(e)} \right], \left[K_F^{(e)} \right]$ and $\left[K_T^{(e)} \right]$ are element stiffness matrix, Pasternak foundation stiffness matrix and element thermal matrix respectively. $P(t)$ can be written in terms of P^{cr}, here the fundamental static buckling load of an isotropic metallic plate, having same dimensions of the FGM plate considered. $P(t) = \alpha P^{cr} + \beta P^{cr} \cos \Omega t$ with α and β as static and dynamic load factors respectively.

The equation of motion of the plate on elastic foundation in global matrix form can be expressed as

$$[M]\{\ddot{q}\} + \left[\left[K_{ef} \right] - P^{cr} (\alpha + \beta \cos \Omega t) \left[K_g \right] \right] \{q\} = 0 \tag{5.7}$$

where $\left[K_{ef} \right] = \left[K \right] + \left[K_F \right] - \left[K_T \right]$

$\left[K_{ef} \right]$ is the effective global stiffness matrix and $[K], [K_T], [K_F], [M]$ and $\left[K_g \right]$ are global elastic stiffness matrix, thermal stiffness matrix, Pasternak foundation stiffness matrix, mass matrix and geometric stiffness matrix respectively and $\{q\}$ is global displacement vector.

The condition for existence of the boundary solutions with period 2T is given by

$$\left(\left[K_{ef} \right] - \left(\alpha \pm \frac{\beta}{2} \right) P^{cr} \times \left[K_g \right] - \frac{\Omega^2}{4} [M] \right) \{q\} = 0 \tag{5.8}$$

The instability boundaries can be determined from the solution of the equation

$$\left| \left[K_{ef} \right] - \left(\alpha \pm \frac{\beta}{2} \right) P^{cr} \times \left[K_g \right] - \frac{\Omega^2}{4} [M] \right| = 0 \tag{5.9}$$

Following the procedure described in section 3.3.1, the natural frequencies, critical buckling load and instability regions of FGM plate resting on elastic foundation can be determined.

5.4 Results and Discussion

5.4.1 Validation of the formulation

In this section, the validation of the present method is established using available results in the literature for fully simply supported FGM plates. For a square FGM (*Al/Al₂O₃*) plate, the natural frequency parameter (ϖ) values from the present work are compared with those of Baferani et al. [49], and are listed in Table 5.1. The result shows good agreement achieved between these works. The small variation may be due to the different shear deformation theories considered. Then, the results for free vibration analysis of FGM thick plates with SCSC boundary conditions supported on Pasternak foundation are presented in Table 5.2. The present numerical experiment results are verified with the results of the higher-order theory of Baferani et al. [49].

Table 5.1 The natural frequency parameter of FG square plate versus the shear and Winkler parameters, power law index and thickness–length ratio for simply supported boundary conditions. $\varpi = \omega h \sqrt{\rho_m / E_m}$

K_w	K_s	h/L	ϖ					
			k=0		*k=1*		*k=2*	
			Present	Baferani et al.[49]	Present	Baferani et al.[49]	Present	Baferani et al.[49]
0	0	0.05	0.0292	0.0291	0.0243	0.0227	0.0219	0.0209
		0.1	0.1137	0.1134	0.0946	0.0891	0.0855	0.0819
	100	0.05	0.0407	0.0406	0.0391	0.0382	0.0384	0.0380
		0.1	0.1602	0.1599	0.1543	0.1517	0.1518	0.1508
100	0	0.05	0.0299	0.0298	0.0252	0.0238	0.0230	0.0221
		0.1	0.1166	0.1162	0.0985	0.0933	0.0901	0.0867
	100	0.05	0.0412	0.0411	0.0397	0.0388	0.0391	0.0386
		0.1	0.1622	0.1619	0.1568	0.1542	0.1545	0.1535

Table 5.2 The natural frequency parameter of FG square plate versus the shear and Winkler parameters, power law index and thickness–length ratio for SCSC boundary conditions.

K_w	K_s	h/L	ϖ					
			$k=0$		$k=1$		$k=2$	
			Present	Baferani et al.[49]	Present	Baferani et al.[49]	Present	Baferani et al.[49]
0	0	0.05	0.0423	0.0421	0.0352	0.0324	0.0318	0.0295
		0.1	0.1594	0.1589	0.1326	0.1239	0.1198	0.1125
	100	0.05	0.0517	0.0515	0.0476	0.0457	0.0458	0.0443
		0.1	0.1977	0.1972	0.1829	0.1777	0.1764	0.1729
100	0	0.05	0.0428	0.0426	0.0359	0.0332	0.0326	0.0304
		0.1	0.1615	0.1609	0.1354	0.1268	0.1231	0.1161
	100	0.05	0.0521	0.0519	0.0481	0.0462	0.0463	0.0449
		0.1	0.1993	0.1988	0.1850	0.1799	0.1787	0.1751

5.4.2 Natural Frequency and buckling analysis

The side and thickness of square (SUS304/Al$_2$O$_3$) FGM plate are L=1 and h=0.1m, and the Winkler and shear layer constants are k$_w$=50 and k$_s$=50, respectively. Figures 5.2-5.4 illustrate the effect of temperature rise on the first two dimensionless natural frequency of simply supported FGM plate on elastic foundation for uniform, linear and nonlinear temperature thermal environments. It is perceived that the first and second mode dimensionless natural frequencies have decreasing tendency with increase in temperature and it is different for different thermal environments. A distinct decrease is observed for increase in index value, k=1, 2 and 5.
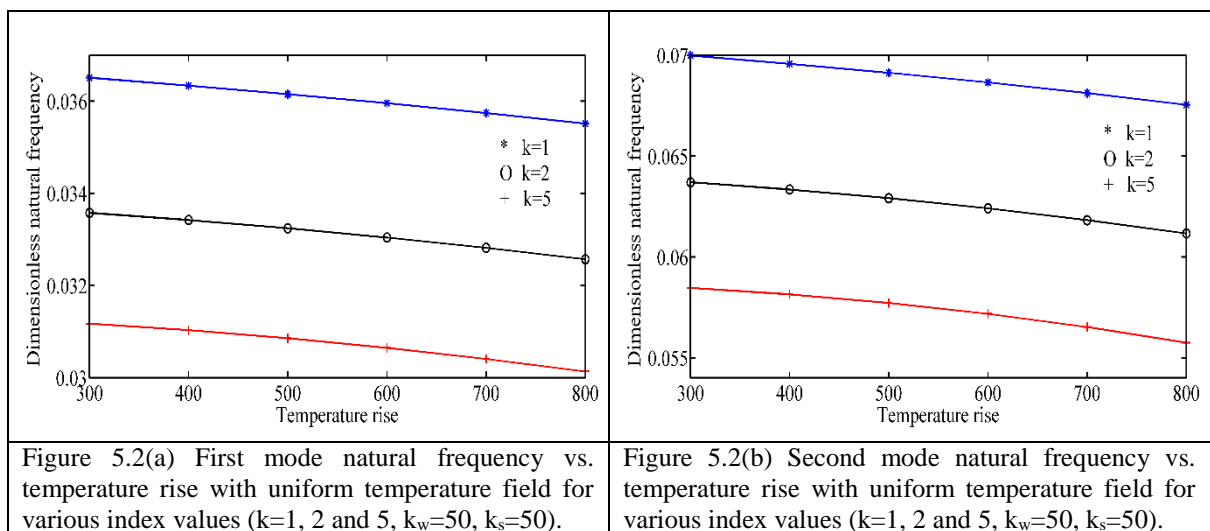
| Figure 5.2(a) First mode natural frequency vs. temperature rise with uniform temperature field for various index values (k=1, 2 and 5, k$_w$=50, k$_s$=50). | Figure 5.2(b) Second mode natural frequency vs. temperature rise with uniform temperature field for various index values (k=1, 2 and 5, k$_w$=50, k$_s$=50). |

| Figure 5.3(a) First mode natural frequency vs. linear temperature rise for various index values (k=1, 2 and 5, k_w=50, k_s=50). | Figure 5.3(b) Second mode natural frequency vs. linear temperature rise for various index values (k=1, 2 and 5, k_w=50, k_s=50). |

| Figure 5.4(a) First mode natural frequency vs. nonlinear temperature rise for various index values (k=1, 2 and 5, k_w=50, k_s=50). | Figure 5.4(b) Second mode natural frequency vs. nonlinear temperature rise for various index values (k=1, 2 and 5, k_w=50, k_s=50). |
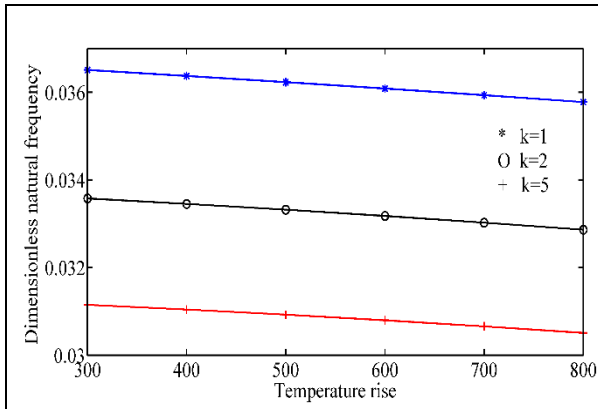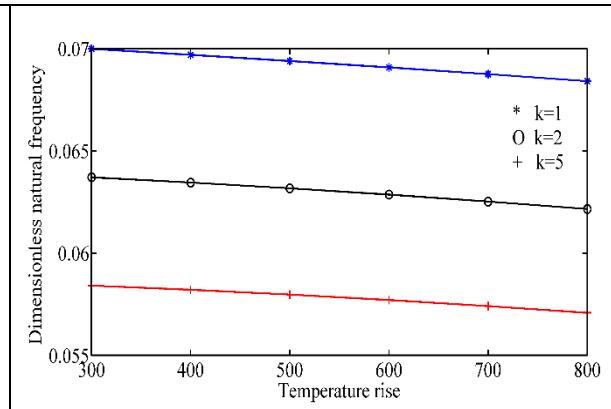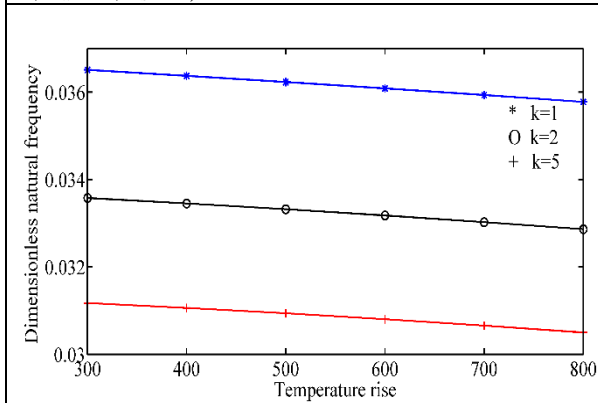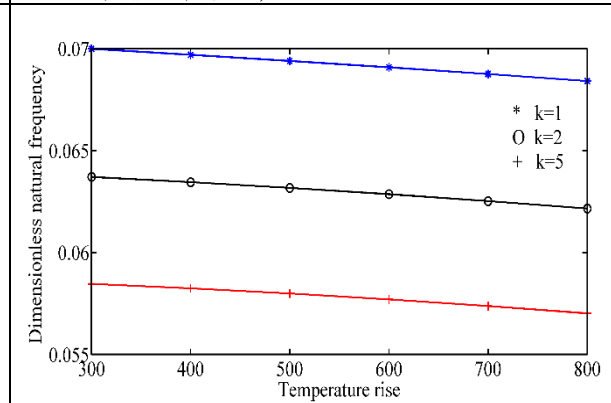
Figures 5.5 (a) and (b) display the effect of temperature rise on first and second mode dimensionless natural frequency for FGM plate k=5 on elastic foundation for different thermal environments, respectively. It is observed that the effect of temperature variation of uniform type on natural frequencies is more pronounced than linear and nonlinear temperature distribution.
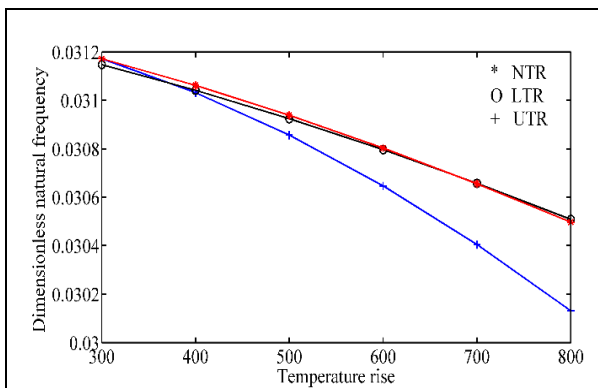
| Figure 5.5(a) First mode natural frequency vs. temperature rise for different thermal environments uniform, linear and nonlinear temperature fields (k= 5, k_w=50, k_s=50). | Figure 5.5(b) Second mode natural frequency vs. temperature rise for different thermal environments uniform, linear and nonlinear temperature fields (k= 5, k_w=50, k_s=50). |
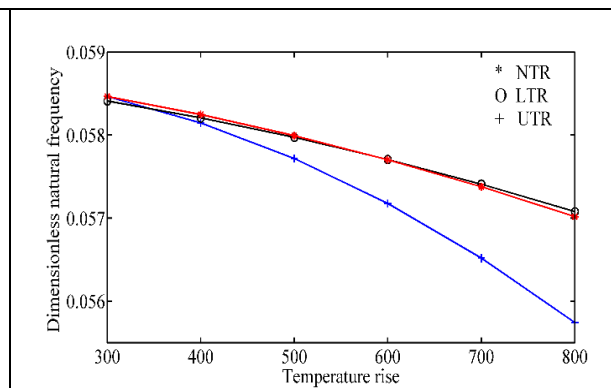
The first and second mode natural frequency parameter variation with the thickness ratio (h/L) for different values of Winkler foundation constant is shown in figures 5.6 (a) and (b), respectively. It can be seen that with increase in thickness ratio, the natural frequencies increase. With the increase in thickness of the plate there is relative increase in stiffness of the plate, which results in higher natural frequencies.

| Figure 5.6(a) First mode natural frequency vs. thickness ratio for different Winkler coefficients (k_w=0, 100 and 500, k_s=50, k=1). | Figure 5.6(b) Second mode natural frequency vs. thickness ratio for different Winkler coefficients (k_w=0, 100 and 500, k_s=50, k=1). |
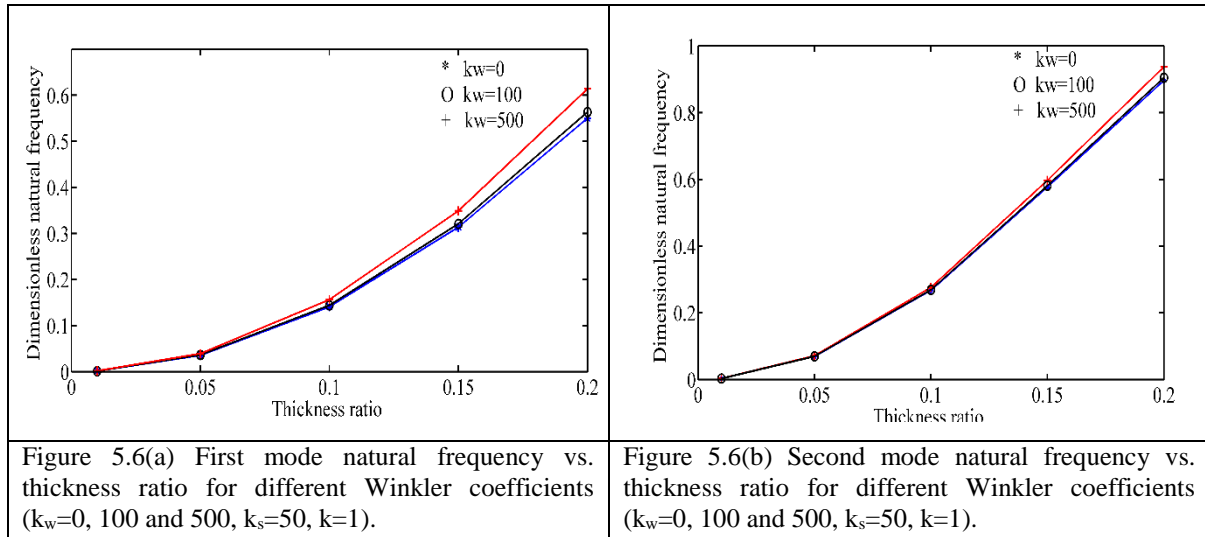
Figure 5.7 (a) illustrates the variation of first mode natural frequency with thickness ratio for the Winkler foundation constant (k_w=50) and different values of shear layer constant (k_s=0, 100 and 500). It can be observed that the frequency increase with increase in thickness ratio for various shear layer constant values. Figure 5.7 (b) represents the effect of thickness ratio on second mode natural frequency of FGM plate. The second mode natural frequency also exhibits an increasing tendency with increase in thickness ratio.

| Figure 5.7(a) First mode natural frequency vs. thickness ratio for different Winkler coefficients (k_s=0, 100 and 500, k_w=50, k=1). | Figure 5.7(b) Second mode natural frequency vs. thickness ratio for different Winkler coefficients (k_s=0, 100 and 500, k_w=50, k=1). |
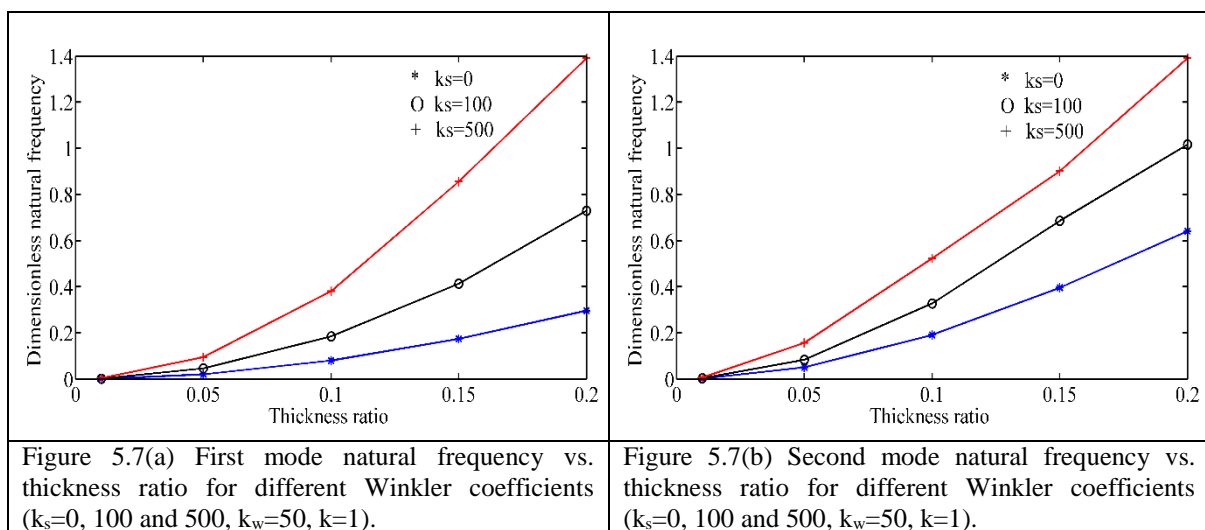
Figure 5.8(a) and (b) show the effect of Winkler foundation constant on natural frequency of FGM plate for first and second mode, respectively. The Winkler foundation

constant varies from 0 to 500. It can be observed that the first two mode natural frequencies increase as the Winkler foundation constant increases. The increase of index value reduces the frequency parameter.

| Figure 5.8 (a) Effect of Winkler constant on first mode frequency parameters (k_s=50, ΔT =200 K). | Figure 5.8(b) Effect of Winkler constant on second mode frequency parameters (k_s=50, ΔT =200 K). |
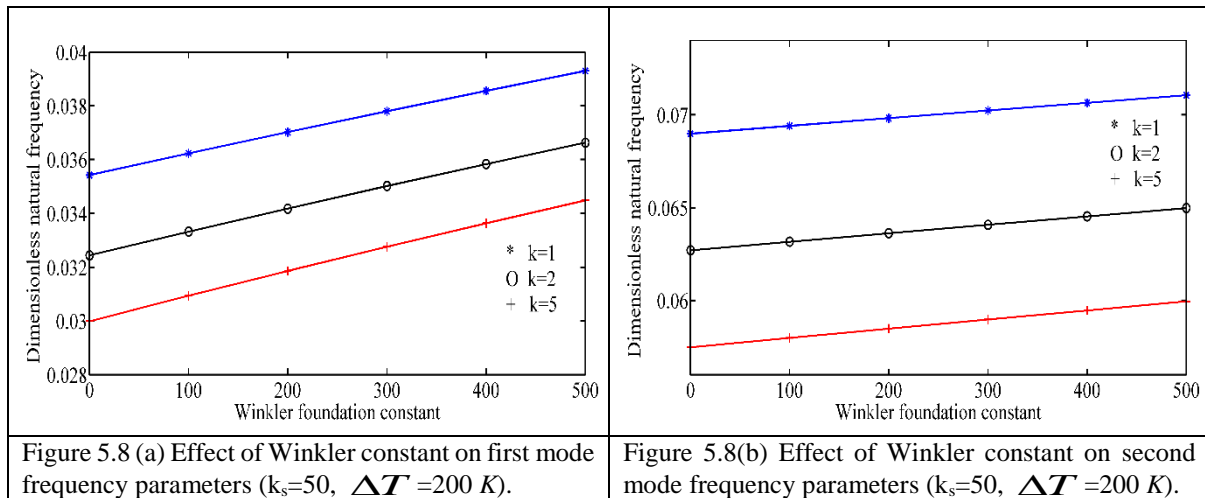
Figures 5.9(a) and (b) describe the effect of shear layer constant on the first two mode natural frequencies for different values of power law index k=1, 2 and 5, respectively. Figure 5.9, depicts that the natural frequency of FGM plate increases with the increase in the value of shear layer constant. This tendency is observed because effective stiffness becomes higher as the shear layer constant increases and consequently, the larger effective stiffness increases the natural frequencies.

| Figure 5.9(a) Effect of shear layer constant on first mode frequency parameters (k_w=50, ΔT =200 K). | Figure 5.9(b) Effect of shear layer constant on second mode frequency parameters (k_w=50, ΔT =200 K). |

Figure 5.10(a) Effect of Winkler constant on critical buckling load for various index values (k=1, 2 and 5, ΔT =200K). (k$_s$=50)	Figure 5.10(b) Effect of shear layer constant on critical buckling load for various index values (k=1, 2 and 5, ΔT =200K). (k$_w$=50)

The effect of elastic foundation parameters on critical buckling load of biaxially loaded simply supported FGM plate under nonlinear temperature rise is depicted in figure 5.10. It can be observed that increasing the Winkler foundation constant increases the critical buckling load of the FGM plate for various index values k=1, 2 and 5 as shown in figure 5.10 (a). The buckling load increases by increasing the shear layer constant as illustrated in figure 5.10(b). It is observed that the increase in power law index value reduces the critical buckling load.

5.4.3 Dynamic stability analysis

The fundamental natural frequency and the critical buckling load of simply supported steel plates are calculated from equations (3.39) and (3.40) respectively without considering foundation. For the dynamic stability study of FGM plate on elastic foundation these parameters are considered as reference frequency ω_1 and reference buckling load P^{cr}.

Figure 5.11 Regions of instability for first and second mode of FGM plates with steel-rich bottom resting on Pasternak foundation (k$_w$=50, k$_s$=50), '——' $2\omega_1$, '– – –' $2\omega_2$
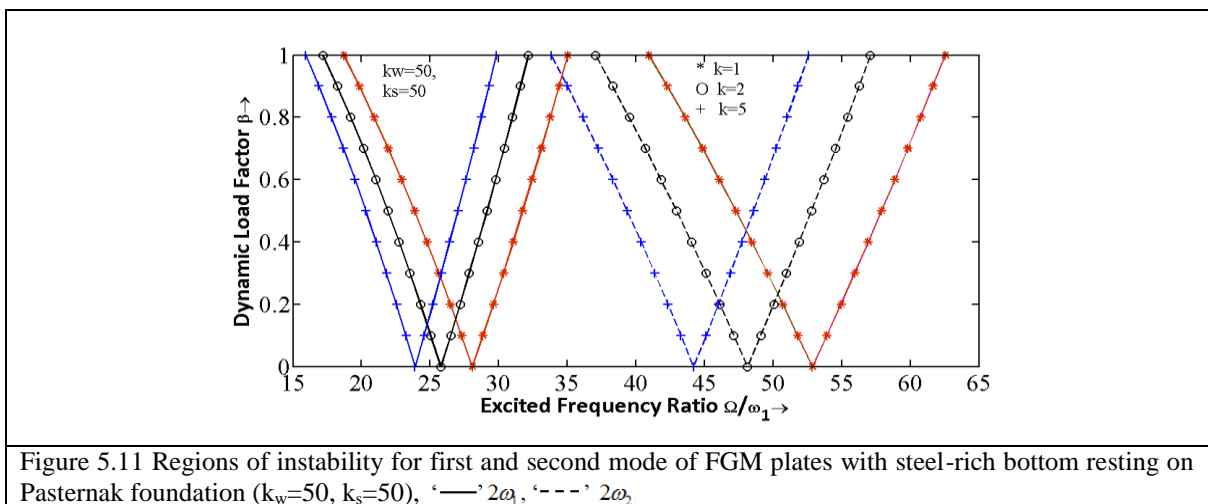
The first and second mode primary instability regions of FGM plate resting on Pasternak foundation (k$_w$=50, k$_s$=50) for different index values k=1, 2 and 5 is shown in figure

5.11. It is observed that the first and second mode instability regions shift towards the dynamic load axis with increase in index value k=1, 2 and 5. So the increase in power law index value increases the instability of FGM plate supported on elastic foundation.

Figure 5.12 illustrates the influence of the temperature rise on the first two mode instability regions of FGM plate on Pasternak foundation (k_w=50, k_s=50). The first and second mode instability regions are farthest from the dynamic load axis for the temperature 0K case. The increase in temperature to 300 K and 600 K increases the instability of FGM plate. Because with increase in temperature the instability regions occur at lower excitation frequencies. Hence, chance of occurrence of instability is more. The effect of temperature rise on second mode instability regions is found to be more prominent than on the first mode which can be noticed from figure 5.12.
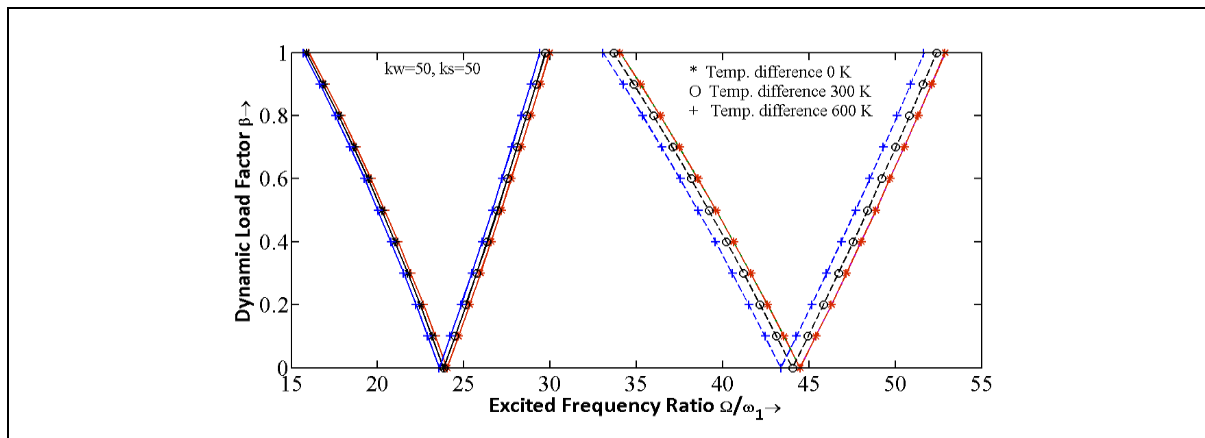
Figure 5.12 Dynamic instability regions of FGM plate resting on Pasternak foundation ((k_w=50, k_s=50)) for temperature changes 0K, 300K and 600K. (k=1), key as in fig. 5.11.

Figure 5.13 represents the effect of thickness ratio on first and second mode instability regions of FGM plate resting on Pasternak foundation. It can be seen that with increase in thickness ratio the instability regions shift to higher frequencies of excitation. Which means increase in thickness ratio ensures better dynamic stability. When the thickness of the plate increases its natural frequencies increase and this leads to occurrence of instability at higher excitation frequencies. The effect is more pronounced on the second principal instability regions than on the first principal instability regions.

Figures 5.14(a) and (b) show the first two mode instability regions of FGM plate supported on Winkler foundation (k_w=0, 200 and 400) and shear layer constant (k_s=50) for index values k=1 and 5 respectively. It is also found that increase in Winkler foundation constant value increases the stability of plate. It is also observed that the effect of k_w is more

prominent on first mode instability regions than on the second mode instability regions of the plate.
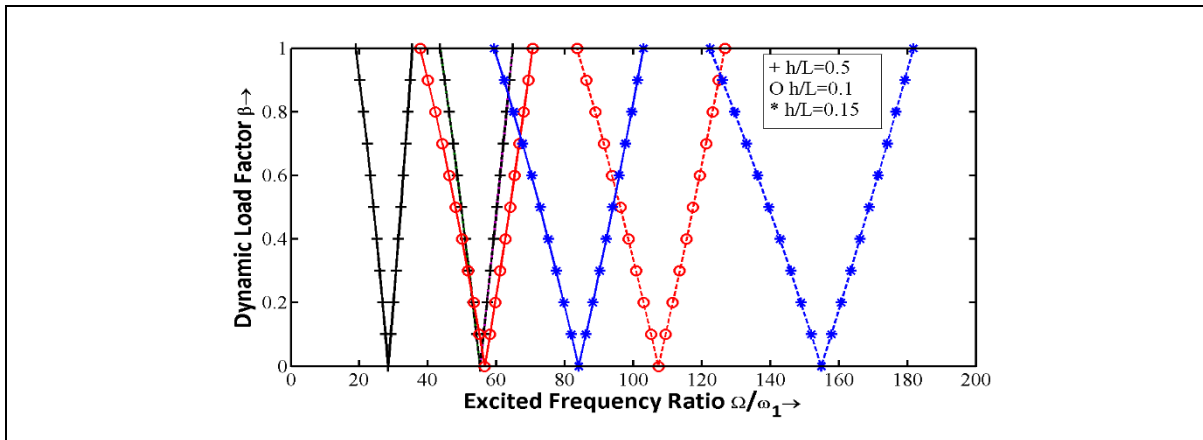
Figure 5.13 Effect of thickness ratio on first and second mode instability of FGM plate resting on Pasternak foundation (k_w=50, k_s=50), $\Delta T = 200\,K$, key as in fig. 5.11.
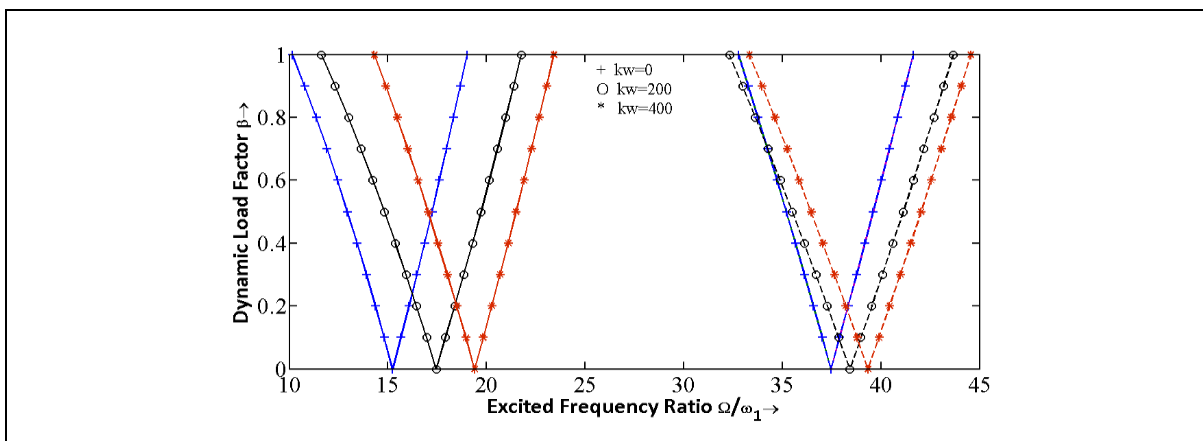
Figure 5.14(a) Effect of Winkler foundation constant on first and second mode instability of FGM plate for index value k=1, $k_s = 50$, $\Delta T = 200\,K$, key as in fig. 5.11.
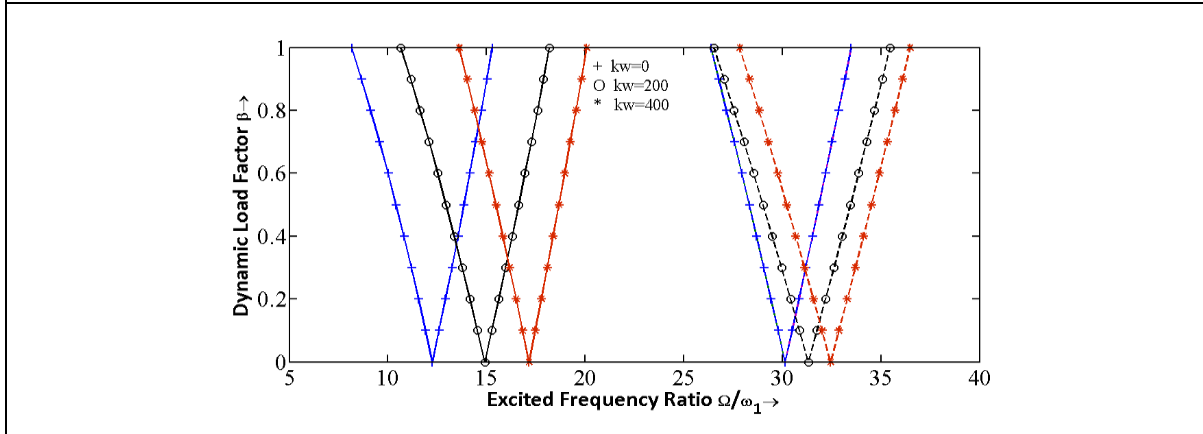
Figure 5.14(b) Effect of Winkler foundation constant on first and second mode instability of FGM plate for index value k=5, $k_s = 50$, $\Delta T = 200$ K, key as in fig. 5.11.
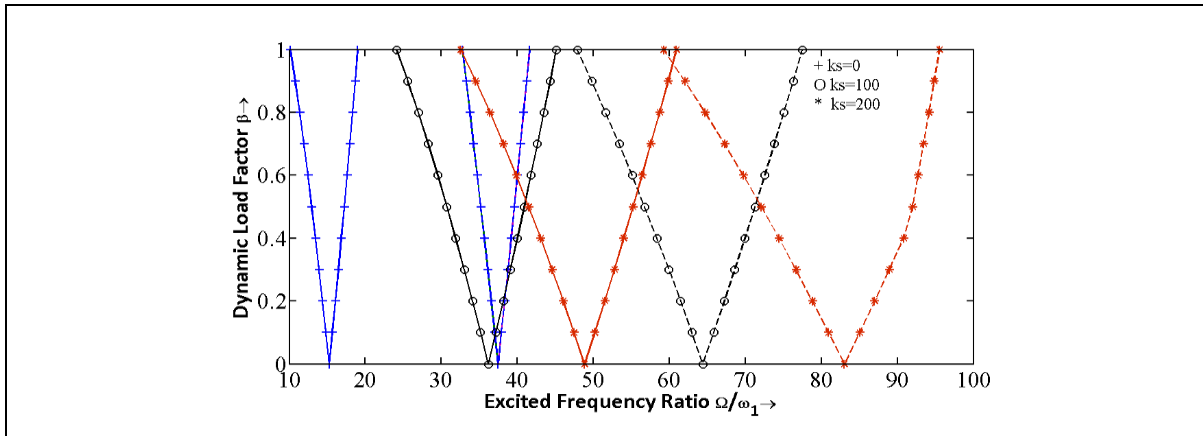
Figure 5.15(a) Effect of Shear layer constant on first and second mode instability of FGM plate with index value k=1, $k_w = 50$, $\Delta T = 200\,K$, key as in fig. 5.11.
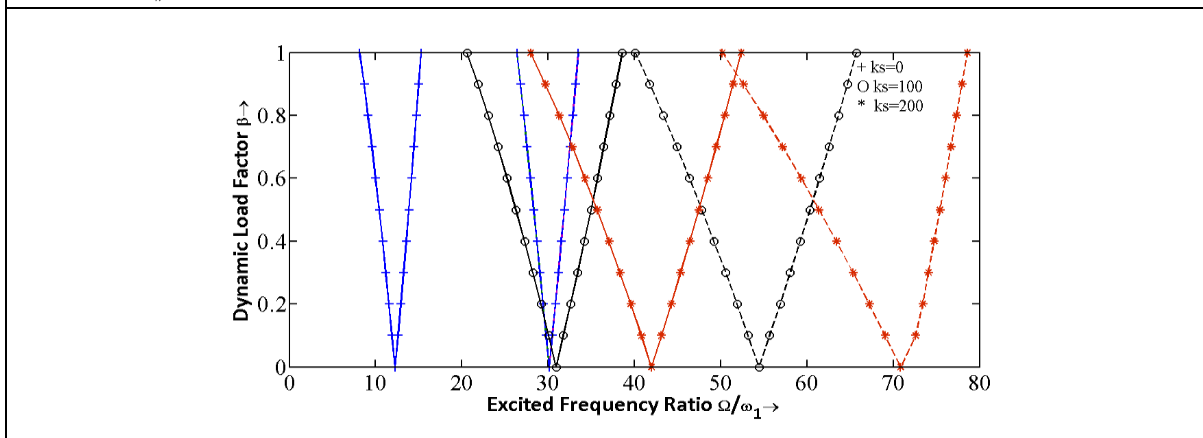
Figure 5.15(b) Effect of Shear layer constant on first and second mode instability of FGM plate with index value k=5, $k_w = 50$, $\Delta T = 200\,K$, key as in fig. 5.11.

The first two mode instability regions of FGM plate, k=1 and k=5 resting on Winkler foundation (k_w=50) and shear layer constant (k_s=0, 100 and 200) are shown in figures 5.15 (a) and (b) respectively. Here the instability regions are relocated farther from the dynamic load factor axis with increase in shear layer constant of the Pasternak foundation. So increase of shear layer constant value increases the stability of the FGM plate.

Figure 5.16 (a) and (b) display the effect of Winkler's foundation constant and shear layer constant on the dynamic stability of FGM plate with index value k=1 and 5, respectively. It can be observed that increase of Winkler foundation constant (k_w=50 to 100) slightly increases the stability of the FGM plate. Similarly, with an increase of shear layer constant (k_s=50 to 100) increases the stability of FGM plate significantly. So it is evident that foundation shear layer constant has got more enhancing effect on the stability of plate as compared to Winkler foundation constant. It is because higher excitation frequency occurs with an increase of shear layer constant.
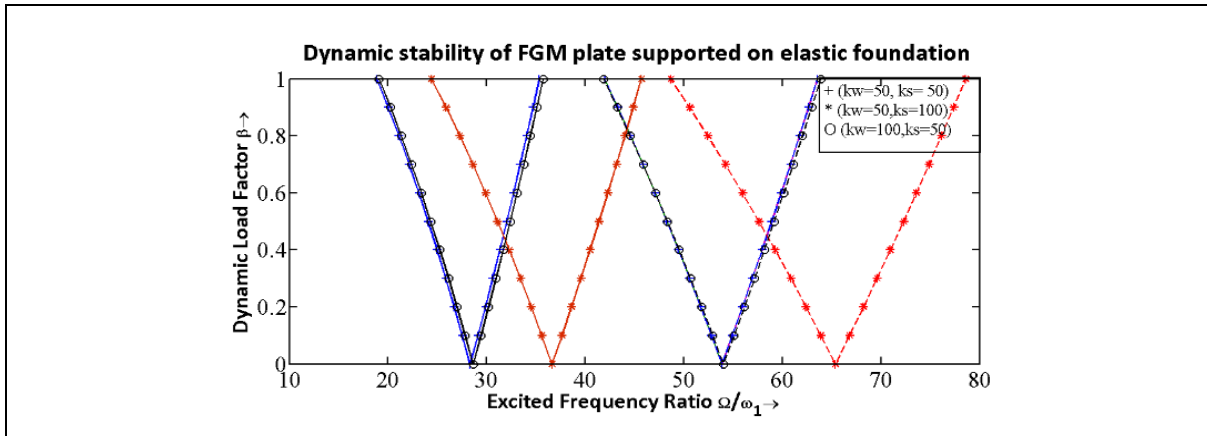
Figure 5.16(a) Effect of Pasternak foundation constants on first and second mode instability of FGM plate for index value k=1, $\Delta T = 200\,\mathrm{K}$, key as in fig. 5.11.
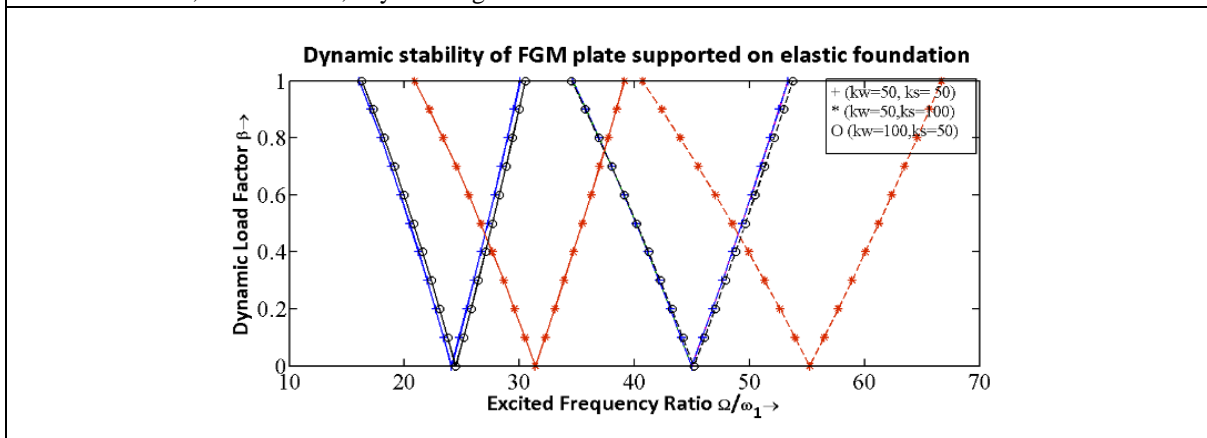
Figure 5.16(b) Effect of Pasternak foundation constants on first and second mode instability of FGM plate for index value k=5, $\Delta T = 200\,\mathrm{K}$, key as in fig. 5.11.

5.5 Conclusion

A rigorous numerical work has been carried out to study the effects of the elastic foundation constants on the vibration, critical buckling as well as the dynamic stability of FGM plate in uniform, linear and nonlinear thermal environments. Increase of temperature and power law index value reduces the first two natural frequencies of simply supported FGM plate resting on elastic foundation. With an increase of Winkler foundation constant there is increase of the first two natural frequencies of FGM plate. With Pasternak foundation, increase of shear layer constant increases the first two natural frequencies of FGM plate. An increase of Winkler foundation constant and shear layer constant increases the critical buckling load of the simply supported FGM plate under biaxial loading condition.

The instability of FGM plate increases with the rise in environment temperature. The dynamic stability of FGM plate increases with a rise of Winkler foundation constant. Increase of shear layer constant increases the dynamic stability of FGM plate resting on the elastic

foundation. Increase of shear layer constant and Winkler foundation constant has a combined effect of enhancing the stability of the plate. However the effect of shear layer constant is more pronounced than the Winkler elastic constant.

Chapter 6

DYNAMIC STABILITY OF FUNCTIONALLY GRADED MATERIAL PLATES IN HYGROTHERMAL ENVIRONMENT UNDER PARAMETRIC EXCITATION

6.1 Introduction

Functionally graded material plates are extensively used in the high performance application such as aerospace, gas turbine blades, automobile parts and other application areas in high temperature environment which can affect the overall strength. During their service life, they may be exposed to moisture and temperature environment. Temperature and moisture have significant effects on the stiffness of the plates and hence on its vibration and dynamic stability. It is important to understand their dynamic characteristics under different loading conditions. The FGM plate structures may be subjected to periodic in-plane load. These periodic loads may cause the system to become unstable for certain combinations of dynamic load amplitude and excitation frequency. This phenomenon is called as dynamic instability or parametric resonance of elastic structures. Thus the dynamic stability characteristics of FGM plate subjected to hygrothermal loads are of a great significance for understanding the dynamic system under periodic loads.

Parhi et al. [144] developed a finite element method for free vibration and transient response analysis of multiple delaminated composite plates and shells under uniform moisture content and temperature separately. B-spline finite strip method (FSM) by Wanga and Dawe [214] was based on the first-order shear deformation plate theory in the analysis of the dynamic instability of composite laminated rectangular plates and prismatic plate structures. Rao and

Sinha [156] investigated the free vibration and transient response of multidirectional composites, where the effects of temperature and moisture concentration were also included. The parametric instability of woven fiber laminated composite plates subjected to in-plane periodic loadings in hygrothermal environment was studied by Rath and Dash [160]. Ramu and Mohanty [152] studied the dynamic instability of FGM plates in high temperature environment. Lee and Kim [97] investigated the effect of hygrothermal environment on post-buckling behavior of FGM plates based on first order shear deformation theory and Von Karman strain displacement relations.

Though, in most of the above literature, studies on dynamic instability of composite plate in hygrothermal environment are reported, there is no reported work on dynamic stability of a FGM plate in hygrothermal environment. The change of temperature and moisture concentration affects the natural frequencies and critical buckling load of the FGM plates. The following work investigates the effects of the moisture content, temperature difference and power law index on the parametric resonance characteristics of FGM plate under high temperature and moisture environment.

6.2 Mathematical Modelling

A typical four noded rectangular element with 7-degrees of freedom per node as described in chapter-3 is chosen for the analysis.

FGM plate experiences hygrothermal stresses and strains when exposed to temperature and moisture. Such stresses can be expressed as

$$\begin{Bmatrix} \sigma_{xx}^{HT} \\ \sigma_{yy}^{HT} \\ \tau_{xy}^{HT} \end{Bmatrix} = \begin{bmatrix} Q_{11} & Q_{12} & 0 \\ Q_{21} & Q_{22} & 0 \\ 0 & 0 & Q_{66} \end{bmatrix} \begin{bmatrix} \begin{Bmatrix} 1 \\ 1 \\ 0 \end{Bmatrix} \left(\psi(z',T)\Delta T(z') \right) + \begin{Bmatrix} 1 \\ 1 \\ 0 \end{Bmatrix} \Gamma(z',T)\Delta C(z') \end{bmatrix} \tag{6.1}$$

where $Q_{11} = Q_{22} = \dfrac{E(z',T)}{\left(1-\nu^2(z',T)\right)}, Q_{12} = Q_{21} = \dfrac{\nu(z',T)E(z',T)}{\left(1-\nu^2(z',T)\right)}, Q_{66} = \dfrac{E(z',T)}{2\left(1+\nu(z',T)\right)}$

where $\Delta C = C_m - C_c$ in here C_m and C_c are the reference moisture concentration at metal and ceramic side. Also Γ is moisture expansion coefficient.

Hygrothermal stresses and strains relationship can be expressed as

$$\begin{Bmatrix} \sigma_{xx}^{HT} \\ \sigma_{yy}^{HT} \\ \tau_{xy}^{HT} \end{Bmatrix} = \begin{Bmatrix} \sigma_{xx}^{T} \\ \sigma_{yy}^{T} \\ \tau_{xy}^{T} \end{Bmatrix} + \begin{Bmatrix} \sigma_{xx}^{H} \\ \sigma_{yy}^{H} \\ \tau_{xy}^{H} \end{Bmatrix} \tag{6.2}$$

The thermal stress concept assumed and described in chapter 4 by equation (4.10) has also been adopted here.

$$\begin{Bmatrix} \sigma_{xx}^T \\ \sigma_{yy}^T \\ \tau_{xy}^T \end{Bmatrix} = \begin{bmatrix} Q_{11} & Q_{12} & 0 \\ Q_{21} & Q_{22} & 0 \\ 0 & 0 & Q_{66} \end{bmatrix} \begin{Bmatrix} 1 \\ 1 \\ 0 \end{Bmatrix} \left(\psi(z',T)\Delta T(z') \right) \tag{4.10}$$

When there is a moisture concentration by ΔC, the stress-strain relationships of the FGM plate in the global x, y and z coordinates system can be written as

$$\begin{Bmatrix} \sigma_{xx}^H \\ \sigma_{yy}^H \\ \tau_{xy}^H \end{Bmatrix} = \begin{bmatrix} Q_{11} & Q_{12} & 0 \\ Q_{21} & Q_{22} & 0 \\ 0 & 0 & Q_{66} \end{bmatrix} \begin{Bmatrix} 1 \\ 1 \\ 0 \end{Bmatrix} \Gamma(z',T)\Delta C(z') \tag{6.3}$$

The force resultants, moments and higher order moments due to moisture concentration are expressed as

$$\left. \begin{aligned} \begin{bmatrix} N_{xx}^H \\ N_{yy}^H \end{bmatrix} &= \int_{-h/2-d}^{h/2-d} \begin{bmatrix} \sigma_{xx}^H \\ \sigma_{yy}^H \end{bmatrix} dz' \\ \begin{bmatrix} M_{xx}^H \\ M_{yy}^T \end{bmatrix} &= \int_{-h/2-d}^{h/2-d} \begin{bmatrix} \sigma_{xx}^H \\ \sigma_{yy}^H \end{bmatrix} z' dz' \\ \begin{bmatrix} P_{xx}^H \\ P_{yy}^H \end{bmatrix} &= \int_{-h/2-d}^{h/2-d} \begin{bmatrix} \sigma_{xx}^H \\ \sigma_{yy}^H \end{bmatrix} z'^3 dz' \end{aligned} \right\} \tag{6.4}$$

Substituting equation (6.4) in equation (6.3) yields the following relations

$$\begin{bmatrix} N^H \\ M^H \\ P^H \end{bmatrix} = \begin{bmatrix} [A^H] & [B^H] & [E^H] \\ [B^H] & [D^H] & [F^H] \\ [E^H] & [F^H] & [H^H] \end{bmatrix} \begin{Bmatrix} \varepsilon^{(n)H} \\ \varepsilon^{(1)H} \\ \varepsilon^{(3)H} \end{Bmatrix}, \tag{6.5}$$

The stiffness components are expressed as:

$$\begin{aligned} & \left(A_{ij}^H \quad B_{ij}^H \quad D_{ij}^H \quad E_{ij}^H \quad F_{ij}^H \quad H_{ij}^H \right) \\ & = \int_{-h/2-d}^{h/2-d} Q_{ij} \left(\Gamma(z',T)\Delta C(z') \right) \left(1, z', z'^2, z'^3, z'^4, z'^6 \right) dz' \\ & (i, j = 1, 2) \end{aligned} \tag{6.6}$$

The strain-displacement relationship about the neutral plane due to moisture presence can be written as

$$\left\{\varepsilon^{bH}\right\} = \left\{\begin{matrix}\varepsilon_x^H \\ \varepsilon_y^H\end{matrix}\right\} = \left\{\begin{matrix}\varepsilon_x^{(n)H} \\ \varepsilon_y^{(n)H}\end{matrix}\right\} + z'\left\{\begin{matrix}\varepsilon_x^{(1)H} \\ \varepsilon_y^{(1)H}\end{matrix}\right\} - z'^3\left\{\begin{matrix}\varepsilon_x^{(3)H} \\ \varepsilon_y^{(3)H}\end{matrix}\right\} \tag{6.7}$$

$$\left.\begin{aligned}
\varepsilon^{(n)H} &= \left\{\begin{matrix}\varepsilon_x^{(n)H} \\ \varepsilon_y^{(n)H}\end{matrix}\right\} = \left\{\begin{matrix}u_{n,x} + w_{n,x} \\ v_{n,x} + w_{n,y}\end{matrix}\right\}, \\[2mm]
\varepsilon^{(1)H} &= \left\{\begin{matrix}\varepsilon_x^{(1)H} \\ \varepsilon_y^{(1)H}\end{matrix}\right\} = \left\{\begin{matrix}\theta_{x,x} \\ \theta_{y,y}\end{matrix}\right\}, \\[2mm]
\varepsilon^{(3)H} &= \left\{\begin{matrix}\varepsilon_x^{(3)H} \\ \varepsilon_y^{(3)H}\end{matrix}\right\} = \left\{\begin{matrix}\theta_{x,x} + w_{n,x} \\ \theta_{y,y} + w_{n,y}\end{matrix}\right\}
\end{aligned}\right\} \tag{6.8}$$

The strain vector can be expressed in terms of nodal displacement vector $\left\{q^{(e)}\right\}$ as

$$\left\{\varepsilon^{bH}\right\} = \left[B_b^H\right]\left\{q^{(e)}\right\} \tag{6.9}$$

where $\left[B_b^H\right] = \left[B_0^H\right] + z'\left[B_1^H\right] + z'^3\left[B_2^H\right]$

$\left[B_0^H\right]$, $\left[B_1^H\right]$ and $\left[B_2^H\right]$ are defined as follows

$$\left[B_0^H\right] = \begin{bmatrix}\dfrac{\partial}{\partial x} & 0 & \dfrac{\partial}{\partial x} & 0 & 0 & 0 & 0 \\[3mm] 0 & \dfrac{\partial}{\partial y} & \dfrac{\partial}{\partial y} & 0 & 0 & 0 & 0\end{bmatrix}[N], \quad \left[B_1^H\right] = \begin{bmatrix}0 & 0 & 0 & \dfrac{\partial}{\partial x} & 0 & 0 & 0 \\[3mm] 0 & 0 & 0 & 0 & \dfrac{\partial}{\partial y} & 0 & 0\end{bmatrix}[N]$$

$$\left[B_2^H\right] = \begin{bmatrix}0 & 0 & 0 & \dfrac{\partial}{\partial x} & 0 & \dfrac{\partial}{\partial x} & 0 \\[3mm] 0 & 0 & 0 & 0 & \dfrac{\partial}{\partial y} & 0 & \dfrac{\partial}{\partial y}\end{bmatrix}[N]$$

6.2.1 Finite Element Analysis

The element strain energy $U_H^{(e)}$ of the plate duo to moisture concentration is expressed as

$$U_H^{(e)} = \frac{1}{2}\int_0^b\int_0^a\left[\left[N^H\right]^T\left\{\varepsilon^{(n)H}\right\} + \left[M^H\right]^T\left\{\varepsilon^{(1)H}\right\} + \left[P^H\right]^T\left\{\varepsilon^{(3)H}\right\}\right]dxdy \tag{6.10}$$

Substituting equation (6.5) and (6.8) in equation (6.10), the element strain energy due to moisture concentration can be expressed as

$$U_H^{(e)} = \frac{1}{2}\left[\left\{q^{(e)}\right\}^T\left[K_H^{(e)}\right]\left\{q^{(e)}\right\}\right] \tag{6.11}$$

The element moisture stiffness matrix is derived as

$$\left[K_H^{(e)} \right] = \left[K_{00}^{(e)H} \right] + \left[K_{11}^{(e)H} \right] + \left[K_{22}^{(e)H} \right] \tag{6.12}$$

$$\left.\begin{aligned}
\left[K_{00}^{(e)H} \right] &= \int_0^a \int_0^b \left[B_0^H \right]^T \left[A^H \right] \left[B_0^H \right] dxdy \\[2mm]
\left[K_{11}^{(e)H} \right] &= \int_0^a \int_0^b \left[B_1^H \right]^T \left[D^H \right] \left[B_1^H \right] dxdy \\[2mm]
\left[K_{22}^{(e)H} \right] &= \int_0^a \int_0^b \left[B_2^H \right]^T \left[H^H \right] \left[B_2^H \right] dxdy
\end{aligned}\right\}$$

6.3 Governing Equations of Motion

The total work done on the plate is due to axial force as given in equation (3.42) and strain energy due to thermal load is as given in equation (4.16). The elastic stiffness and mass matrices of the FGM plate element derived in section 3.2.6 are also applicable in this case and hence have not been repeated.

The equations of motion for a FGM plate element, referring section 3.3 can be modified for hygrothermal environment case and is given as

$$\left[M^{(e)} \right]\{\ddot{q}^{(e)}\} + \left[K_{ef}^{(e)} \right]\{q^{(e)}\} - P(t)\left[K_g^{(e)} \right]\{q^{(e)}\} = 0 \tag{6.13}$$

where $\left[K_{ef}^{(e)} \right] = \left[K^{(e)} \right] - \left[K_T^{(e)} \right] - \left[K_H^{(e)} \right]$

$\left[K_{ef}^{(e)} \right]$ is effective stiffness matrix and $\left[K^{(e)} \right], \left[K_T^{(e)} \right]$ and $\left[K_H^{(e)} \right]$ are element stiffness matrix, thermal stiffness matrix and moisture stiffness matrix.

The governing equation of motion of FGM plate in terms of global displacement matrix is obtained as follows

$$[M]\{\ddot{q}\} + \left[K_{ef} \right]\{q\} - P(t)\left[K_g \right]\{q\} = 0 \tag{6.14}$$

where $P(t)$ is the time dependent dynamic load, which can be represented in terms of static critical buckling load P^{cr} of metallic plate having similar applied boundary conditions. Hence substituting, $P(t) = \alpha P^{cr} + \beta P^{cr} \cos \Omega t$ with α and β called as static and dynamic load factors respectively, equation (6.14) can be expressed as

$$[M]\{\ddot{q}\}+\left[\left[K_{ef}\right]-P^{cr}\left(\alpha+\beta\cos\Omega t\right)\left[K_{g}\right]\right]\{q\}=0 \qquad (6.15)$$

where $\left[K_{ef}\right]=\left[K\right]-\left[K_{T}\right]-\left[K_{H}\right]$

$\left[K_{ef}\right]$ is the effective stiffness matrix and $\left[K\right],\left[K_{T}\right],\left[K_{T}\right],\left[M\right]$ and $\left[K_{g}\right]$ are global elastic stiffness matrix , thermal matrix, moisture matrix, mass matrix and geometric stiffness matrix respectively and $\{q\}$ is global displacement vector.

The condition for existence of the boundary solutions with period 2T is given by

$$\left(\left[K_{ef}\right]-\left(\alpha\pm\frac{\beta}{2}\right)P^{cr}\times\left[K_{g}\right]-\frac{\Omega^{2}}{4}\left[M\right]\right)\{q\}=0 \qquad (6.16)$$

The instability boundaries can be determined from the solution of the equation

$$\left|\left[K_{ef}\right]-\left(\alpha\pm\frac{\beta}{2}\right)P^{cr}\times\left[K_{g}\right]-\frac{\Omega^{2}}{4}\left[M\right]\right|=0 \qquad (6.17)$$

Following the procedure described in section 3.3.1, the natural frequencies, critical buckling load and instability regions of FGM plate in hygrothermal environment are determined.

6.4 Results and Discussion

6.4.1 Comparison study

Validation of the present computational method has been carried out by considering a (*Si3N4/SUS304*) FGM plate in uniform temperature environment with clamped boundary condition. For this numerical study the typical values of temperature-dependent material property coefficients are adopted from table 4.1 shown in chapter 4.

For simplicity, the non-dimensional natural frequency parameter is expressed as:

$$\varpi=\frac{\omega W^{2}}{\pi^{2}}\sqrt{\frac{I_{0}}{D}}$$

where, $I_{0}=\rho h, D=E_{m}h^{3}/12\left(1-v^{2}\right)$. The material properties $v=v_{m}$, $\rho=\rho_{m}$ and E_{m} are chosen to be the values of metal at $T=300K$.

The numerical results of natural frequency parameters of first six modes of clamped FGM (*Si3N4/SUS304*) rectangular plates are obtained by applying third order shear deformation theory. The obtained numerical results are compared with the available literature results of

Senthil and Batra [175] and Yang and Shen [222]. The following non-dimensional natural frequencies presented in table 6.1 are obtained by considering a combination of *Si₃N₄/SUS304,* where the upper surface is ceramic-rich and the lower surface is metal-rich. The FGM plates, subjected to the uniform temperature rise condition is considered for aspect ratios L/W = 1.0 and 1.5, and power law index k = 2 and 10. There is good agreement between the results predicted by present method and the results of Senthil and Batra [175] and Yang and Shen [222].

Table 6. 1 Comparisons of first six natural frequency parameters for CCCC (Si_3N_4/SUS304) FGM rectangular plates subjected to uniform temperature rise (L=0.2m, h/W =0.1, Tm = 300K, ΔT = 300K).

L/W	k	Source	Frequency parameters					
			ω_1	ω_2	ω_3	ω_4	ω_5	ω_6
1	2	Yang [222]	3.6636	7.2544	7.2544	10.3924	11.7054	12.3175
		Senthil [175]	3.7202	7.3010	7.3010	10.3348	12.2256	12.3563
		Present	3.6618	7.2832	7.2832	10.2549	12.5202	12.6552
	10	Yang [222]	3.1835	6.3001	6.3001	9.0171	10.2372	10.6781
		Senthil [175]	3.1398	6.1857	6.1857	8.7653	10.3727	10.4866
		Present	3.1032	6.2780	6.2780	8.8216	10.5657	10.6823
1.5	2	Yang [222]	2.7373	4.2236	6.6331	6.6331	7.9088	9.8122
		Senthil [175]	2.7904	4.2839	6.6401	6.7227	7.8941	9.8528
		Present	2.7572	4.2212	6.6635	6.6775	7.8474	9.8760
	10	Yang [222]	2.3753	3.6672	5.7618	5.7618	6.8690	8.5206
		Senthil [175]	2.3470	3.6147	5.6234	5.6910	6.6888	8.3553
		Present	2.3058	3.5409	5.6113	5.6198	6.6110	8.3264

6.4.2 Free vibration and buckling analysis

Numerical analysis has been performed using FGM square plate made up of *Al₂O₃/SUS305*; with length of 0.2m and thickness of 0.02m. Natural frequencies of FGM plates are obtained from numerical experiments for different thermal environments. Figures 6.1-6.3 display the first two frequency parameters vs temperature rise of FGM plate in thermal environments with simply supported boundary conditions. Figures 6.1 (a), 6.2 (a) and 6.3 (a) show the variation of fundamental frequency parameter for power law indices k=1 and 5 subjected to uniform, linear and nonlinear temperature rise conditions. Similarly, the figures 6.1 (b), 6.2 (b) and 6.3 (b) illustrate the variation of second mode frequency parameters of simply supported FGM plate under uniform, linear and nonlinear temperature rise conditions for volume fraction indices k=1 and 5. Observations from these plots show that increase of temperature change reduces the first two mode frequency parameters. This happens due to the decrease of plate stiffness at increased temperature.
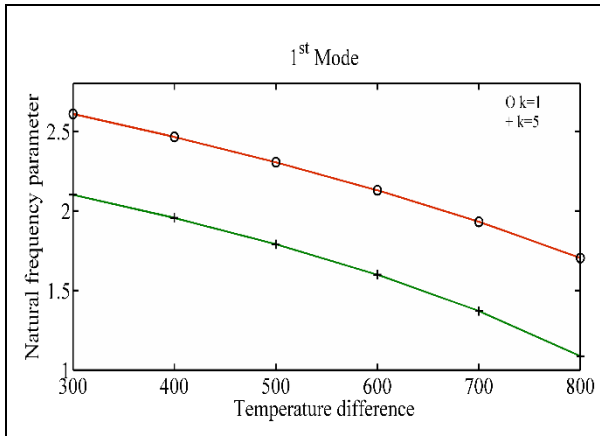
Figure 6.1(a) Temperature rise verses first mode natural frequency parameter of FGM plates with uniform temperature field for k=1 and k=5. $\left(\Delta C = 1\% \right)$
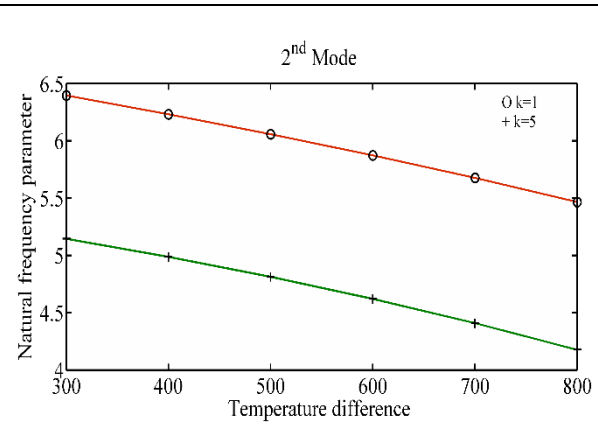
Figure 6.1(b) Temperature rise verses second mode natural frequency parameter of FGM plates with uniform temperature field for k=1 and k=5,. $\left(\Delta C = 1\% \right)$
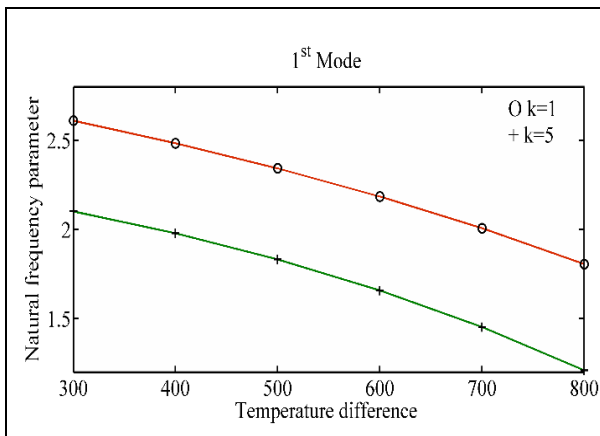
Figure 6.2(a) Temperature rise verses first mode natural frequency parameter of FGM plates with linear temperature field for k=1 and k=5, $\left(\Delta C = 1\% \right)$.
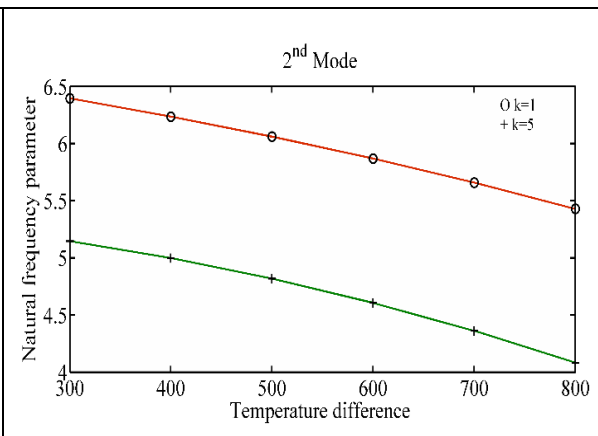
Figure 6.2(b) Temperature rise verses natural frequency parameter of FGM plates with linear temperature field for k=1 and k=5, $\left(\Delta C = 1\% \right)$.
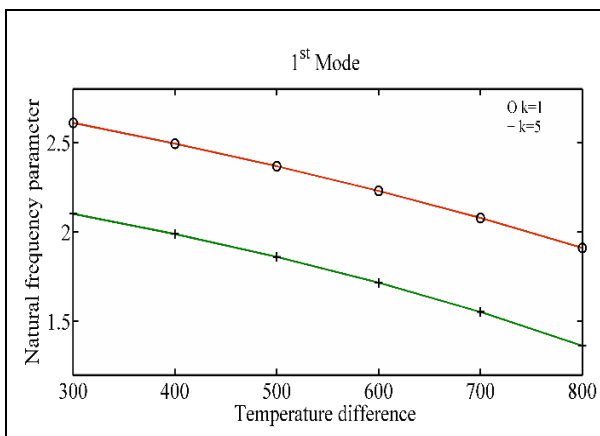
Figure 6.3(a) Temperature rise verses first mode natural frequency parameter of FGM plates with nonlinear temperature field for k=1 and k=5, $\left(\Delta C = 1\% \right)$
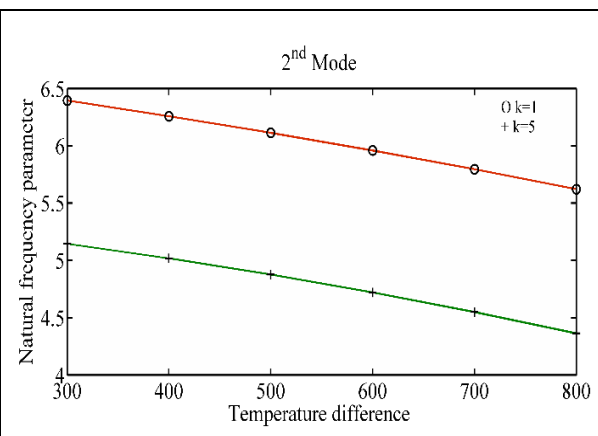
Figure 6.3(b) Temperature rise verses second mode natural frequency parameter of FGM plates with nonlinear temperature field for k=1 and k=5, $\left(\Delta C = 1\% \right)$

The uniform temperature environment affects the natural frequency parameters more significantly than the linear and nonlinear temperature fields. It can be explained by figure 6.4 where the temperature rise of the uniform temperature environment is more intensive than those of linear and nonlinear temperature environments.

Figure 6.4 Variation of fundamental frequency parameter verses temperature change for uniform, linear and nonlinear thermal environments, $\left(k = 1, \Delta C = 1\% \right)$.
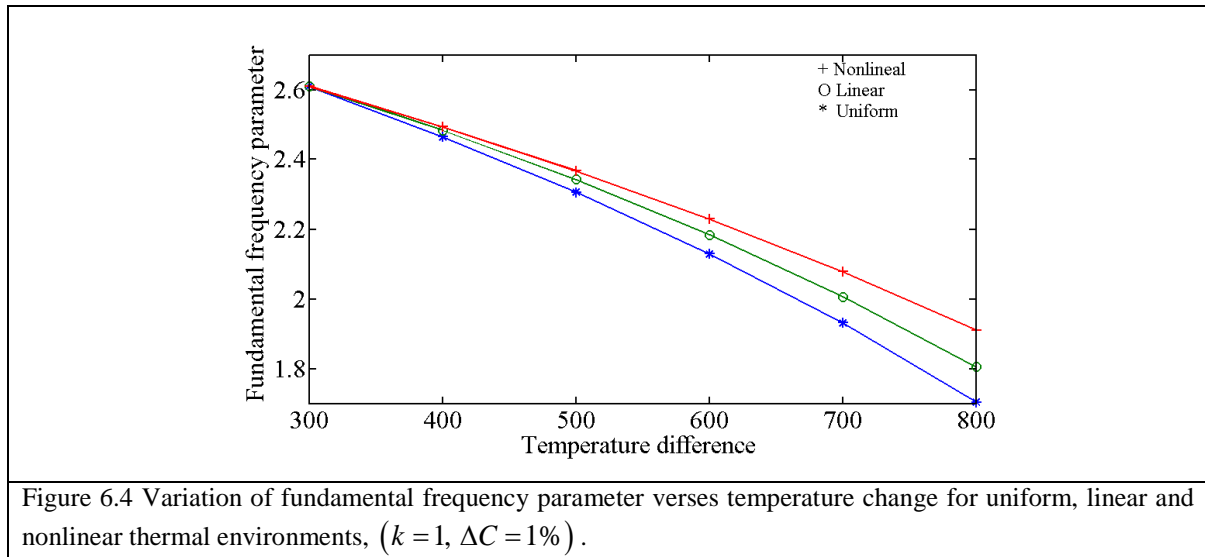
The natural frequencies of the FGM plate are shown in figures 6.5 (a) and (b) against moisture concentration for different power law index values ($k=1$, $k=5$, $\Delta T = 200 \ K$) with simply supported boundary condition. It is observed that the first and second mode frequency parameters reduce with increase in moisture concentration. Increase of moisture concentration reduces the effective stiffness of the plate, so the natural frequencies drop.

Figure 6.5(a) Moisture concentration verses first mode natural frequency parameter of FGM plates in hygrothermal environment, $\left(\Delta T = 200K \right)$.

Figure 6.5(b) Moisture concentration verses second mode natural frequency parameter of FGM plates in hygrothermal environment, $\left(\Delta T = 200K \right)$.
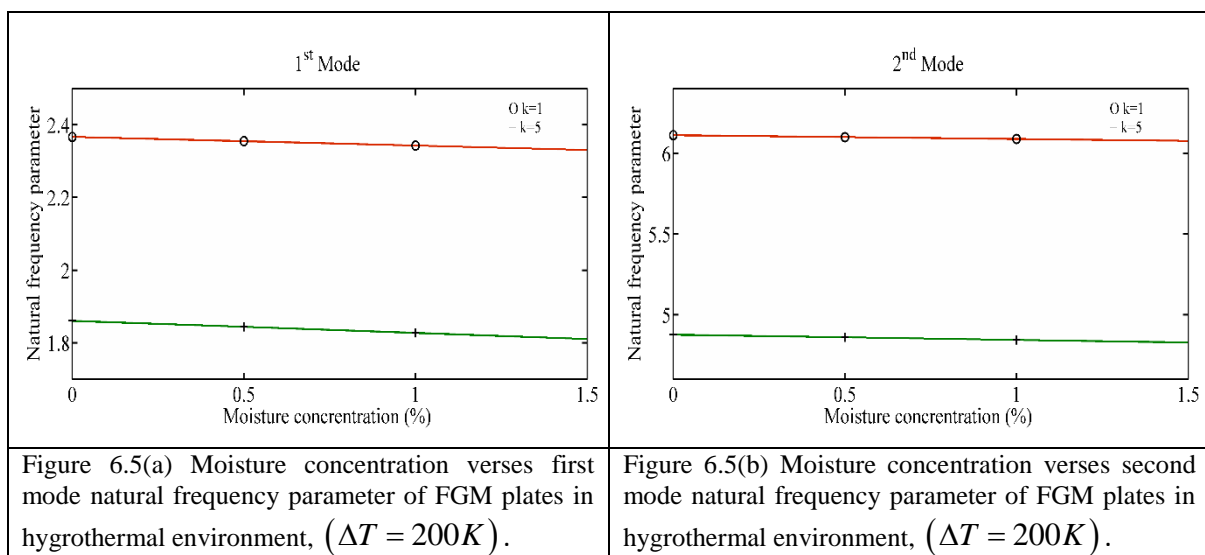
Figures 6.6 (a) and 6.6 (b) depict natural frequencies variation with increase in moisture concentration (%) for simply supported FGM plate with power law index k=2 and 10 and with $\Delta T = 500K$. The first and second mode natural frequencies of the FGM plates are reduced

with rise in moisture concentration from 0% to 1.5%. There is significant reduction in natural frequency parameters of FGM plate in hygrothermal environment with increasing moisture concentration. The reason behind this reduction of natural frequencies is that the presence of moisture concentration in hygrothermal environment reduces the stiffness of the FGM plate. The first and second mode natural frequencies decrease with increase in power law index, due to the fact that the effective modulus of elasticity is decreased.

Figures 6.7 (a) and (b) illustrate the effect of moisture concentration on the critical buckling load of the FGM plates in hygrothermal environment for k=1 and 5. The moisture concentration is varied from 0% to 1.5%. The increased moisture concentration reduces the critical buckling load. The critical buckling load results show that the FGM plate is sensitive to the amount of moisture concentration and then moisture may cause to degrade the structural characteristics.

Figure 6.6(a) First mode natural frequency parameter variation with respective moisture concentration. $(\Delta T = 500K)$	Figure 6.6(b) Second mode natural frequency parameter variation with respective moisture concentration. $(\Delta T = 500K)$
Figure 6.7(a) Variation of critical buckling load of FGM plate with moisture concentration (%), $\Delta T = 200K$, k=1 and 5.	Figure 6.7(b) Variation of critical buckling load of FGM plate with moisture concentration (%), $\Delta T = 500K$, k=2 and 10

6.4.3 Dynamic stability analysis

The effects of temperature rise on the dynamic stability of FGM plates are illustrated in figures 6.8-6.9 for power law indices k=1 and k=5. It is observed that the parametric instability regions are shifted towards the dynamic load axis with increase in temperature change in the order of $0K$, $200K$ and $400K$. Increase in temperature reduces the structural stiffness causing the reduction in the excitation frequency of parametric resonance, hence the probability of instability increases.
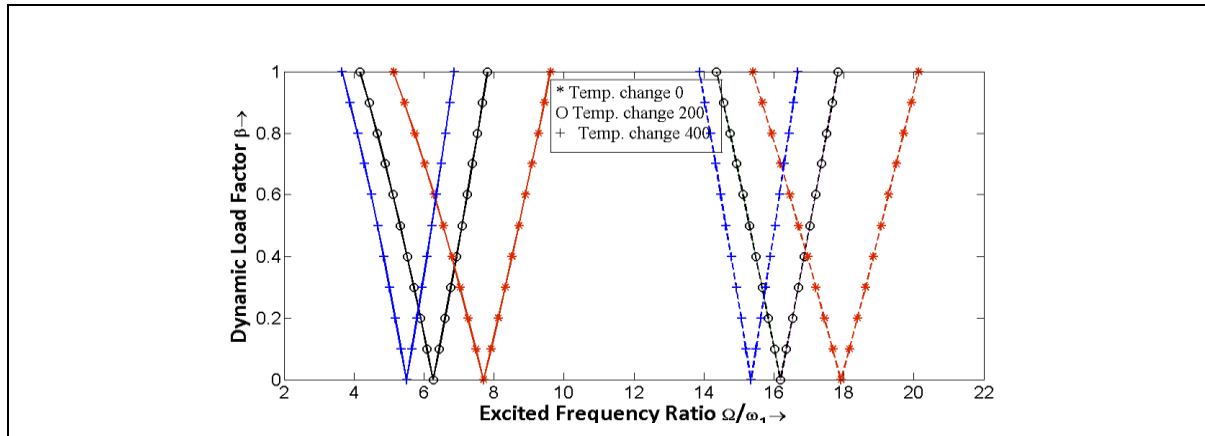
Figure 6.8 Effects of temperature change on dynamic stability of FGM plate with simply supported boundary condition at power law index ($k=1$), '——' $2\omega_1$, '– – –' $2\omega_2$
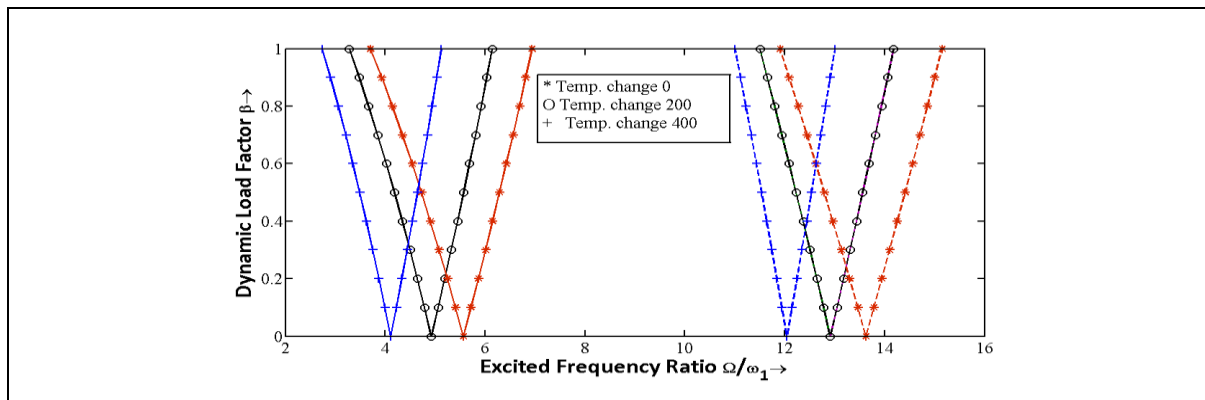
Figure 6.9 Effects of temperature change on dynamic stability of FGM plate with simply supported boundary condition at power law index ($k=5$), key as in fig. 6.8.

Figures 6.10 and 6.11 show the effect of moisture on dynamic stability of FGM plate in hygrothermal environment keeping temperature change ($100K$) constant. Increase in moisture concentration (0%, 0.75% and 1.5%) increases the dynamic instability of FGM plate with k=1 and k=5. The increasing moisture concentration lowers the excitation frequency and the first two stability regions shift towards the dynamic load axis, so the chance of instability becomes more.
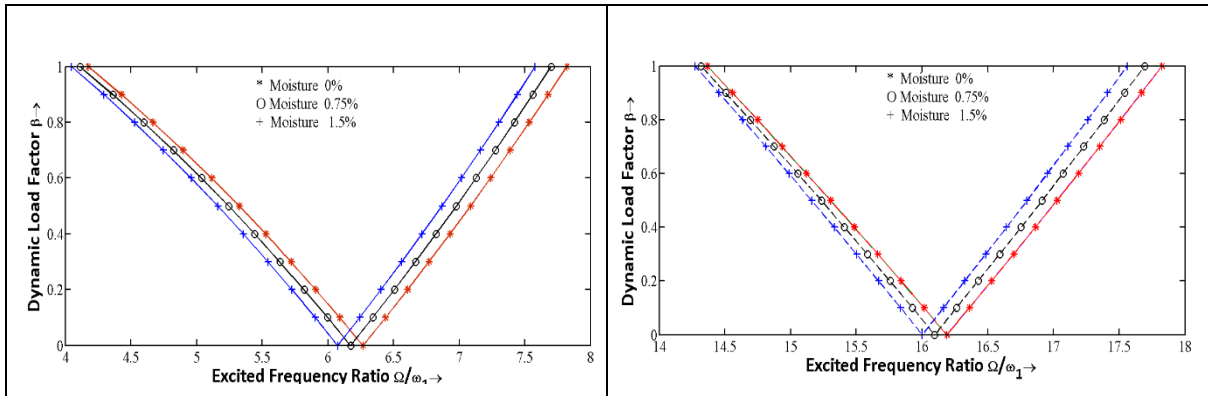
Figure 6.10(a) Effect of moisture concentration on first mode instability region of FGM plate in hygrothermal environment, (100 K, k=1)	Figure 6.10(b) Effect of moisture concentration on second mode instability region of FGM plate in hygrothermal environment, (100 K, k=1)
Figure 6.11(a) Effect of moisture concentration on first mode instability region of FGM plate in hygrothermal environment, (100 K, k=5)	Figure 6.11(b) Effect of moisture concentration on second mode instability region of FGM plate in hygrothermal environment, (100 K, k=5)
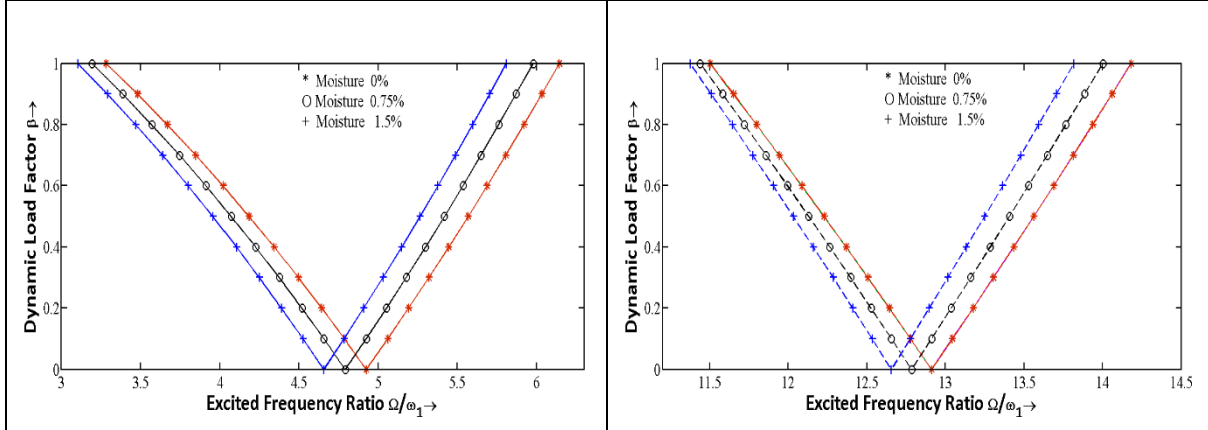
Figures 6.12(a) and (b) present the dynamic stability of FGM plates in hygrothermal environment for different combination of temperature change and moisture concentration (100, 0.5%), (300, 1%) and (500, 1.5%) with power law index value, k=1. In this case increase of both the temperature rise and moisture concentration degrades the overall structural stiffness. The reduced structural stiffness decreases the excitation frequency and the dynamic instability regions shift towards the dynamic load axis.

The effects of increasing both temperature rise and moisture concentration on the excitation frequencies are analyzed for FGM plates and shown in figures 6.13 (a) and (b) with power law index k=5. In this case also the combined effect of increase of temperature and moisture concentration is same as that observed in figures 6.12(a) and (b) only difference is that the instability occurs at further lower excitation frequencies, this is due to increased value of k.
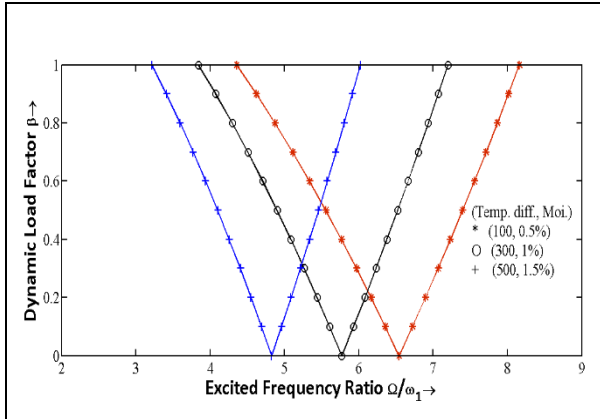
Figure 6.12(a) First mode principal instability region of FGM plate in hygrothermal environment at temperature change (100 K) with power law index values (k=1).	Figure 6.12(b) Second mode principal instability region of FGM plate in hygrothermal environment at temperature change (100 K) with power law index values (k=1).
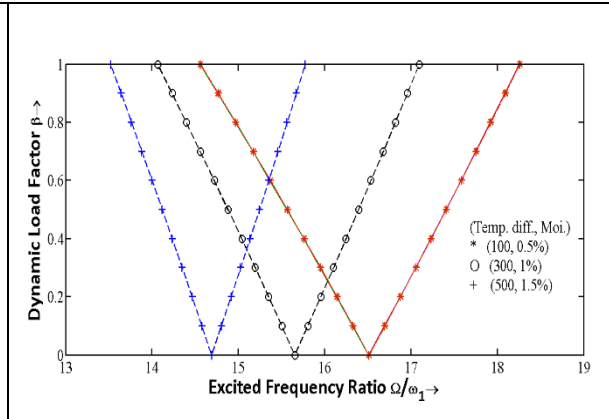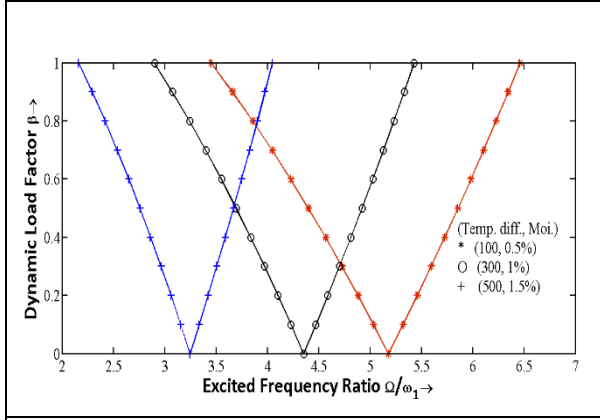
| Figure 6.13(a) First mode dynamic instability region of FGM plate in hygrothermal environment at temperature change (100K) with power law index values (k=5). | Figure 6.13(b) Second mode dynamic instability region of FGM plate in hygrothermal environment at temperature change (100K) with power law index values (k=5). |
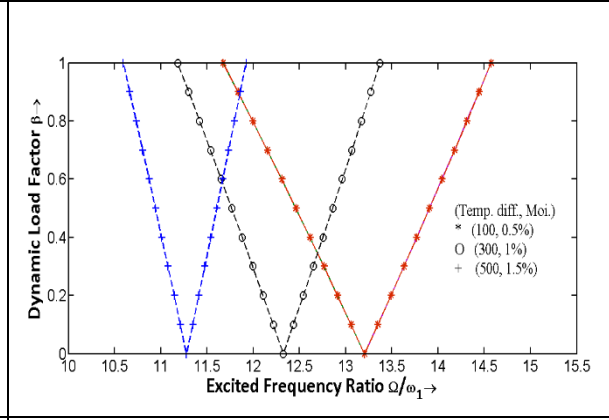
6.5 Conclusion

Vibration and parametric instability study of FGM plates with power law property distribution along the thickness in hygrothermal environments has been carried out based on third order shear deformation theory using finite element method in conjunction with Hamilton's principle. The first two natural frequencies of FGM plate in uniform, linear and nonlinear temperature environments are reduced by increase of temperature difference. With increase in power law index value, the natural frequencies are decreased. The natural frequencies of FGM plates decrease with increase of temperature and moisture concentration. The FGM plates in hygrothermal environment with higher values of power law index are more responsive to change of the temperature rise than those with lower values of index. The moisture concentration reduces the critical buckling load of FGM plate in hygrothermal environment. Specifically, the effect of moisture is considerably more for higher values of power law index.

The parametric instability of FGM plates subjected to biaxial periodic in-plane loads in hygrothermal environment is studied. FGM plates are less stable with increased temperature in hygrothermal environment. The increasing moisture concentration increases the dynamic instability of FGM plate. The combined effect of both moisture and temperature rise reduces the excitation frequency, the dynamic stability region shift towards lower excitation frequencies.

Chapter 7

DYNAMIC STABILITY OF ROTATING FUNCTIONALLY GRADED MATERIAL PLATES UNDER PARAMETRIC EXCITATION

7.1 Introduction

Advanced composite materials, especially functionally graded materials (FGMs) have been widely used for specific applications for aerospace, aircrafts and other engineering structures under high temperature environment. Now FGMs are developed for general use as structural elements. Dynamic characteristics of rotating structures are more significant than non-rotating structures. Many industrial structures such as turbine blades, turbo-machinery, helicopter rotor blades, aircraft engine, impeller and fan blades etc., can be modeled as rotating plate. Acquaintance with the natural frequencies of these structures is important in the design stages for studying their parametric resonance. The variation of natural frequencies is significant when the plate rotates. As the rotational speed of the structure increases so does the centrifugal inertia force, which can affect the transverse bending vibration of the rotating plates. This change will affect the dynamic characteristics of rotating plates.

Most of the studies introduced in literature are based on rotating isotropic and composite plates. This work is aimed to present the bending vibration and dynamic stability of rotating FGM plate in high temperature environment. For this purpose, the rotating structure is modeled as a cantilever thick plate using third order shear deformation theory. The finite element method presented in the previous chapters can be easily used for vibration and stability analysis of rotating plates. The effects of different parameters such as temperature change, hub radius ratio and rotational speed on vibration and dynamic stability of rotating plates are discussed.

7.2 Mathematical Formulation

Figure 7.1 shows a rotating cantilever FGM plate of a length L, width B, and thickness h, which is fixed to a rigid hub with a radius R. The cantilever FGM plate is subjected to a dynamic load $P(t) = P_s + P_t \cos \Omega t$ acting along neutral axis as shown in figure 7.1. Where P_s and P_t are the static and dynamic components of the axial force. The frequency of the dynamic component of the force is Ω and t is time. The coordinate system of the typical four noded rectangular element used to derive the governing equations of motion is shown in figure 4.4 of chapter 4. The neutral plane is preferred as the reference plane for expressing the displacements.

The elastic stiffness matrix, thermal stiffness matrix and mass matrix for the FGM plate element derived in section 3.2 are also applicable in this case and hence the expressions have not been repeated.

The effect of rotation is introduced as centrifugal stiffness matrix which is derived from the work done by the centrifugal force and presented as follows.
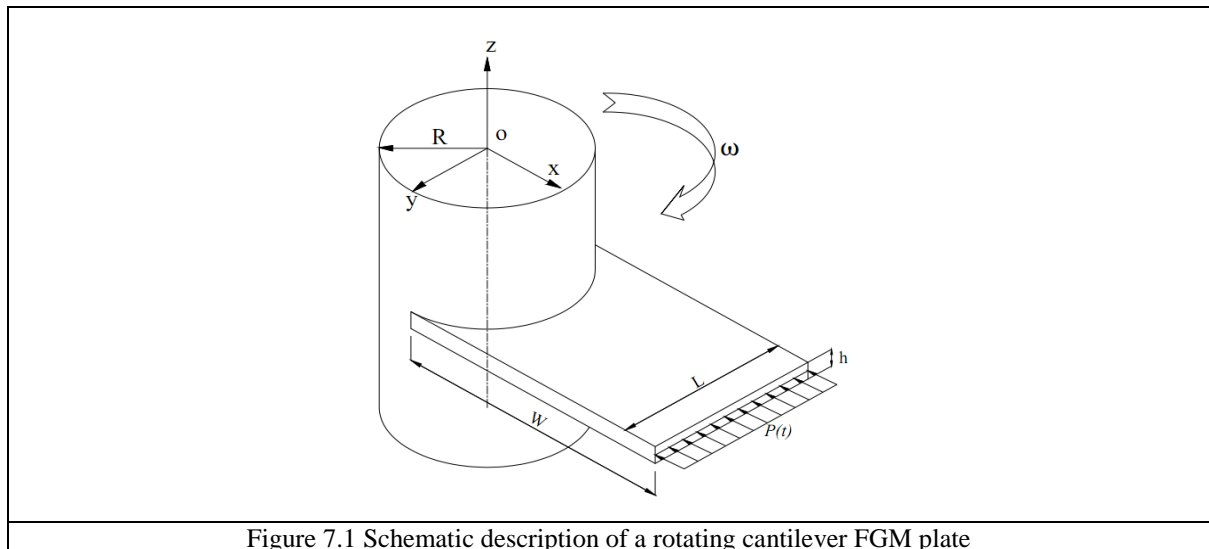
Figure 7.1 Schematic description of a rotating cantilever FGM plate

7.2.1 Temperature field along the thickness of FGM plate

According to power law graded change in temperature along the thickness of the FGM plate is assumed. Let us consider that the temperature of the ceramic surface is Tc and according to a power law along the thickness to the pure metal surface temperature it varies from T_c to T_m. The variation of power law temperature distribution is as shown in figure 7.2.

The temperature across the thickness is expressed as

$$T(z) = T_m + (T_c - T_m)\left(\frac{1}{2} + \frac{z}{h}\right)^n \tag{7.1}$$
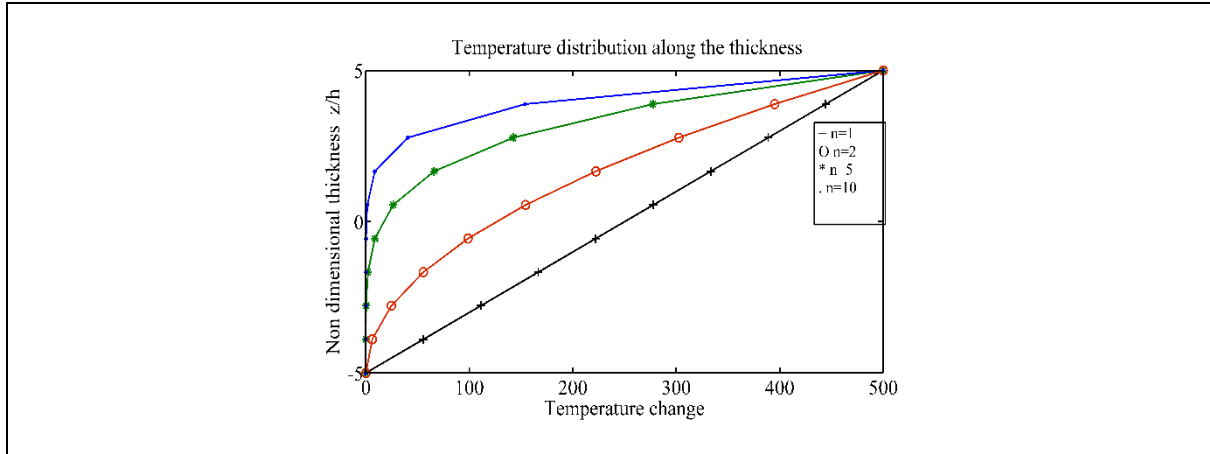
Figure 7.2 variation of temperature distribution along the thickness direction

7.2.2 Element centrifugal stiffness matrix

As the FGM plate is rotating it is subjected to centrifugal forces. Hence, the work done by the plate due to rotation is expressed as

$$W_c^{(e)} = \frac{1}{2}\int_A F_c^{(e)} w^2 dx dy = \frac{1}{2}\left\{q^{(e)}\right\}^T \left[K_c^{(e)}\right]\left\{q^{(e)}\right\} \tag{7.2}$$

The centrifugal force on an element of the FGM plate can be expressed as

$$F_c^{(e)} = \int_{x_i}^{x_i+l} \int_{-h/2-d}^{h/2-d} b\rho(z')\varpi_r^2 (H+x) dz' dx \tag{7.3}$$

where x_i is the distance of ith node from axis of rotation, ϖ_r *(rad/s)* is angular speed of plate element and H is the radius of hub.

Element centrifugal stiffness matrix

$$\left[K_c^{(e)}\right] = F_c \iint [N_w]^T [N_w] dx dy \tag{7.4}$$

7.3 Governing Equations of Motion

The elastic stiffness, mass matrix and geometric stiffness matrix of the FGM plate element derived in section 3.2.6 are also applicable in this case, hence have not been repeated. The strain energy due to thermal load is given in equation (4.16). Work done by plate element due to rotation is given in equation (7.2).

The equation of motion for FGM plate element referring section 3.3 can be modified for the present case and is given as

$$\left[M^{(e)}\right]\left\{\ddot{q}^{(e)}\right\} + \left[K_{ef}^{(e)}\right]\left\{q^{(e)}\right\} - P(t)\left[K_g^{(e)}\right]\left\{q^{(e)}\right\} = 0 \tag{7.5}$$

where $\left[K_{ef}^{(e)}\right]=\left[K^{(e)}\right]-\left[K_T^{(e)}\right]+\left[K_C^{(e)}\right]$

$\left[K_{ef}^{(e)}\right]$ is effective element stiffness matrix, $\left[K^{(e)}\right],\left[K_T^{(e)}\right]$ and $\left[K_C^{(e)}\right]$ are element stiffness matrix, thermal matrix and centrifugal stiffness matrix respectively.

Assembling the element matrices in equation (7.5), the equation in terms of global matrices which is the equation of motion for the rotating plate, can be expressed as

$$[M]\{\ddot{q}\}+\left[K_{ef}\right]\{q\}-P(t)\left[K_g\right]\{q\}=0 \tag{7.6}$$

where $P(t)$ is the time dependent dynamic load, which can be represented in terms of static critical buckling load P^{cr} of metallic plate having applied boundary conditions. Hence substituting, $P(t)=\alpha P^{cr}+\beta P^{cr}\cos\Omega t$ with α and β as called static and dynamic load factors respectively, equation (7.6) can be expressed as

$$[M]\{\ddot{q}\}+\left[\left[K_{ef}\right]-P^{cr}\left(\alpha+\beta\cos\Omega t\right)\left[K_g\right]\right]\{q\}=0 \tag{7.7}$$

where $\left[K_{ef}\right]=\left[K\right]-\left[K_T\right]+\left[K_C\right]$

$\left[K_{ef}\right]$ is the effective stiffness matrix and $\left[K\right],\left[K_T\right],\left[K_C\right],[M]$ and $\left[K_g\right]$ are global elastic stiffness, thermal matrix, centrifugal matrix, mass matrix and geometric stiffness matrix respectively and $\{q\}$ is global displacement vector.

The condition for existence of the boundary solutions with period 2T is given by

$$\left(\left[K_{ef}\right]-\left(\alpha\pm\frac{\beta}{2}\right)P^{cr}\times\left[K_g\right]-\frac{\Omega^2}{4}[M]\right)\{q\}=0 \tag{7.8}$$

The instability boundaries can be determined from the solution of the equation

$$\left|\left[K_{ef}\right]-\left(\alpha\pm\frac{\beta}{2}\right)P^{cr}\times\left[K_g\right]-\frac{\Omega^2}{4}[M]\right|=0 \tag{7.9}$$

Following the procedure described in section 3.3.1, the natural frequencies, critical buckling load and instability regions of FGM plate in hygrothermal environment are determined.

7.4 Results and Discussion

7.4.1 Validation

In all presented tables and figures, δ, η, σ, ϖ and γ represent aspect ratio, thickness ratio, hub radius ratio, dimensionless natural frequency and dimensionless rotation speed, respectively, and are defined as: $\delta = L/W$, $\eta = h/L$, $\sigma = R/L$, $\varpi = \omega L^2 \sqrt{\rho h / D}$, $\gamma = \Upsilon T$, $D = Eh^3 / \left(12\left(1-v^2\right)\right)$, $T = \sqrt{\rho h L^4 / D}$

where E and v are Young's modulus of elasticity and Poisson's ratio of the metal phase, respectively. Υ is constant angular speed.

The plate is discretized into 10X10 elements. First of all, the numerical results obtained by using the present method are compared to those of Yoo and Kim [229] and Hashemi et al. [53] for rotating isotropic material plate frequency parameters. As shown in tables 7.1 and 7.2, the lowest five natural frequencies obtained by the present modeling method agree well with those of Yoo and Kim [229] and Hashemi et al. [53].

Table 7. 1 Comparison of lowest five natural frequencies by the present and by the Yoo and Kim [229] and Hashemi et al. [53]. $\left(\delta = 1, \sigma = 0\right)$

	$\gamma = 1$			$\gamma = 2$		
	Hashemi et al. [53]	Yoo and Kim[229]	Present	Hashemi et al. [53]	Yoo and Kim[229]	Present
ϖ_1	3.6437	3.6528	3.5421	4.1051	4.1131	3.9487
ϖ_2	8.6289	8.6459	8.5109	8.9790	9.0031	9.0739
ϖ_3	21.4378	21.5337	21.4160	21.8630	21.9664	21.9660
ϖ_4	27.2592	27.3847	27.0952	27.4993	27.6231	27.7049
ϖ_5	31.0695	31.2185	30.8993	31.4258	31.5854	31.3487

Table 7. 2 Comparison of lowest five natural frequencies by the present and by the Yoo and Kim [229] and Hashemi et al. [53]. $\left(\delta = 1, \sigma = 1\right)$

	$\gamma = 1$			$\gamma = 2$		
	Hashemi et al. [53]	Yoo and Kim[229]	Present	Hashemi et al. [53]	Yoo and Kim[229]	Present
ϖ_1	3.8532	3.8618	3.8195	4.8069	4.8138	4.8176
ϖ_2	8.7157	8.7358	8.8905	9.3079	9.3435	10.3977
ϖ_3	21.6205	21.7196	21.7848	22.5615	22.6798	23.0773
ϖ_4	27.3009	27.4257	27.5030	27.6713	27.7901	29.0710
ϖ_5	31.2101	31.3624	31.1998	31.9771	32.1493	32.1498

7.4.2 Vibration and buckling analysis

The following numerical results are obtained by considering the combination of steel (SUS304) and Alumina (Al_2O_3) for the FGM. The geometry of the rotating square FGM plate is as follows: side to thickness ratio L/h=0.01, hub radius ratio R/L=0, rotational speed=100 rpm.

Figures 7.3-7.6 illustrate the natural frequencies versus temperature variation of rotating cantilever FGM (SUS304/Al_2O_3) plate for first and second mode. For all thermal conditions the metallic side (bottom) temperature is kept as constant $300K$. The ceramic (upper) surface temperature varies from $300K$ to $800K$ in all thermal conditions. FGM plates of three volume fraction indices k=0, 0.5 and 2 subjected to temperature environments n=0, 1, 5 and 10 are considered. It is observed that increase in temperature reduces the first two natural frequencies of rotating FGM plate. Also, the increase in power law index value reduces the first two natural frequencies of rotating plate.
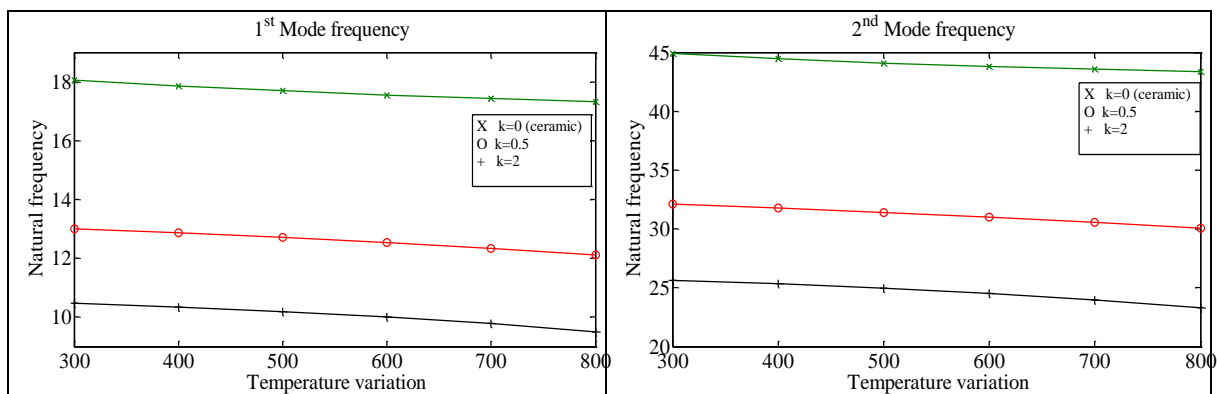
Figure 7.3(a) First mode frequency verses temperature variation for different power law index values at thermal field (n=0).

Figure 7.3(b) Second mode frequency verses temperature variation for different power law index values at thermal field (n=0).

Figure 7.4(a) First mode frequency verses temperature variation for different power law index values at thermal field (n=1).

Figure 7.4(b) Second mode frequency verses temperature variation for different power law index values at thermal field (n=1).

| Figure 7.5(a) First mode frequency verses temperature variation for different power law index values at thermal field (n=5). | Figure 7.5(b) Second mode frequency verses temperature variation for different power law index values at thermal field (n=5). |

| Figure 7.6(a) First mode frequency verses temperature variation for different power law index values at thermal field (n=10). | Figure 7.6(b) Second mode frequency verses temperature variation for different power law index values at thermal field (n=10). |
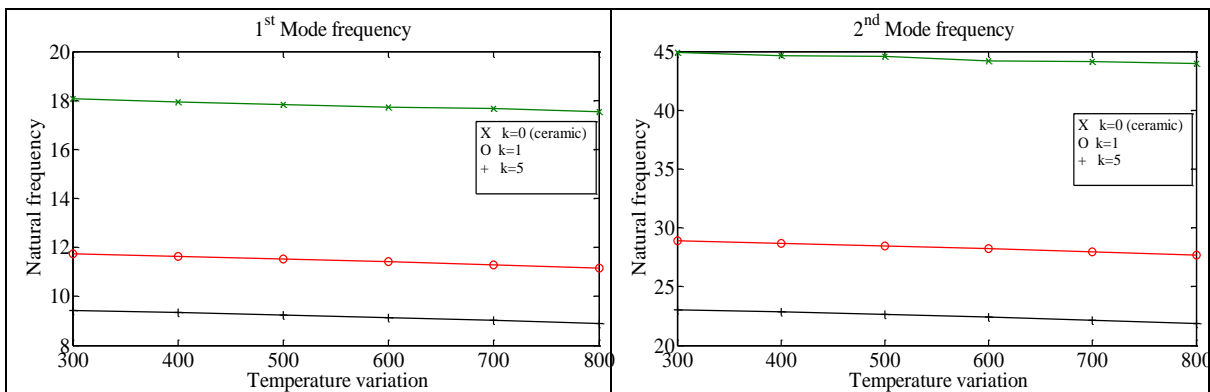
The figure 7.7 is a plot of natural frequency versus temperature variation for four thermal environment conditions namely n=0, 1, 5, 10. The effect of temperature rise on fundamental frequency is most severe for the case n=0, i.e. uniform temperature case. With increase in the index value, the reduction in fundamental natural frequency diminishes. The effect of increase of index becomes very insignificant for high values of n, say above n=5. The temperature rise decreases the effective Young's modulus which leads to reduction in the stiffness of the plate. The reduced stiffness decreases the natural frequencies of the rotating plate.
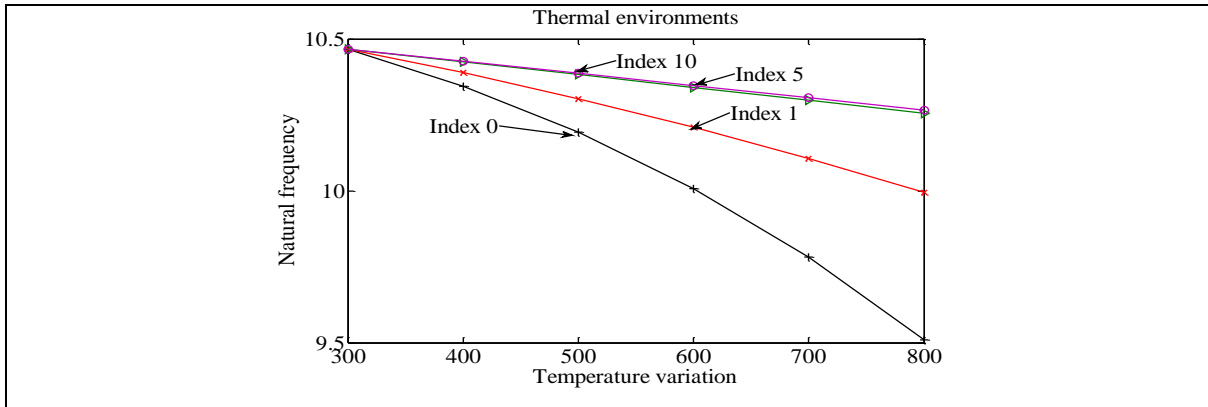
Figure 7.7 Variation of fundamental frequency of rotating FGM plate in for thermal environments (n=0, 1, 5 and 10).

Figure 7.8-7.9 show the effect of hub radius on the rotating cantilever FGM plate natural frequencies in nonlinear (n=10) thermal condition for power law index values k=0, 1 and 5. It can be observed from the figures that with the increase of hub radius the first two natural frequencies increase.

Figure 7.8 Variation of first mode frequency with hub radius ratio at thermal field (n=10) for power law index k=0, 1 and 5.

Figure 7.9 Variation of second mode frequency with hub radius ratio at thermal field (n=10) for power law index k=0, 1 and 5.
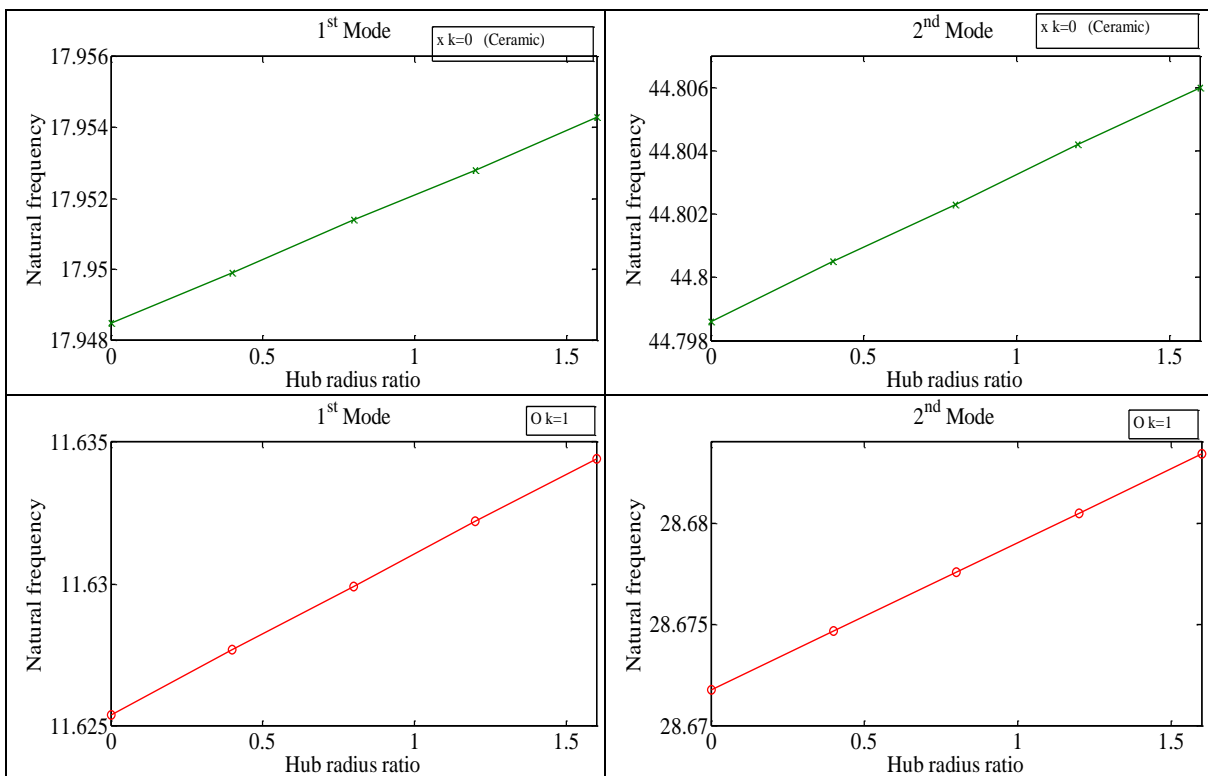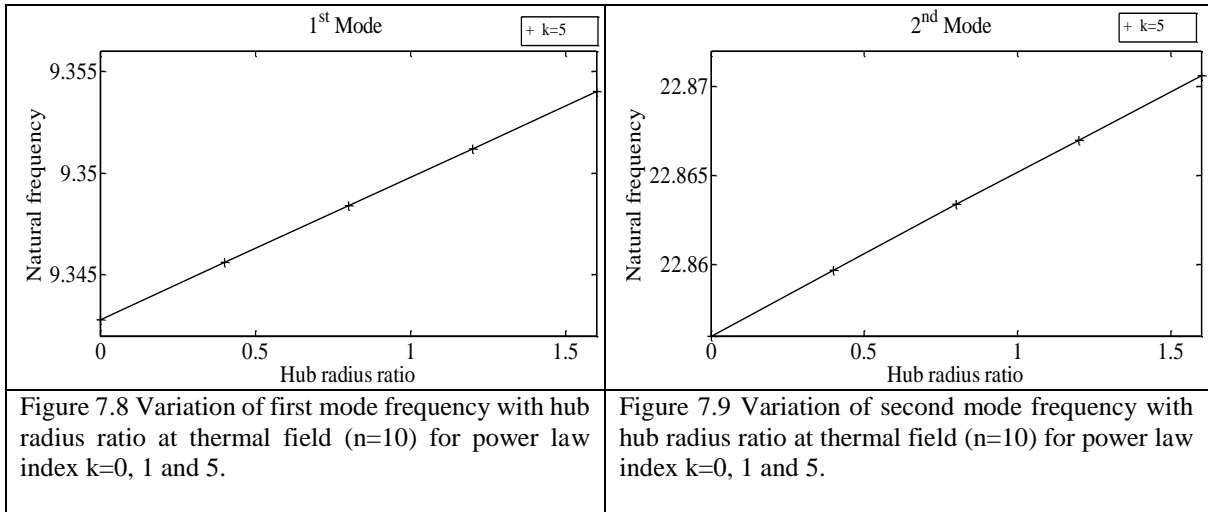
Figure 7.10(a) and (b) describe the effect of rotational speed on natural frequencies of cantilever FGM plate in nonlinear (n=10) thermal environment. The increased rotational speed increases the first two natural frequencies and it is due to the centrifugal stiffening of the plate.
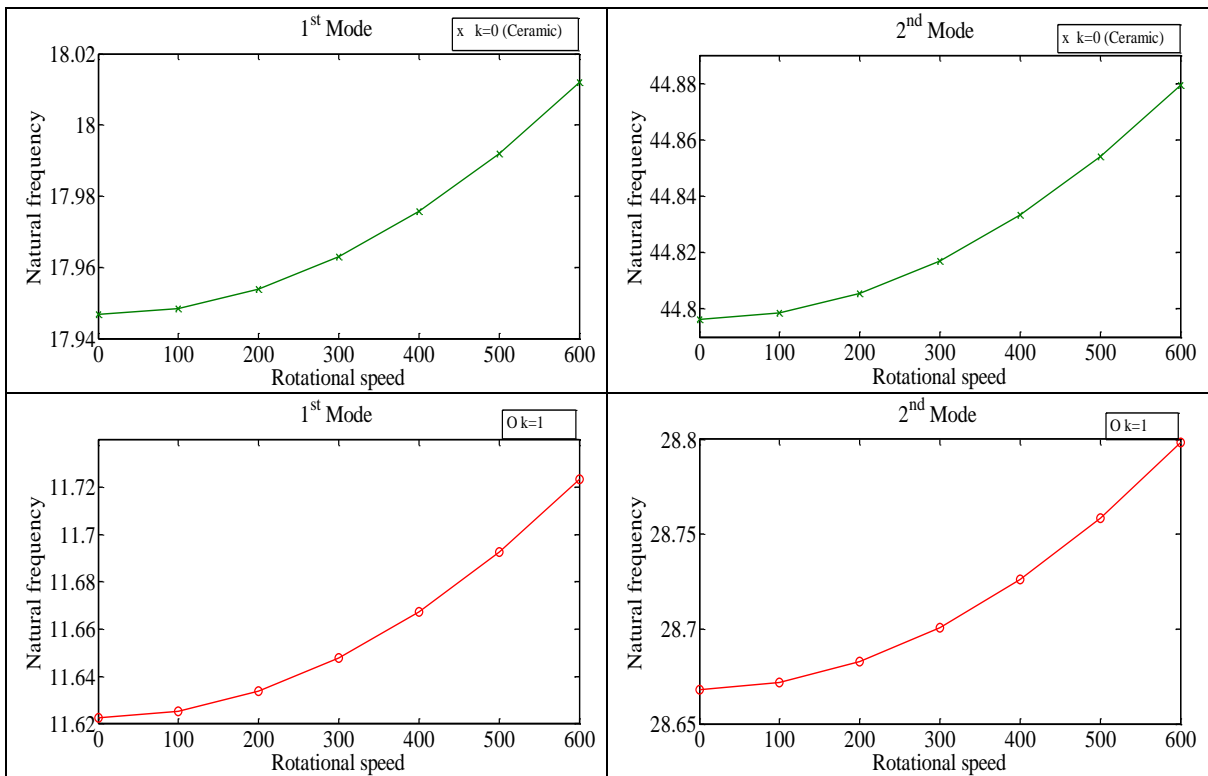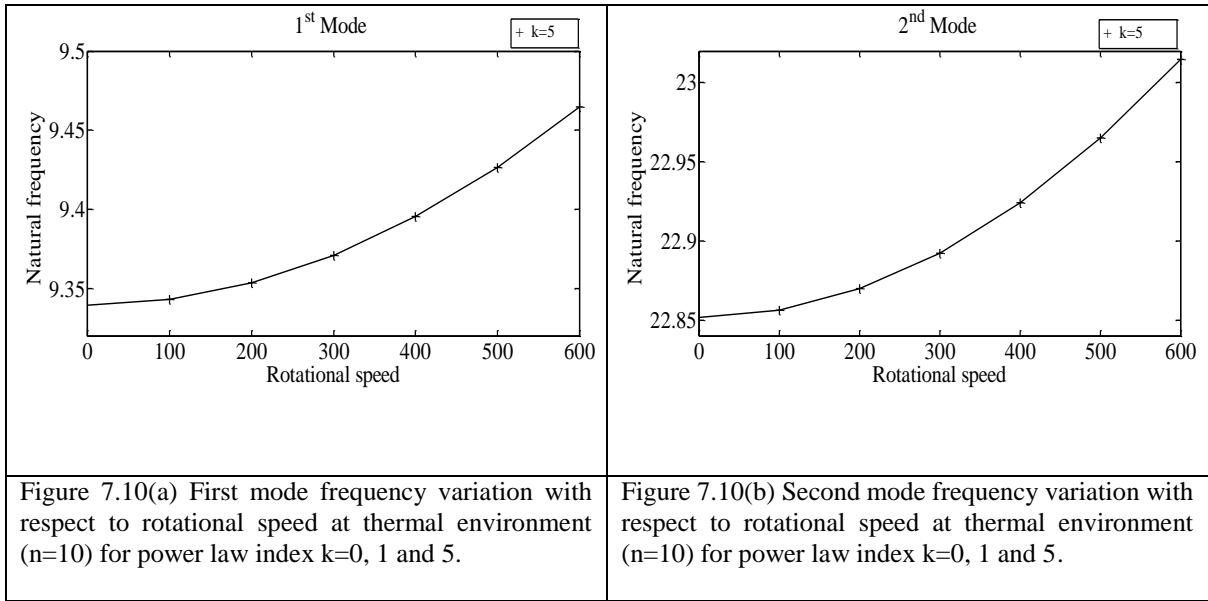
| Figure 7.10(a) First mode frequency variation with respect to rotational speed at thermal environment (n=10) for power law index k=0, 1 and 5. | Figure 7.10(b) Second mode frequency variation with respect to rotational speed at thermal environment (n=10) for power law index k=0, 1 and 5. |

| Figure 7.11(a) Critical buckling load variation with respect to rotational speed k=1 | Figure 7.11(b) Critical buckling load variation with respect to rotational speed k=5 |
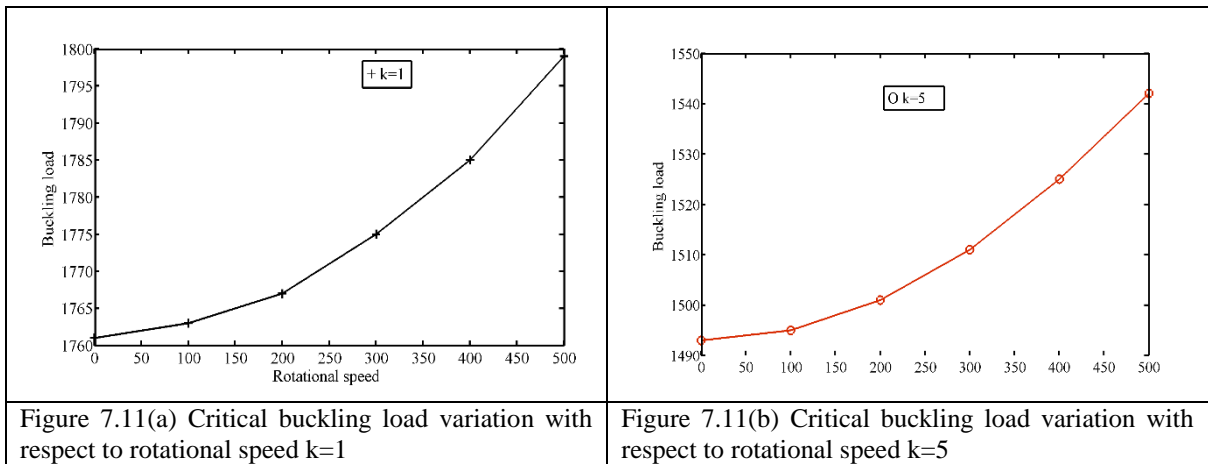
Figure 7.11(a) and (b) show the variation of critical buckling load with respect to rotational speed of the plate. It can be seen that increase in rotational speed increases the critical buckling load of FGM plate for power law index values, k=1 and k=5.
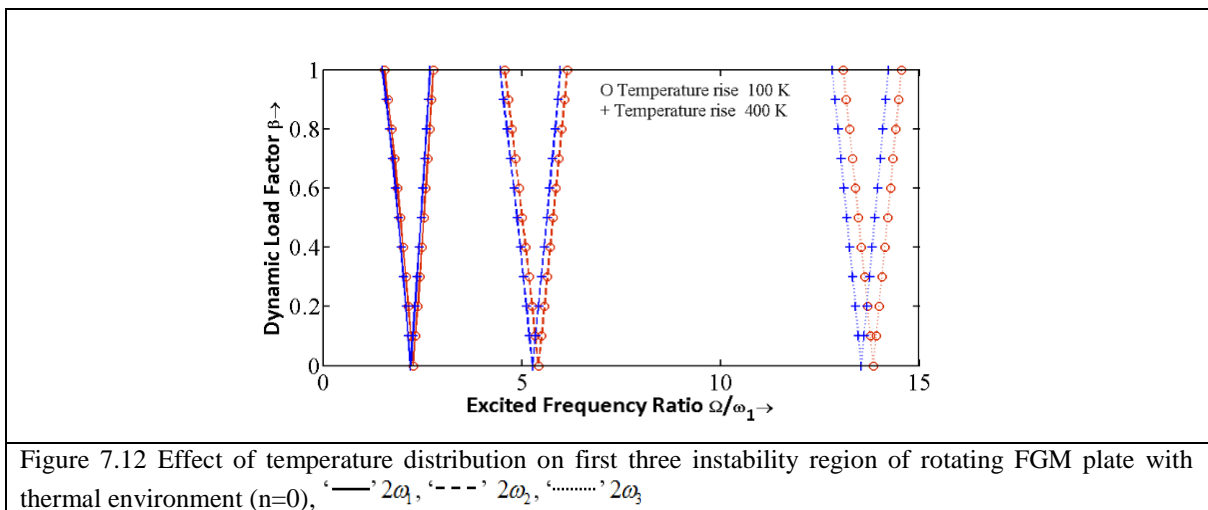
Figure 7.12 Effect of temperature distribution on first three instability region of rotating FGM plate with thermal environment (n=0), '——' $2\omega_1$, '- - -' $2\omega_2$, '..........' $2\omega_3$

7.4.3 Dynamic stability analysis

Figure 7.12 shows the effect of temperature rise on the principal instability regions of first three modes of FGM plate in thermal environment (n=0) for temperature difference of 100K and 400K. It can been seen from the figure that with increase in temperature, the instability regions shift to lower frequencies of excitation, thereby increasing the probability of occurrence of instability. The effect of change in temperature is more for higher modes compared to fundamental mode. With increase in temperature the strength of the plate decreases that leads to decrease in natural frequencies. Hence instability occurs at lower excitation frequencies.

Figure 7.13(a) Effect of temperature distribution on first mode instability region of rotating FGM plate with thermal environment (n=1).	Figure 7.13(b) Effect of temperature distribution on second mode instability region of rotating FGM plate with thermal environment (n=1).
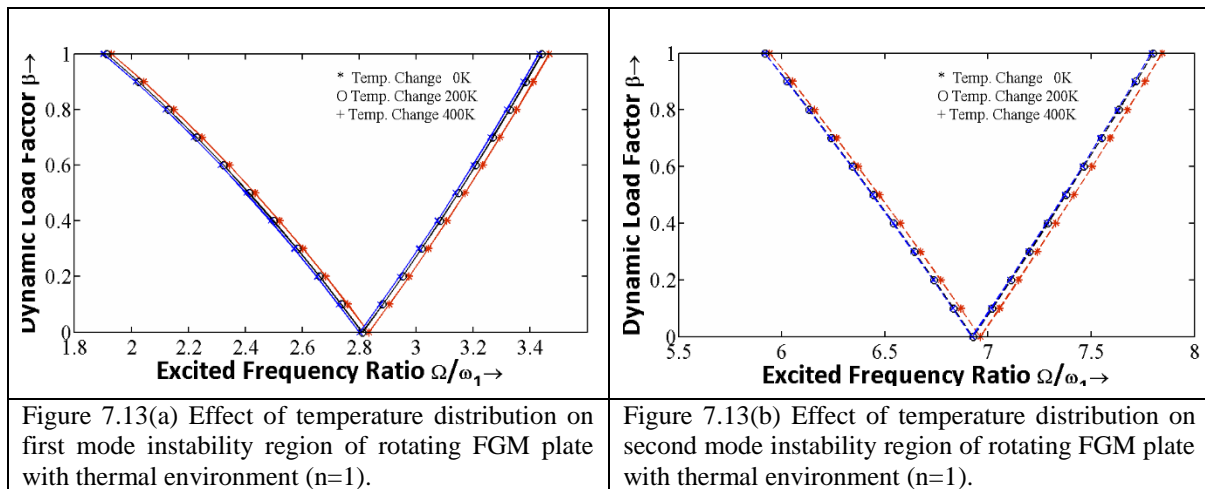
Figure 7.13 presents the diagrams of dynamic instability of first two modes of FGM plate in linear temperature distribution thermal environment (n=1). The temperature rises considered are 0, 200 and 400 K. When temperature difference is 0K the plate is most stable, the increased temperature rise decreases the stability, in terms of shifting of the instability regions to lower excitation frequencies.

Figure 7.14(a) Effect of temperature distribution on first mode instability region of rotating FGM plate with thermal environment (n=5).	Figure 7.14(b) Effect of temperature distribution on second mode instability region of rotating FGM plate with thermal environment (n=5).
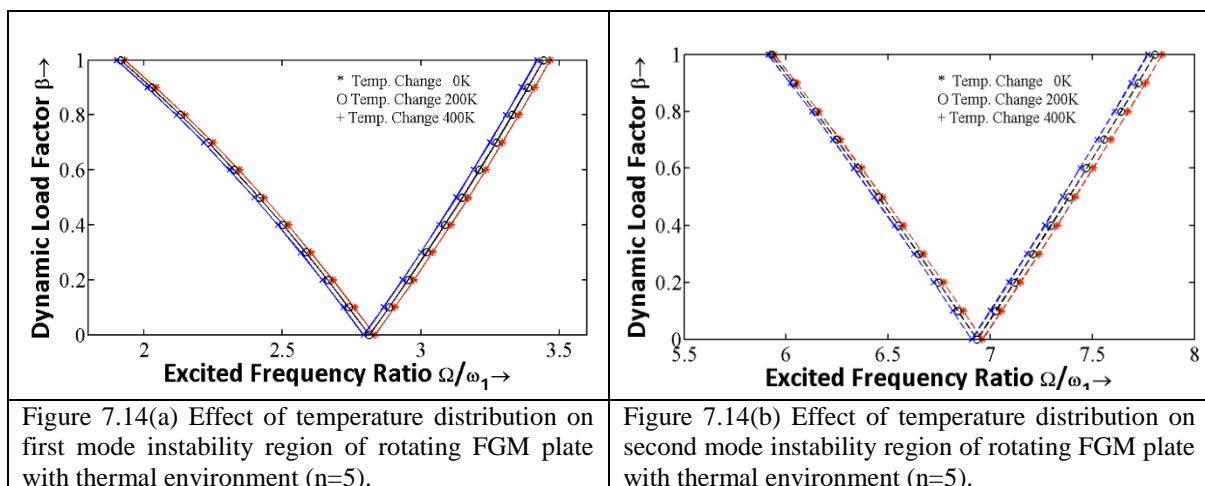
The first and second principal instability regions of rotating FGM plates in thermal environment (n=5) and thermal environment (n=10) are shown in figures 7.14(a, b) and 7.15(a,

b) respectively. As expected when there is no temperature rise (0 K) the instability regions occur at highest excitation frequencies, with increase in environment temperature the instability regions occurs at lower excitation frequencies. This indicates, with increase in temperature, the stability of the plate deteriorates. The increase of temperature rise reduces the Young's modulus which causes the reduction in the overall stiffness of rotating plate and decrease in natural frequencies. So instability occurs at lower excitation frequencies.

| Figure 7.15(a) Effect of temperature distribution on first mode instability region of rotating FGM plate with thermal environment (n=10), key as in fig. 3.25. | Figure 7.15(b) Effect of temperature distribution on second mode instability region of rotating FGM plate with thermal environment (n=10), key as in fig. 3.25. |

| Figure 7.16(a) Effect of hub radius ratio on first mode instability region of rotating FGM plate, key as in fig. 3.25. | Figure 7.16(b) Effect of hub radius ratio on second mode instability region of rotating FGM plate, key as in fig. 3.25. |

The effect of hub radius on dynamic stability of rotating FGM plate in thermal environment is presented in figures 7.16(a) and 7.16(b) for first and second mode respectively. The hub radius ratio is varied from 0 to 1. From the figures it is found that for first and second mode the stability increases appreciably with the increase in hub radius. This happens due to increased centrifugal stiffening of the plate with increased hub radius.
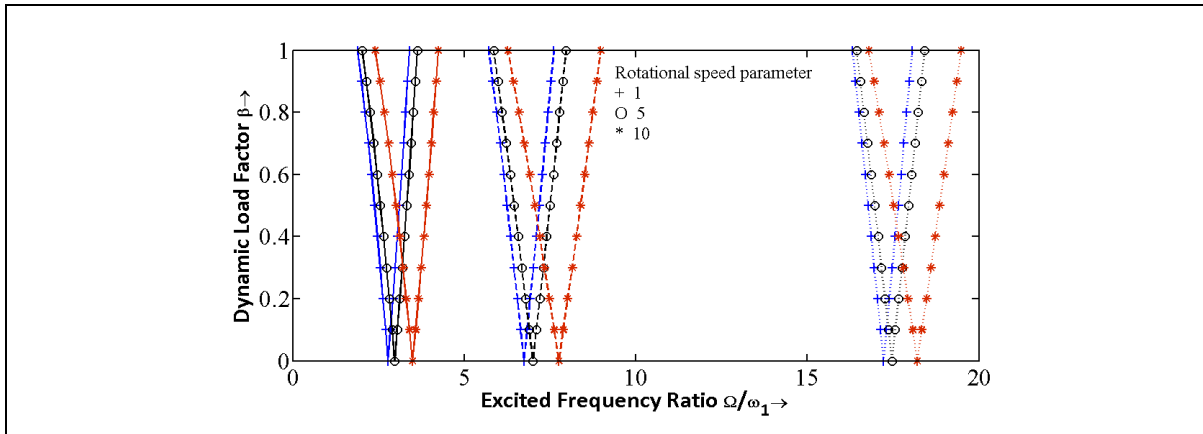
Figure 7.17(a) Effect of rotational speed on first three instability regions of FGM plate for h=0.05m, and temperature rise 100^0 K, k=1, key as in fig. 3.15.
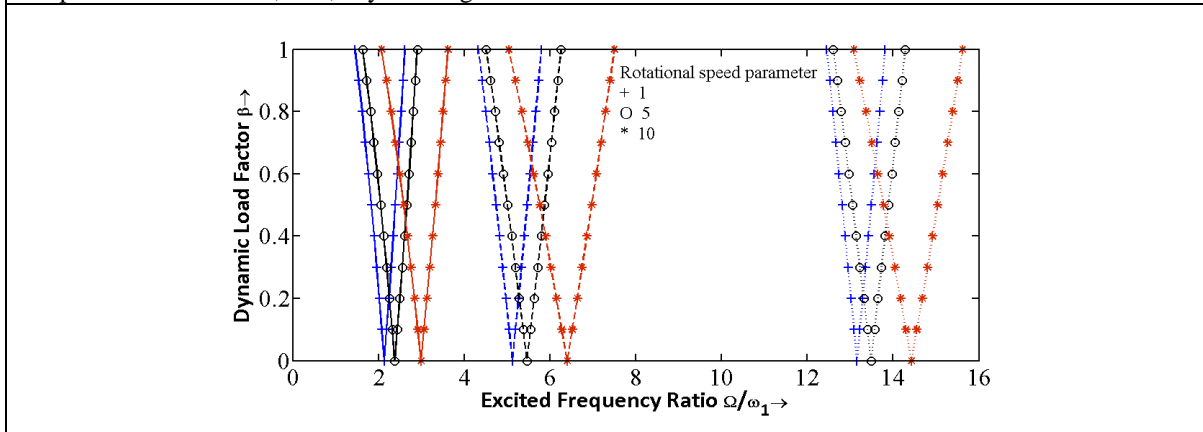
Figure 7.17(b) Effect of rotational speed on first three instability regions of FGM plate for h=0.05m, and temperature rise 100^0 K, k=10, key as in fig. 3.15.

Figures 7.17(a) and 7.17(b) show the effect of rotational speed on the first three mode instabilities of FGM plate with k=1 and k=10, respectively. It is found that for the first three modes stability increases with the increase in rotational speed of plates. When the rotational speed increases the centrifugal force increases. Increased centrifugal force causes centrifugal stiffening of the plate, hence the natural frequencies increase. Due to the increase in natural frequencies the instability occurs at higher excitation frequencies.

7.5 Conclusion

Flapwise bending vibration and dynamic stability of rotating FGM plates with different temperature environments are investigated by using finite element method. The third order shear deformation theory is used for theoretical formulation. The temperature dependent material properties are considered and vary along the thickness direction of the plate following a power law distribution of constituent's volume fraction. Based on the numerical results, the following conclusions are reached.

Increase in power law index value reduces the first two natural frequencies of rotating FGM plate. Rise in temperature reduces the first two mode natural frequencies of rotating plate in thermal environment. The first two natural frequencies increase with an increase of the hub radius and the rotational speed of FGM plates. The critical buckling load increases with an increase of the rotational speed of FGM plate.

It is observed that dynamic stability of rotating plate in thermal environment reduces as the temperature increases. The dynamic instability increases with increase in hub radius. Increase in rotational speed has a stabilizing effect on the plate.

Chapter 8

DYNAMIC STABILITY OF SKEW FUNCTIONALLY GRADED PLATES UNDER PARAMETRIC EXCITATION

8.1 Introduction

A novel model material which combines the finest properties such as high strength, high stiffness, toughness, and temperature resistance of both metals and ceramics has been developed for structural applications. By varying the constituents of two or more materials spatially, new materials of desired property progression in preferred directions may be formed and is termed as functionally graded material (FGM). This material property gradation can reduce the stresses such as residual and thermal. The increased use of FGM in various applications such as skew plate structural components of tails, panels in skew bridges, wings and fins of swept wing missile have required a robust necessity to understand their dynamic stability characteristics under different thermo-mechanical loading conditions. The skew plate structures are sometimes subjected to inplane pulsating load and become dynamically unstable i.e. transverse vibration grows without bound for certain combinations of dynamic load amplitude and excitation frequency. This phenomenon is termed as parametric resonance or dynamic instability. Bolotin [14] studied the theory of dynamic stability of elastic structures. Young and Chen [230] investigated the stability of skew plates under aerodynamic and inplane forces. Noh and Lee [136] used higher order shear deformation theory along with finite element

method for the dynamic instability study of delaminated composite skew plates under various periodic in-plane loads. Young et al. [231] examined the dynamic stability of skew plates subjected to an aerodynamic force in the chordwise direction and a random in-plane force in the spanwise direction.

Previous studies on the dynamic stability of FGM plates subjected to time-dependent compressive axial loads are mainly based on temperature independent material. It is evident from the available literature that the dynamic instability of temperature dependent FGM skew plates has not been thoroughly studied. The present work attempts to study the dynamic stability of a skew plate under high temperature environment. Based on Bolotin's method the boundary frequencies of instability regions are plotted. The dynamic instability of FGM skew plate is affected by power law index, skew angle, aspect ratio, and thermal load. The fundamental frequency and critical buckling of FGM skew plate have been studied in detail for all sides simply supported (SSSS) and all sides clamped (CCCC) boundary conditions.

8.2 Mathematical Formulation

8.2.1 Oblique boundary transformation

Figure 8.1 shows that the thick skew plate edges are not parallel to global axes X and Y, therefore it is required to define the boundary conditions in terms of the displacements u, v, w, $\theta_x, \theta_y, \dfrac{\partial w}{\partial x}$ and $\dfrac{\partial w}{\partial y}$. The local reference plane edge displacements u_S, v_T, w, θ_T, θ_S, $\dfrac{\partial w}{\partial S}$ and $\dfrac{\partial w}{\partial T}$ are tangential and normal to the oblique edge. Here, θ_T and θ_s represent the average rotations of the normal to the reference plane and normal to the oblique edge. So it is necessary to transform the element matrices along the oblique coordinates corresponding to x-axis and y-axis. The oblique boundary transformation displacement for i^h node is given by

$$
\begin{Bmatrix} u_x \\ v_y \\ w \\ \theta_x \\ \theta_y \\ \dfrac{\partial w}{\partial x} \\ \dfrac{\partial w}{\partial y} \end{Bmatrix} = \begin{bmatrix} \cos\phi & -\sin\phi & 0 & 0 & 0 & 0 & 0 \\ \sin\phi & \cos\phi & 0 & 0 & 0 & 0 & 0 \\ 0 & 0 & 1 & 0 & 0 & 0 & 0 \\ 0 & 0 & 0 & \cos\phi & -\sin\phi & 0 & 0 \\ 0 & 0 & 0 & \sin\phi & \cos\phi & 0 & 0 \\ 0 & 0 & 0 & 0 & 0 & \cos\phi & -\sin\phi \\ 0 & 0 & 0 & 0 & 0 & \sin\phi & \cos\phi \end{bmatrix} \begin{Bmatrix} u_S \\ v_T \\ w \\ \theta_T \\ \theta_s \\ \dfrac{\partial w}{\partial S} \\ \dfrac{\partial w}{\partial T} \end{Bmatrix} \tag{8.1}
$$

The relationship of transformation can be written as

$$\left\{q_i^{(e)}\right\} = \left[T_i\right]\left\{\overline{q}_i^{(e)}\right\} \qquad (8.2)$$

$$\left\{q^{(e)}\right\} = \left[T\right]\left\{\overline{q}^{(e)}\right\} \qquad (8.3)$$

where $\left[T_i\right]$ is the transform matrix for the ith node.

For the complete element, the complete element transformation matrix $\left[T^{(e)}\right]$ is written as

$$\left[T^{(e)}\right] = diag\left[\left[T_i\right]\ \left[T_i\right]\ \left[T_i\right]\ \left[T_i\right]\right] \qquad (8.4)$$

| Figure 8.1(a) Geometry of the plate in the skew co-ordinate system. | Figure 8.1(b) Inplane periodic loading of the plate in the skew co-ordinate system. |

Figure 8.1(a) Geometry of the plate in the skew co-ordinate system.

Figure 8.1(b) Inplane periodic loading of the plate in the skew co-ordinate system.
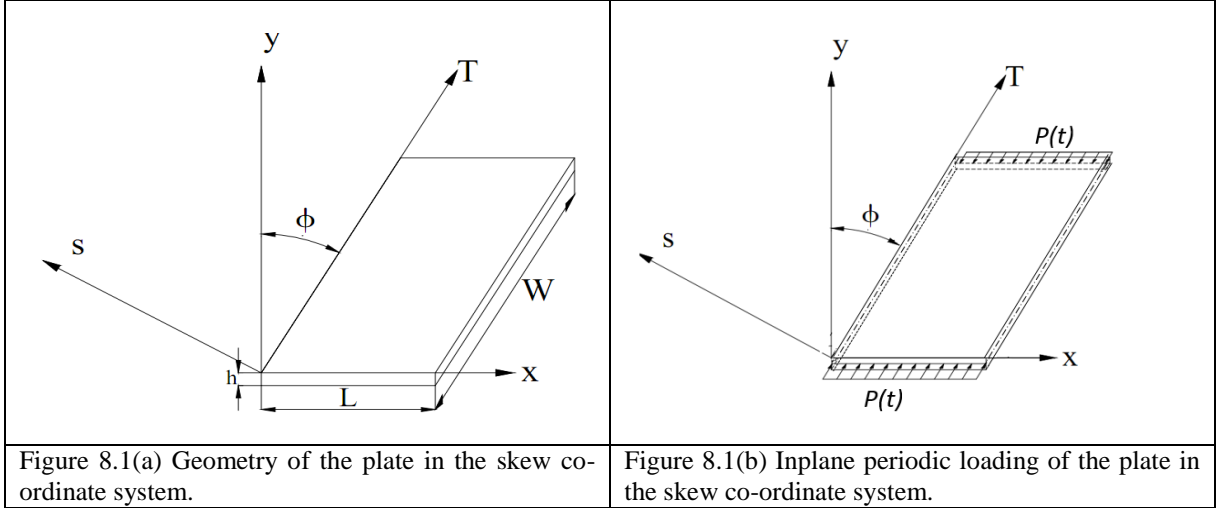
8.2.2 Finite Element Analysis

The skew FGM plate in thermal environment is as shown in figure 8.1. A four node rectangular element is considered for the analysis of skew FGM plate in thermal environment. The stiffness, thermal stiffness and mass matrices can be computed in skew coordinates as follows.

The strain energy $U^{(e)}$ and kinetic energy $T^{(e)}$ of the skew FGM plate element can be expressed as

$$U^{(e)} = U_p^{(e)} + U_T^{(e)} \qquad (8.5)$$

$$U_P^{(e)} = \frac{1}{2}\int_0^b\int_0^a \left[T^{(e)}\right]^T\left[\left[N\right]^T\left\{\varepsilon^{(n)}\right\} + \left[M\right]^T\left\{\varepsilon^{(1)}\right\} + \left[P\right]^T\left\{\varepsilon^{(3)}\right\} + \left[Q^s\right]^T\left\{\gamma^{(n)}\right\} + \left[R^s\right]^T\left\{\gamma^{(2)}\right\}\right]\left[T^{(e)}\right]dxdy \qquad (8.6)$$

$$U_T^{(e)} = \frac{1}{2}\int_0^b\int_0^a\left[T^{(e)}\right]^T\left[\left[N^T\right]^T\left\{\varepsilon^{(n)T}\right\} + \left[M^T\right]^T\left\{\varepsilon^{(1)T}\right\} + \left[P^T\right]^T\left\{\varepsilon^{(3)T}\right\}\right]\left[T^{(e)}\right]dxdy \qquad (8.7)$$

$$T^{(e)} = \frac{1}{2}\rho\int_A\left(\dot{u}^2 + \dot{v}^2 + \dot{w}^2\right)dA \qquad (3.21)$$

Following the procedure described in chapter 3and 4 the skew element stiffness matrix $\left[K^{(se)}\right]$ is derived as

$$U_p^{(e)} = \frac{1}{2}\left[\left\{q^{(e)}\right\}^T \left[T^{(e)}\right]^T \left[K^{(e)}\right]\left[T^{(e)}\right]\left\{q^{(e)}\right\}\right] \tag{8.8}$$

$$\left[K^{(se)}\right] = \left[T^{(e)}\right]^T \left[K^{(e)}\right]\left[T^{(e)}\right] \tag{8.9}$$

$$\left[K^{(e)}\right] = \left[K_b^{(e)}\right] + \left[K_s^{(e)}\right] \tag{3.31}$$

$$\left[K_b^{(e)}\right] = \left[K_{00}^{(e)}\right] + \left[K_{01}^{(e)}\right] + \left[K_{11}^{(e)}\right] + \left[K_{02}^{(e)}\right] + \left[K_{12}^{(e)}\right] + \left[K_{22}^{(e)}\right] \tag{3.32}$$

$$\left[K_s^{(e)}\right] = \left[K_{33}^{(e)}\right] + \left[K_{34}^{(e)}\right] + \left[K_{44}^{(e)}\right] \tag{3.34}$$

Similarly the element mass matrix is expressed as

Element kinetic energy

$$T^{(e)} = \frac{1}{2}\left[\left\{q^{(e)}\right\}^T \left[T^{(e)}\right]^T \left[M^{(e)}\right]\left[T^{(e)}\right]\left\{q^{(e)}\right\}\right]$$
$$= \frac{1}{2}\left[\left\{q^{(e)}\right\}^T \left[M^{(se)}\right]\left\{q^{(e)}\right\}\right] \tag{8.10}$$

$$\left[M^{(e)}\right] = \int_0^a \int_0^b \left[I_0\left(\left[N_{u_n}\right]^T\left[N_{u_n}\right] + \left[N_{v_n}\right]^T\left[N_{v_n}\right] + \left[N_{w_n}\right]^T\left[N_{w_n}\right]\right) + \right.$$
$$I_1\left(\left[N_{u_n}\right]^T\left[N_{\theta_x}\right] + \left[N_{\theta_x}\right]^T\left[N_{u_n}\right] + \left[N_{v_n}\right]^T\left[N_{\theta_y}\right] + \left[N_{\theta_y}\right]^T\left[N_{v_n}\right]\right) +$$
$$I_2\left(\left[N_{\theta_x}\right]^T\left[N_{\theta_x}\right] + \left[N_{\theta_y}\right]^T\left[N_{\theta_y}\right]\right) +$$
$$I_3\left(\left[N_{u_n}\right]^T\left[\left[N_{\theta_x}\right] + \left[N_{\partial w/\partial x}\right]\right] + \left[\left[N_{\theta_x}\right] + \left[N_{\partial w/\partial x}\right]\right]^T\left[N_{u_n}\right] + \right.$$
$$\left.\left[N_{v_n}\right]^T\left[\left[N_{\theta_y}\right] + \left[N_{\partial w/\partial y}\right]\right] + \left[\left[N_{\theta_y}\right] + \left[N_{\partial w/\partial y}\right]\right]^T\left[N_{v_n}\right]\right) +$$
$$I_4\left(\left[N_{\theta_x}\right]^T\left[\left[N_{\theta_x}\right] + \left[N_{\partial w/\partial x}\right]\right] + \left[\left[N_{\theta_x}\right] + \left[N_{\partial w/\partial x}\right]\right]^T\left[N_{\theta_x}\right] + \right.$$
$$\left.\left[N_{\theta_y}\right]^T\left[\left[N_{\theta_y}\right] + \left[N_{\partial w/\partial y}\right]\right] + \left[\left[N_{\theta_y}\right] + \left[N_{\partial w/\partial y}\right]\right]^T\left[N_{\theta_y}\right]\right) +$$
$$\left. I_6\left(\left[\left[N_{\theta_x}\right] + \left[N_{\partial w/\partial x}\right]\right]^T\left[\left[N_{\theta_x}\right] + \left[N_{\partial w/\partial x}\right]\right] + \left[\left[N_{\theta_y}\right] + \left[N_{\partial w/\partial y}\right]\right]^T\left[\left[N_{\theta_y}\right] + \left[N_{\partial w/\partial y}\right]\right]\right)\right] dx\, dy$$

$$\left[M^{(se)}\right] = \left[T^{(e)}\right]^T \left[M^{(e)}\right]\left[T^{(e)}\right] \tag{8.11}$$

The element strain energy due to thermal stresses can be expressed as

$$U_T^{(e)} = \frac{1}{2}\left[\left\{q^{(e)}\right\}^T \left[T^{(e)}\right]^T \left[K_T^{(e)}\right]\left[T^{(e)}\right]\left\{q^{(e)}\right\}\right] \tag{8.12}$$

The skew element thermal stresses stiffness matrix $\left[K_T^{(se)} \right]$ is derived as

$$\left[K_T^{(se)} \right] = \left[T^{(e)} \right]^T \left[K_T^{(e)} \right] \left[T^{(e)} \right] \tag{8.13}$$

$$\left[K_T^{(e)} \right] = \left[K_{00}^{(e)T} \right] + \left[K_{11}^{(e)T} \right] + \left[K_{22}^{(e)T} \right]$$

$$\left. \begin{aligned} \left[K_{00}^{(e)T} \right] &= \int_0^a \int_0^b \left[B_0^T \right]^T \left[A^T \right] \left[B_0^T \right] dx\, dy \\[4pt] \left[K_{11}^{(e)T} \right] &= \int_0^a \int_0^b \left[B_1^T \right]^T \left[D^T \right] \left[B_1^T \right] dx\, dy \\[4pt] \left[K_{22}^{(e)T} \right] &= \int_0^a \int_0^b \left[B_2^T \right]^T \left[H^T \right] \left[B_2^T \right] dx\, dy \end{aligned} \right\} \tag{4.18}$$

Work done by the skew plate due to the in-plane loads can be expressed as

$$\begin{aligned} W^{(e)} &= \frac{1}{2} \int_A \left\{ q^{(e)} \right\}^T \left[T^{(e)} \right]^T \left[P(t) \left[N_{\partial w/\partial x} \right]^T \left[N_{\partial w/\partial x} \right] \right] \left[T^{(e)} \right] \left\{ q^{(e)} \right\} dA \\[4pt] &= \frac{1}{2} \left\{ q^{(e)} \right\}^T \left[K_g^{(se)} \right] \left\{ q^{(e)} \right\} \end{aligned} \tag{8.14}$$

The skew element geometric stiffness matrix $\left[K_g^{(se)} \right]$ is derived as

$$\left[K_g^{(se)} \right] = \int_0^a \int_0^b \left[T^{(e)} \right]^T \left[\left[N_{\partial w/\partial y} \right]^T \left[N_{\partial w/\partial y} \right] \right] \left[T^{(e)} \right] dx\, dy \tag{8.15}$$

$$\left[K_g^{(se)} \right] = \left[T^{(e)} \right]^T \left[K_g^{(e)} \right] \left[T^{(e)} \right]$$

$$\left[K_g^{(e)} \right] = \int_0^a \int_0^b \left[\left[N_{\partial w/\partial y} \right]^T \left[N_{\partial w/\partial y} \right] \right] dx\, dy \tag{3.60}$$

8.3 Governing Equations of Motion

The equation of motion for the element subjected to axial force $P(t)$ can be expressed in terms of nodal degrees of freedom as

$$\left[M^{(e)} \right] \left\{ \ddot{q}^{(e)} \right\} + \left[K_{ef}^{(se)} \right] \left\{ q^{(e)} \right\} - P(t) \left[K_g^{(se)} \right] \left\{ q^{(e)} \right\} = 0 \tag{8.16}$$

where $\left[K_{ef}^{(se)} \right] = \left[K^{(se)} \right] - \left[K_T^{(se)} \right]$ effective element stiffness matrix, which is sum of element stiffness matrix $\left[K^{(se)} \right]$ and element thermal stiffness matrix $\left[K_T^{(se)} \right]$.

The governing equation of motion of skew plate in terms of global displacement matrix obtained as follows

$$[M]\{\ddot{q}\} + [K_{ef}]\{q\} - P(t)[K_g]\{q\} = 0 \tag{8.17}$$

where $\left[K_{ef}^{(se)}\right] = [K] - [K_T]$

$[K_{ef}]$ is global effective stiffness matrix. $[M]$ and $[K_g]$ are global mass and geometric stiffness matrix respectively. $P(t) = \alpha P^{cr} + \beta P^{cr} \cos \Omega t$ with α and β as static and dynamic load factors respectively. Equation (8.16) can be expressed as

$$[M]\{\ddot{q}\} + \left[[K_{ef}] - P^{cr}(\alpha + \beta \cos \Omega t)[K_g]\right]\{q\} = 0 \tag{8.18}$$

where $[K_{ef}] = [K] - [K_T]$

$[K_{ef}]$ is the effective stiffness matrix and $[K], [K_T], [M]$ and $[K_g]$ are global elastic stiffness matrix , thermal stiffness matrix, mass matrix and geometric stiffness matrix respectively and $\{q\}$ is global displacement vector.

The condition for existence of the boundary solutions with period 2T is given by

$$\left([K_{ef}] - \left(\alpha \pm \frac{\beta}{2}\right)P^{cr} \times [K_g] - \frac{\Omega^2}{4}[M]\right)\{q\} = 0 \tag{8.19}$$

The instability boundaries can be determined from the solution of the equation

$$\left| [K_{ef}] - \left(\alpha \pm \frac{\beta}{2}\right)P^{cr} \times [K_g] - \frac{\Omega^2}{4}[M] \right| = 0 \tag{8.20}$$

Following the procedure described in section 3.3.1, the natural frequencies, critical buckling load and instability regions of the skew FGM plate in high thermal environment are determined.

8.4 Numerıcal Results and Dıscussıon

8.4.1 Comparison studies

The natural frequencies of an ordinary plate is calculated with the present computational program and compared with those of Liew [103]. The results are found to be in very good agreement. The results are presented in Table-8.1, S represents simply supported, F represents the free end and C denotes clamped end condition as shown in all tables and figures. The results

of the present numerical model has also been validated in terms of critical buckling load parameter for skew plates with different boundary conditions. Isotropic material properties are considered for comparison with results available in Liew et al. [103], the results are shown in Table-8.2. The results are seen to be in very good agreement.

Table 8.1 Comparison of frequency parameters, λ of skew plates having different boundary condition and W/L=1, h=0.1 m, Poison's ratio $\nu = 0.3$.

SSSS		Mode sequence number							
Deg.		1	2	3	4	5	6	7	8
0	Liew [103]	1.931	4.605	4.605	7.064	8.605	8.605	10.793	10.793
	Present	1.952	4.699	4.699	7.182	8.862	8.862	11.038	11.038
15	Liew [103]	2.037	4.506	5.184	7.071	9.007	9.374	10.227	11.894
	Present	2.089	4.560	5.247	7.141	9.068	9.634	10.402	12.033
30	Liew [103]	2.419	4.888	6.489	7.453	10.398	10.398	11.665	13.611
	Present	2.620	4.668	6.505	7.220	9.487	10.053	11.713	13.165
45	Liew [103]	3.354	6.034	8.733	9.304	11.677	13.548	14.656	16.795
	Present	4.062	5.810	8.537	9.991	11.753	12.01	15.232	15.975
SCSC									
0	Liew [103]	2.699	4.971	5.990	7.973	8.787	10.250	11.338	12.024
	Present	2.735	5.041	6.095	8.085	8.971	10.485	11.523	12.245
15	Liew [103]	2.848	5.122	6.395	7.968	9.444	10.867	11.070	12.860
	Present	2.940	5.221	6.738	8.293	9.702	11.613	11.728	13.551
30	Liew [103]	3.370	5.708	7.738	8.444	11.174	11.373	12.994	14.564
	Present	3.361	5.322	7.933	8.301	10.424	11.417	13.776	14.774
45	Liew [103]	4.596	7.152	9.953	10.701	12.885	14.627	15.801	18.061
	Present	4.412	5.772	8.257	10.447	11.334	12.149	14.405	15.409
CCCC									
0	Liew [103]	3.292	6.276	6.276	8.793	10.357	10.456	12.524	12.524
	Present	3.339	6.385	6.385	8.929	10.594	10.694	12.759	12.759
15	Liew [103]	3.474	6.223	6.959	8.870	10.818	11.282	12.037	13.643
	Present	3.470	6.275	7.010	8.972	10.961	11.575	12.290	13.881
30	Liew [103]	4.114	6.829	8.531	9.471	12.395	12.413	13.743	15.543
	Present	3.892	6.554	8.325	9.388	11.843	12.590	14.031	15.737
45	Liew [103]	5.604	8.477	9.471	11.785	14.104	15.872	16.989	19.059
	Present	5.311	8.113	11.99	12.069	15.165	16.315	20.674	21.089

8.4.2 Free vibration and buckling analysis

For this analysis, FGM plate composed of steel (*SUS304*) and alumina (*Al₂O₃*) has been considered. The properties of each constituent such as Young's modulus, coefficient of linear thermal expansion, Poisson's ratio and thermal conductivity which have been considered for this analysis are adapted from chapter 4. The plate has been discretized into 10X10 elements. For all the cases thickness ratio b/h has been taken as 0.15. Five values of skew angle in degrees (0, 15, 30, 45, and 60) have been considered for the analysis.

Table 8. 2 Critical buckling load factors, K_b; for skew plates with various boundary conditions and under uniaxial loads.

Boundary condition	h/W	Skew angle	Liew et al. [103]	Present
SSSS	0.1	0	3.7870	3.8030
		15	4.1412	4.0472
		30	4.9324	4.9969
		45	7.7236	7.4012
FCFC	0.1	0	3.5077	3.560
		15	3.7937	3.881
		30	4.8043	4.812
		45	6.3311	6.0399
CCCC	0.1	0	8.2917	8.3875
		15	8.7741	8.8102
		30	10.3760	10.4869
		45	13.6909	13.0740

Variation of the fundamental frequency parameter of the skew FGM plate versus power law index for uniform, linear and nonlinear temperature distribution through thickness are shown in figures 8.2-8.7. The obtained results in figures 8.2-8.4 indicate the frequency parameter variation with the index value for simply supported FGM skew plates. It can be seen that the frequency parameter reduces with the increase of index value and on the contrary increasing the skew angle increases the fundamental frequency parameter with UTD, LTD and NTD. Figures 8.5-8.7 show the frequency parameter variation of a fully clamped skew FGM plate for different skew angles and thermal environments. It is observed that the increase in power law index value reduces the first five natural frequencies of skew FGM plate. Increase of skew angle increases the five natural frequencies of FGM plate. From figures 8.2 -8.7 it is clearly observed that variation of frequency parameter drastically changes with respect to power law index value from 0 to 3. The volume fraction of metal increases with increase of index value, and the effective stiffness of the plate is reduced. With higher values of index the metal and ceramic content of the FGM becomes saturated, so there is not much variation in effective Young's modulus and hence of the frequencies.
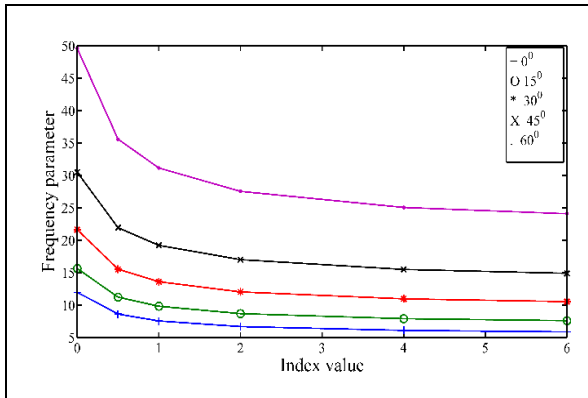
Figure 8.2 Fundamental frequency parameter for Al$_2$O$_3$/ SUS304 (SSSS) plate in thermal environment (UTD).
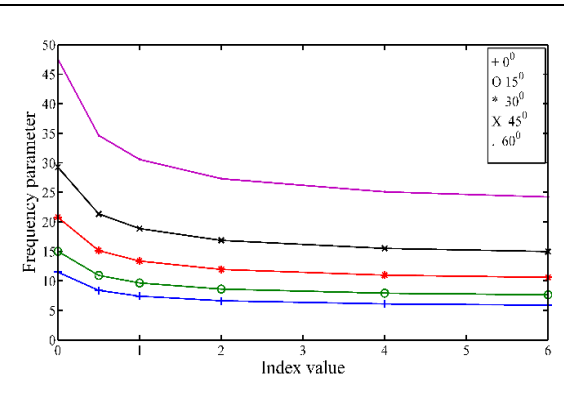
Figure 8.3 Fundamental frequency parameter for Al$_2$O$_3$/SUS304 (SSSS) plate in thermal environment (LTD).
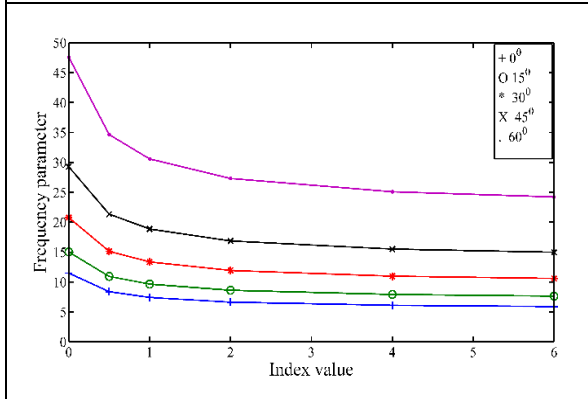
Figure 8.4 Fundamental frequency parameter for Al$_2$O$_3$/ SUS304 (SSSS) plate in thermal environment (NTD).
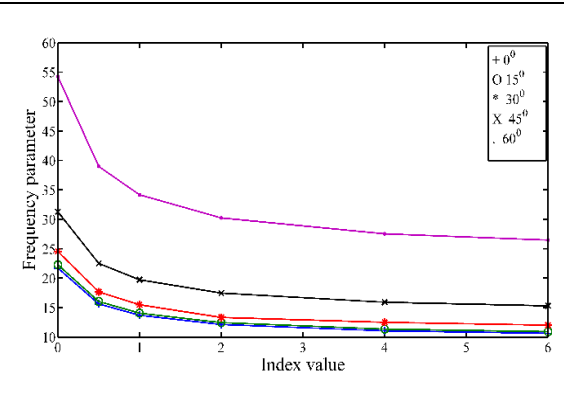
Figure 8.5 Fundamental frequency parameter for Al$_2$O$_3$/SUS304 (CCCC) plate in thermal environment (UTD).
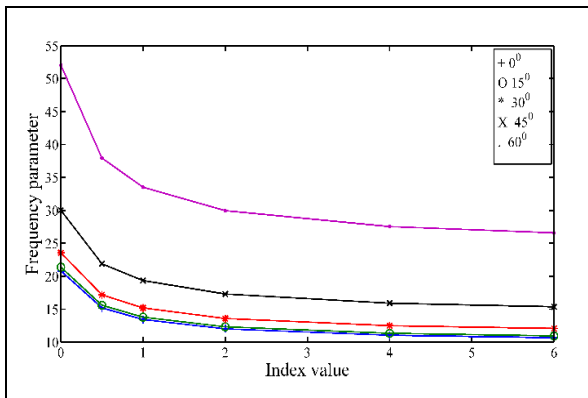
Figure 8.6 Fundamental frequency parameter for Al$_2$O$_3$/ SUS304 (CCCC) plate in thermal environment (LTD).
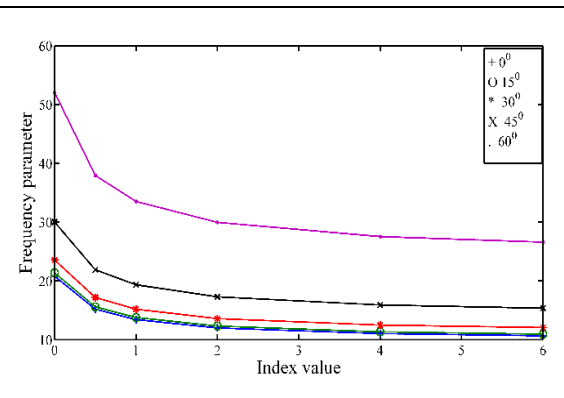
Figure 8.7 Fundamental frequency parameter for Al$_2$O$_3$/SUS304 (CCCC) plate in thermal environment (NTD).

The variation of the frequency parameter versus temperature difference is plotted in figures 8.8-8.10 for a simply supported FGM skew plate with uniform, linear and nonlinear temperature distribution. From these plots it is observed that the first five natural frequencies reduce with increase in temperature, but with increase in skew angle there is increase in the natural frequencies.
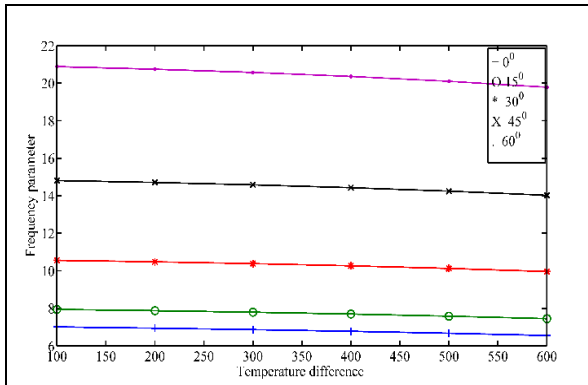
| Figure 8.8 Variation of frequency parameter of a simply supported (SSSS) FGM skew plate for temperature change (UTD).k=1 | Figure 8.9 Variation of frequency parameter of a simply supported (SSSS) FGM skew plate for temperature change (LTD). k=1 |
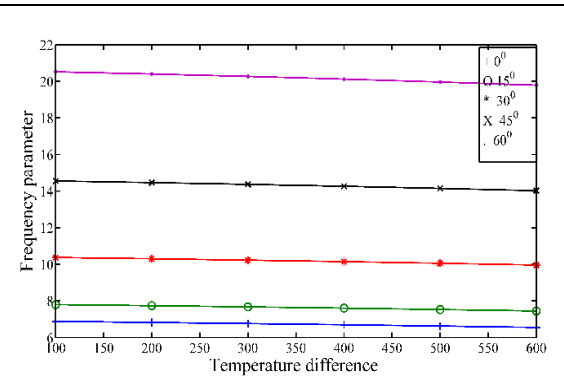
Figures 8.11-8.13 show the variation of frequency parameters with respect to temperature change of FGM skew plate with CCCC boundary. It is observed that increase of temperature rise reduces the first five natural frequencies, also increase in skew angle increases the first five natural frequencies of FGM plate.
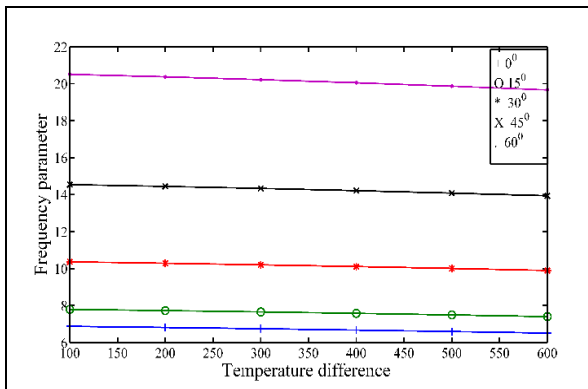
| Figure 8.10 Variation of frequency parameter of a clamped FGM skew plate with temperature change (NTD). k=1 | Figure 8.11 Variation of frequency parameter of a clamped FGM skew plate with temperature change (UTD). k=1 |
| Figure 8.12 Variation of frequency parameter of a clamped FGM skew plate with linear temperature distribution. k=1 | Figure 8.13 Variation of frequency parameter of a clamped FGM skew plate with nonlinear temperature distribution. k=1 |
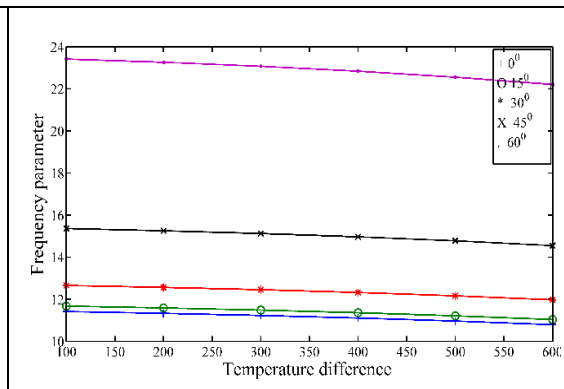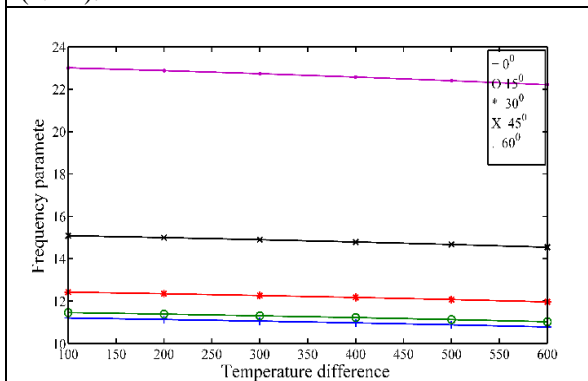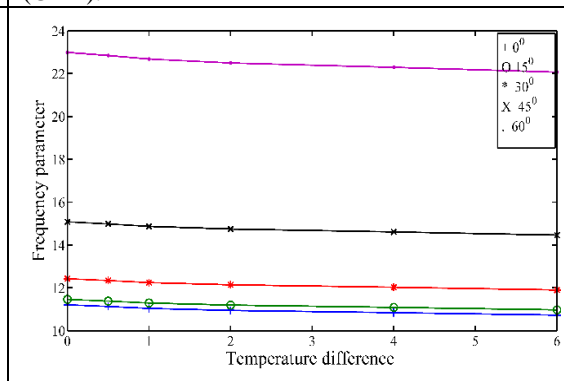
The variation of critical buckling load with respect to power law index values for SSSS and CCCC skew FGM plate are shown in figures 8.14 and 8.15, respectively. It can be

123

observed that the critical buckling load parameter is reduced with increase of power law index value and is increased with the increase of skew angle.
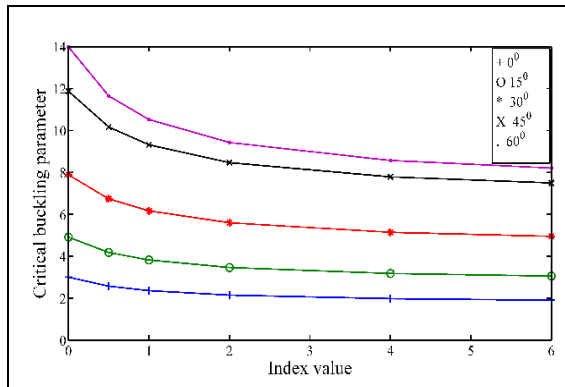
Figure 8.14 Variation of critical buckling parameter of the SSSS FGM skew plate.	Figure 8.15 Variation of critical buckling parameter of the CCCC FGM skew plate.
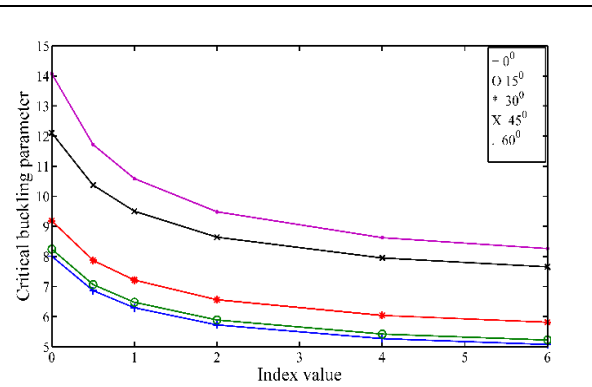
8.4.3 Parametric instability study

The effect of power law index on the dynamic stability of simply supported FGM skew plate is shown in figures 8.16, 8.17 and 8.18 with skew angles 15^0, 30^0 and 45^0, respectively. Thermal environment UTD is considered for this analysis with temperature difference of $100K$. From the figures it is observed that with increase power law index, instability occurs at lower excitation frequency. Hence increase in power law index enhances the dynamic instability.
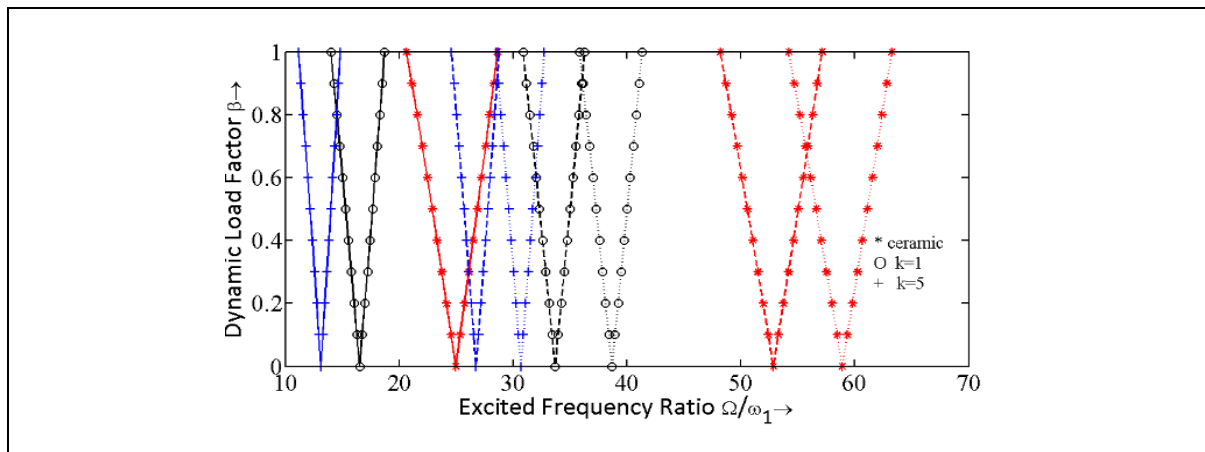
Figure 8.16 Dynamic stability regions for simply supported FGM skew plate with different index values k=1, 5. (L/W=1, h/L=0.15, Φ =15^0), '——' $2\omega_1$, '- - -' $2\omega_2$, '··········' $2\omega_3$
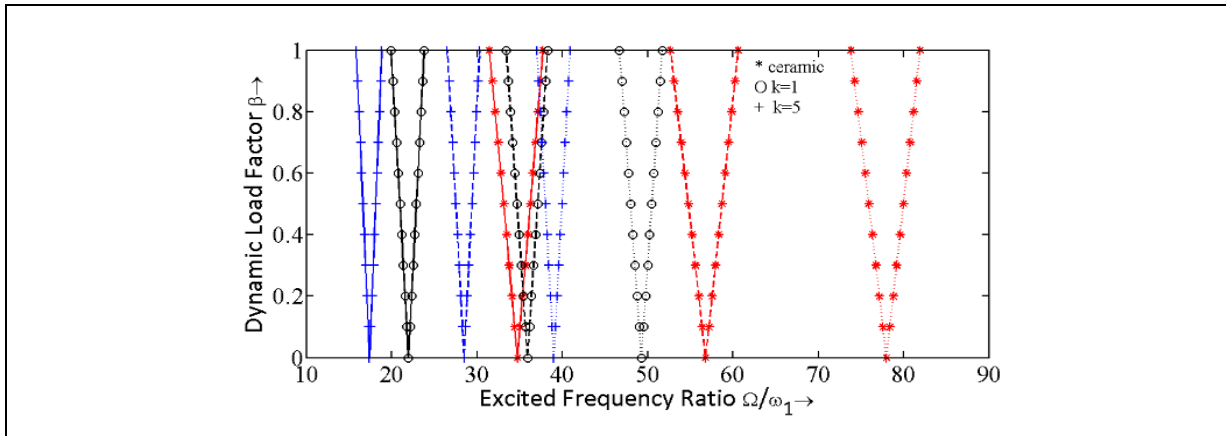
Figure 8.17 Dynamic stability regions for simply supported FGM skew plate with different index values k=1, 5. (L/W=1, h/L=0.15, Φ=30⁰), key as in fig. 8.16.
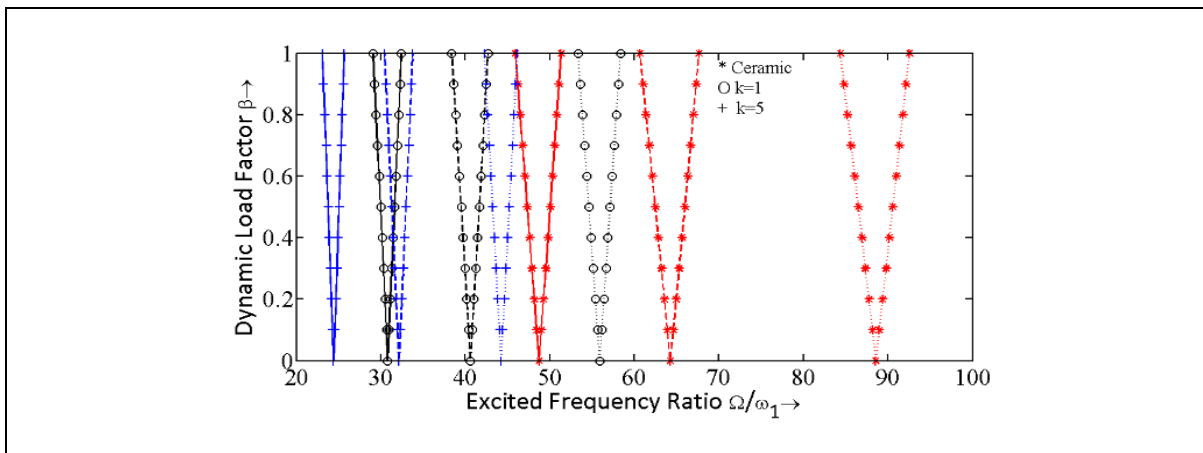
Figure 8.18 Dynamic stability regions for simply supported FGM skew plate with different index values k=0, 1, 5. (L/W=1, h/L=0.15, Φ=45⁰), key as in fig. 8.16.
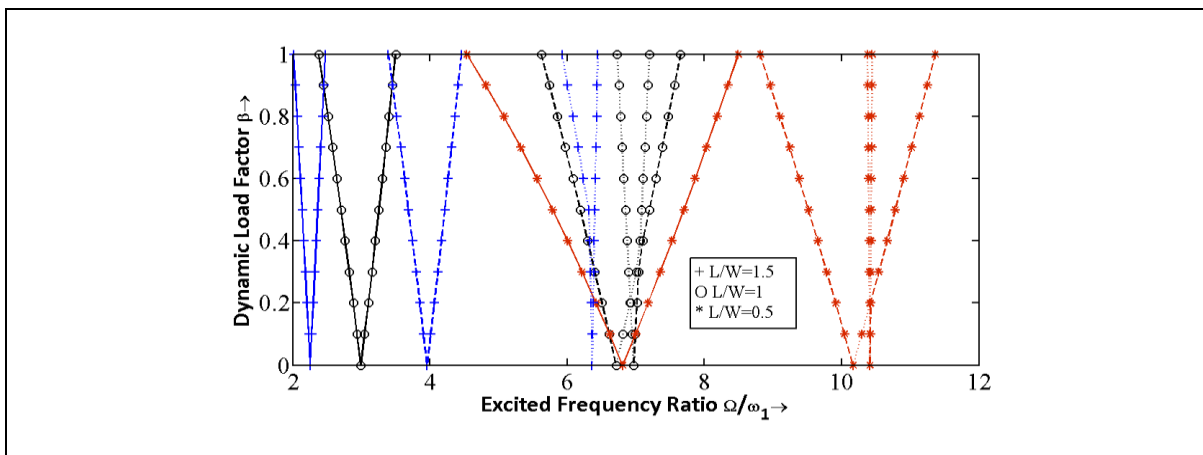
Figure 8.19 Dynamic stability regions for simply supported FGM plate with various aspect ratios L/W=0.5, 1, 1.5. (h/L=0.15, Φ=15⁰), key as in fig. 8.16.

Figure 8.19 shows the effect of increase in aspect ratio on dynamic stability of skew plate. Here the nonlinear temperature distribution with temperature change of 100*K* and power law index *k* =1 is considered. Figure 8.19 displays, increase in aspect ratio L/W=0.5, 1 and 1.5

of FGM skew $\left(\phi = 15^{0}\right)$ plate results in the increase of the dynamic instability, since the instability region move to lower excitation frequencies with increase in aspect ratio.
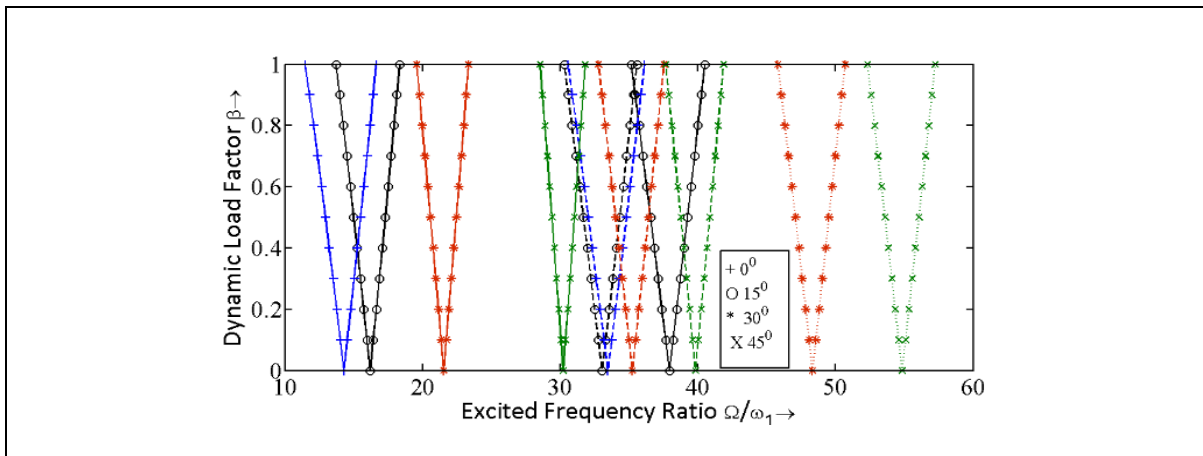
Figure 8.20 Dynamic stability of simply supported FGM skew plate with UTD thermal condition (L/W=1, k=1, h/L=0.15), key as in fig. 8.16.

Figures 8.20-8.22 show the dynamic stability diagrams of FGM skew plate with uniform, linear and nonlinear thermal environments. Geometrical properties considered are aspect ratio L/W = 1, thickness ratio is h/L = 0.15 and the power law index k = 1. When the skew angle increases the stability regions shift from low excitation frequency to high excitation frequency in dynamic stability diagram, this indicates increase in stability of the plate.
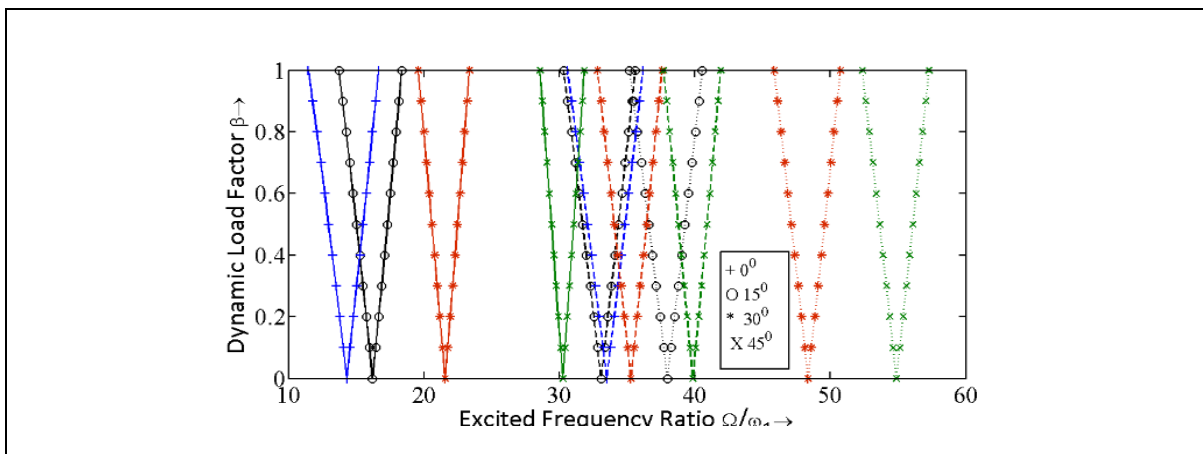
Figure 8.21 Dynamic stability of simply supported FGM skew plate with LTD thermal condition (L/W=1, k=1, h/L=0.15), key as in fig. 8.16.
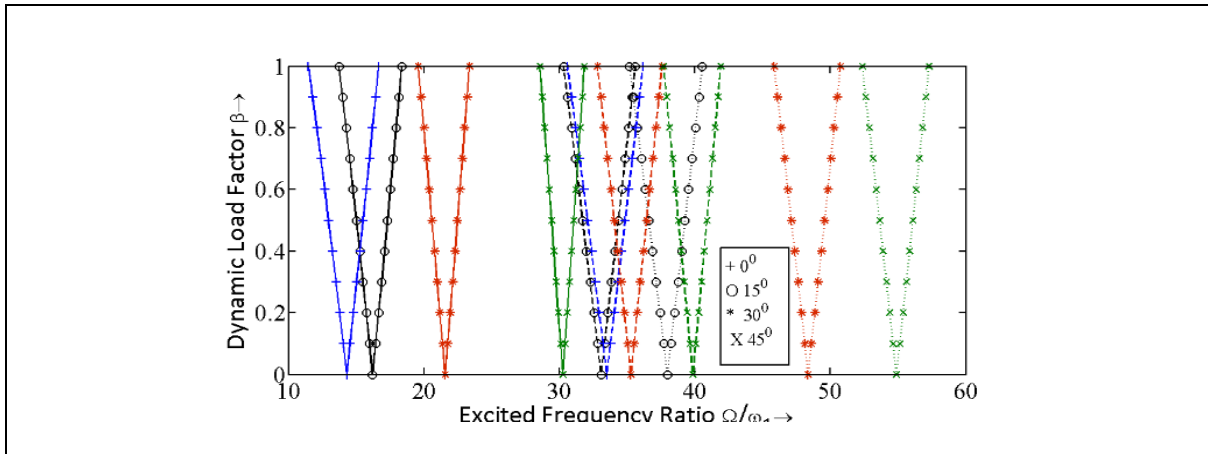
Figure 8.22 Dynamic stability of simply supported FGM skew plate with NTD thermal condition (L/W=1, k=1, h/L=0.15), key as in fig. 8.16.

Figures 8.23 (a) and (b) show the effect of type of temperature distribution on the dynamic stability of skew plate for temperature rise of 100K and 300K respectively. It can be seen that UTD has more prominent effect than compared to linear and nonlinear temperature distribution. The UTD shifts the instability regions to lower excitation frequencies more than compared to linear and nonlinear temperature distribution for the same temperature rise.
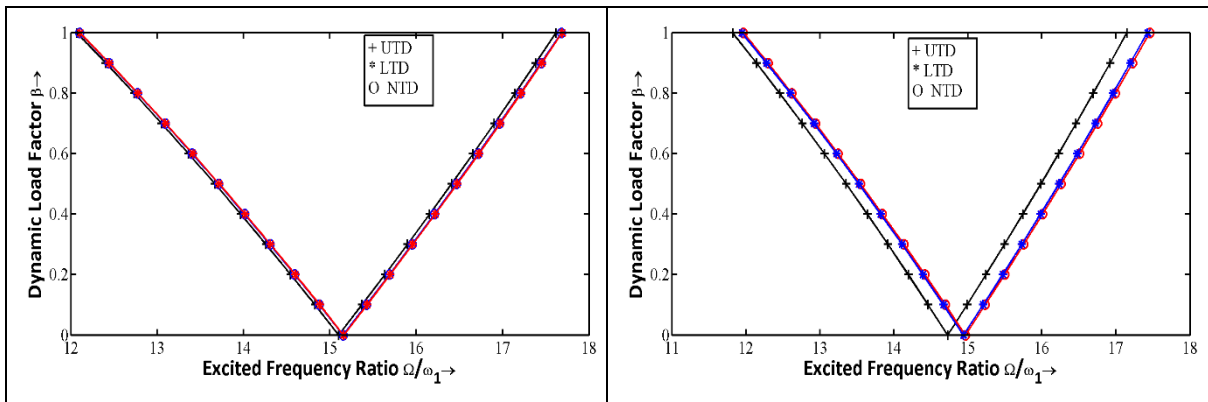
| Figure 8.23(a) First principal instability region of simply supported FGM skew plate with uniform, linear and nonlinear thermal environments. (L/W=1, Φ=15^0, k=2). $\Delta T = 100K$ | Figure 8.23(b) First principal instability region of simply supported FGM skew plate with uniform, linear and nonlinear thermal environments. (L/W=1, Φ=15^0, k=2). $\Delta T = 300K$ |

Figures 8.24-8.26 show the effect of temperature rise on first three principal instability regions of a simply supported skew FGM plate with uniform, linear and nonlinear temperature distribution. It can be observed that increase in temperature reduces the stability of skew plate for all thermal conditions.
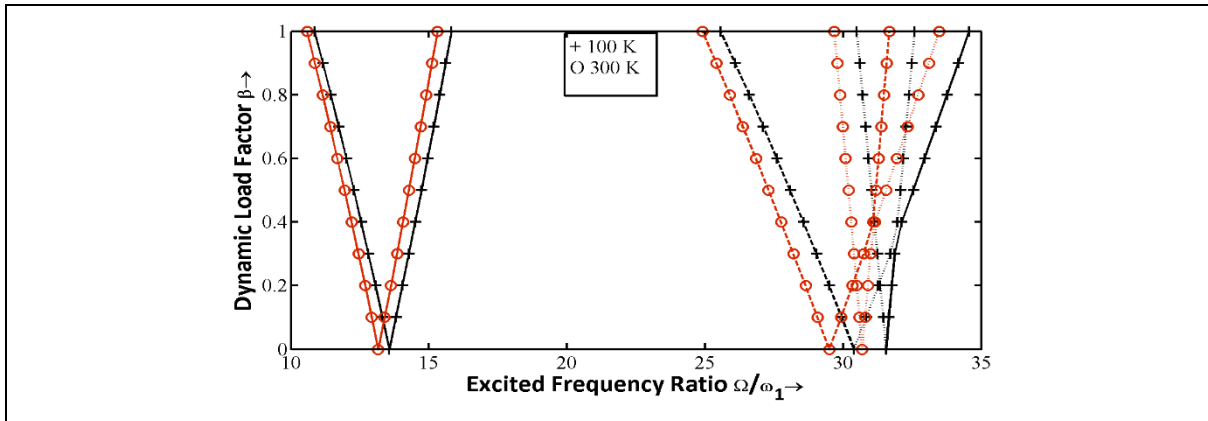
Figure 8.24 First three mode principal instability regions of simply supported FGM skew plate with uniform thermal environments. (L/W=1, $\Phi=15^0$, k=5), key as in fig. 8.16
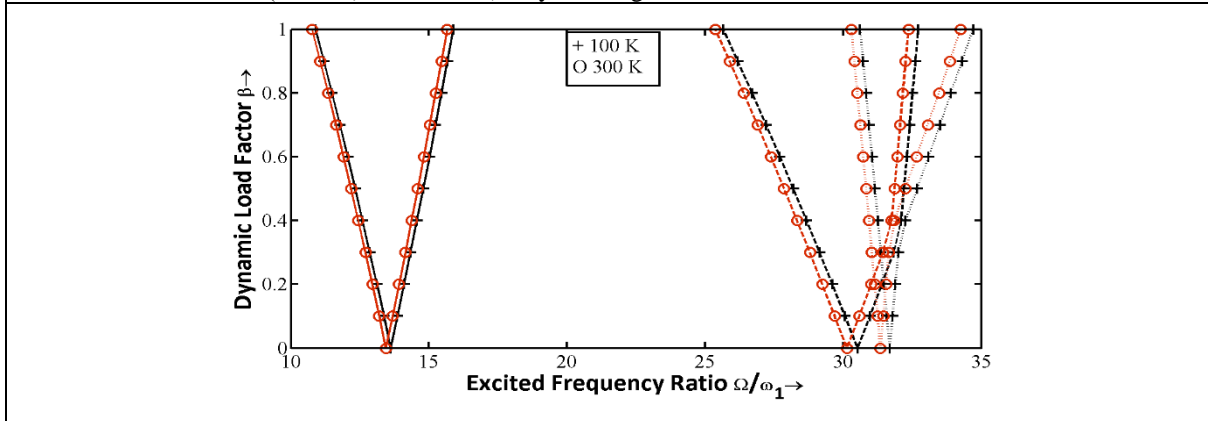
Figure 8.25 First three mode principal instability regions of simply supported FGM skew plate with linear thermal environments. (L/W=1, $\Phi=15^0$, k=2), key as in fig. 8.16
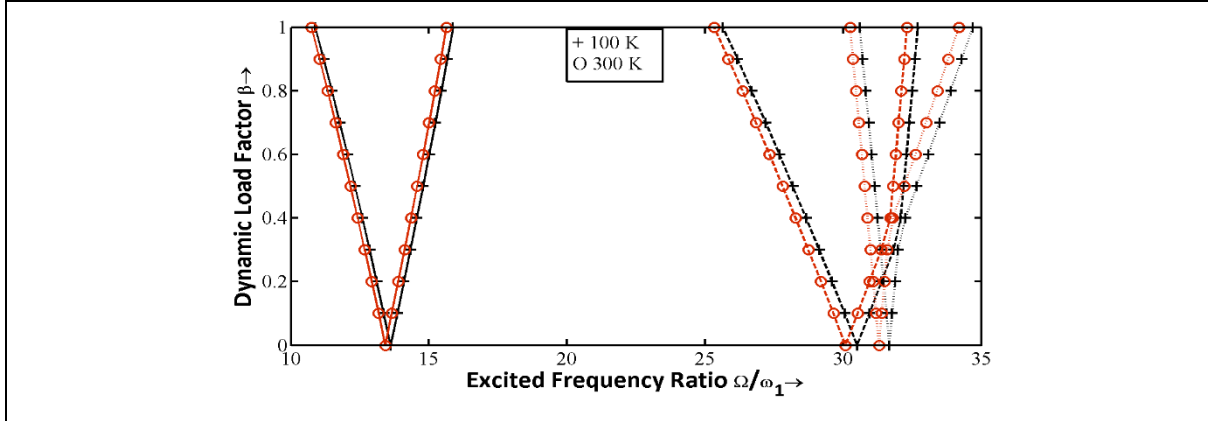
Figure 8.26 First three mode principal instability region of simply supported FGM skew plate with nonlinear thermal environments. (L/W=1, $\Phi=15^0$, k=2). key as in fig. 8.16

8.5 Conclusion

The free vibration, buckling and dynamic stability of FGM skew plate under thermal field is studied in this work. The material properties are assumed to be temperature dependent and the effective material properties are calculated by using a simple power law. An efficient finite element model which is based on the third order shear deformation theory is used for this study. The fundamental natural frequency and critical buckling load of the FGM skew plate are

affected by skew angle, power law index and temperature change. In high temperature environment with the increase in power law index value there is decrease in the fundamental frequency and critical buckling load. Whereas with increase in skew angle there is increase of fundamental frequency and buckling load.

The dynamic stability of FGM skew plate is found to be highly sensitive to changes in the temperature between the bottom and top surfaces. By increasing the power law index value the instability regions move from higher excitation frequency to lower excitation frequency. It shows that there is deterioration of the dynamic stability. Similarly with increase in aspect ratio of FGM skew plate results in overall enhancement of instability of the plate. The stability of the plate is enhanced with increase of skew angle.

Chapter 9

CONCLUSION AND SCOPE FOR FUTURE WORK

9.1 Introduction

The FGMs have many advantages over traditional/regular composite material and those are classified as new composite materials. These advanced composite materials are used in aerospace, automotive, optical, biomechanical, electronic, chemical, nuclear, civil, mechanical, and shipbuilding industries. FGMs possess a number of advantages such as high resistance to temperature gradients, significant reduction in residual and thermal stresses. In the present work, an attempt has been made to study the dynamic stability of FGM plates for different environments and operating conditions such as in the thermal environment, on elastic foundation, hygrothermal environment, under rotation and with a skew angle.

9.2 Summary Report of Key Findings

In this work, finite element method is used to investigate the vibration, buckling and dynamic stability of functionally graded material plates. Finite element modeling technique is applied to carry out the theoretical formulations based on third-order shear deformation theory of FGM plates, with different boundary conditions and various operating conditions. Floquet's theory has been used to establish the dynamic instability regions. The effect of various parameters like boundary conditions, power law index value, temperature rise, angular speed, skew angle and dynamic load factor on the vibration and dynamic instability characteristics of FGM plate under

parametric excitation have been investigated. The conclusions drawn with respect to different studies are presented below.

9.2.1 FGM plates

✓ The first five natural frequencies decrease with an increase of the power law index for SFSF, SSSS and CCCC boundary conditions.

✓ The critical buckling load of SSSS FGM plate decreases with the increase of the power law index value for both uniaxial and biaxial compression loadings.

✓ Increase in aspect ratio (width to length) reduces the critical buckling load of FGM plate.

✓ Increase in the power law index value enhances the parametric instability of FGM plates for both uniaxial and biaxial loadings.

✓ Increase in aspect ratio enhances the dynamic instability of FGM plates.

9.2.2 FGM plates in high temperature thermal environments

✓ Increase in temperature reduces the first two natural frequencies of FGM plates under uniform, linear and nonlinear temperature fields.

✓ In high temperature thermal environment, increase of the power law index reduces the dynamic stability of the FGM plate.

✓ Increase in temperature enhances the chance of parametric instability of FGM plates.

9.2.3 FGM plate resting on elastic foundation

✓ Increase in the power law index value reduces the first two mode frequencies of FGM plate on elastic foundation.

✓ The first two natural frequencies of FGM plates increase with an increase of foundation Winkler and shear layer constants.

✓ Increase in the Winkler foundation constant increases the critical buckling load of the FGM plate, the increase in index value reduces the critical buckling load of FGM plate.

✓ The dynamic stability of FGM plates is improved with an increase of Winkler foundation constant.

✓ With increase in shear layer constant the dynamic stability of FGM plate is also improved.

9.2.4 FGM plate in hygrothermal environment

✓ Increase in the value of the power law index reduces the first two natural frequencies and critical buckling load.

- ✓ The natural frequencies of FGM plates decrease with an increase of temperature and moisture concentration.
- ✓ The critical buckling load decrease with an increase of moisture concentration of FGM plate in hygrothermal environment.
- ✓ The dynamic instability of FGM plate is enhanced with an increase in moisture concentration as well as increase in temperature.
- ✓ The combined effect of both temperature and moisture concentration on the dynamic instability of FGM plates is more severe than the individual effects.

9.2.5 Rotating FGM plates

- ✓ Increase in the power law index reduces the first two-mode natural frequencies of rotating FGM plates.
- ✓ Increase in temperature reduces the first two natural frequencies of rotating FGM plates.
- ✓ The first two natural frequencies of FGM plates increases with an increase of hub radius and rotational speed.
- ✓ Increase in rotational speed of FGM plates increases their stability.
- ✓ With increase in hub radius, the dynamic stability of rotating FGM plate increases.
- ✓ Increase in environment temperature enhances the chance of dynamic instability of rotating FGM plate.

9.2.6 Skew FGM plates

- ✓ Increase of the power law index value reduces the natural frequencies.
- ✓ The critical buckling load of the FGM skew plate decreases with an increase in the power law index value.
- ✓ The first five natural frequencies increase with an increase in skew angle of the plate.
- ✓ Parametric instability enhances with increase of power law index.
- ✓ Increase in skew angle of the plate, enhances the dynamic stability of first and second mode regions.

9.3 Important conclusions with respect to dynamic stability of FGM plates

- ✓ There is an enhanced dynamic instability of FGM plates with an increase of power law index value.
- ✓ In high thermal environment increase in the power law index value increases the dynamic instability of the FGM plate.

- The dynamic instability of FGM plate increases with an increase of environment temperature.
- In increase of Winkler's foundation constant improves the dynamic stability of FGM plate.
- The dynamic stability of FGM plate resting on Pasternak foundation is enhanced with increase of shear layer constant.
- The instability increases with an increase of moisture concentration and temperature of FGM plate in hygrothermal environment.
- Increase in hub radius and rotational speed of FGM plates enhance the dynamic stability of the rotating plate.
- Increase of skew angle improves the dynamic stability of FGM plate in the thermal environment.

9.4 Some design guidelines with respect to dynamic stability of FGM plates.

- The designer has to look at power law distribution features along the thickness. Smaller value of the power law index should be selected to ensure better dynamic stability of the FGM plate.
- For FGM plates with the power law property distribution used at higher temperature, uniform temperature distribution may be assumed to have safer design.
- For FGM plates resting on elastic foundation, higher Pasternak foundation constant should be preferred to Winkler's foundation constant, to ensure better dynamic stability.
- Increased radius of the hub, enhances the dynamic stability of rotating FGM plate. Hence, the rotating plate should be designed for least hub radius, which will ensure better dynamic stability for larger hub radius.
- For rotating FGM plate dynamic stability enhances with centrifugal stiffening. The design of rotating plates should be done for the minimum speed and this will ensure the further enhancement of the dynamic stability at higher speeds.
- For skew FGM plates, increase of skew angle increases the dynamic stability. Hence, the optimum skew angle taking in to other design requirement should be decided to ensure better dynamic stability.

9.5 Scope for Future Work

Present research examines some main reasons of the dynamic instability of functionally graded material plates. There are some other factors of the plates that stay as start problems. The works those can be performed later on are provided as follows.

The particular resistances of elastic foundation in existing research are supposed to be constant. But in practice these resistances may be different along the length of the plates. The effect of a variable foundation on dynamic stability of functionally graded material plate may be taken up as a future problem of research.

In the present analysis, the dynamic stability analysis of rotating functionally graded material un-twisted plates are conducted. Since, turbomachinery blades are pre-twisted rotating rotor blades, the dynamic stability analysis of rotating pre-twisted plates can be carried out.

Sometimes the loading may be such that the structural parts are focused on beyond the elastic limit. At that point, the structure carries on nonlinearly. In the present study, the plates are considered to be concentrated within the elastic limit. The investigation of dynamic stability of FGM plates considering geometrical nonlinearity may be embraced in a future work of exploration. So also material non-linearity may be included.

The effects of high temperature environment on the dynamic stability of plates have been studied in the present work. But in space applications, FGMs are subjected low temperature environment. Hence vibration and dynamic stability of FGM plates subjected to low temperature thermal environment can be taken up for future study.

The outcomes need to be confirmed by experimental results. Hence, experimental investigation of dynamic stability of functionally graded material plates may be taken as a future work to approve the utilized computational method and experimentally validate the obtained theoretical results.

REFERENCES

[1] Abbas, B. A. H. and Thomas, J. (1978) Dynamic stability of Timoshenko beams resting on an elastic foundation. *Journal of sound and vibration*, 60, 33–44.

[2] Abdalla, J. and Ibrahim, M. (2006) Development of a discrete Reissner–Mindlin element on Winkler foundation. *Finite Elements in Analysis and Design*, 42(8-9), 740–748.

[3] Abrate, S. (2006) Free vibration, buckling, and static deflections of functionally graded plates. *Composites Science and Technology*, 66, 2383–2394.

[4] Akhavan, H., Hashemi, S.H., Taher, R., Alibeidloo, A. and Vahabi, Sh. (2009) Exact solutions for rectangular Mindlin plates under in-plane loads resting on Pasternak elastic foundation. Part II: Frequency analysis. *Computational Materials Science*, 44(3), 951–961.

[5] Alexanderson, E. F. (1916) A magnetic amplifier for audio telephony. *Proceedings of the Institute of Radio Engineers*, 4, 101–149.

[6] Altay, G. and Dokmeci, M. C. (2005) Variational principles and vibrations of a functionally graded plate. *Computers and Structures*, 83, 1340–1354.

[7] Ariarathnam, S.T. (1986) Parametric resonance. *proceedings of the tenth U.S. National Congress of applied Mechanics*.

[8] Bahmyari, E. and Khedmati, M.R. (2013) Vibration analysis of nonhomogeneous thick plates with point supports resting on Pasternak elastic foundation using element free Galerkin method. *Engineering Analysis with Boundary Elements*, 37(10), 1212–1238.

[9] Beena, K. P. and Parvathy, U. (2014) Linear static analysis of Functionally Graded Plate using Spline Finite Strip Method. *Composite Structures*, 117, 309–315.

[10] Belabed, Z. Ahmed Houari, M. S. Tounsi, A. (2014) An efficient and simple higher order shear and normal deformation theory for functionally graded material (FGM) plates. *Composites Part B: Engineering*, 60, 274–283

[11] Beliaev, N. M. (1924) Stability of prismatic rods subjected to variable longitudinal forces. *Collection of papers: Eng. Construct, Struct. Mech., Put', Leningrad,* 149 – 167.

[12] Benkhedda, A. Tounsia, E. A. Bedia, A. (2008) Effect of temperature and humidity on transient hygrothermal stresses during moisture desorption in laminated composite plates. *Composite Structures*, 82, 629–635.

[13] Bodaghi, M. and Saidi, (2010) Levy-type solution for buckling analysis of thick functionally graded rectangular plates based on the higher-order shear deformation plate theory. *Applied Mathematical Modelling 34 (2010) 3659–3673*, 34, 3659–3673.

[14] Bolotin, V. V. (1962) The dynamic stability of elastic Systems. *Holden – Day, Inc., san Frasncisco,.*

[15] Bouazza, M. Tounsi, Adda-Bedia, E. (2010) Thermoelastic stability analysis of functionally graded plates: An analytical approach. *Computational Materials Science*, 49(4), 865–870.

[16] Bouazza, M. Hammadi, F. Seddiki, S. (2013) Mechanical Stability of Moderately Thick Functionally Graded Plates. 2, 60–65.

[17] Briseghella, L., Majorana, C. E. and Pellegrino, C. (1998) Dynamic stability of elastic structures: a finite element approach. *Computors and Structures*, 69, 11-25.

[18] Brown, J. E., Hutt, J. M. and Salama, A.E. (1968) Finite element solution to dynamic stability of bars. *AIAA J.*, 6, 1423–1425.

[19] Buczkowski, R. and Torbacki, W. (2001) Finite element modelling of thick plates on two-parameter elastic foundation. *International Journal for Numerical and Analytical Methods in Geomechanics*, 25(14), 1409–1427.

[20] Burney, S. Z. H. and Jaeger, L.G. (1971) A method of determining the regions of instability of a column by a numerical method approach. *Journal of Sound and Vibration*, 15(1), 75–91.

[21] Carrera, E. Filippi, M. and Zappino, E. (2013) Free vibration analysis of rotating composite blades via Carrera Unified Formulation. *Composite Structures*, 106, 317–325.

[22] Celep, Z. (1985) Dynamic stability of pre-twisted columns under periodic axial loads. *Journal of sound and vibration*, 103, 35–48.

[23] Chattopadhyay, A. and Radu, A.G. (2000) Dynamic instability of composite laminates using a higher order theory. *Computers & Structures*, 77(5), 453–460.

[24] Chen, L.W. and Ku, M.K. (1992) Dynamic stability of a cantilever shaft-disk system. *Journal of Vibration and Acoustics, Trans of ASME*, 114, 326–329.

[25] Cheng Xiang-sheng (1992) A free rectangular plate on elastic foundation. *Applied Mathematics and Mechanics*, 13(10), 977–982.

[26] Chinnaboon, B. Katsikadelis, J.T. and Chucheepsakul, S. (2007) A BEM-based meshless method for plates on biparametric elastic foundation with internal supports. *Computer Methods in Applied Mechanics and Engineering*, 196(33-34), 3165–3177.

[27] Choi, H. (2012) An efficient and simple reined theory for buckling analysis of functionally graded plates. *Applied Mathematical Modelling*, 36(3), 1008–1022.

[28] Chucheepsakul, S. and Chinnaboon, B. (2002) An alternative domain/boundary element technique for analyzing plates on two-parameter elastic foundations. *Engineering Analysis with Boundary Elements*, 26(6), 547–555.

[29] Civalek, Ö. (2007) Nonlinear analysis of thin rectangular plates on Winkler–Pasternak elastic foundations by DSC–HDQ methods. *Applied Mathematical Modelling*, 31(3), 606–624.

[30] Da-Guang Zhang and You-He Zhou (2008) A theoretical analysis of FGM thin plates based on physical neutral surface. *Computational Materials Science*, 44, 716–720.

[31] Dehghan, M. and Baradaran, G.H. (2011) Buckling and free vibration analysis of thick rectangular plates resting on elastic foundation using mixed finite element and differential quadrature method. *Applied Mathematics and Computation*, 218(6), 2772–2784.

[32] Desai, Y. M., Ramtekkar, G. S. and Shah, A.H. (2003) Dynamic analysis of laminated composite plates using a layer-wise mixed finite element model. *Composite Structures, 59, 237–249, 2003.*, 59, 237–249.

[33] Dehghany, M. and Farajpour (2013) Free vibration of simply supported rectangular plates on Pasternak foundation: An exact and three-dimensional solution. *Engineering Solid Mechanics*, 2, 29–42.

[34] Dutta, P. K. and Nagraj, C.S. (1989) Dynamic instability behaviour of tapered bars with flaws supported on an elastic foundation. *Journal of Sound and Vibration*, 131(2), 229–237.

[35] Efraim, M.E. (2007) Exact vibration analysis of variable thickness thick annular isotropic and FGM plates. *Journal of Sound and Vibration*, 299, 720–738.

[36] Eftekhari, S. and Jafari, A. (2013) Modified mixed Ritz-DQ formulation for free vibration of thick rectangular and skew plates with general boundary conditions. *Applied Mathematical Modelling*, 37(12-13), 7398–7426.

[37] Evan – Iwanowski, R. M. (1965) On the parametric response of structures. *Applied Mechanics review*, 18, 699–702.

[38] Eratll, N. and Akiiz, A. Y. (1997) The mixed finite element formulation for the thick plates on elastic foundations. *composites and structures*, 65(4), 515–529.

[39] Faraday, M. (1831) On a peculiar class of acoustical figures and on certain forms assumed by a group of particles upon vibrating elastic surfaces. *Phil. Trans., Roy. Soc., London*, 299–318.

[40] Fares, A. D., Elmarghany, M. K. (2009) An efficient and simple refined theory for bending and vibration of functionally graded plates. *Composite Structures*, 91, 296–305.

[41] Farhadi, S. and Hosseini-Hashemi, S.H. (2011) Aeroelastic behavior of cantilevered rotating rectangular plates. *International Journal of Mechanical Sciences*, 53(4), 316–328.

[42] Ferreira, J.M., Batra, R.C., Roque, C.M.C. (2006) Natural frequencies of functionally graded plates by a meshless method. *Composite Structures*, 75(1-4), 593–600.

[43] Ferreira, J.M., Castro, L.M.S. and Bertoluzza, S. (2010) Analysis of plates on Winkler foundation by wavelet collocation. *Meccanica*, 46(4), 865–873.

[44] Ganapathi, M. and Prakash, T. (2006) Thermal buckling of simply supported functionally graded skew plates. *Composite Structures*, 74(2), 247–250.

[45] Gulshan Taj, M.N., Chakrabarti, A. and Sheikh, A.H. (2013) Analysis of functionally graded plates using higher order shear deformation theory. *Applied Mathematical Modelling*, 37(18-19), 8484–8494.

[46] Geoige, Z., Voyiadjis, M. (1986) Thick Rectangular Plates on an Elastic Foundation. *journal of engineering mechanics*, 112(11), 1218–1240.

[47] Guoyong Jin, S.G., Zhu Su, Shuangxia Shi, T.Y. (2014) Three-dimensional exact solution for the free vibration of arbitrarily thick functionally graded rectangular plates with general boundary conditions. *Composite Structures*, 108, 565–577.

[48] Han, J. B. and Liew, K.M. (1997) Numarical differential quadrature method for Reissner/Mindlin plates on two-parameter foundations. *International Journal of Mechanical Sciences*, 39(9), 977–989.

[49] Hasani Baferani, Saidi, R. and Ehteshami, H. (2011) Accurate solution for free vibration analysis of functionally graded thick rectangular plates resting on elastic foundation. *Composite Structures*, 93(7), 1842–1853.

[50] Hasani Baferani, A. R. and Saidi, E. J. (2010) An exact solution for free vibration of thin functionally graded rectangular plates. *Proceedings IMechE Part C: Journal of Mechanical Engineering Science*, 225, 526–536.

[51] Hashemi, H., Fadaee, M. (2011) A new exact analytical approach for free vibration of Reissner–Mindlin functionally graded rectangular plates. *International Journal of Mechanical Sciences*, 53(1), 11–22.

[52] Hashemi, H., Taher, H.R.D., Akhavan, H. (2010) Free vibration of functionally graded rectangular plates using first-order shear deformation plate theory. *Applied Mathematical Modelling*, 34(1276-1291).

[53] Hashemi, S.H., Farhadi, S. and Carra, S. (2009) Free vibration analysis of rotating thick plates. *Journal of Sound and Vibration*, 323(1-2), 366–384.

[54] Hosseini, R., Eghtesad, M., Khayatian, A. (2008) Boundary control of large vibration of FGM rectangular plates. In: *WAC 2008, Automation Congress, Hawaii*, p. World page(s): 1–6.

[55] Hosseini-Hashemi, S., Fadaee, M. and Atashipour, S.R. (2011a) A new exact analytical approach for free vibration of Reissner–Mindlin functionally graded rectangular plates. *International Journal of Mechanical Sciences*, 53(1), 11–22.

[56] Hosseini-Hashemi, S., Fadaee, M. and Atashipour, S.R. (2011b) Study on the free vibration of thick functionally graded rectangular plates according to a new exact closedform procedure. *Composite Structures*, 93(2), 722–735.

[57] Hosseini-Hashemi, Sh., Rokni Damavandi Taher, H., Akhavan, H. (2009) Free vibration of functionally graded rectangular plates using first-order shear deformation plate theory. *Applied Mathematical Modelling*, 34(5), 1276–91.

[58] Hsu, C. S. (1963) On the parametric excitation of a dynamic system having multiple degrees of freedom. *J. Appl. Mech., Trans. ASME*, 30, 367–372.

[59] Hsu, C. S. (1965) Further results on parametric excitation of a dynamic system. *J. Appl. Mech., Trans. ASME*, 32, 373–377.

[60] Hsu, M. (2006) Vibration Characteristics of Rectangular Plates Resting on Elastic Foundations and Carrying any Number of Sprung Masses. *International Journal of Applied science and engineering*, 4(1), 83–89.

[61] Hu, H-T and Tzeng, W-L (2000) Buckling analysis of skew laminate plates subjected to uniaxial inplane loads. *Thin-Walled Structures*, 38(1), 53–77.

[62] Hu, X. X., Sakiyama, T., Matsuda, H. (2004) Fundamental vibration of rotating cantilever blades with pre-twist. *Journal of Sound and Vibration*, 271(1-2), 47–66.

[63] Huang, M. and Thambiratnam, D.P. (2001) Analysis of plate resting on elastic supports and elastic foundation by finite strip method. *Composite Structures*, 79, 2547–2557.

[64] Hiroyuki, M. (2000) Vibration and stability of thick plates on elastic foundations. *Journal of Engineering Mechanics*, 126(1), 27–34.

[65] Huang, X-L. and Shen, H-S. (2004) Nonlinear vibration and dynamic response of functionally graded plates in thermal environments. *International Journal of Solids and Structures*, 41(9-10), 2403–2427.

[66] Huu-Tai Thai and Dong-Ho Choi (2013) A simple first-order shear deformation theory for the bending and free vibration analysis of functionally graded plates. *Composite Structures*, 101, 332–340.

[67] Ibrahim, R.A. (1978a) Parametric vibration, Part III: Current problems (1). *Shock vib. Dig.,* 10(3), 41–57.

[68] Ibrahim, R.A. (1978b) Parametric vibration, Part IV: Current problems (2). *Shock Vib Dig.*, 10(4), 19–47.

[69] Ibrahim, R.A. (1981) Parametric vibration, Part Vi: Stochastic problems (2). *Shock Vib. Dig.*, 13(9), 23–35.

[70] Ibrahim, R.A. (1985) Parametric Random Vibration. *Research Studies Press Ltd., England.*

[71] Ibrahim, R.A. and Barr, A.D.S. (1978a) Parametric vibration, Part I: Mechanics of linear problems. *Shock Vib. Dig.*, 10(1), 15–29.

[72] Ibrahim, R. A. and Barr, A.D.S. (1978b) Parametric vibration, part II: Mechanics of nonlinear problems. *Shock Vib. Dig.,* 10(20), 9–24.

[73] Ibrahim, R. A., and Roberts, J.W. (1978) parametric vibration, Part V: Stochastic problems. *Shock Vib. Dig.*, 10(5), 17–38.

[74] Ishida, Y., Ikeda, T., Yamamoto, T. and Esaka T. (1988) Parametrically excited oscillations of a rotating Shaft under a periodic axial force. *JSME Int. J., Series III*, 31, 698 − 704.

[75] Iwatsubo, T., Saigo, M. and Sugiyama, Y. (1973) Parametric instability of clamped − clamped and clamped − simply supported columns under periodic axial load. *Journal of sound and vibration*, 30, 65 − 77.

[76] Iwatsubo, T., Sugiyama, Y. and Ogino, S. (1974) Simple and combination resonances of columns under periodic axial loads. *Journal of sound and vibration*, 33, 211 − 221.

[77] Jahromi, H.N., Aghdam, M.M. and Fallah, A. (2013) Free vibration analysis of Mindlin plates partially resting on Pasternak foundation. *International Journal of Mechanical Sciences*, 75, 1–7.

[78] Jha, D. K., Kant, T. and Singh, R. K. (2013a) A critical review of recent research on functionally graded plates. *Composite Structures*, 96, 833–849.

[79] Jha, D. K., Kant, T. and Singh, R. K. (2013b) Free vibration response of functionally graded thick plates with shear and normal deformations effects. *Composite Structures*, 96, 799–823.

[80] Jha, D. K., Tarun Kant, Singh, R. K. (2013) Free Vibration of Functionally Graded Plates With A Higher-Order Shear and Normal Deformation Theory. *International Journal of Structural Stability and Dynamics*, 13(1), 13500041– 26.

[81] Karmakar Amit and Singh, P.K. (1997) Finite element free vibration analysis of rotating laminated composite pretwisted cantilever plates. *Journal of Reinforced Plastics and Composites*, 16, 1461–1491.

[82] Karmakar, A. and Sinha, P. K. (2001) Failure Analysis of Laminated Composite Pretwisted Rotating Plates. *Journal of Reinforced Plastics and Composites*, 20(14-15), 1326–1357.

[83] Kee, Y. J. and Kim, J. H. (2004) Vibration characteristics of initially twisted rotating shell type composite blades. *Composite Structures*, 64(2), 151–159.

[84] Khorramabadi, M. K., Najafizadeh, M. M., Shahraki J. A. (2008) Effect of Shear Theories on Free Vibration of Functionally Graded Plates. *World Academy of Science, Engineering and Technology*, 48.

[85] Kim, S. K. (2002) Vibration Analysis of Rotating Composite Cantilever Plates. *KSME International Journal*, 16(3), 320–326.

[86] Kima, J. H. and Kim, H. S. (2000) A study on the dynamic stability of plates under a follower force. *Computers and Structures,* 74, 351–363.

[87] Krishna Reddy, A. R. and Palaninathan, R. (1999) Free vibration of skew laminates. *Computers & Structures*, 70(4), 415–423.

[88] Kugler, S., Fotiu, P. A. and Murin, J. (2014) Enhanced functionally graded material shell finite elements. *Journal of Applied Mathematics and Mechanics*, 94(1-2), 72-84.

[89] Kumar, S., Reddy, B. S., Redd,y C. E. (2011) Higher Order Theory for Free Vibration Analysis of Functionally Graded Material Plates. *ARPN Journal of Engineering and Applied Sciences*, 2006–2011.

[90] Kumar, Y. (2013) Free vibration analysis of isotropic rectangular plates on winkler foundation using differential transform method. *International Journal of Applied Mechanics and Engineering*, 18(2), 589–597.

[91] Lai S. K., Zhou, L., Zhang, Y. Y. (2011) Application of the DSC-Element method to flexural vibration of skew plates with continuous and discontinuous boundaries. *Thin-Walled Structures*, 49(9), 1080–1090.

[92] Lal, A., Jagtap, K. R. (2013) Post buckling response of functionally graded materials plate subjected to mechanical and thermal loadings with random material properties. *Applied mathematical modelling*, 37, 2900–2920.

[93] Lam, K. Y., Wang, C. M. (2000) Canonical exact solutions for Levy-plates on two-parameter foundation using Green's functions. *Engineering Structures*, 22, 364–378.

[94] Lucia, D. C. and Paolo, V. (2004) Finite elements for functionally graded Reissner–Mindlin plates. *Computer Methods in Applied Mechanics and Engineering*, 193(9-11), 705–725.

[95] Latifi, M., Farhatnia, F. and Kadkhodaei, M. (2013) Buckling analysis of rectangular functionally graded plates under various edge conditions using Fourier series expansion. *European Journal of Mechanics - A/Solids*, 41, 16–27.

[96] Lau, S. L., Cheung, Y. K. and Wu, S. Y. (1982) A variable parameter incrementation method for dynamic instability if linear and nonlinear elastic systems. *J. Appl. Mech., Trans. ASME*, 49, 849–853.

[97] Lee, C. Y. and Kim, J. H. (2013) Hygrothermal postbuckling behavior of functionally graded plates. *Composite Structures*, 95, 278–282.

[98] Leetsch, R. Wallmersperger, T. and Kroplin, B. (2009) Thermo mechanical Modeling of Functionally Graded Plates. *Journal of Intelligent Material Systems and Structure*, 20, 1799–1813.

[99] Li Q., Iu, V. P. and Kou, K. P. (2009) Three-dimensional vibration analysis of functionally graded material plates in thermal environment. *Journal of Sound and Vibration*, 324(3-5), 733–750.

[100] Li, S.and Zhang, W. (2011) Global dynamics of a functionally graded material rectangular plate. *IEEE*, 978.

[101] Liew, K. M., Han, J. B. and Du, H. (1996) Differential quadrature method for Mindlin plates on Winkler foundation. *International Journal of Mechanical Sciences*, 38(4), 405–421.

[102] Liew, K. M. and Han, J. B. (1997) Bending analysis of simply supported shear deformable skew plates. *Journal of Engineering Mechanics*, 123, 214–221.

[103] Liew, K. M., Xiang, Y., Kitipornchai, S. and Wang, C. M. (1993) Vibration of thick skew plates based on Mindlin shear deformation plate theory. *Journal of Sound and Vibration*, 168(1), 39–69.

[104] Liew, K. M., Wang, J., Ng, T. Y., Tan, M. J. (2004) Free vibration and buckling analyses of shear-deformable plates based on FSDT meshfree method. *Journal of Sound and Vibration*, 276, 997–1017.

[105] Liu, C., Lee, J. and Lee, Y. (2000) Axisymmetric vibration analysis of rotating annular plates by a 3D finite element. *International Journal of Solids and Structures*, 37, 5813–5827.

[106] Liu, F. (2000) Rectangular thick plates on winkler foundation : differential quadrature element solution. *International Journal of Solids and Structures*, 37, 1743–1763.

[107] Machado, S. P., Filipich, C. P. and Cortinez, V. H. (2007) Parametric vibration of thin-walled composite beams with shear deformation. *Journal of Sound and Vibration*, 305, 563–581.

[108] Mahapatra, T. R., Panda, S. K. and Kar, C. (2014) Vibration Behaviour of Laminated Composite Flat Panel Under Hygrothermal Environment. International Revirew of Applied Engineering Reasearch, 4(5), 455–464.

[109] Mahato, P. K. and Maiti, D. K. (2010) Aeroelastic analysis of smart composite structures in hygro-thermal environment. *Composite Structures*, 92(4), 1027–1038.

[110] Malekzadeh, P. (2008) Differential quadrature large amplitude free vibration analysis of laminated skew plates based on FSDT. *Composite Structures*, 83(2), 189–200.

[111] Malekzadeh, P. (2009) Three-dimensional free vibration analysis of thick functionally graded plates on elastic foundations. *Composite Structures*, 89(3), 367–373.

[112] Malekzadeh, P. and Alibeygi Beni, A. (2010) Free vibration of functionally graded arbitrary straight-sided quadrilateral plates in thermal environment. *Composite Structures*, 92(11), 2758–2767.

[113] Malekzadeh, P., Shahpari, S. A. and Ziaee, H. R. (2010) Three-dimensional free vibration of thick functionally graded annular plates in thermal environment. *Journal of Sound and Vibration*, 329(4), 425–442.

[114] Mantari, J. L., Oktem, A. S. and Guedes Soares, C. (2012) Bending response of functionally graded plates by using a new higher order shear deformation theory. *Composite Structures*, 94(2), 714–723.

[115] Mantari, J.L., Granados, E.V., Hinostroza, M.A. (2014) Modelling advanced composite plates resting on elastic foundation by using a quasi-3D hybrid type HSDT. *Composite Structures*, 118, 455–471.

[116] Mantari, J.L., Granados, E.V. and Guedes Soares, C. (2014) Vibrational analysis of advanced composite plates resting on elastic foundation. *Composites Part B: Engineering*, 66, 407–419.

[117] Matsunaga, H. (2009) Thermal buckling of functionally graded plates according to a 2D higher-order deformation theory. *Composite Structures*, 90(1), 76–86.

[118] Matsunaga, H. (2008) Free vibration and stability of functionally graded plates according to a 2-D higher-order deformation theory. *Composite Structures*, 82, 499–512.

[119] Maziar Janghorban and Amian Zare (2011) Thermal effect on free vibration analysis of functionally graded arbitrary straight-sided plates with different cutouts. *latin american journal of solids and structures*, 8, 245–257.

[120] Melde, F. (1859a) über erregung stehender wellen eines fadenformigen korpers. *ANN. PHys. Chem.*, 109, 193 – 215.

[121] Mizusawa, T. and Kajita, T. (1987) Vibrations of skew plates resting on point supports. *Journal of Sound and Vibration*, 115(2), 243–251.

[122] Mohanty, J., Sahu, S. K. and Parhi, P. K. (2015) Parametric instability of delaminated composite plates subjected to periodic in-plane loading. *Journal of Vibration and Control*, 21, 419-434.

[123] Mohanty, S. C. (2007) Parametric instability of a pretwisted cantilever beam with localised damage. *International Journal of Acoustics and Vibration*, 12(4), 153–161.

[124] Mohanty, S. C., Dash, R.R. and Rout, T. (2011) Parametric instability of a functionally graded Timoshenko beam on Winkler's elastic foundation. *Nuclear Engineering and Design*, 241, 2698–2715.

[125] Mohanty, S. C., Dash, R. R. and Rout, T. (2012) Static dynamic stability analysis of a functionally graded Timoshenko beam. *International Journal of Structural Stability and Dynamics*, 12(4).

[126] Mokhtar, B., Djamel, O. (2012) Buckling of thin plates under uniaxial and biaxial compression. *Journal of Materials Science and Engineering B*, 2(8), 487–492.

[127] Muhammad, T. and Singh, A. V (2004) A p-type solution for the bending of rectangular, circular, elliptic and skew plates. *International Journal of Solids and Structures*, 41(15), 3977–3997.

[128] Myung-Hyun Noh and Sang-Youl Lee (2014) Dynamic instability of delaminated composite skew plates subjected to combined static and dynamic loads based on HSDT. *Composites: Part B*, 58, 113–121.

[129] Nair, P. S. and Durvasula, S. (1973) vibration of skew plates. *Journal of Sound and Vibration*, 26(1), 1–19.

[130] Nayak, N., Meher, S. and Sahu, S. K. (2013) Experimental Study on Effect of Hygrothermal Loading on Vibration of Industry Driven Woven Fiber Carbon / Epoxy Laminated Composite Plates. Proc. of Int. Conf. on Advances in Civil Engineering, AETACE, 896-902,

[131] Nayfeh, A. H. and Mook, D. T. (1979) Nonlinear Oscillations. *John Willey & Sons, Inc., New York*.

[132] Neves, A. M., Ferreira, A. J. M., Carrera, E. (2012) A quasi-3D hyperbolic shear deformation theory for the static and free vibration analysis of functionally graded plates. *Composite Structures*, 94(5), 1814–1825.

[133] Ng, T. Y., Lam, K. Y., Liew, K. M., Reddy, J. N. (2001) Dynamic stability analysis of functionally graded cylindrical shells under periodic axial loading. *International Journal of Solids and Structures*, 38, 1295–1309.

[134] Nguyen, T., Sab, K. (2008) First-order shear deformation plate models for functionally graded materials. *Composite Structures*, 83, 25–36.

[135] Nobakhti, S. and Aghdam, M.M. (2011) Static analysis of rectangular thick plates resting on two-parameter elastic boundary strips. *European Journal of Mechanics - A/Solids*, 30(3), 442–448.

[136] Noh, M.H. and Lee, S.Y. (2014) Dynamic instability of delaminated composite skew plates subjected to combined static and dynamic loads based on HSDT. *Composites Part B: Engineering*, 58, 113–121.

[137] Nuttawit, W. Gangadhara, B. P. and Donald, W. K. (2013) Free and forced vibration analysis using improved third-order shear deformation theory for functionally graded plates under high temperature loading. *Journal of Sandwich Structures and Materials*, 15(5), 583–606.

[138] Ozgan, K. and Daloglu, A. T. (2008) Effect of transverse shear strains on plates resting on elastic foundation using modified Vlasov model. *Thin-Walled Structures*, 46(11), 1236–1250.

[139] Öztürk, H. and Sabuncu, M. (2005) Stability analysis of a cantilever composite beam on elastic support. *Composite Science and Technology*, 65, 1982–1995.

[140] Özdemir, Y.I. (2012) Development of a higher order finite element on a Winkler foundation. *Finite Elements in Analysis and Design*, 48, 1400–1408.

[141] Panda, H. S., Sahu, S. K. and Parhi, P. K. (2013) Hygrothermal effects on free vibration of delaminated woven fiber composite plates - Numerical and experimental results. *Composite Structures*, 96, 502–513.

[142] Pang-jo Chun and Yun Mook Lim (2011) Analytical Behavior Prediction for Skewed Thick Plates on Elastic Foundation. *Mathematical Problems in Engineering*, 509724–29.

[143] Patel, B. P. Ganapathi, M. Prasad, K. R., Balamurugan, V. (1999) Dynamic instability of layered anisotropic composite plates on elastic foundations. *Engineering structures*, 21(11), 988–995.

[144] Parhi, P. K., Bhattacharyya, S. K. and Sinha, P. K. (2001) Hygrothermal Effects on the Dynamic Behavior of Multiple Delaminated Composite Plates and Shells. *Journal of Sound and Vibration*, 248(2), 195–214.

[145] Partha Dey and Singha, M. K. (2006) Dynamic stability analysis of composite skew plates subjected to periodic in-plane load. *Thin-Walled Structures*, 44(9), 937–942.

[146] Patel, B. P., Ganapathi, M. (2002) Hygrothermal effects on the structural behaviour of thick composite laminates using higher-order theory. *Composite Structures*, 56, 25–34.

[147] Piovan, M. T. and Machado, S. P. (2011) Thermoelastic dynamic stability of thin-walled beams with graded material properties. *Thin-Walled Structures*, 49, 437–447.

[148] Praveen, G. N. and Reddy, J.N. (1998) Nonlinear transient thermo elastic analysis of functionally graded ceramic-metal Plates. *International Journal of Solids and Structures*, 35, 4457–4476.

[149] Qin, Q. H. (1995) Hybrid-Trefftz finite element method for Reissner plates on an elastic foundation. *Comput Methods Appl Mech Eng.*, 122(3-4), 379–392.

[150] Rajamohan, C. and Ramachandran, J. (1997) Boundar element analysis of skew plates using a new fundamental solution. *Mechanical research communications*, 24(4), 407–414.

[151] Rajesh, K. and Patil, H. S. (2013) Hygrothermally Induced Nonlinear Free Vibration Response of Nonlinear Elastically Supported Laminated Composite Plates with Random System Properties : Stochastic Finite Element Micromechanical Model. *Frontiers in Aerospace Engineering*, 2(2), 143–156.

[152] Ramu, I. and Mohanty, S. C. (2014) Dynamic stability of functionally graded material plates in high temperature environment. *International Journal of Aerospace and Lightweight Structures*, 4(1), 1-20.

[153] Ramu, I. and Mohanty, S. C. (2012) A review on free, forced vibration analysis and dynamic stability of ordinary and functionally grade material plates. *Caspian Journal of Applied Sciences Research*, 1(13), 57–70.

[154] Ramu, I. and Mohanty, S. C. (2014a) Buckling Analysis of Rectangular Functionally Graded Material Plates under Uniaxial and Biaxial Compression Load. Procedia Engineering, 86, 748-757.

[155] Ramu, I. and Mohanty, S. C. (2014b) Modal analysis of Functionally Graded material Plates using Finite Element Method. In: *Procedia Materials Science 6*, 460–467.

[156] Rao, V. and Sinha, V. (2004) Dynamic response of multidirectional composites in hygrothermal environments. *Composite Structures*, 64, 329–338.

[157] Rashed, Y. F., Aliabadi, M. H. and Brebbia, C. (1999) A boundary element formulation for a Reissner plate on a Pasternak foundation. *Computers & Structures*, 70(5), 515–532.

[158] Ramesh, C. M. and Sekhar K. C. (1996) Rctangular plates resting on tensionless elastic foundation: some new results. *Journal of Engineering Mechanics*, 122(4), 385–387.

[159] Rastgoftar, H., Eghtesad, M., Khayatian, A. (2008) Boundary Control of a Vibrating FGM Rectangular Plate. *International Conference on Intelligent Engineering Systems*, IEEE Xplore.

[160] Rath, M. K. and Dash, M. K. (2014) Parametric Instability of Woven Fiber Laminated Composite Plates in Adverse Hygrothermal Environment. *American Journal of Mechanical Engineering*, 2(3), 70–81.

[161] Rath, M. K. and Sahu, S. K. (2013) Experimental Investigation for Free Vibration of Woven Fiber Composite Plates Subjected to hygrothermal loading. *Thermal Energy and Power Engineering*, 2(3), 94–103.

[162] Reddy, J. N. and Chin, C. D. (1998) Thermomechanical Analysis of Functionally Graded Cylinders and Plates. *Journal of Thermal Stresses*, 21(6), 593–626.

[163] Reddy, J. N. (2000) Analysis of functionally graded plates. *International Journal of Numerical Methods in Engineering*, 47, 663–684.

[164] Rohit, S. and Maiti, P. R. (2012) Buckling of simply supported FGM plates under uniaxial load. *International Journal of Civil and Structural Engineering*, 2(4), 1035–1050.

[165] Saeidifar, M. and Ohadi, A. (2010) Bending vibration and buckling of non-uniform plate with time-dependent boundary conditions. *Journal of Vibration and Control*, 17(9), 1371–1393.

[166] Saha, K. N. (2004) Large Amplitude Free Vibration Study of Square Plates under Different Boundary Conditions Through a Static Analysis. *Journal of Vibration and Control*, 10(7), 1009–1028.

[167] Sahu, S. K. and Datta, P. K. (2000) Dynamic instability of laminated composite rectangular plates subjected to non-uniform harmonic in-plane edge loading. *Proceedings of the Institution of Mechanical Engineers, Part G: Journal of Aerospace Engineering*, 214(5), 295–312.

[168] Sai Ram, K.and Sinha, P (1992) Hygrothermal effects on the buckling of laminated composite plates. *Composite Structures*, 21, 233–247.

[169] Saito, H. and Otomi, K. (1979) Parametric response of viscoelastically supported beams. *Journal of Sound and Vibration*, 63, 169–178.

[170] Samsam Shariat, B. A. and Eslami, M. R. (2007) Buckling of thick functionally graded plates under mechanical and thermal loads. *Composite Structures*, 78, 433–439.

[171] Sathyamoorthy, M. (1978) Vibration of skew plates at large amplitudes including shear and rotatory inertia effects. *International Journal of Solids and Structures*, 14, 869–880.

[172] Seyedemad, M. Massood, M., John, A. (2012) On the free vibration response of rectangular plates, partially supported on elastic foundation. *Applied Mathematical Modelling*, 36, 4473–4482.

[173] Schmidt, G. (1975) Parametererregte Schwingungen. *VEB Deutscher verlag der Wissenschaften, Berlin*.

[174] Sengupta, D. (1995) Performance study of a simple finite element in the analysis of skew rhombic plates. *Computer and structures*, 54(6), 1173–1182.

[175] Senthil, S. Vel and Batra, R. C. (2004) Three-dimensional exact solution for the vibration of functionally graded rectangular plates. *Journal of Sound and Vibration*, 272, 703–730.

[176] Shahrjerdi, A., Mustapha, F., Bayat, M. (2011) Free vibration analysis of solar functionally graded plates with temperature-dependent material properties using second order shear deformation theory. *Journal of Mechanical Science and Technology*, 25(9), 2195–2209.

[177] Shariat, B. S., Javaheri, R. and Eslami, M. R. (2005) Buckling of imperfect functionally graded plates under in-plane compressive loading. *Thin-Walled Structures*, 43(7), 1020–1036.

[178] Sharma, A. K., Mittal, N. D. and Sharma, A. (2011) Free vibration analysis of moderately thick antisymmetric cross-ply laminated rectangular plates with elastic edge constraints. *International Journal of Mechanical Sciences*, 53(9), 688–695.

[179] Shastry, B. P. and Rao, G. V. (1987a) Dynamic stability of a cantilever column with an intermediate concentrated periodic load. *Journal of Sound and Vibration*, 113, 194–197.

[180] Shastry, B. P. and Rao, G. V. (1987b) Stability boundaries of a cantilever column subjected to an intermediate periodic concentrated axial load. *Journal of Sound and Vibration,* 116, 195–198.

[181] Sheikholeslami, S. and Saidi, R. (2013) Vibration analysis of functionally graded rectangular plates resting on elastic foundation using higher-order shear and normal deformable plate theory. *Composite Structures*, 106, 350–361.

[182] Shen, H. S., Yang, J. and Zhang, L. (2001) Free and Forced Vibration of Reissner–Mindlin Plates With Free Edges Resting on Elastic Foundations. *Journal of Sound and Vibration*, 244(2), 299–320.

[183] Shiaut, T. N., Yu, Y. D. and Kuot, C. P. (1996) Vibration and optimum design of rotating laminated blades. *Composites Part B:*, 27B, 395–405.

[184] Sidda Reddy, B., Suresh Kumar, J., Eswara Reddy, C. and Vijaya Kumar Reddy J. (2013) Buckling Analysis of Functionally Graded Material Plates Using Higher Order Shear Deformation Theory. *Journal of Composites*, 1–12.

[185] Simitses, G. J. (1987) Instability of dynamically – loaded structures. *Appl. Mech, Rev.*, 40, 1403 –1408.

[186] Singh, J. M. and Kari, R. (2010) Buckling and Vibration Analysis of FGM Plates and Shells. *ieee*, 978.

[187] Singha, M. K. and Prakash, T. (2011) Finite element analysis of functionally graded plates under transverse load. *Finite Elements in Analysis and Design*, 47, 453–460.

[188] Sreenivasamurthy, S. and Ramamurti, V. (1981) Coriolis effect on the vibration of flat rotating low aspect ratio cantilever plates. *The Journal of Strain Analysis for Engineering Design*, 16(2), 97–106.

[189] Srinivasa, C. V. Suresh, Y. J. Prema Kumar, W. P. (2014) Experimental and finite element studies on free vibration of skew plates. *International Journal of Advance Structural Engineering*, 6(48), 1–11.

[190] Stevens, K. K. (1966) On the parametric excitation of a viscoelastic column. *AIAA journal*, 4, 2111–2115.

[191] Strutt, J. W. (Lord R (1883) On maintained vibrations. *Philosophical Magazine*, 15, 229–235.

[192] Strutt, J. W. (Lord R (1945) The Theory of Sound. *2nd. ed. (N.Y., N.Y.: Dover)*, 1, 81–85.

[193] Strutt, J. W. (Lord R (1987) On the maintenance of vibrations by forces of double frequency, and on the propagation of waves through a medium endowed with periodic structure. *Philosophical Magazine*, 24, 145–159.

[194] Sun, J., Kari, L. and Lopez Arteaga, I. (2013) A dynamic rotating blade model at an arbitrary stagger angle based on classical plate theory and the Hamilton's principle. *Journal of Sound and Vibration*, 332(5), 1355–1371.

[195] Suresh Kumar, J., Sidda Reddy, Eswara, R. C. and Vijayakumar, R. (2011) Higher Order Theory for Free Vibration Analysis of Functionally Graded Material Plates. *ARPN Journal of Engineering and Applied Sciences*, 6(10), 105–111.

[196] Tahmasebi nejad A. and Shanmugam, N. E. (2011) Elastic buckling of uniaxially loaded skew plates containing openings. *Thin-Walled Structures*, 49(10), 1208–1216.

[197] Takahashi, K. (1981) An approach to investigate the instability of the multiple-degree-of-freedom parametric dynamic systems. *Journal of Sound and Vibration*, 78, 519–529.

[198] Talha, M. and Singh, B. N. (2010) Thermomechanical-induced vibration characteristics of shear deformable functionally graded ceramic–metal plates using finite-element method. *Proceedings of the Institution of Mechanical Engineers, Part C: Journal of Mechanical Engineering Science*, 1(-1), 1–16.

[199] Talha, M. and Singh, B. N. (2011) Thermo-Mechanical Buckling Analysis of Finite Element Modeled Functionally Graded Ceramic-Metal Plates. *International Journal of Applied Mechanics*, 03(04), 867–880.

[200] Talha M. and Singh, B. N. (2011) Thermo-mechanical induced vibration characteristics of shear deformable functionally graded ceramic–metal plates using the finite element method. *Proceedings of the Institution of Mechanical Engineers, Part C: Journal of Mechanical Engineering Science*, 225, 50–65.

[201] Talha, M. and Singh, B. N. (2010) Static response and free vibration analysis of FGM plates using higher order shear deformation theory. *Applied mathematical modelling*, 34, 3991–4011.

[202] Tawfik, M. (2010) Limit-cycle Oscillations of Functionally Graded Material Plates Subject to Aerodynamic and Thermal Loads. *Journal of Vibration and Control*, 16(14), 2147–2166.

[203] Thai, H. T. and Choi, D. H. (2011) A refined plate theory for functionally graded plates resting on elastic foundation. *Composites Science and Technology*, 71(16), 1850–1858.

[204] Thai, H. T. and Choi, D. H. (2012) A refined shear deformation theory for free vibration of functionally graded plates on elastic foundation. *Composites Part B: Engineering*, 43(5), 2335–2347.

[205] Thai, H. T. and Kim, S. E. (2013) Closed-form solution for buckling analysis of thick functionally graded plates on elastic foundation. *International Journal of Mechanical Sciences*, 75, 34–44.

[206] Thai, H. T., Park, M. and Choi, D. H. (2013) A simple refined theory for bending, buckling, and vibration of thick plates resting on elastic foundation. *International Journal of Mechanical Sciences*, 73, 40–52.

[207] Tylikowski Andrzej, (2005) Dynamic Staibility of Functonally graded plate under in-plane compression. Mathematical Problems in Engineering, 4, 411-424.

[208] Upadhyay, A. K. and Shukla, K. K. (2012) Large deformation flexural behavior of laminated composite skew plates: An analytical approach. *Composite Structures*, 94(12), 3722–3735.

[209] Victor, B. and Larry, W. B. (2007) Modeling and analysis of functionally graded materials and structures. *Appl. Mech. Rev.*, 60, 195–216.

[210] Wang, J.T-S., Shaw, D. and Mahrenholtz, O. (1987) Vibration of rotating rectangular plates. *Journal of Sound and Vibration*, 112(3), 455–468.

[211] Wang, S. (1997) Buckling analysis of skew fibre-reinforced composite laminates based on first-order shear deformation plate theory. *Composite Structures*, 37(1), 5–19.

[212] Wang, X., Tan, M. and Zhou, Y. (2003) Buckling analyses of anisotropic plates and isotropic skew plates by the new version differential quadrature method. *Thin-Walled Structures*, 41(1), 15–29.

[213] Wang, X., Wang, Y. and Yuan, Z. (2014) Accurate vibration analysis of skew plates by the new version of the differential quadrature method. *Applied Mathematical Modelling*, 38(3), 926–937.

[214] Wanga, S. D. (2002) Dynamic instability of composite laminated rectangular plates and prismatic plate structures. *Computer Methods Applied Mechanics and Engineering*, 191, 1791–1826.

[215] Woo, K. S., Honga, C. H., Basua, P. K., Seo, C. G. (2003) Free vibration of skew Mindlin plates by p-version of F.E.M. *Journal of Sound and Vibration*, 268, 637–656.

[216] Wu, C-P. and Li, H-Y. (2014) Three-dimensional free vibration analysis of functionally graded carbon nanotube-reinforced composite plates with various boundary conditions. *Journal of Vibration and Control*, 106, 128-138.

[217] Xiang, S. and Kang, G. (2013) Static analysis of functionally graded plates by the various shear deformation theory. *Composite Structures*, 99, 224–230.

[218] Xiang, Y. (2003) Vibration of rectangular Mindlin plates resting on non-homogenous elastic foundations. *International Journal of Mechanical Sciences*, 45(6-7), 1229–1244.

[219] Xinwei Wang, Lifei Gan, Y. Z. (2008) Differential quadrature analysis of the buckling of thin rectangular plates with cosine-distributed compressive loads on two opposite sides. *Advances in Engineering Software*, 39, 497–504.

[220] Xinwei Wang, Yongliang Wang, Z. Y. (2014) Accurate vibration analysis of skew plates by the new version of the differential quadrature method. *Applied Mathematical Modelling*, 38, 926–937.

[221] Yaghoobi, H. and Fereidoon, A. (2014) Mechanical and thermal buckling analysis of functionally graded plates resting on elastic foundations: An assessment of a simple refined nth-order shear deformation theory. *Composites Part B: Engineering*, 62, 54–64.

[222] Yang, J. and Shen, H-S. (2002) Vibration Characteristics and Transient Response of Shear-Deformable Functionally Graded Plates in Thermal Environments. *Journal of Sound and Vibration*, 255(3), 579–602.

[223] Yang, J., Liew, K. M. and Kitipornchai, S. (2004) Dynamic stability of laminated FGM plates based on higher-order shear deformation theory. *Computational Mechanics*, 33(4), 305–315.

[224] Yang, J., Liew, K. M. and Kitipornchai, S. (2005) Second-order statistics of the elastic buckling of functionally graded rectangular plates. *Composites Science and Technology*, 65(7-8), 1165–1175.

[225] Yang, J. and Shen, H. S. (2002) Three-dimensional free vibration of thick functionally graded annular plates in thermal environment. *Journal of Sound and Vibration*, 255(3), 255(3), 579–602.

[226] Yang, Zhong, Yuan-yuan, G. and Fangin, B. (2012) Solution for a Rectangular Plate on Elastic Foundation with Free Edges Using Reciprocal Theorem Method. *mathematica Aeterna*, 2(4), 335–343.

[227] Yas, M. H. and Aragh, B. S. (2010) Free vibration analysis of continuous grading fiber reinforced plates on elastic foundation. *International Journal of Engineering Science*, 48(12), 1881–1895.

[228] Yoo, H. H., kim, S. K. and Inman, D. J. (2002) Modal Analysis of Rotating Composite Cantilever Plates. *Journal of Sound and Vibration*, 258(2), 233–246.

[229] Yoo, H. H. and Kim, S. K. (2002) Flapwise bending vibration of rotating plates. *International Journal for Numerical Methods in Engineering*, 55(7), 785–802.

[230] Young, T. H. and Chen, F. Y. (1994) Stability analysis of skew plate subjected areo dynamic and in-plane forces. *Journal of Sound and Vibration*, 171(5), 603–615.

[231] Young, T. H., Lee, C. W. and Chen, F. Y. (2002) Dynamic stability of skew plates subjected to aerodynamic and random in–plane forces. *Journal of Sound and Vibration*, 250(3), 401–414.

[232] Young-Wann, K. (2005) Temperature dependent vibration analysis of functionally graded rectangular plates. *Journal of Sound and Vibration*, 284(3-5), 531–549.

[233] Zarrinzadeh, H., Attarnejad, R. and Shahba, (2011) Free vibration of rotating axially functionally graded tapered beams. *Proceedings of the Institution of Mechanical Engineers, Part G: Journal of Aerospace Engineering*, 226(4), 363–379.

[234] Zenkour, M., Allam, M. N. M., Shaker, M. O. (2011) On the simple and mixed first-order theories for plates resting on elastic foundations. *Acta Mechanica*, 220(1-4), 33–46.

[235] Zenkour, A. M. (2009) The refined sinusoidal theory for FGM plates on elastic foundations. *International Journal of Mechanical Sciences*, 51(11-12), 869–880.

[236] Zhao, X., Lee, Y. Y., Liew, K. M. (2009) Free vibration analysis of functionally graded plates using the element-free kp-Ritz method. *Journal of Sound and Vibration*, 319, 918–939.

[237] Zhibo Yang, Xuefeng Chen, Xingwu Zhang, Z. H. (2012) Free vibration and buckling analysis of plates using B-spline wavelet on the interval Mindlin element. *Applied Mathematical Modelling*, 7–55.

[238] Zhou, D., Liu, W. and Yang, Q. (2008) Three-dimensional vibration analysis of cantilevered skew plates. *Journal of Sound and Vibration*, 313(1-2), 134–148.

[239] Zhou, L. and Zheng, W. X. (2008) Vibration of skew plates by the MLS-Ritz method. *International Journal of Mechanical Sciences*, 50(7), 1133–1141.

[240] Zhu, P. and Liew, K. M. (2011) Free vibration analysis of moderately thick functionally graded plates by local Kriging meshless method. *Composite Structures*, 93, 2925–2944.

Appendix-A

```
                          ╔═══════════╗
                          ⟨   Start   ⟩
                          ╚═══════════╝
                                │
                                ▼
              ┌──────────────────────────────────────┐
              │ Read plate geometry and material properties │
              └──────────────────────────────────────┘
                                │
                                ▼
              ┌──────────────────────────────────────┐
              │   Generate nodal connectivity and mesh   │
              └──────────────────────────────────────┘
                                │
                                ▼
       ┌────────────────────────────────────────────────────┐
       │  Generate Element stiffness matrix, Element mass matrix and │
       │  Element geometric stiffness matrix due to mechanical loads and │
       │       thermo-mechanical loads of FGM plates        │
       └────────────────────────────────────────────────────┘
                                │
                                ▼
              ┌──────────────────────────────────────┐
              │    Assemble element matrices to global    │
              └──────────────────────────────────────┘
                                │
                                ▼
              ┌──────────────────────────────────────┐
              │  Apply boundary conditions and generate reduced │
              │            global matrices             │
              └──────────────────────────────────────┘
                                │
                                ▼
              ┌──────────────────────────────────────┐
              │ Read Natural frequency, Critical buckling load α, β │
              └──────────────────────────────────────┘
```

Flow chart of program in MATLAB for calculating the lower and upper boundary limits of instability regions based on Floquet's theory.

Publications related to the Ph.D. thesis work

International Journal:
Published/To be published:

[1] Ramu, I. and Mohanty, S.C. (2015) Free Vibration and Dynamic Stability of FGM Plates on Elastic Foundation, *Defense Science Journal*, 65(3), 245-251.

[2] Ramu, I. and Mohanty, S.C. (2014) Dynamic Stability of Functionally Graded Material Plates in High Temperature Environment, *International Journal of Aerospace and Lightweight Structures*, 4(1), 1–20.

[3] Ramu, I. and Mohanty, S.C. (2014) Vibration and Parametric Instability of Functionally Graded Material Plates, *Journal of Mechanical Design and Vibration*, 2(4), 102-110.

[4] Ramu I. and Mohanty, S.C. (2012) A Review on Free, Forced Vibration Analysis and Dynamic Stability of Ordinary and Functionally Grade Material Plates, *Caspian Journal of Applied Sciences Research*, 1(13), 5770-5779.

[5] Ramu, I. and Mohanty, S.C. (2012) Study on Free Vibration Analysis of Rectangular Plate Structures Using Finite Element Method, *Elsevier Procedia Engineering,* 38, 2758 – 2766.

[6] Ramu, I. and Mohanty, S.C. (2014) Buckling Analysis of Rectangular Functionally Graded Material Plates under Uniaxial and Biaxial Compression Load, *Elsevier Procedia Engineering*, 86, 748–757.

[7] Ramu, I. and Mohanty, S.C. (2014) Modal analysis of Functionally Graded Material Plates using Finite Element Method, *Elsevier Procedia Material Science*, 6, 460-467.

[8] Ramu, I. and Mohanty, S.C. Free vibration analysis of rotating FGM plates in high thermal environment using the finite element method, *International Journal of Acoustics and Vibration* (Accepted).

[9] Ramu, I. and Mohanty, S.C. Flap wise bending vibration and dynamic stability of rotating FGM plates in thermal environments, *Journal of Aerospace Engineering* (SAGE), Accepted.

Work communicated:

[1] Ramu, I. and Mohanty, S.C. Vibration and Parametric Instability Characteristics of FGM Plates in Hygrothermal Environment, *Journal of Materials: Design and Applications* (SAGE), under review.

International conferences presented

[1] Ramu, I. and Mohanty, S.C. Study on free vibration analysis of rectangular plate structures using finite element method, ICMOC-2012, Noorul Islam University, 10-11 Apr. 2012, Kumaracoil-629180. Tamil Nadu, India.

[2] Ramu, I. and Mohanty, S.C. Study on free vibration analysis of temperature dependent functionally graded material plates, International Conference on Smart Technologies for Mechanical Engineering, (STME-2013) (25-26 October, 2013), Delhi Technological University, Delhi, India.

[3] Ramu, I. and Mohanty, S.C. Buckling Analysis of Rectangular Functionally Graded Material Plates under Uniaxial and Biaxial Compression Load, First international conference on structural integrity (ICONS-2014), FEB 4-6, Indira Gandhi Centre for Atomic Research Kalpakkam, India.

[4] Ramu, I. and Mohanty, S.C. Modal analysis of Functionally Graded material Plates using Finite Element Method, 3rd international conference on material processing and characterization 8th -9th march-2014, ICMPC-2014, GRIET, Hyderabad, India.

BIBLIOGRAPHY

Mr. Ramu Inala is a Research scholar in the Department of Mechanical Engineering, National Institute of Technology-Rourkela, Odisha-769008, India. He has 4 years of research and two year teaching experience in his field. He is a graduate of Bachelor of Engineering in Mechanical from the Andhra University (2005), M.Tech. in Machine Design and Analysis (2010) from National Institute of Technology, Rourkela. This dissertation is being submitted for the fulfillment the Ph.D. degree.

Permanent address

RAMU INALA, Door No. 6-42,

Madepalli (Lingaraogudem),

Jali pudi (post), Eluru (mandal),

West Godavari district,

Andhra Pradesh-534004. India

E mail:ramuinala@gmail.com,

Phone: 08500675526 (M)